UC San Diego

UC San Diego Electronic Theses and Dissertations

Title

Development of a seismic design procedure for metal building systems

Permalink

https://escholarship.org/uc/item/3vp4k1pf

Author

Hong, Jong-Kook

Publication Date

2007

Peer reviewed|Thesis/dissertation

eScholarship.org Powered by the California Digital Library
University of California

UNIVERSITY OF CALIFORNIA, SAN DIEGO

Development of A Seismic Design Procedure for Metal Building Systems

A Dissertation submitted in partial satisfaction of the requirements

for the degree Doctor of Philosophy

in

Structural Engineering

by

Jong-Kook Hong

Committee in charge:

Professor Chia-Ming Uang, Chair
Professor David Benson
Professor Enrique Luco
Professor Sia Nemat-Nasser
Professor Benson Shing

2007

Copyright

Jong-Kook Hong, 2007

All rights reserved.

The Dissertation of Jong-Kook Hong is approved, and it is acceptable in quality and form for publication on microfilm:

Chair

University of California, San Diego

2007

To my wife, Ha-Jeong

and my daughter, Joanne

Ignorance is not innocence, but sin.

- Robert Browning

TABLE OF CONTENTS

SIGNATURE PAGE iii
DEDICATION iv
EPIGRAPH v
TABLE OF CONTENTS vi
LIST OF ABBREVIATIONS x
LIST OF SYMBOLS xi
LIST OF FIGURES xiv
LIST OF TABLES xviii
ACKNOWLEDGEMENTS xix
VITA xx
ABSTRACT OF THE DISSERTATION xxi
1 INTRODUCTION 1
1.1 Introduction 1
1.2 Current Seismic Design Philosophy 2
1.3 Metal Building Systems 4
1.4 Current Seismic Design Practice of Metal Buildings 5
1.5 Statement of Problem 6
1.6 Dissertation Outline and Chapter Summary 7
1.6.1 Chapter 1 8
1.6.2 Chapter 2 8
1.6.3 Chapter 3 8
1.6.4 Chapter 4 9
1.6.5 Chapter 5 9
1.6.6 Chapter 6 9
1.6.7 Chapter 7 10
2 LITERATURE REVIEW 13
2.1 Introduction 13
2.2 LRFD Strength Evaluation of Web-Tapered Members 13
2.2.1 Axial Compressive Strength 13
2.2.2 Flexural Strength 16
2.2.3 Combined Axial Compression and Flexure 18
2.2.4 Shear Strength 20
2.3 Metal Building Testing 22

2.3.1 Forest and Murray (1982) 22
2.3.2 Hwang et al. (1989 and 1991) 23
2.3.3 Sumner (1995) 23
2.3.4 Heldt and Mahendran (1998) 24
2.3.5 Chen et al. (2006) 24
2.4 Finite Element Analysis 25
2.4.1 Davids (1996) 25
2.4.2 Miller and Earls (2003 and 2005) 25
2.5 Summary and Conclusions 26
3 CYCLIC TESTING OF A METAL BUILDING SYSTEM 32
3.1 Introduction 32
3.2 Design of Test Building 32
3.2.1 Test Building 32
3.2.2 Design Load 33
3.2.3 Governing Load Combination 34
3.3 Testing Program 35
3.3.1 General 35
3.3.2 Material Properties 36
3.3.3 Test Setup 36
3.3.4 Instrumentation 37
3.3.5 Loading History 38
3.4 Test Results 39
3.4.1 Gravity Load Test 39
3.4.2 Cyclic Test 40
3.5 Overstrength of Test Frame 44
3.6 Member Strength Correlation 44
3.7 Flange Brace Force 46
3.8 Summary and Conclusions 49
4 FINITE ELEMENT ANALYSIS OF TEST FRAME 117
4.1 Introduction 117
4.2 Finite Element Modeling Technique 117
4.2.1 General 117
4.2.2 Geometry and Element 117
4.2.3 Material Properties 119
4.2.4 Gravity Load and Monotonic Push 119
4.2.5 Post-Buckling Response 119
4.3 Correlation with Test Results 120

4.3.1 Gravity Load Analysis 120
4.3.2 Lateral Load Analysis 121
4.4 Initial Geometric Imperfection 122
4.5 Summary and Conclusions 122
5 DEVELOPMENT OF A SEISMIC DESIGN PROCEDURE 132
5.1 Introduction 132
5.2 Drift-Based Design Concept 132
5.3 System Overstrength Factor, Ω_o 134
5.4 Fundamental Period 135
5.4.1 Design Seismic Base Shear 135
5.4.2 T versus T_a 136
5.4.3 Story Drift Evaluation 137
5.5 Influence of Damping 137
5.6 Influence of R-Factor 138
5.7 Simplified Design Procedure 138
5.8 Summary and Conclusions 140
6 APPLICATIONS OF THE PROPOSED SEISMIC DESIGN PROCEDURE 148
6.1 Introduction 148
6.2 Case 1 (40 ft×12 ft) 148
6.2.1 Step 1: Preliminary Design 148
6.2.2 Step 2: Compute Actual Fundamental Period, T 149
6.2.3 Step 3: Compute Ω_o Based on the Revised Earthquake Load 150
6.2.4 Step 4: Check Ω_o/R Ratio 151
6.2.5 Step 5: Connection Design 151
6.3 Case 2 (100 ft×20 ft) 151
6.3.1 Step 1: Preliminary Design 151
6.3.2 Step 2: Compute Actual Fundamental Period, T 152
6.3.3 Step 3: Compute Ω_o Based on the Revised Earthquake Load 152
6.3.4 Step 4: Check Ω_o/R Ratio 153
6.3.5 Step 5: Connection Design 154
6.4 Case 3 (150 ft×20 ft) 154
6.4.1 Step 1: Preliminary Design 154
6.4.2 Step 2: Compute Actual Fundamental Period, T 155
6.4.3 Step 3: Compute Ω_o Based on the Revised Earthquake Load 155
6.4.4 Step 4: Check Ω_o/R Ratio 156
6.4.5 Step 5: Connection Design 157

6.5 Summary and Conclusions 157
7 SUMMARY AND CONCLUSIONS 186
7.1 Summary 186
7.2 Conclusions 189
APPENDIX A. MEMBER STRENGTH CHECK OF TEST FRMAE 192
APPENDIX B. OVERSTRENGTH FACTOR OF EXAMPLE BUILDINGS 205
APPENDIX C. PARAMETRIC STUDIES ON PANEL ZONE THICKNESS 219
REFERENCES 228

LIST OF ABBREVIATIONS

AISC	American Institute of Steel Construction,
AISI	American Iron and Steel Institute,
ASCE	American Society of Civil Engineers,
ASD	Allowable Stress Design,
BSSC	Building Seismic Safety Committee,
DCR	Demand/Capacity Ratio,
DCR_E	Demand/Capacity Ratio under Earthquake Load,
DCR_G	Demand/Capacity Ratio under Gravity Load,
FEA	Finite Element Analysis,
FEMA	Federal Emergency Management Agency,
ICC	International Code Council,
IBC	International Building Code,
LRFD	Load and Resistance Factor Design,
MBMA	Metal Building Manufacturers Association,
OMF	Ordinary Moment Frame,
SMF	Special Moment Frame, and
UCSD	University of California, San Diego.

LIST OF SYMBOLS

A_g	Area of cross-section,
A_w	Area of web,
C_b	Bending coefficient dependent on moment gradient,
C_d	Displacement amplification factor,
C_{eu}	Required strength to respond elastically,
C_s	Code-specified seismic force level,
C_u	Coefficient for upper limit of fundamental period,
C_v	Shear coefficient,
C_y	Ultimate strength level,
E	Elastic modulus,
$F_{b\gamma}$	Critical flexural stress,
F_{cr}	Critical buckling stress,
$F_{s\gamma}$	St. Venant's term of critical flexural stress,
F_u	Tensile stress,
$F_{w\gamma}$	Warping term of critical flexural stress,
F_y	Specified minimum yield stress,
F_{ye}	Design expected yield strength,
F_{yw}	Web yield stress,
K	Effective length factor for prismatic members,
K_γ	Effective length factor for web-tapered members,
L_b	Unbraced length of a segment,
M_n	Nominal flexural strength,
M_{nt}	Required flexural strength with no lateral translation,
M_{lt}	Required flexural strength with lateral translation,
M_p	Nominal plastic flexural strength,
M_u	Required flexural strength,
P_n	Nominal compressive strength,

P_u Required axial strength,

P_y Nominal tensile strength,

Q Slenderness member reduction factor,

Q_a Slenderness member reduction factor for stiffened compression members,

Q_s Slenderness member reduction factor for unstiffened compression elements,

S_a Spectral response acceleration,

S_{DS} Design, 5 percent damped, spectral response acceleration parameter at short periods,

S_{D1} Design, 5 percent damped, spectral response acceleration parameter at a period of 1 second,

R Response modification factor,

R_μ System ductility reduction factor,

S_x' Section modulus at larger member end,

T Actual fundamental period,

T_a Fundamental period by approximate method,

V_n Nominal shear strength,

V_u Required shear strength,

d_o Depth of beam at smaller end,

d_i Depth of beam at larger end,

h Tapered member length factor,

k_v Web plate buckling coefficient,

g Acceleration of gravity,

r_o Radius of gyration about strong axis,

r_{oy} Radius of gyration about weak axis,

Δ_C Drift capacity,

Δ_D Drift demand,

Δ_S Drift at design seismic force level,

Ω_o System overstrength factor,

δ_e	Elastic story drift,
δ_s	Inelastic story drift,
$\bar{\varepsilon}^{pl}$	Plastic strain,
γ	Tapering ratio,
λ	Section compactness ratio,
σ_{taper}	Stress of tapered member,
$\sigma\|_0$	Yield surface size as zero plastic strain, and
ξ	Damping ratio.

LIST OF FIGURES

Figure 1.1 General Structural Response Envelope (Uang 1991) 12
Figure 1.2 Typical Components of a Metal Building System (Newman 2003) 12
Figure 2.1 Tapered Beam Geometry and Presumed Loading (Lee et al. 1972) 29
Figure 2.2 Length Modification Factor (Lee et al. 1972) 30
Figure 2.3 Panel Zone Plate with Stiffener 31
Figure 2.4 Tension Field in the Panel Zone 31
Figure 3.1 Elevation and Top View of Test Building 55
Figure 3.2 Sidewall Elevation 56
Figure 3.3 Column Base 57
Figure 3.4 Design Wind Load 58
Figure 3.5 SAP Modeling Scheme 58
Figure 3.6 Force Demand under Governing Loading Combination 59
Figure 3.7 Test Building 60
Figure 3.8 Flange Brace 61
Figure 3.9 Test Setup 62
Figure 3.10 Actuator-to-Column Connection Details 63
Figure 3.11 Column Base Connection Details 64
Figure 3.12 Instrumentation for Panel Zone, End Plate, and Column Base 65
Figure 3.13 Gravity Load and Cyclic Load 66
Figure 3.14 Vertical Deflection at Midspan 67
Figure 3.15 Frame 1: Rotation Angle at Column Base 67
Figure 3.16 Stress Distribution due to Gravity Load 68
Figure 3.17 Moment Diagram (Gravity Load Only) 69
Figure 3.18 Derived and Simplified Support Reactions (Gravity Load Only) 70
Figure 3.19 Frame 1: Axial Force and Bending Moment Diagrams (Gravity Load Only) 71
Figure 3.20 Frame 2: Axial Force and Bending Moment Diagrams (Gravity Load Only) 72

Figure 3.21 Frame 1: Behavior at 1.5% Drift 73
Figure 3.22 Frame 2: Behavior at 1.5% Drift 74
Figure 3.23 Lateral Buckling at South Column and Rafter of Frame 2 75
Figure 3.24 Flange Brace Reinforcement and Addition after First 2% Drift 76
Figure 3.25 Flange Braces Added during 2% Drift Cycles 77
Figure 3.26 Frame 1: Failure Mode at First Positive Excursion to 3% Drift 78
Figure 3.27 Frame 2: Failure Mode at First Positive Excursion to 3% Drift 78
Figure 3.28 Failure Mode at First Negative Excursion to 3% Drift 79
Figure 3.29 Base Shear versus Column Top Displacement 80
Figure 3.30 Frame 1: Moment versus Panel Zone Shear Deformation 81
Figure 3.31 Frame 2: Moment versus Panel Zone Shear Deformation 82
Figure 3.32 Moment versus End-Plate Opening Displacement 83
Figure 3.33 Frame 1: Measured Strains at Rafter Flanges (Positive Excursions) 84
Figure 3.34 Frame 1: Measured Strains at North Column (Positive Excursions) 85
Figure 3.35 Frame 1: Measured Strains at South Column (Positive Excursions) 86
Figure 3.36 Frame 1: Measured Strains at Rafter Flanges (Negative Excursions) 87
Figure 3.37 Frame 1: Measured Strains at North Column (Negative Excursions) 88
Figure 3.38 Frame 1: Measured Strains at South Column (Negative Excursions) 89
Figure 3.39 Frame 2: Measured Strains at Rafter Flanges (Positive Excursions) 90
Figure 3.40 Frame 2: Measured Strains at North Column (Positive Excursions) 91
Figure 3.41 Frame 2: Measured Strains at South Column (Positive Excursions) 92
Figure 3.42 Frame 2: Measured Strains at Rafter Flanges (Negative Excursions) 93
Figure 3.43 Frame 2: Measured Strains at North Column (Negative Excursions) 94
Figure 3.44 Frame 2: Measured Strains at South Column (Negative Excursions) 95
Figure 3.45 Load versus Measured Strain at Rod Braces 96
Figure 3.46 Strain Deviation at 1.5% Drift 97
Figure 3.47 Support Reactions of Frame 1 at Positive 2.6% Drift (Lateral Load Only) 98
Figure 3.48 Measured Rotation Angle at Column Bases of Frame 1 99
Figure 3.49 Shear Force at South Column of Frame 1 100

Figure 3.50 Internal Forces at Positive 2.6% Drift due to Lateral Load Only 101
Figure 3.51 Frame 1: Internal Forces at Positive 2.6% Drift due to Combined Loads 102
Figure 3.52 Frame 2: Internal Forces at Positive 2.6% Drift due to Combined Loads 103
Figure 3.53 Support Reactions of Frame 1 at Negative 2.3% Drift (Lateral Load Only) 104
Figure 3.54 Internal Forces at Negative 2.3% Drift due to Lateral Load Only 105
Figure 3.55 Frame 1: Internal Forces at Negative 2.3% Drift due to Combined Loads 106
Figure 3.56 Frame 2: Internal Forces at Negative 2.3% Drift due to Combined Loads 107
Figure 3.57 Frame 1: Axial Force and Moment Interaction 108
Figure 3.58 Frame 2: Axial Force and Moment Interaction 109
Figure 3.59 South Rafter Strength Check at Positive 2.6% Drift 110
Figure 3.60 North Rafter Strength Check at Negative 2.3% Drift 111
Figure 3.61 Flange Brace Force on HSS Supporting Beam 112
Figure 3.62 Flange Brace Angle Section (L2½×2½×3/16) 112
Figure 3.63 Moment due to Axial Load at Flange Brace 113
Figure 3.64 Frame 1: Measured Strain at Flange Brace 114
Figure 3.65 Frame 2: Measured Strain at Additional Flange Brace 116
Figure 4.1 ABAQUS Model of Test Frame (Loading in Positive Direction) 125
Figure 4.2 First Eigen Buckling Mode Shape for Models 2 and 3 125
Figure 4.3 Stress-Strain Relationship (Mays 2000) 126
Figure 4.4 Typical Unstable Static Response (ABAQUS Inc. 2005) 126
Figure 4.5 Normal Stress Comparison 127
Figure 4.6 Flange Buckling Failure Mode of Model 1 128
Figure 4.7 Lateral Buckling Failure Mode of Model 2 128
Figure 4.8 Flange Local Buckling and Lateral Buckling Failure Mode of Model 3 129
Figure 4.9 Base Shear versus Lateral Displacement Comparison 129

Figure 4.10 Predicted Failure Mode of Model 4 130
Figure 4.11 Global Response Comparison 130
Figure 4.12 Initial Imperfection Effect on Global Response 131
Figure 5.1 Seismic Design Concept 144
Figure 5.2 Design Response Spectrum (ASCE 7-05) 145
Figure 5.3 Prototype Building for Dynamic Test (Sockalingam 1988) 145
Figure 5.4 General Response Spectrum (FEMA 273) 146
Figure 5.5 General Design Procedure 147
Figure 6.1 Case 1 (40 ft×12 ft) 164
Figure 6.2 Case 1: Demand/Capacity Ratio under Governing Load Combination 165
Figure 6.3 Case 1: Spectral Response Acceleration and Drift Demand 166
Figure 6.4 Case 1: Overstrength Factor for Building A 167
Figure 6.5 Case 1: Overstrength Factor for Building B 169
Figure 6.6 Case 1: Failure Mode and Drift Capacity Verification of Building A 171
Figure 6.7 Case 1: Failure Mode and Drift Capacity Verification of Building B 172
Figure 6.8 Case 2 (100 ft×20 ft) 173
Figure 6.9 Case 2: Demand/Capacity Ratio under Governing Load Combination 174
Figure 6.10 Case 2: Spectral Response Acceleration and Drift Demand 175
Figure 6.11 Case 2: Overstrength Factor at Critical Segment 176
Figure 6.12 Case 2: Failure Mode and Drift Capacity Verification of Building A 177
Figure 6.13 Case 2: Failure Mode and Drift Capacity Verification of Building B 178
Figure 6.14 Case 3 (150 ft×20 ft) 179
Figure 6.15 Case 3: Connection Details (Nucor Building Systems) 180
Figure 6.16 Case 3: Demand/Capacity Ratio under Governing Load Combination 181
Figure 6.17 Case 3: Spectral Response Acceleration and Drift Demand 182
Figure 6.18 Case 3: Overstrength Factor at Critical Segment 183
Figure 6.19 Case 3: Failure Mode and Drift Capacity Verification of Building A 184
Figure 6.20 Case 3: Failure Mode and Drift Capacity Verification of Building B 185

LIST OF TABLES

Table 1.1 Design Coefficients and Factors for Steel Seismic Force-Resisting Systems (ASCE 7-05) 11
Table 2.1 Section Properties at the Smaller End (Lee et al. 1972) 28
Table 3.1 Member Properties 51
Table 3.2 Design Load 52
Table 3.3 Mechanical Properties of Steel 52
Table 3.4 Strength Check of Frame 1 at Positive 2.6% Drift 53
Table 3.5 Strength Check of Frame 2 at Positive 2.6% Drift 53
Table 3.6 Strength Check of Frame 1 at Negative 2.3% Drift 54
Table 3.7 Strength Check of Frame 2 at Negative 2.3% Drift 54
Table 4.1 ABAQUS Modeling Matrix 124
Table 4.2 Initial Imperfection Amplitude Effect on Ultimate Load Prediction 124
Table 5.1 Coefficient for Upper Limit on Calculated Period (ASCE 7-05) 142
Table 5.2 Values of Approximate Period Parameters C_t and x (ASCE 7-05) 142
Table 5.3 Dynamic Properties of a Metal Building from Free Vibration Tests (Sockalingam 1988) 143
Table 5.4 Damping Coefficients B_S and B_1 as a Function of Effective Damping β (FEMA 273) 143
Table 6.1 Design Loads for Case 1 (40 ft×12 ft) 159
Table 6.2 Case 1: Section Properties – Building A 159
Table 6.3 Case 1: Section Properties – Building B 159
Table 6.4 Design Loads for Case 2 (100 ft×20 ft) 160
Table 6.5 Case 2: Section Properties – Building A 161
Table 6.6 Case 2: Section Properties – Building B 161
Table 6.7 Design Loads for Case 3 (150 ft×20 ft) 162
Table 6.8 Case 3: Section Properties – Building A 163
Table 6.9 Case 3: Section Properties – Building B 163

ACKNOWLEDGEMENTS

Funding for this research was provided by Metal Building Manufacturers Association (MBMA) and American Iron and Steel Institute (AISI); Dr. W. Lee Shoemaker was the contract administrator. Nucor Building Systems Group provided the test building and Butler Manufacturing Company provided the construction of the test building. Mr. Scott Russell at Nucor Building Systems Group and Mr. Al Harrold at Butler Manufacturing Company provided the design examples in Chapter 6. The MBMA Seismic Research Steering Group consisted of Messrs. Scott Russell and Al Harrold, Professors Michael Engelhardt and Donald White.

The testing was conducted in the Charles Lee Powell Structures Laboratories at the University of California, San Diego. Assistance from Messrs. James Newell and Hyoung-Bo Sim throughout the testing phase is much appreciated.

Professor Chia-Ming Uang has served as my advisor and mentor throughout my graduate studies. His support and guidance have made this work possible.

VITA

1999	Bachelor, Chonnam National University, Korea
2001	Master of Engineering, Chonnam National University, Korea
2001-2002	Visiting Researcher, Posco-Hyundai Project
2002-2007	Graduate Research Assistant, University of California, San Diego
2007	Doctor of Philosophy, University of California, San Diego

PUBLICATIONS

Technical Reports

Hong, J. K. and Uang, C. M. (2004), "Cyclic Testing of a Type of Cold-Formed Steel Moment Connections For Pre-Fabricated Mezzanines," *Report No. TR-04/03*, Department of Structural Engineering, University of California, San Diego, La Jolla, CA.

Hong, J. K. and Uang, C. M. (2006), "Cyclic Performance Evaluation of Metal Building System with Web-Tapered Members," *Report No. SSRP-06/23*, Department of Structural Engineering, University of California, San Diego, La Jolla, CA.

Conferences

Hong, J. K., Uang, C. M., and Wood, K. (2006), "Cyclic Behavior of Bolted Moment Connection for a Type of Cold-Formed Pre-Fabricated Mezzanines," Proceedings, 8th U.S. National Conference on Earthquake Engineering, Earthquake Engineering Research Institute.

Hong, J. K. and Uang, C. M. (2006), "Cyclic Performance of Metal Building Frame," Proceedings, International Symposium Commemorating the 10th Anniversary of Earthquake Engineering Society of Korea, Earthquake Engineering Society of Korea.

ABSTRACT OF THE DISSERTATION

Development of A Seismic Design Procedure for Metal Building Systems

by

Jong-Kook Hong

Doctor of Philosophy in Structural Engineering

University of California, San Diego, 2007

Professor Chia-Ming Uang, Chair

Metal building systems are widely used in low-rise (1- or 2-story) building construction for economic reasons. Maximum cost efficiency is usually achieved through optimization of steel weight and the fabrication process by adopting web-tapered members and bolted end-plate connections. However, the cyclic behavior of this kind of system has not been investigated, and no specific seismic design guidelines are available in the United States. Based on both experimental and analytical studies, this dissertation introduces a new design concept utilizing drift evaluation, and proposes a seismic design procedure for metal building systems.

Full-scale cyclic testing on a metal building with web-tapered members demonstrated that the system has high deformability, but little ductility. Proper flange bracing was essential to prevent premature lateral-torsional buckling. Test results also showed that the overstrength of this system was very high since the non-seismic load combination governed the design. A correlation study indicated that the failure modes corresponded well with the strength evaluation contained in the *AISC LRFD Specification*.

Numerical simulation using the finite element analysis program ABAQUS demonstrated that good correlations in both the failure mode and the system strength characteristics could be achieved when a proper assumption on the initial geometric imperfections was made. A parametric study showed that the best correlation was found in the models with the first eigen buckling mode shape and an amplitude of $L_b/1000$ as an initial imperfection (L_b = unbraced length).

A drift-based seismic design procedure was then developed. The design goal is to ensure that the elastic drift capacity of the system is larger than the drift demand with a sufficient margin. The drift capacity is calculated using the system overstrength factor, and both drift capacity and demand are estimated utilizing the actual fundamental period. The proposed factor of safety (= 1.4) partially reflects the influence of low damping nature of metal buildings. Case studies using the proposed design procedure indicated that metal frames with heavy walls (i.e., masonry or concrete) based on the current design procedure are very vulnerable to collapse under major earthquake events, but the impact to the design of typical metal buildings without heavy wall attachments is insignificant.

1 INTRODUCTION

1.1 Introduction

FEMA 450: NEHRP Recommended Provisions for Seismic Regulations for New Buildings and Other Structures (BSSC 2003) presents criteria for the design and construction of structures to resist earthquake ground motions as follows:

1. For most structures, structural damage from the design earthquake ground motion would be repairable although perhaps not economically so.
2. For essential facilities, it is expected that the damage from the design earthquake ground motion would not be so severe as to preclude continued occupancy and function of the facility.

The design basis is that individual members shall be provided with adequate strength at all sections to resist the shear, axial forces, and moments determined in accordance with FEMA 450, and connections shall develop the strength of the connected members or the force indicated above. It is also advised that the design of a structure shall consider the potentially adverse effect that the failure of a single member, connection, or component of the seismic-force-resisting system would have on the stability of the structure

Generally accepted seismic design philosophy for structural steel buildings is to remain elastic under minor earthquake events and to provide stability without collapse under strong earthquake events. To achieve this goal economically, the lateral load is reduced to the reasonable level based on the assumption that the inherent inelastic characteristics (i.e., plastic hinge formation, sufficient ductility,

system redundancy, etc.) could significantly contribute to resisting the earthquake shaking.

However, there are cases that such assumption cannot be applied explicitly. While the conventional steel buildings are multi-story and the prismatic compact sections are used, metal building are low-rise (1-, or 2-story) and the web-tapered non-compact (or slender) sections are usually adopted for economic reasons. Metal buildings are a unique system and different approach is needed for the seismic design, but the same methodology used for conventional steel buildings is accepted by engineering professionals. In this chapter, the current seismic design practice of metal buildings is discussed and the motivation for the development of a new seismic design procedure for metal buildings is addressed. The dissertation outline and the summary of each chapter then follow.

1.2 Current Seismic Design Philosophy

Historically, the response modification factors (*R*-factor) are established empirically. A rational formula of the *R*-factor was first developed by Uang (1991):

$$R = R_\mu \Omega_o \tag{1.1}$$

where R_μ is the system ductility reduction factor, and Ω_o is the system overstrength factor (see Figure 1.1**Error! Reference source not found.**). R_μ depends on the ductility capacity of energy dissipating members and Ω_o represents the ratio between the ultimate strength level, C_y, of the system and the code-prescribed seismic force level, C_s. Assuming the system has sufficient energy dissipation capacity, the seismic force level, C_{eu}, which represents the required structural strength to respond

elastically during a major earthquake event, could be significantly reduced to C_s by using the R-factor:

$$C_s = \frac{C_{eu}}{R} \tag{1.2}$$

Then, the elastic story drift, δ_e, can be computed from elastic structural analysis and the displacement amplification factor, C_d, is used to estimate the inelastic design story drift.

$$\delta_s = C_d \delta_e \tag{1.3}$$

The basic concept of this procedure is that certain structural components are designed as the structural fuses and detailed to respond in the inelastic range to dissipate the seismic energy during a major earthquake event. However, the rest of the components are designed to remain elastic under the maximum loads that can be delivered by the structural fuses. This approach greatly simplifies the seismic design process since the only elastic analysis is required even though the structure would behave in the inelastic range. The R, Ω_o, and C_d values for structural steel building systems specified in the ASCE 7: *Minimum Design Loads for Buildings and Other Structures* (ASCE 2005), hereinafter referred as the ASCE 7, are summarized in Table 1.1 and the seismic design procedure is well established in the *AISC Seismic Provisions for Structural Steel Buildings* (AISC 2005), hereinafter referred as the *AISC Seismic Provisions*.

1.3 Metal Building Systems

Today, metal building systems dominate the low-rise (1- or 2-story) non-residential building construction in the United States with several advantages such as cost efficiency, ability to long spanning, fast construction, and so on. Since the primary cornerstone of metal building construction is to minimize the building cost, the goal is usually achieved through optimization of steel weight and the fabrication process by adopting the built-up I-shaped web-tapered primary framing members with bolted end-plate connections and the cold-formed secondary structural members. Figure 1.2 shows a typical framing system of a single-story metal building. The system is supported by main frames forming a number of bays, and the secondary framing members (i.e., purlins and girts) are located between the main frames to carry the structural load to the main frames. Lateral stability is provided by rigid moment resisting ability of main frames in the transverse direction and diagonal rod braces in the longitudinal direction. Columns can be inserted in the middle of clear span for optimum efficiency. Metal buildings are usually clad with metal panels; however, hard walls (i.e., masonry and concrete walls) are increasingly used nowadays.

The structural design loads are dead (D), live (L), rain (R), snow (S), wind (W) and earthquake (E) loads, and additionally collateral (C) load which accounts for a specific type of dead load other than the permanent construction such as the weight of mechanical ducts, sprinklers and future ceilings is considered. The design of metal building systems is generally governed by non-seismic loads (i.e., gravity and wind loads) since they are very light, and the design procedure for the web-tapered members are presented in the *AISC LRFD Specification* (AISC 2001) and the *AISC*

ASD Specification (AISC 1989). When heavy attachments are installed, the governing factor is often the seismic load; however, there are no seismic design guidelines for this unique building system.

1.4 Current Seismic Design Practice of Metal Buildings

Since no seismic design procedure for metal building systems exists, the industry takes advantage of all allowed code exceptions and options that frequently result in lighter and more economical structures than are normally found in other types of building construction (Bachman and Shoemaker 2004). In accordance with the ASCE 7-05, single-story steel buildings up to a height of 65 ft (and with some dead load restrictions) assigned to Seismic Design Category D, E, or F can be designed as an Ordinary Steel Moment Frames (OMF) with R = 3½, Ω_o = 3, and C_d = 3. OMF is expected to withstand minimal inelastic deformations in their members and connections when subjected to the forces resulting from the motions of the design earthquake (AISC 2005) and the stringent slenderness requirements for both local buckling and lateral buckling are not required, and therefore, non-compact or slender elements are usually used.

The bolted end-plate connections shall be designed for the lesser of (1) $1.1R_yM_p$ (LRFD) or $(1.1/1.5)R_yM_p$ (ASD) of the beam (rafter) or (2) the maximum moment that can be delivered by the system (AISC 2005). Item (1) is routinely used for the seismic design of multi-story conventional steel building, but the *AISC Seismic Provisions* do not define how to determine item (2). Therefore, *Seismic Design Guide for Metal Building Systems* (MBMA 2004) interprets it as three (= Ω_o) times the

design earthquake forces at that location. The connection design procedure including panel zone design follows the *AISC/MBMA Design Guide 16: Flush and Extended Multiple-Row Moment End-Plate Connections* (AISC 2002).

1.5 Statement of Problem

Research that was conducted after the Northridge, California Earthquake in 1994 has made a significant improvement to the *AISC Seismic Provisions* (AISC 2005). The Northridge problem is mainly associated with the brittle fracture of welded joints at beam-to-column welded moment connections in multi-story steel buildings composed of (seismically) compact wide flange sections. However, the design of metal building systems adopts the seismic design codes developed for conventional steel buildings due to a lack of research. Despite that past earthquakes have demonstrated good performance, the direct application is not reasonable to the completely different building system and the adoption of stringent requirements in seismic design provisions has also impacted the design and construction of this type of system. Followings are the issues that can be discussed:

- *Plastic Hinge Formation*: Metal building frames designed as OMFs use member sections that significantly exceed the limiting slenderness ratio, λ_p, (and thus the λ_{ps} values for seismic design) for compact section specified in the *AISC Seismic Provisions* (AISC 2005), it is questionable that a yield mechanism through plastic hinge formation can be developed.
- *Location of Plastic Hinges*: For prismatic wide-flange beams in conventional multi-story construction, cyclic test data is abundant to establish the rule for

determining the plastic hinge location (FEMA 2000). However, since metal buildings usually use the web-tapered members, both demand and capacity in the section vary along member span, in turn, the location of plastic hinges is not obvious even if the plastic hinge can be developed.

- *System Redundancy*: Metal buildings are used in low-rise construction, mostly singe-story, and the columns are designed as hinge based. In this case, the system requires only two plastic hinges to form a yield mechanism.
- *Building Period Calculation*: Fundamental period of the building is a very important factor to determine the design base shear. Since the approximate fundamental period, T_a, (ASCE 2005) is intended for the conventional multi-story steel buildings, the application to the metal buildings is not appropriate.

Therefore, research is needed to address these issues before a seismic design procedure for metal buildings can be developed.

1.6 Dissertation Outline and Chapter Summary

This dissertation begins with the general introduction and the problems of current seismic design procedure for metal building systems, and a review of the past studies follows. Chapters 3 and 4 discuss the experimental and analytical studies of a typical metal building system. Chapters 5 and 6 introduce the new seismic design concept for the metal building systems and demonstrate how to apply it with design examples. Each chapter starts with background information, and a brief summary follows.

1.6.1 Chapter 1

This chapter discusses the basic philosophy of current design and the current seismic design application to metal building systems. The problems of the current seismic design procedure for metal buildings are presented and the need for a new design procedure is addressed. Then, the outline of the dissertation and the summary of each chapter are provided.

1.6.2 Chapter 2

This chapter reviews the previous studies of metal building systems in three points of view. The general design procedure for strength of the web-tapered members is first addressed, and the testing of metal building follows. Then, the numerical analysis method is discussed.

1.6.3 Chapter 3

This chapter describes the cyclic performance evaluation of a typical web-tapered metal building system. Test results indicate that lateral buckling is the governing failure mode and the system has little ductility with sudden strength degradation, although it shows high deformability. The observed system overstrength is very high compare to the design base shear since the metal building is governed by non-seismic load combinations. The derived internal member forces and corresponding failures from the testing correspond well with the code provisions for strength evaluation of web-tapered members. Lateral force at flange brace is measured up to 2.6% of the nominal yield strength of the rafter compression flange.

1.6.4 Chapter 4

This chapter addresses the finite element modeling techniques for correlation with the test results. The analytical correlation studies indicate that the initial geometric imperfection assumed in the frame is very important parameter to predict the response accurately. A model without considering any initial imperfection overestimates the system ultimate strength, and the predicted failure (flange local buckling) is not consistent with that (lateral buckling) observed in the test. The correlation on the lateral stiffness of the system is also improved when the semi-rigid nature of the column base connection is considered in the model.

1.6.5 Chapter 5

This chapter introduces a new concept for seismic design of metal building systems based on the observation from testing. Considering the elastic performance only, the drift-based design procedure is developed. The drift capacity of the building is calculated using inherent system overstrength and compared with the drift demand. It is proposed to use the actual fundamental period, T, rather than the approximated fundamental period, T_a, for the determination of both drift capacity and demand.

1.6.6 Chapter 6

This chapter describes the application of the drift-based seismic design procedure for a total of six examples. Case study indicates that the proposed design procedure has little impact on the current design for typical frames, but not the cases with heavy walls. In such cases, the increase of member size is required.

1.6.7 Chapter 7

This chapter summarizes the work presented in this dissertation and addresses the original contributions to the seismic design of metal building. Then, the dissertation ends with future work and concluding remarks.

Table 1.1 Design Coefficients and Factors for Steel Seismic Force-Resisting Systems (ASCE 7-05)

Seismic Force-Resisting System	R	Ω_o	C_d
B. Building Frame Systems			
1.Steel eccentrically braced frames, moment resisting connections at columns away from links	8	2	4
2.Steel eccentrically braced frames, non-moment-resisting, connections at columns away from links	7	2	4
3.Special steel concentrically braced frames	6	2	5
4.Ordinary steel concentrically braced frames	3¼	2	3¼
C. Moment-Resisting Frame Systems			
1. Special steel moment frames	8	3	5½
2. Special steel truss moment frames	7	3	5½
3. Intermediate steel moment frames	4½	3	4
4. Ordinary steel moment frames	3½	3	3
D. Dual Systems With Special Moment Frames Capable Of Resisting At Least 25% of Prescribed Seismic Forces			
1. Steel eccentrically braced frames	8	2½	4
2. Special steel concentrically braced frames	7	2½	5½
E. Dual Systems With Intermediate Moment Frames Capable of Resisting At Least 25% of Prescribed Seismic Forces			
1. Special steel concentrically braced	6	2½	5
G. Cantilevered Column Systems Detailed To Conform To The Requirements For:			
1. Special steel moment frames	2½	1¼	2½
2. Intermediate steel moment frames	1½	1¼	1½
3. Ordinary steel moment frames	1¼	1¼	1¼
H. Steel Systems Not Specifically Detailed For Seismic Resistance, Excluding Cantilever Column Systems	3	3	3

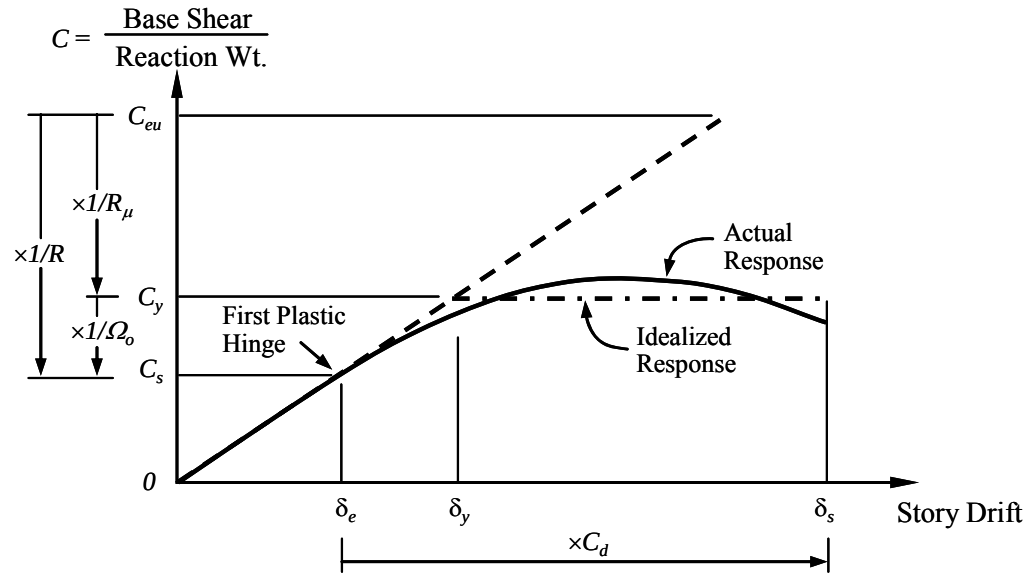

Figure 1.1 General Structural Response Envelope (Uang 1991)

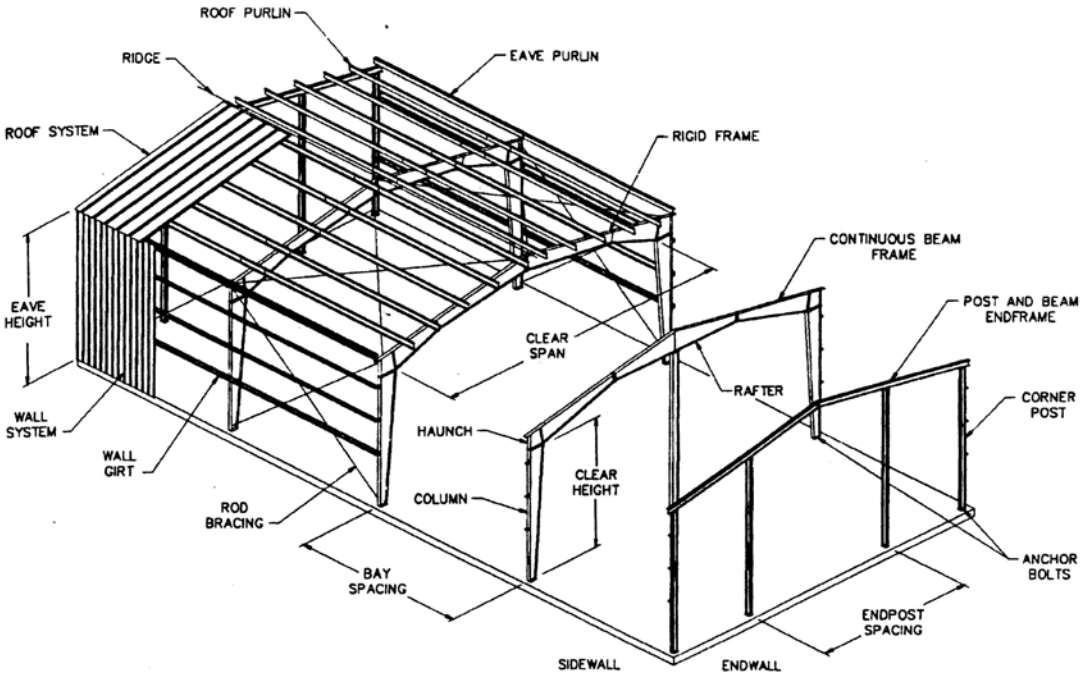

Figure 1.2 Typical Components of a Metal Building System (Newman 2003)

2 LITERATURE REVIEW

2.1 Introduction

Research on the behavior of metal building systems, especially for seismic applications, is very limited. This chapter reviews the previous available studies on metal building systems in three areas. Section 2.2 examines the design basis for strength evaluation of web-tapered members. Sections 2.3 and 2.4 summarize the metal building testing and the finite element analysis studies.

2.2 LRFD Strength Evaluation of Web-Tapered Members

Tapered structural elements which have a continuously varying cross section along their longitudinal axes were first proposed in 1950s for economic reasons. Since the stiffness (i.e., axial, flexural, and torsional) of the member varies along the length of the member, stability check of tapered members is complicated. Due to the lack of understanding, extensive research was conducted at the State University of New York (SUNY), Buffalo in the 1960s and their results formed the basis of the current *AISC ASD Specification* (AISC 1989) and *AISC LRFD Specification* (AISC 2001) for web-tapered member strength evaluation.

2.2.1 Axial Compressive Strength

For the linearly tapered member [see Figure 2.1(a)], the depth at any distance z from the smaller end can be expressed as

$$d_z = d_o\left(1+\frac{z}{l}\gamma\right) \tag{2.1}$$

where d_o represents the smallest depth at $z = 0$, and γ represents the tapering ratio. In terms of the depths at the ends of the member, the tapering ratio is defined by

$$\gamma = \frac{d_l}{d_o} - 1 \tag{2.2}$$

For a prismatic member, γ is equal to 0; for a member whose depth at the larger end is three times of its smaller end, γ is equal to 2. The assumed loading condition for a typical member is shown in Figure 2.1(b) (Lee et al. 1972; 1981).

Lee et al. (1972; 1981) adopted the principle of virtual displacement using five smaller, singly tapered cross-sections (see Table 2.1) with other variables such as member length, member ratio, tapering ratio, and eccentricity to obtain buckling strength of web-tapered member since it was not practically possible to non-dimensionalize the many parameters in tapered members. Two approaches for deriving the buckling strength were possible. The first approach was to use a multivariable curve fitting technique, starting from polynomial expressions containing all the variables could be developed. Another approach was based on the assumption that adequate design allowable stresses were available for prismatic members, and these could be modified to handle the tapered problem by introducing a factor.

$$f(\gamma, d_o, b, t_f, t_w, l) = \frac{\text{Strength of tapered member}}{\text{Strength of prismatic member based on the smaller cross-section}} \tag{2.3}$$

with the restriction that when $\gamma = 0$ (prismatic), $f = 1.0$.

The second approach was adopted because the designers were familiar with AISC code formulas for prismatic members although modification factor was

introduced, and the factors should give the designer an intuitive feeling of the increase in strength of the tapered member over its prismatic counterpart. Figure 2.2(a) shows the basic idea of axial strength estimation.

Since buckling can occur about either the strong or weak axis of the member, the function, *f*, in Eq. (2.3) is different for each case. Observing that the variation of the weak-axis radius of gyration along the length was small (equal flanges), no modification factor was considered:

$$\sigma_{taper} = \frac{\pi^2 E}{(l / r_{yo})^2} \quad \text{(weak axis)} \tag{2.4}$$

For strong axis buckling, the length modification was necessary and the factor, g, was chosen (Lee et al. 1972):

$$\sigma_{taper} = \frac{\pi^2 E}{(gl / r_{o})^2} \quad \text{(strong axis)} \tag{2.5}$$

where $g = 1.000 - 0.375\gamma + 0.080\gamma^2(1.000\text{-}0.0775\gamma)$. This idea was further extended to other boundary conditions and doubly tapered cross-sections, and the effective length factor, K_γ, was developed by Lee et al. (1972; 1979; and 1981) and was adopted by the *AISC LRFD Specification* (AISC 2001). The axial compressive strength can then be calculated using the same principles for prismatic members.

$$P = A_g F_{cr} \tag{2.6}$$

where A_g is the cross-section area, and F_{cr} is the critical buckling stress at the smaller end:

$$\lambda_{eff} = \frac{S}{\pi}\sqrt{\frac{QF_y}{E}} \tag{2.7}$$

$$F_{cr} = Q(0.658^{\lambda_{eff}^2})F_y \quad (\lambda_{eff} \le 1.5) \tag{2.8}$$

$$F_{cr} = \left(\frac{0.877}{\lambda_{eff}^2}\right)F_y \quad (\lambda_{eff} > 1.5) \tag{2.9}$$

where $S = KL/r_{oy}$ (weak-axis buckling) and $K_\gamma L/r_{ox}$ (strong-axis buckling), and Q = slenderness member reduction factor to account for the effect of local buckling.

2.2.2 Flexural Strength

The same methodology for the flexural strength of prismatic members can be applied to the limit states of flange local buckling and web local buckling. The flexural strength for lateral-torsional buckling for tapered members was first developed by Lee et al. (1972) and further extended by Morrell and Lee (1974).

The length modification factor, h, was introduced as shown in Figure 2.2(b). The critical lateral buckling stress for a prismatic beam subjected to a uniform bending moment is given by

$$\sigma_{cr} = \frac{1}{S_x}\sqrt{\frac{\pi^2 EI_y GJ}{l^2} + \frac{\pi^4 EI_y EC_w}{l^4}} \tag{2.10}$$

where σ_{cr} = prismatic member elastic critical stress (ksi), S_x = strong-axis elastic section modulus (in^3), EI_y = bending rigidity about weak-axis, GJ = St. Venant's torsional rigidity, l = unbraced length (in), and C_w = warping constant (in^4). The critical buckling stress for a tapered beam by introducing the length modification factor, h, is then,

$$(\sigma_{cr})_\gamma = \frac{M_o}{S_{xo}} = \frac{1}{S_{xo}}\sqrt{\frac{\pi^2 EI_{yo} GJ_o}{(hl)^2} + \frac{\pi^4 EI_{yo} EC_{wo}}{(hl)^4}} \tag{2.11}$$

where $(\sigma_{cr})_\gamma$ = tapered member elastic critical stress (ksi), S_{xo} = strong-axis elastic section modulus at smaller end (in^3), EI_{yo} = bending rigidity about weak-axis at smaller end, GJ_o = St. Venant's torsional rigidity at smaller end, h = tapered member length modification factor, l = unbraced length (in), and C_{wo} = warping constant at smaller end (in^4). Solving the (2.11) for h yields

$$h = \left[\frac{\pi^2 EI_{yo} GK_o}{l^2 (\sigma_{cr})_\gamma^2 S_{xo}^2} \left[1 + \sqrt{1 + \frac{[(\sigma_{cr})_\gamma S_{xo} d_o]^2}{(GK_o)^2}} \right] \right]^{1/2} \tag{2.12}$$

Lee et al. (1972) used Eq. (2.12) for calculating the first four cross-sections shown in Table 2.1 and found that the resulting values were quite dependent on the tapering ratio [also see Galambos (1998)]. Excluding Sections II and IV in Table 2.1 since they were representatives of typical column sections, two different length modification factors were introduced by curve fitting for thick and shallow sections (Sections I and III) and thin and deep section (Section V).

$$h_s = 1.00 + 0.0230\gamma \sqrt{\frac{ld_o}{A_f}} \tag{2.13}$$

$$h_w = 1.00 + 0.00385\gamma \sqrt{\frac{l}{r_{To}}} \tag{2.14}$$

This idea was accepted by code provisions and the design flexural strength of tapered members for the limit state of lateral-torsional buckling in the *AISC LRFD Specification* (AISC 2001) is calculated as

$$M_n = (5/3) S_x' F_{b\gamma} \tag{2.15}$$

where S_x' is the section modulus based on the larger end of the unbraced section under consideration, and $F_{b\gamma}$ is the critical flexural stress which consists of the St. Venant's term, $F_{s\gamma}$, and the warping term, $F_{w\gamma}$.

$$F_{b\gamma} = \frac{2}{3}\left(1.0 - \frac{F_y}{6B\sqrt{F_{s\gamma}^2 + F_{w\gamma}^2}}\right)F_y \le 0.6F_y \tag{2.16}$$

Unless $F_{b\gamma} \le F_y/3$, in which case

$$F_{b\gamma} = B\sqrt{F_{s\gamma}^2 + F_{w\gamma}^2} \tag{2.17}$$

In Eqs. (2.16) and (2.17),

$$F_{s\gamma} = \frac{0.41E}{h_s l d_o / A_f} \tag{2.18}$$

$$F_{w\gamma} = \frac{5.9E}{(h_w l / r_{To})^2} \tag{2.19}$$

The factor B developed by Morrell and Lee (1974) accounts for the effect of the moment gradient along the member length and acts as the C_b factor for the prismatic members.

2.2.3 Combined Axial Compression and Flexure

For web-tapered members subjected to both compression and bending, interaction of all unbraced segments should be evaluated as a beam-column in accordance with Chapter H of the *AISC LRFD Specification* (AISC 2001) with some modifications. The interaction of axial compression and flexure for prismatic members shall be limited by the following equations:

$$\frac{P_u}{\phi P_n} + \frac{8}{9}\left(\frac{M_u}{\phi_b M_n}\right) \le 1.0 \quad \text{for} \quad \frac{P_u}{\phi P_n} \ge 0.2 \tag{2.20}$$

$$\frac{P_u}{2\phi P_n} + \left(\frac{M_u}{\phi_b M_n}\right) \le 1.0 \quad \text{for} \quad \frac{P_u}{\phi P_n} < 0.2 \tag{2.21}$$

where P_u = required compressive strength (kips), P_n = nominal compressive strength (kips), M_u = required flexural strength (kip-in), M_n = nominal flexural strength (kip-in), $\phi = \phi_c$ = resistance factor for compression (= 0.85), and ϕ_b = resistance factor for flexure (= 0.90). M_u for beam-columns shall be determined from a second-order elastic analysis or from the following approximate second-order analysis procedure:

$$M_u = B_1 M_{nt} + B_2 M_{lt} \tag{2.22}$$

where M_{nt} = required flexural strength in member assuming there is no lateral translation of the frame, M_{lt} = required flexural strength in member as a result of lateral translation of the frame only. The amplification factors B_1 and B_2 are defined as follows:

$$B_1 = \frac{C_m}{(1 - P_u / P_{e1})} \ge 1 \tag{2.23}$$

$$B_2 = \frac{1}{1 - \left(\frac{\sum P_u}{\sum P_{e2}}\right)} \tag{2.24}$$

where P_{e1} and P_{e2} are in-plane Euler buckling strength.

For tapered members, P_n and P_{ex} shall be determined for the properties of the smaller end using the appropriate effective length factors discussed in Section 2.2.1,

but M_u and M_n shall be determined for the larger end (Section 2.2.2). In addition, the coefficient C_m in Eq. (2.23) is replaced by C_m' determine as follows:

(a) When the member is subjected to end moments which cause single curvature bending and approximately equal computed moments at the ends:

$$C_m' = 1.0 + 0.1\left(\frac{P_u}{\phi_b P_{ex}}\right) + 0.3\left(\frac{P_u}{\phi_b P_{ex}}\right)^2 \tag{2.25}$$

(b) When the computed bending moment at the smaller end of the unbraced length is equal to zero:

$$C_m' = 1.0 - 0.9\left(\frac{P_u}{\phi_b P_{ex}}\right) + 0.6\left(\frac{P_u}{\phi_b P_{ex}}\right)^2 \tag{2.26}$$

2.2.4 Shear Strength

Shear strength of tapered members is determined based on the shear yielding, elastic buckling, or inelastic buckling of the web plate, and the same approach for plate girder (Chapter G of the *AISC LRFD Specification*) can be made. For a relatively thick web plate, the shear strength is governed by shear yielding. For a relatively thin web plate, the elastic or inelastic buckling would control the shear strength. Two different sets of equations (with tension field action and without tension filed action) are given in Appendix G; however it is stated that tension filed action strength is not permitted for web-tapered plate girders. Then, the nominal shear strength is:

$$V_n = 0.6F_{yw}A_wC_v \tag{2.27}$$

where A_w = area of web plate and C_v = shear coefficient determined as follows:

(a) For $1.10\sqrt{\frac{k_v E}{F_{yw}}} \le \frac{h}{t_w} \le 1.37\sqrt{\frac{k_v E}{F_{yw}}}$:

$$C_v = \frac{1.10\sqrt{k_v E / F_{yw}}}{h/t_w} \tag{2.28}$$

(b) For $\frac{h}{t_w} > 1.37\sqrt{\frac{k_v E}{F_{yw}}}$:

$$C_v = \frac{1.51 k_v E}{(h/t_w)^2 F_{yw}} \tag{2.29}$$

The web plate buckling coefficient, k_v is given as

$$k_v = 5 + \frac{5}{(a/h)^2} \tag{2.30}$$

except that k_v shall be taken as 5.0 if a/h exceeds 3.0 or $[260/(h/t_w)]^2$, where a = clear distance between transverse stiffeners.

Although tension field action of web-tapered members is not allowed in the *AISC LRFD Specification* (AISC 2001), the *AISC/MBMA Steel Design Guide No. 16* (AISC 2003) utilizes the tension field action in the panel zone based on research by Murray (1986) and Young and Murray (1996). Major research finding is that all limit states (elastic buckling, inelastic buckling, and post-buckling) are possible for negative moment loading and the tension field action can be developed in the panel zone with full depth stiffeners [see Figure 2.3(a)]. Figure 2.4 shows the tension field action in a buckled web plate; tension field must be anchored at both ends (points A and B) to develop the additional post-buckling strength. The tension field will not anchor in a panel zone with partial depth stiffener [see Figure 2.3(b)]. Similarly, the

outside corner of the knee area does not have sufficient anchorage to fully develop tension field action under positive moment. Therefore, the design shear strength of panel zone with full depth stiffeners under negative moment can take advantage of the tension field action, and the required shear strength is (see Figure 2.3)

$$V_u = \frac{M_u}{h} - \frac{P_u}{2} \tag{2.31}$$

2.3 Metal Building Testing

2.3.1 Forest and Murray (1982)

A total of eight full-scale tests were conducted to determine the structural strength and stiffness by Forest and Murray (1982) under five different combinations of gravity and wind loads. The objectives of the testing was (1) to verify the existing design procedures used by a metal building manufacturer to predict deflections and strength, (2) to verify the design procedures established by Lee et al. (1981), and (3) to determine bracing requirements for tapered steel members.

Test results showed that the measured sidesway deflections were consistently less than predicted due to the assumption of column base hinge although the measured vertical deflections were very accurate. The correlation with the procedures by Lee et al. (1981) indicated that no consistent set of design rules which adequately predicted frame strength for all loading combinations was found. Caution was recommended if a flange brace is located at an unrestrained purlin, for instance, near a sky light, but no specific suggestions were made. It was also noted that no failure was attributed to the end-plate connections.

2.3.2 Hwang et al. (1989 and 1991)

Two shaking table test of 1/5-scale steel gable frames were conducted at the State University of New York at Buffalo; the first frame incorporated prismatic members (Hwang et al. 1989) and the second frame incorporated web-tapered members (Hwang et al. 1991).

Test results of the first frame showed that the system had high deformability (i.e., very flexible). The elastic behavior was noted up to 3% drift; recall the elastic range of typical Special Moment Frames (SMFs) for multi-story construction is about 1% drift. Local buckling at column top was the governing failure mode. Test results of the second frame indicated that energy dissipation capacity was much less than that of the first frame due to lateral-torsional buckling of the rafter, even though the wide-spread inelastic deformation was observed in the web-tapered members. Therefore, it was concluded that strict requirement for lateral bracing is needed, but no specific recommendation was given.

2.3.3 Sumner (1995)

Sumner (1995) investigated the behavior of rigid knee joints typically found in single-story, rigid gable frames. A total of eight rafter-column subassemblages were tested with three different types of loading; positive bending (two specimens), negative bending (four specimens), cyclic (two specimens). The correlation study with the *AISC LRFD* strength evaluation for web-tapered members was also conducted.

The failure mode for all test specimens was flange local buckling. The correlation study showed that the *AISC LRFD* provisions for axial load and flexure

interaction equation was sufficiently accurate and corresponded well with the failure locations, although the shear strength evaluation without tension filed action was too conservative.

2.3.4 Heldt and Mahendran (1998)

Full-scale test with a two-bay steel portal frame building, which was designed in accordance with the Australian building code and consisted of hollow flange beams, was conducted by Heldt and Mahendran (1998) to study the system behavior under gravity and wind loads.

Test showed that the failure of the secondary framing system such as purlin and flange brace resulted in the failure of the building. No inelastic evidence up to failure was noted and the system failed suddenly. Test results also indicated that cladding with rod brace was effective in reducing the frame deflection and the connection bolt tension force, either sung-tight or fully tensioned, did not make a large difference on the deflection.

2.3.5 Chen et al. (2006)

An experimental study on non-compact prismatic H-shaped members and frames subjected to cyclic loads was conducted by Chen et al. (2006).

Component test results showed that the ductile behavior was noted in the hysteresis loop and the non-compact or slender section was able to sustain a certain level of load after the ultimate load. Two-story frame tests demonstrated the plate buckling and plastic deformation in the member as well as local buckling. It was then concluded that the energy dissipation capacity of the system was small, but

enough. It was also recommended that the width-to-thickness (w/t) ratio or the height-to-thickness (h/t) ratio be limited to ensure the ductility of non-compact sections.

2.4 Finite Element Analysis

2.4.1 Davids (1996)

Finite element analysis using ABAQUS (HKS 1996) was conducted on an unbraced segment which was composed of one tapered rafter welded to one prismatic rafter and compared with the test data (Davids 1996). Initial geometric imperfection was introduced by applying a small lateral load (either 0.001 kips or 0.01 kips) at the web-bottom flange intersection at the welded splice. Riks method (Riks 1970) was used to trace the non-linear equilibrium path.

Lateral-torsional buckling failure mode was predicted from the analysis while flange local buckling was the governing failure mode from the test. Analysis results also indicated that the predicted buckling loads were close to those from the test, but lower. Correlation study with the *AISC LRFD Specification* showed that the provisions concerning combined axial force and flexure are very accurate when the flexural strength is controlled by flange local buckling.

2.4.2 Miller and Earls (2003 and 2005)

A parametric study was carried out by Miller and Earls (2003 and 2005) in the pursuit of the revisions to the web-tapered member flexural design provision contained in the *AISC LRFD Specification*. A simply supported tapered beam subjected to pure bending (Prawel. et al. 1974) and rafter-to-column subassemblages (Sumner 1995)

were modeled and the effects of various cross-sectional proportions and beam geometries on flexural ductility of web-tapered I-shaped beams were studied. For the initial imperfection, the first buckling mode shape from a linearized eigen buckling analysis was introduced with a maximum amplitude of $L_b/500$ for the beam model based on the suggestion by Winter (1960) and $L_b/1000$ for the subassemblages.

It was determined that the buckling loads of the web-tapered beams are somewhat insensitive to the change in the maximum imperfection amplitude of between $L_b/1200$ and $L_b/100$. Analysis results demonstrated that the *AISC LRFD Specification* is too conservative for compact section, but unconservative for non-compact section. It was also observed that an ultra compact section is needed in order to attain the plastic hinge.

2.5 Summary and Conclusions

The behavior of web-tapered members was investigated and the correlation studies with the strength evaluation presented in the *AISC LRFD Specification* were conducted through experimental tests and analytical works by previous researchrs. Most of these studies were dealing with the non-seismic application. From the experimental tests, the following conclusions can be made:

(1) Forest and Murray (1982) found no consistency with the strength prediction in the design procedure while Sumner (1995) demonstrated a good agreement with the *AISC LRFD Specification*.

(2) Although the system with web-tapered members exhibited the wide-spread inelastic deformation, the energy dissipation capacity was much smaller than

that with prismatic members due to lateral-torsional buckling failure under seismic load [Hwang et al. (1989 and 1991)].

(3) No inelastic deformation was noted up to the failure of the system [Heldt and Mahendran (1998)]; on the other hand, the non-compact section was able to sustain a certain level of load after the ultimate load and the plastic hinge could be developed [Chen et al. (2006)].

From the analytical works, the following conclusions can be made:

(1) The predicted failure mode of a rafter with initial geometric imperfection by applying a small lateral load was different from that from test although the buckling load was close [Davids (1996)].

(2) Miller and Earls (2003 and 2005) showed good agreements with test results by using the frist eigen buckling mode shape with an initial geometric imperfection amplitude of $L_b/500$ and $L_b/1000$ for the beam segment and the rafter-to-column subassembalges, respectively.

(3) Miller and Earls (2003 and 2005) pointed out the *AISC LRFD Specification* is not conservative for compact sections, and that ultra compact sections ($\lambda << \lambda_{ps}$) are required to ensure a required rotational capacity.

Table 2.1 Section Properties at the Smaller End (Lee et al. 1972)

	I	II	III	IV	V
	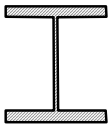	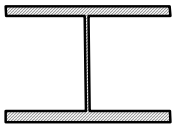	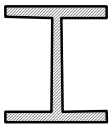	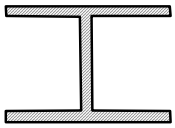	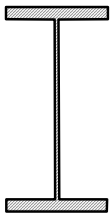
d_o (in.)	6.00	6.00	6.00	6.00	12.00
b (in.)	4.00	12.00	4.00	12.00	6.00
t_f (in.)	0.25	0.25	0.75	0.75	0.25
t_w (in.)	0.10	0.10	0.25	0.25	0.10

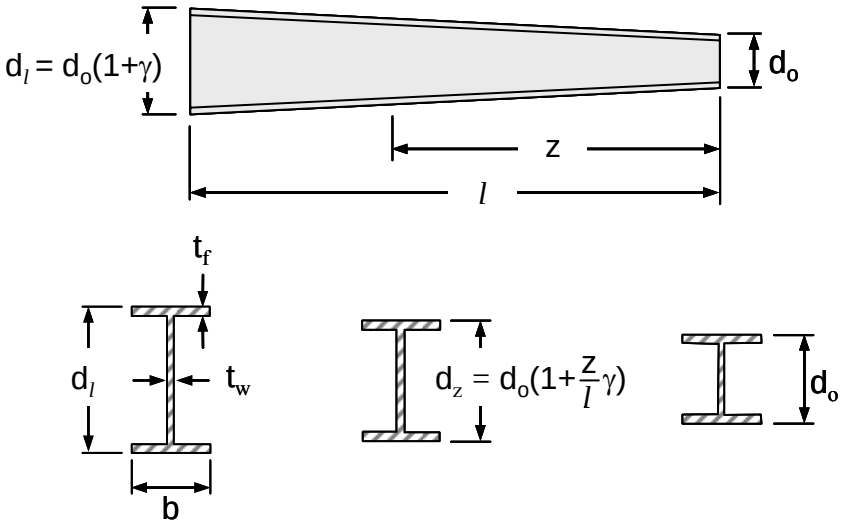

(a) Tapered Member Geometry

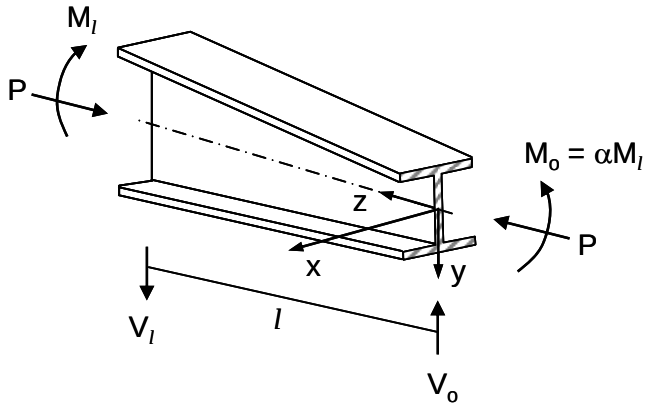

(b) Presumed Loading

Figure 2.1 Tapered Beam Geometry and Presumed Loading (Lee et al. 1972)

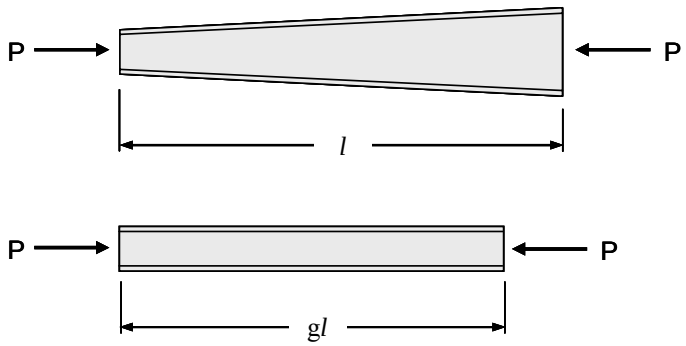

(a) Definition of the Length Modification Factor, g, for Columns

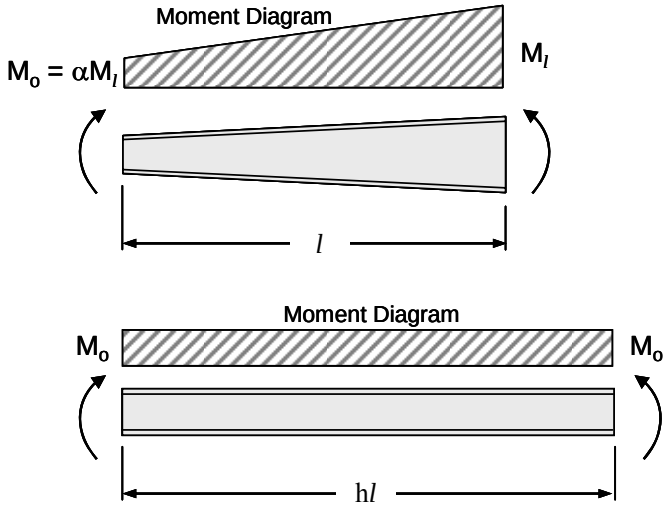

(b) Definition of the Length Modification Factor, h, for Beams

Figure 2.2 Length Modification Factor (Lee et al. 1972)

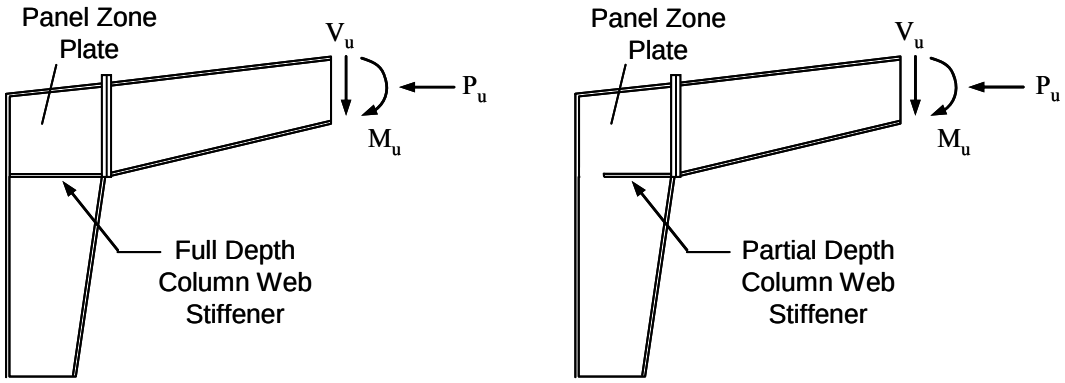

(a) Knee with Full Depth Stiffener (b) Knee with Partial Depth Stiffener

Figure 2.3 Panel Zone Plate with Stiffener

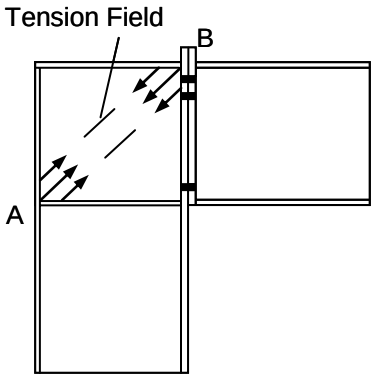

Figure 2.4 Tension Field in the Panel Zone

3 CYCLIC TESTING OF A METAL BUILDING SYSTEM

3.1 Introduction

The cyclic performance of a metal building system with web-tapered members was evaluated at University of California, San Diego, through a full-scale cyclic testing (Sections 3.2 through 3.4). Section 3.5 discusses the overstrength of the test frame. Section 3.6 summarizes the correlation of test results with the current design code provisions for strength evaluation of web-tapered members, and Section 3.7 presents lateral bracing force. The test results provides useful information for the numerical correlation studies in Chapter 4.

3.2 Design of Test Building

3.2.1 Test Building

A metal building with a dimension of 60 ft wide by 20 ft long by 20 ft eave height and a 0.5:12 roof pitch was designed in accordance with the *International Building Code* (ICC 2003). The elevation and top view of the building with overall dimensions are shown in Figure 3.1. The built-up singly-symmetric, doubly-tapered rafters and singly-tapered columns were assembled through eight-bolt extended end-plate moment connections; 1 in.-diameter A325 high-strength bolts were used for the rafter-to-column connections and ¾ in.-diameter A325 high-strength bolts were used for the rafter-to-rafter connections. One side of the building was clad with a metal sidewall, while the other side was completely opened. The columns at the sidewall side were laterally braced by girts at their outside flanges and by flange braces at their

inside flanges, whereas no lateral brace was added at the open side columns other than diagonal rod braces (see Figure 3.2). The rafters were braced by purlins and flange braces at their outside and inside flanges, respectively. The typical four-bolt base plate detail with ¾ in.-diameter A307 Grade A anchor bolts was specified for all column bases as shown in Figure 3.3. The member section properties are summarized in Table 3.1.

3.2.2 Design Load

Table 3.2 summarizes the design loads. The gravity load was 7.5 psf, 20 psf, and 30.1 psf for dead load, roof live load, and snow load, respectively. For wind load, the basic wind speed of 85 mph was considered and the wind exposure category was B. According to Section 6.5.12.2.2 of ASCE 7-02 (ASCE 2002), the wind pressure for the main wind force-resisting system of low-rise buildings shall be determined by the following equation (Method 2):

$$p = q_h[(GC_{pf}) - (GC_{pi})] \tag{3.1}$$

where q_h is the velocity pressure evaluated at mean roof height, h. GC_{pf} and GC_{pi} are the external and internal pressure coefficients, respectively. Figure 3.4 shows the design wind load based on the above equation.

The building was assumed to be located in San Bernardino, California, a high seismic region, for earthquake load. The seismic design category was D, and the response modification factor, R, of 3.5 for Ordinary Moment Frames was used. Based on an S_{DS} value of 1.035 at 0.12 second, an S_{D1} value of 0.600 at 1 second, the

approximate fundamental period (T_a) was 0.31 second for the building frame according to ASCE 7-02:

$$T_a = C_t h_n^x = (0.028)(20)^{0.8} = 0.31 \text{ sec.} \quad (3.2)$$

Then, the seismic response coefficient, C_s, was determined to be 0.296 (= S_{DS}/R) and the design base shear, V, was 4.8 kips.

3.2.3 Governing Load Combination

According to Section 1605 of IBC 2003, the following load combinations for Load and Resistance Factor Design (LRFD) were considered:

$$1.4D \quad (3.3)$$

$$1.2D + 0.5(L_r \text{ or } S) \quad (3.4)$$

$$1.2D + 1.6(L_r \text{ or } S) + 0.8W \quad (3.5)$$

$$1.2D + 1.6W + 0.5(L_r \text{ or } S) \quad (3.6)$$

$$1.2D + 1.0E + 0.2S \quad (3.7)$$

$$0.9D + (1.0E \text{ or } 1.6W) \quad (3.8)$$

where D, L_r, S, W, and E are dead load, roof live load, snow load, wind load and earthquake load, respectively. In Eqs. (3.7) and (3.8), the earthquake load, E, can be rewritten as $E_h + 0.2S_{DS}D = E_h + 0.207D$, where E_h is the effect of horizontal seismic forces.

To check the governing load combination, structural analysis considering second order effects was conducted on the moment resisting frame in the transverse direction by using the commercial finite element analysis software, SAP2000 (Computer and Structures 2005). The modeling scheme is shown in Figure 3.5; each

member was modeled as a series of prismatic beams which have the section property at mid point between two nodes. Ideal hinges were considered at the column bases.

The largest axial force and moment were noted for the non-seismic load combination in Eq. (3.5):

$$1.2D + 1.6S + 0.8W \tag{3.9}$$

Figure 3.6 shows the axial force, shear, and bending moment diagram; the axial force was 34.1 kips and the maximum moment was 3,370 kip-in in the column with a sidewall. The axial force and the maximum moment was 32.3 kips and 3,110 kip-in, respectively, in the column at open side. The maximum moment in the rafter was 3,284 kip-in. Strength check at three critical locations under the governing load combination was performed (see APPENDIX A); the frame was optimally designed.

3.3 Testing Program

3.3.1 General

The test building is shown in Figure 3.7. The building was constructed at the Charles Lee Powell Structures Laboratories at the University of California, San Diego (UCSD) following the U.S. construction practices; all pre-fabricated members were assembled through bolted end-plate moment connections. After the columns were erected and braced by diagonal rod bracing, the rafters assembled on the ground were lifted and connected to the columns with eight 1-in. diameter high-strength bolts. Purlins, girts, and diagonal flange braces were then installed. Diagonal flange braces, which had a long-slotted hole at both ends, were connected from the purlin or girt to the inside flanges of rafters or columns with snug-tight ½-in. diameter high-strength

bolts (see Figure 3.8). The building was clad with roof panel and wall panel. Only one sidewall was installed as designed such that the bracing effects on the column could be studied.

3.3.2 Material Properties

ASTM A529 Grade 55 steel was specified for the flange and ASTM A1011 HSLAS Grade 55 Class 1 steel was specified for the web of the rafters and columns. The material properties based on tensile coupon test results are summarized in Table 3.3. All materials except for the 5/16-in.×6-in. plate satisfied the ASTM requirements; this plate had a yield strength (= 53.8 ksi) slightly lower than the ASTM minimum specified value (= 55 ksi). A325 high-strength bolts were used for the end-plate moment connections and the flange brace connections.

3.3.3 Test Setup

The overall test configuration and the top view of the test setup are shown in Figure 3.9. The closed side, which had a sidewall, was located to face the north, and the open side was located to face the south. Four 50-kip hydraulic actuators, one at each top corner of the building, were used to provide lateral load.

Some modifications were made to the test building for testing purposes. Figure 3.10 shows the details for the actuator-to-frame connection [also see Figure 3.8(c)]. A 1 in. thick actuator attachment plate was welded to the column outside flange. In addition, two pairs of ¼ in. thick partial-height stiffeners were added to the column to prevent flange local bending and web crippling from the actuator concentrated forces.

Figure 3.11 shows the column base detail. The column base plates were mounted on short sections of W14×176 reinforced with vertical stiffeners, and were fully tightened with four ¾-in. diameter A325 high-strength bolts instead of using four ¾-in. diameter anchor rods. The W14×176 section was then fully tightened with six 1-in. diameter A325 high-strength bolts to the mounting plate, which was tied to the reaction floor.

3.3.4 Instrumentation

A combination of displacement transducers, inclinometers, strain gage rosettes, and uniaxial strain gages were used to measure global and local responses. A total of eight inclinometers were installed on Frame 1 to measure the rotation angles at column base, column top, panel zone, and rafter [see Figure 3.9(a)]. These rotation angles can be used to investigate the column base behavior from the bolt configuration and the connection behavior at the rafter-to-column bolted end-plate connection.

A total of 27 displacement transducers were used to measure the displacement of the test building. Figure 3.9(b) shows the location of displacement transducers at roof level; five displacement transducers at each frame were used to measure the horizontal, transverse, and vertical displacements of both frames. In addition, the panel zone deformation, the bolted end-plate opening displacement, the column base plate uplift, etc., were monitored (see Figure 3.12). A total of 25 rosettes and 104 uniaxial strain gages were used to measure the strains at various locations.

3.3.5 Loading History

The test program consisted of two stages (gravity load test and cyclic load test). In the first stage, the gravity load component according to the seismic load combination specified in the IBC 2003 was applied before the actuators were connected to the test building.

$$1.2D + 1.0E + 0.2S = 1.412D + 0.2S + 1.0E_h \quad (3.10)$$

The gravity load component ($1.407D + 0.2S$) in Eq. (3.10) is equal to 16.57 psf, which corresponds to 19.9 kips for a tributary floor area of 1200 ft^2. Deducting the self weight (= 6.7 kips) of the test building, an additional weight of 13.2 kips was added by fastening gypsum wall boards and wood panels on top of the roof [see Figure 3.13(a)].

In the second stage for cyclic testing, the loading sequence for beam-to-column moment connection test specified in Appendix S6.2 of the *AISC Seismic Provisions* (AISC 2005) was used [see Figure 3.13(b)] since no guideline for the cyclic testing of this kind of framing system exists. This loading sequence was controlled by story drift angles. The loading history begins with six cycles each at 0.375%, 0.5%, and 0.75%. The next four cycles in loading sequence were at 1% drift, followed by two cycles each at 2%, 3%, 4%, etc., until the test building fails. In the testing, the displacement controlled loading was applied to the north columns based on the measurements of the displacement transducers [see Figure 3.9(b)] and the forces read from the north actuators were imposed to the south actuators such that the same forces were acting on both sides of the columns. The direction of the arrows represents the positive direction.

3.4 Test Results

3.4.1 Gravity Load Test

3.4.1.1 General

The global behavior was monitored at three different loading stages: 28%, 89%, and 100% of the gravity load application. Figure 3.14 shows the vertical deflection at midspan of each frame. The measured deflections at midspan were 0.22 in. and 0.24 in. for Frame 1 and Frame 2, respectively, when the full gravity load was applied. Figure 3.15 shows the rotation angles measured from the inclinometers installed 1 ft above the column bases of Frame 1. The measured rotation angles were 0.005 rad and 0.0032 rad near the north and south column bases, respectively, when the full gravity load was applied.

3.4.1.2 Recorded Responses

Figure 3.16 shows the stress distribution at the outside flanges due to the imposed gravity load. The stress was calculated by multiplying the measured strain by the Young's modulus (E = 29,000 ksi). Larger stresses were noted at both ends of the rafters and the maximum stress was only of 3.3 ksi. Since strain gage readings indicated that the frames remained elastic under gravity load, the moment could be calculated by multiplying the stress by the elastic section modulus. The moment distribution is shown in Figure 3.17. The moments at column bases were estimated by linear extrapolation. Together with the rotation angles measured from the inclinometers at Frame 1, the equivalent rotational stiffnesses were computed to be 12,000 kip-in/rad and 12,500 kip-in/rad at north and south column bases, respectively.

Axial and shear force distributions in the frames could be estimated as follows. (Recall that the frames are indeterminate to the first degree.) Assuming that the frame and the loading were symmetric, the vertical reaction at each column was a half of the applied gravity load. Knowing the moments at the both ends of the columns (see Figure 3.17), the column shear (i.e., horizontal reaction) could be derived from statics. The resulting reactions are shown in Figure 3.18. Note that the horizontal reactions in each frame have opposite sign but slightly different magnitudes. Thus, a simplification for horizontal reactions was made such that horizontal force equilibrium is satisfied.

Moment diagrams thus constructed can be further verified by measurements. Since the frames were extensively instrumented with strain gages, moments that were computed from gage readings based on basic beam theory at a number of locations in the frames are also shown in Figures 3.19 and 3.20. Good correlation is observed in the column and in the negative bending regions of the rafter. The stiffening effect in the positive region of the rafter due to the addition of gypsum wall boards and wood panels on the roof might have caused reduced strain readings.

3.4.2 Cyclic Test

3.4.2.1 Observed Behavior

The test structures remained practically elastic at low drift levels. Figures 3.21 and 3.22 show the observed frame behavior at 1.5% drift. No visual evidence of local yielding or lateral buckling in the rafter or column was noted. Lateral buckling with the maximum amplitudes of 2.5 in. and 2.0 in. at the column and rafter,

respectively, on the south side (without sidewall) of Frame 2 was observed on the first positive excursion to 2% drift (see Figure 3.23), while Frame 1 did not show any sign of buckling. On the north side (with a sidewall), no lateral buckling was observed until the completion of first cycle at 2% drift.

It was noted during testing that flange braces for the rafters were not effective in preventing lateral buckling because these braces were connected to the bottom flange by snug-tight bolt in a long-slotted hole (see Figure 3.8). It was then decided to weld each existing brace to the brace connection plate after the completion of the first 2% drift cycle [see Figure 3.24(a)]. Furthermore, one flange brace was added to the south side of Frame 2 to brace the column [see Figure 3.24(b)]; an HSS3×3×1/8 section was also added to serve as the support for the upper end of the brace.

During the second cycle at 2% drift, the rafter in the south side of Frame 2 still experienced minor lateral buckling due to the existence of a permanent (i.e., residual) deformation from the previous cycle. Upon the completion of the second cycle, two flange braces were added before an extra cycle at 2% drift was applied: one at the top of the south column in Frame 1 and the other one at the buckled region of the south rafter in Frame 2 (see Figure 3.25). Such strengthening was effective to prevent lateral buckling during the additional (third) cycle at 2% drift.

Both frames failed during the first excursion to 3% drift. On the positive excursion at 3% drift, south rafter of Frame 1 and south column of Frame 2 experienced lateral buckling almost simultaneously (see Figures 3.26 and 3.27), which was accompanied by a sudden drop of the applied load. The different failure mode in these two frames was related to the strengthening that was introduced to the test

building during the 2% drift cycles. Rafter buckling in Frame 1 corresponded to the location where one additional flange brace was added to Frame 2 [see Figure 3.25(c)]. On the other hand, the increased lateral strength of the rafter due to the addition of two flange braces in Frame 2 forced the column buckling instead. But a significant amount of axial force developed in these two flange braces, as evidenced from the crippling of the purlin web and the permanent bending deformation of the HSS supporting beam in Figure 3.27(b).

On the negative excursion to 3% drift, the north rafters in both frames buckled laterally as shown in Figure 3.28(a). At the almost same time, the south columns also experienced significant lateral buckling at their outside flanges [see Figure 3.28(b)]. The north columns, which were braced by girts and flange braces, did not buckle. The strength degradation of the test building was significant and the test was then stopped.

3.4.2.2 Global Behavior

Figure 3.29 shows that the overall global responses of both frames were similar. The elastic behavior was noted up to 2% drift. The sudden strength degradation during the 3% drift cycle was due to lateral buckling failure of the web-tapered members; the story drifts at failure were 2.6% and 2.3% in the positive and negative excursions, respectively. The maximum lateral loads measured were 44.68 kips for Frame 1 and 44.05 kips for Frame 2, which were significantly higher than the design base shear (= 4.8 kips). Overstrength of the test frame would be discussed further in Section 3.5. The strength reduction was about 25% in the positive excursion and

about 45% in the negative excursion. Since south columns also experienced lateral buckling when the north rafters buckled, the strength degradation was more significant in the negative excursion than that in the positive excursion.

The average shear deformation of the column-to-rafter panel zone can be computed from the measurements of two diagonally placed displacement transducers [see Figure 3.12(a)]. The moment versus panel zone shear deformation relationships are shown in Figures 3.30 and 3.31, all four panel zones practically remained in the elastic region throughout the test. The opening at one bolted end-plate connection was monitored by a displacement transducer [see Figure 3.12(b)]. Figure 3.32 shows that the gap opening is negligibly small.

3.4.2.3 Strain Profile

Figures 3.33 through 3.44 show the measured strain profiles along the rafter and column flanges of both frames. Dotted lines representing the yield strain, ε_y, based on tensile coupon test results are also added in the plots. The first general observation is that, up to 3% drift, both rafters and columns were strained below ε_y, unless members experienced lateral buckling. Second, rafters were strained closer to ε_y than columns. The measured strains of rod braces at north and south ends were negligible as shown in Figure 3.45.

Lateral buckling of the south portion of Frame 2 was visually observed at 2% drift. But gage readings indicated that such buckling started during the 1.5% drift cycle. This is evident from the deviation of readings from two strain gages that were placed on the inside flange of the rafter near the connection region (see Figure 3.46).

3.5 Overstrength of Test Frame

As was briefly mentioned in the previous section, the measured maximum base shear of test frame was much higher than the design base shear. The system overstrength was 9.31 (= 44.68 kips/4.8 kips) and 9.18 (= 44.05 kips/4.8 kips) for Frame 1 and Frame 2, respectively (see Figure 3.29). These values are more than three times the system overstrength for OMFs (Ω_o = 3) specified in the design code (IBC 2003).

Since the governing load was the non-seismic load combination and the seismic load was small due to the light weight nature of the system, the test building had high inherent reserve strength under earthquake load. The fact explains why this system showed good performance in the past earthquake.

3.6 Member Strength Correlation

The axial force and moment produced by the lateral load only was calculated at incipient failure (i.e., at +2.6% drift) in the positive drift direction (see Figure 3.47). The moment at column bases of Frame 1 was estimated by multiplying the rotation angles from the inclinometers, I4 and I8 (see Figure 3.48), by the rotational stiffness derived from gravity load test (see Section 3.4.1).

Figure 3.49 shows the procedure used to calculate the shear force (= 22.9 kips) at south column of Frame 1 indicated in Figure 3.47. Three rosettes were installed at 2 ft above from the column base; the shear stresses at failure were calculated by multiplying the shear strains by the shear modulus (G = 11,150 ksi). The shear forces were then calculated by multiplying the shear stresses by the web area of the

section. The average of three shear forces was 22.9 kips. Once this column shear is determined, the remaining three reactions of the frame were calculated from statics; second-order effect was considered in determining these reactions. Figure 3.47(a) shows that the procedure resulted in two horizontal reactions with a very similar magnitude; a simplification was thus made such that these two horizontal reactions are equal. These same reactions were also assumed for Frame 2 because it was not as fully instrumented as Frame 1.

Figure 3.50 shows the axial force and the bending moment diagram based on the simplification. From beam theory, available moments derived from strain gage readings are also added in the figure for comparison purposes. Good correlation justifies the simplification made in constructing the internal force distributions.

The internal forces from the gravity load and the lateral load were then superimposed to obtain the internal forces (see Figures 3.51 and 3.52). Based on these force diagrams, each unbraced segment was checked as a beam-column according to Chapter H of the *AISC LRFD Specification* (AISC 2001). The strength check results are summarized in Tables 3.4 and 3.5.

Following the same procedure, the reaction for each frame at incipient failure in the negative drift direction (i.e., at -2.3% drift) were calculated. But the simplification was not made because the shear forces (21.83 kips vs. 14.45 kips) derived in the north and south columns were quite different, probably due to a force redistribution because the south column in Frame 2 was weakened due to lateral buckling in the previous excursion (see Figure 3.53). Figures 3.54 through 3.56

show the internal force diagrams, and the results of strength check are summarized in Tables 3.6 and 3.7.

For columns, the strength check data are also presented in the form of P-M interaction in Figures 3.57 and 3.58. It is first observed that the axial loads were very low and these columns behaved more like a flexural member. Second, the column C4, which was not braced by the sidewall, had the highest demand/capacity (D/C) ratio (= 1.18) at +2.6% drift; this is consistent with the observed lateral buckling in the south column of Frame 2. Third, the D/C ratios of the three unbraced segments (C1, C2, and C3) of the north columns were between 0.61 and 1.0.

The axial load in the rafter was even smaller. Therefore, all the unbraced segments are treated as a flexural member and the D/C ratios are presented in Figures 3.59 and 3.60. At +2.6% drift, only the unbraced segment R2 in the south rafter of Frame 1 buckled laterally, which was consistent with the highest D/C ratio calculated for this segment. Due to the addition of a flange brace at this location during the 2% drift cycles, the D/C ratios of segments R2A and R2B in Frame 2 are less than that of segment R2 in Frame 1 (see Figure 3.59). At -2.3% drift, the D/C ratios of segment R2 in the north rafter of both frames are the highest (see Figure 3.60); which is consistent with the observed lateral buckling in the test.

3.7 Flange Brace Force

Figure 3.24(b) shows one of the two flange braces that were added to strengthen the rafter of Frame 2. The HSS3×3×1/8 beam supporting the upper end of the brace showed a permanent deformation at the end of the test, indicating that a

plastic hinge at the midspan was formed. Such information can be used to estimate the axial force developed in the flange brace. Figure 3.61 shows the model, where the HSS beam is subjected to a bi-axial bending due to the 45-degree brace concentrated force at the midspan. Using the interaction formula specified in Chapter H of the *AISC LRFD Specification* (AISC 2001):

$$\frac{M_y}{M_{py}} + \frac{M_z}{M_{pz}} = 1 \tag{3.11}$$

where M_{py} and M_{pz} correspond to the plastic moment of the HSS section about the y and z axes, respectively, the horizontal component of the bracing force, F, was calculated to be 2.38 kips, which corresponded to 2.6% of the nominal yield strength of the rafter bottom flange.

In addition, strains at two flange braces (one existing flange brace for Frame 1 and one added flange brace for Frame 2) were measured. Using the strain gage readings, the flange brace force was calculated from basic beam theory. The flange brace section (L2½×2½×3/16) is shown in Figure 3.62; the cross section properties are given in the *AISC LRFD Specification* (AISC 2001):

$A = 0.901$ in^2, $I_1 = I_2 = 0.535$ in^4, $r_y = 0.482$ in.

$I_y = A \times r_y^2 = 0.2093$ in^4, $I_z = I_1 + I_2 - I_y = 0.8607$ in^4

Since the axial force acted at A, which was the connection bolt location, the induced stress at any location is

$$\sigma = \frac{P}{A} + \frac{M_y}{I_y} y + \frac{M_z}{I_z} z \tag{3.12}$$

Moments due to the axial force and eccentricity are $M_1 = 0.563P$ and $M_2 = 0.593P$ about axes 1 and 2, respectively [see Figure 3.63(a)]. The moments acting on the principal axes are

$$M_y = M_1 \cos\theta - M_2 \sin\theta = -0.0214P \tag{3.13}$$

$$M_z = M_1 \sin\theta + M_2 \cos\theta = 0.8176P \tag{3.14}$$

as shown in Figure 3.63(b).

The distance from any point, say B, on the section to the principal axes is (see Figure 3.62).

$$y = d_1 \sin\theta + d_2 \cos\theta \tag{3.15}$$

$$z = d_1 \cos\theta - d_2 \sin\theta \tag{3.16}$$

Based on the above equations, the axial force, P, acing on the flange brace can be calculated.

Figure 3.64 shows the gage readings of one flange brace in Frame 1. It was judged that gage S97 had a more reliable measurement than the other gages. With this gage, the derived brace axial force at incipient failure (+2.6% drift) was 1.72 kips (tension). Figure 3.65 shows the reading of one strain gage for a flange brace that was added during the 2% drift cycles. At incipient failure (+2.6% drift), the calculated brace axial force was 3.07 kips (compression).

To summarize, the horizontal component of the above two flange brace forces was 1.22 kips and 2.17 kips, or 1.3% and 2.4% of the nominal yield strength of the rafter bottom flange. Together with the data derived from Eq. (3.11) for the brace

placed at the top end of a column, it is observed that the horizontal component of the flange brace force varied from 1.3% to 2.6% of the yield strength of the rafter flange.

3.8 Summary and Conclusions

The test building, 60 ft wide by 20 ft long by 20 ft eave high and with a 0.5:12 roof pitch, was composed of two nominally identical frames with web-tapered members. Major findings from the testing follow.

(1) Member stresses due to the imposed gravity load were relatively small ($\approx$ 3 ksi).

(2) The dominant failure mode of the test frame under cyclic loading was lateral buckling. Both rafter and column on the side without a sidewall experienced buckling at 2% drift due to a lack of sound lateral bracing to the bottom flange of the rafter. Such premature buckling was probably caused by the slippage at the flange brace connection. Proper detailing is needed to avoid slippage.

(3) Such premature lateral buckling was prevented during the subsequent 2% drift cycles by (i) welding the flange brace to the brace connection plate directly to avoid any slippage, and (ii) adding additional flange braces to strengthen the rafter.

(4) The test frame experienced lateral buckling at 2.6% drift in the first positive excursion to 3% drift. Rafter buckled in one frame that was previously strengthened by adding one additional flange brace. Strengthening of the other frame with two additional flange braces forced the lateral buckling to occur in the column instead of the rafter.

(5) Lateral buckling at 2.3% drift during the subsequent negative excursion to 3% drift occurred in the rafters of both frames. Flange braces and girts that existed on the other side of the test building with a sidewall were effective to prevent column lateral buckling.

(6) The reserve strength of the building was very high; the overstrength was 9.31 and 9.18 for Frame 1 and Frame 2, respectively.

(7) The system showed little ductility, while its deformability in the elastic range ($\approx$ 2% drift) was significantly larger than that ($\approx$ 1% drift) in conventional moment-resisting frames. The strength degradation was significant upon lateral buckling.

(8) Internal forces derived from measurements and corresponding failure modes correlated well with the *AISC LRFD Specification* (AISC 2001) for strength evaluation of web-tapered members.

(9) The horizontal component of the flange brace force ranged from 1.3% to 2.6% of the nominal yield strength of the rafter compression flange.

Table 3.1 Member Properties

Section	Web Depth (in.)	Web Plate (in.)		Outside Flange (in.)	Inside Flange (in.)
	Start / End	Thick.	Length	W×T×L	W×T×L
RF1	12.0 / 31.0	0.200	194.3	6×1/4×229.6	6×5/16×195.2
	31.0 / 31.0	0.313	36.6	6×3/8×39.0	–
RF2	32.0 / 22.0	0.225	140.5	6×1/4×319.1	6×1/4×140.8
	22.0 / 27.0	0.175	180.0	–	6×1/4×178.9
RF3	27.0 / 22.0	0.175	180.0	6×1/4×327.1	6×1/4×178.9
	22.0 / 32.0	0.225	148.5	–	6×1/4×148.8
RF4	31.0 / 31.0	0.313	36.6	8×5/16×31.3	8×3/8×194.9
	31.0 / 12.0	0.200	194.0	8×1/4×229.2	–
P-1	10Z076				
E-1	10E076				
G-1	08Z071				
CB-1	¾ in-diameter Rod				
CB-2	5/8 in-diameter Rod				
Flange Brace	L2½×2½×3/16				

Table 3.2 Design Load

Load Type	Detail	Data
Dead Load	Dead Load	2.5 psf
	Collateral Load	3.0 psf
	Frame Self Weight	2.0 psf
Live Load	Roof Live Load	20.0 psf
Snow Load	Snow Load	30.1 psf
Wind Load	Wind Speed	85 mph
	Wind Exposure	B
	Importance Factor	1.0
Earthquake Load	Site Location	San Bernardino
	Importance Factor	1.0
	Seismic Design Category	D
	R	3.5
	C_s	0.296

Table 3.3 Mechanical Properties of Steel

Member		F_y (ksi)	F_u (ksi)	Elongation (%)
Flange	1/4×8	57.9 (63.4)	80.5 (85.6)	26 (21)
	3/8×8	57.7 (58.4)	79.1 (77.5)	25 (20)
	5/16×6	53.8 (59.1)	80.7 (84.2)	23 (22)
	1/4×6	59.2 (61.2)	81.1 (80.4)	23 (22)
Web	0.175”-thk.	64.2 (56.7)	77.4 (75.7)	26 (27)
	0.2”-thk.	61.1 (61.0)	76.4 (79.0)	29 (31)
	0.225”-thk.	65.4 (62.0)	79.3 (71.0)	27 (25)

[1] Values based on tensile coupon test results
[2] Values in parentheses based on Certified Mill Test Reports

Table 3.4 Strength Check of Frame 1 at Positive 2.6% Drift

Segment		P_u	P_n	P_y	P_u/P_n	M_u	M_{no}	M_{ni}	M_u/M_n	Unity
Column	C1	+9.2	190	311	**0.03**	1477	2491	2672	**0.58**	**0.61**
	C2	+9.2	220	403	**0.02**	2963	3243	3788	**0.91**	**0.92**
	C3	+9.2	224	477	**0.02**	3724	3755	4348	**0.99**	**1.00**
	C4	-15.8	165	427	**0.10**	4430	2869	3939	**1.13**	**1.18**
S. Rafter	R1	-1.4	233	581	**0.01**	4430	4080	4080	**1.09**	**1.10**
	R2	-1.3	194	483	**0.01**	4018	3376	3376	**1.19**	**1.20**
	R3	-0.8	162	405	**0.01**	2483	2623	2623	**0.95**	**0.96**
	R4	-0.4	193	435	**0.00**	945	2820	2820	**0.34**	**0.34**
	R5	-0.0	201	452	**0.00**	219	2868	2868	**0.08**	**0.08**

[1] Unit: kips and kip-in

Table 3.5 Strength Check of Frame 2 at Positive 2.6% Drift

Segment		P_u	P_n	P_y	P_u/P_n	M_u	M_{no}	M_{ni}	M_u/M_n	Unity
Column	C1	+9.2	190	311	**0.03**	1462	2491	2672	**0.59**	**0.61**
	C2	+9.2	220	403	**0.02**	2960	3243	3788	**0.91**	**0.92**
	C3	+9.2	224	477	**0.02**	3729	3755	4348	**0.99**	**1.00**
	C4	-15.8	165	427	**0.10**	4289	2869	3939	**1.09**	**1.14**
S. Rafter	R1	-1.3	233	581	**0.01**	4289	4080	4080	**1.05**	**1.06**
	R2A	-1.2	230	532	**0.01**	3952	3797	3797	**1.04**	**1.05**
	R2B	-1.0	230	483	**0.00**	3234	3645	3645	**0.89**	**0.89**
	R3	-0.7	160	405	**0.00**	2417	2623	2623	**0.92**	**0.92**
	R4	-0.4	192	435	**0.00**	886	2820	2820	**0.31**	**0.31**
	R5	-0.0	200	457	**0.00**	183	2868	2868	**0.06**	**0.06**

[1] Unit: kips and kip-in

Table 3.6 Strength Check of Frame 1 at Negative 2.3% Drift

Segment		P_u	P_n	P_y	P_u/P_n	M_u	M_{no}	M_{ni}	M_u/M_n	Unity
Column	C1	-13.4	190	311	**0.07**	1700	2491	2672	**0.64**	**0.68**
	C2	-13.4	220	403	**0.06**	3384	3243	3788	**0.89**	**0.92**
	C3	-13.4	224	477	**0.06**	4266	3755	4348	**0.98**	**1.01**
	C4	+6.8	165	427	**0.02**	2218	2869	3939	**0.77**	**0.78**
N. Rafter	R1	-5.1	233	581	**0.02**	4266	4080	4080	**1.05**	**1.06**
	R2	-5.0	194	483	**0.03**	4006	3304	3304	**1.21**	**1.23**
	R3	-4.5	162	405	**0.03**	2817	2623	2623	**1.07**	**1.09**
	R4	-4.1	193	435	**0.02**	1524	2820	2820	**0.54**	**0.55**
	R5	-3.7	201	452	**0.02**	877	2868	2868	**0.31**	**0.32**

[1] Unit: kips and kip-in

Table 3.7 Strength Check of Frame 2 at Negative 2.3% Drift

Segment		P_u	P_n	P_y	P_u/P_n	M_u	M_{no}	M_{ni}	M_u/M_n	Unity
Column	C1	-13.4	190	311	**0.07**	1714	2491	2672	**0.64**	**0.68**
	C2	-13.4	220	403	**0.06**	3386	3243	3788	**0.89**	**0.92**
	C3	-13.4	224	477	**0.06**	4261	3755	4348	**0.98**	**1.01**
	C4	+6.8	165	427	**0.02**	2269	2869	3939	**0.79**	**0.80**
N. Rafter	R1	-5.0	233	581	**0.02**	4261	4080	4080	**1.04**	**1.05**
	R2	-4.9	194	483	**0.02**	3999	3304	3304	**1.21**	**1.22**
	R3	-4.5	162	405	**0.03**	2801	2623	2623	**1.07**	**1.09**
	R4	-4.1	193	435	**0.02**	1499	2820	2820	**0.53**	**0.54**
	R5	-3.7	201	452	**0.02**	848	2868	2868	**0.30**	**0.31**

[1] Unit: kips and kip-in

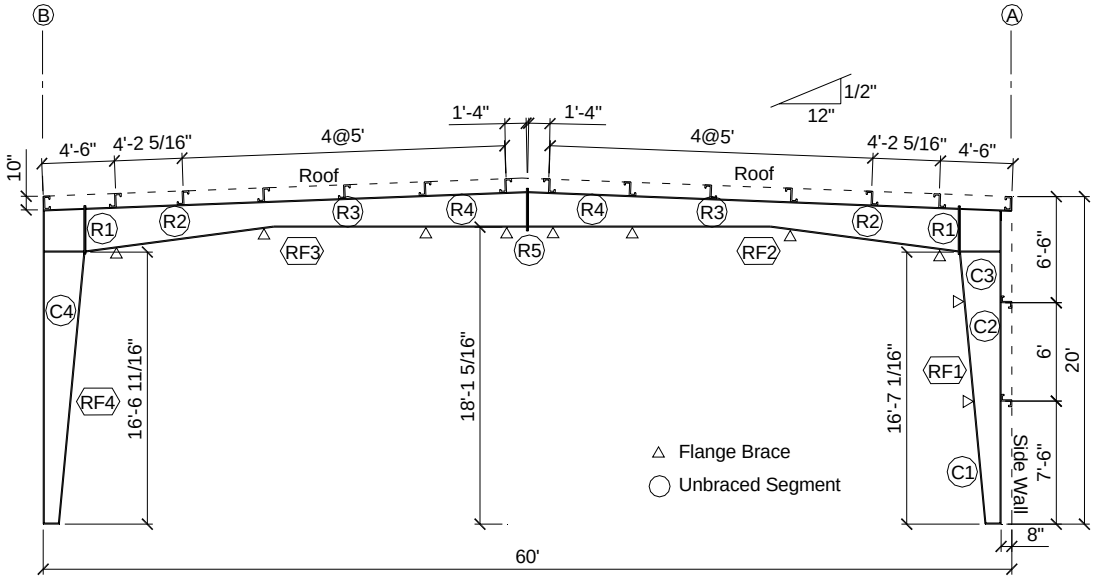

(a) Elevation

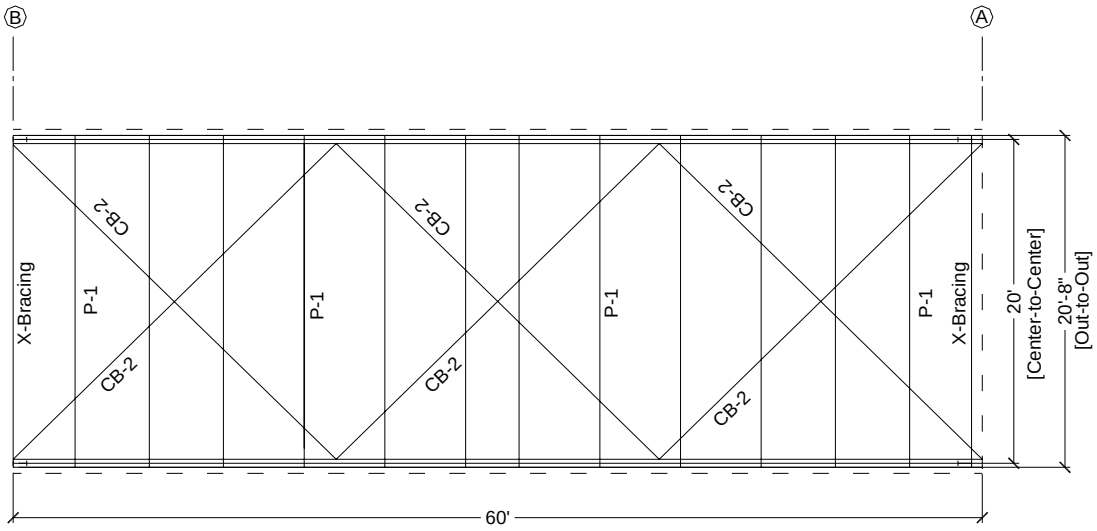

(b) Top View

Figure 3.1 Elevation and Top View of Test Building

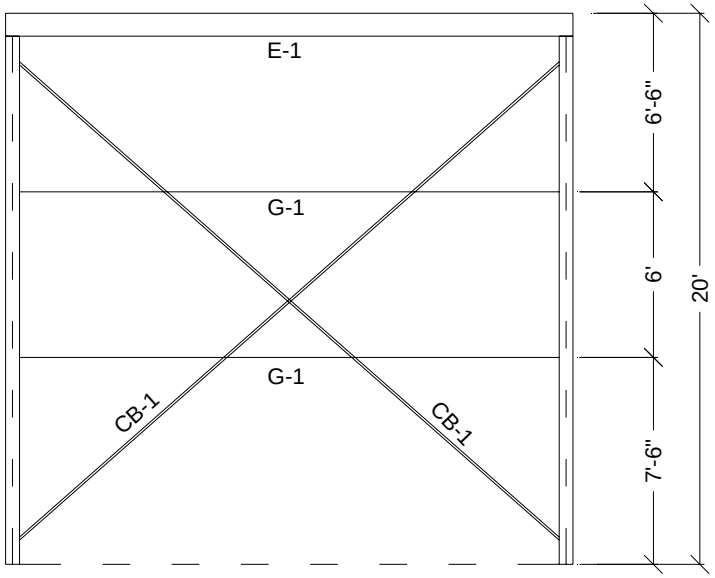

(a) Line A

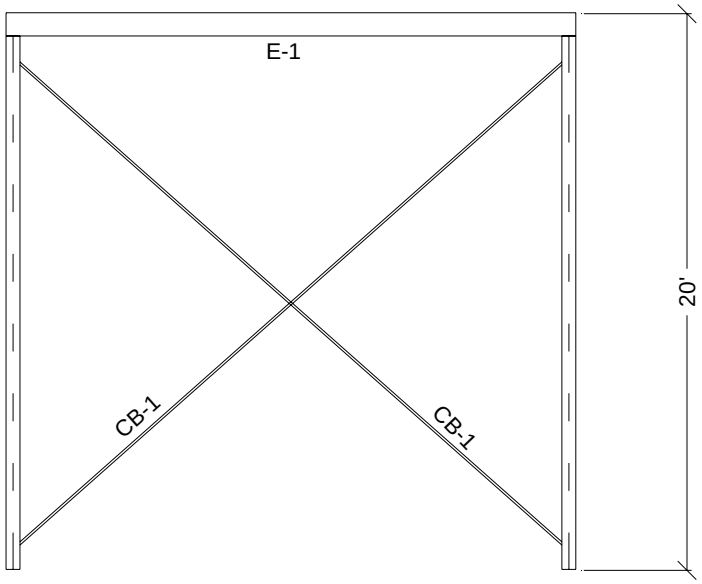

(b) Line B

Figure 3.2 Sidewall Elevation

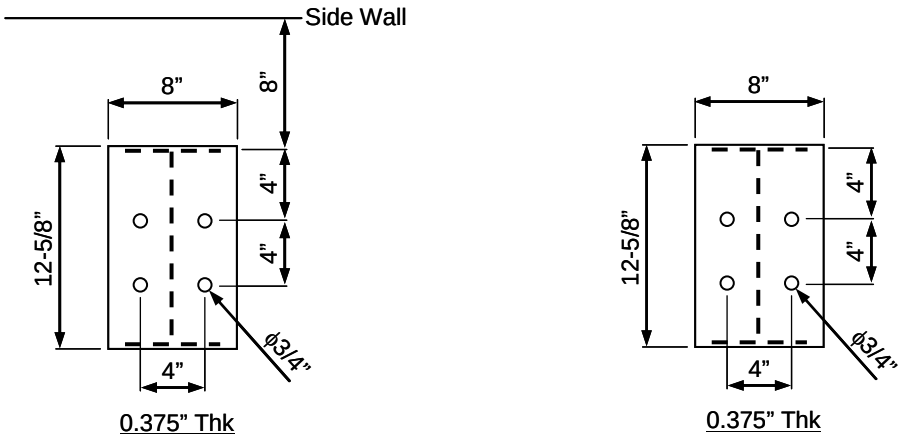

(a) Line A (b) Line B

Figure 3.3 Column Base

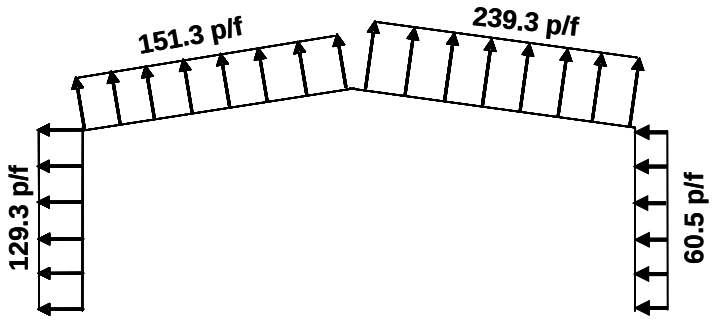

(a) Positive Internal Pressure

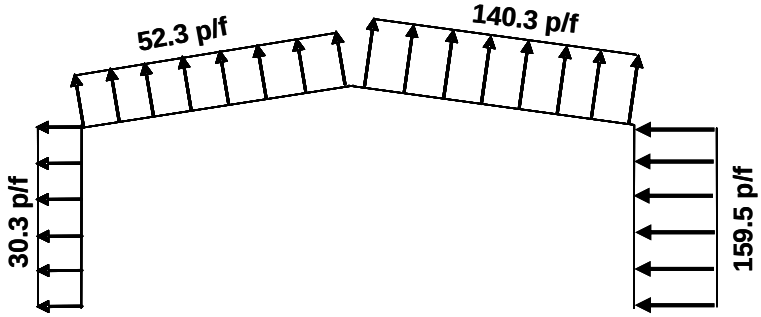

(b) Negative Internal Pressure

Figure 3.4 Design Wind Load

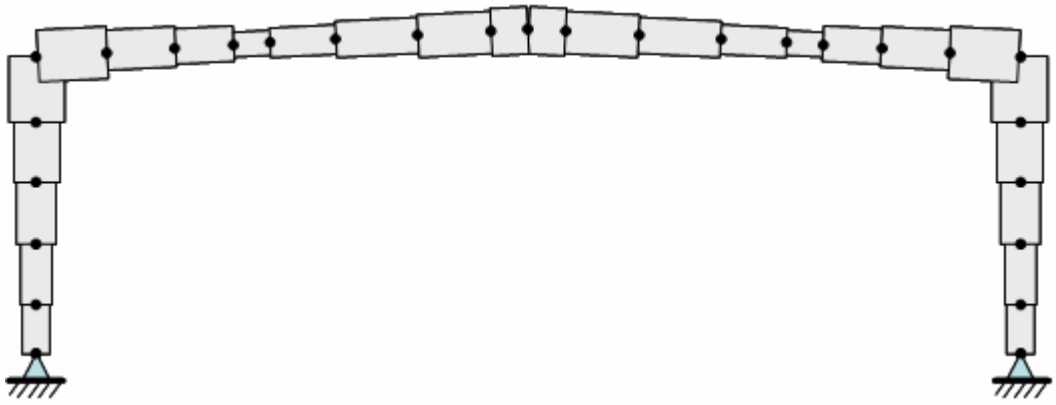

Figure 3.5 SAP Modeling Scheme

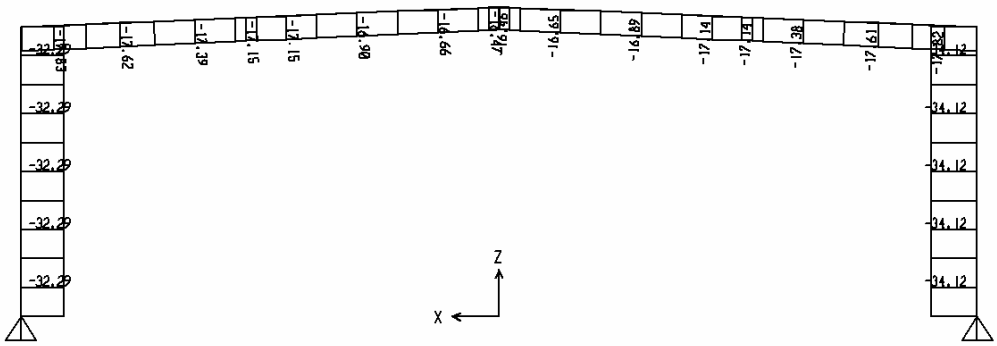

(a) Axial Force Diagram (kips)

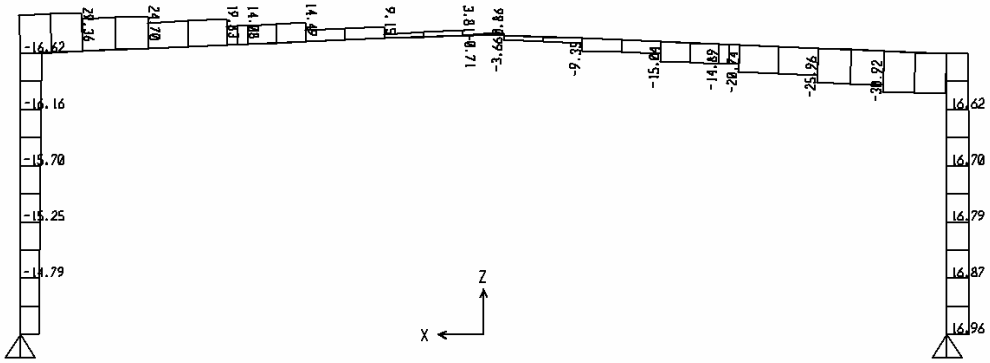

(b) Shear Force Diagram (kips)

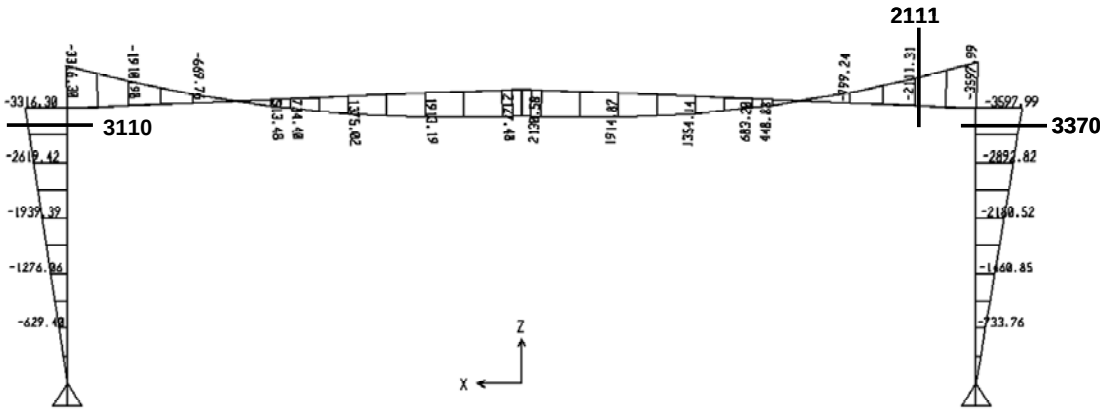

(c) Bending Moment Diagram (kip-in)

Figure 3.6 Force Demand under Governing Loading Combination

Figure 3.7 Test Building

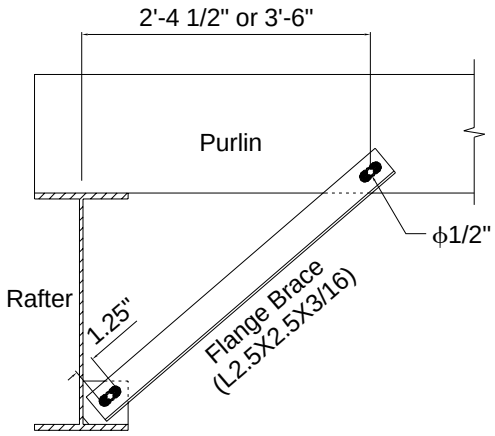

(a) Rafter Flange Brace

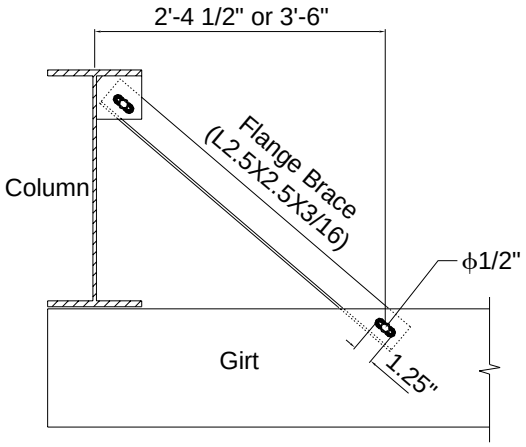

(b) Column Flange Brace

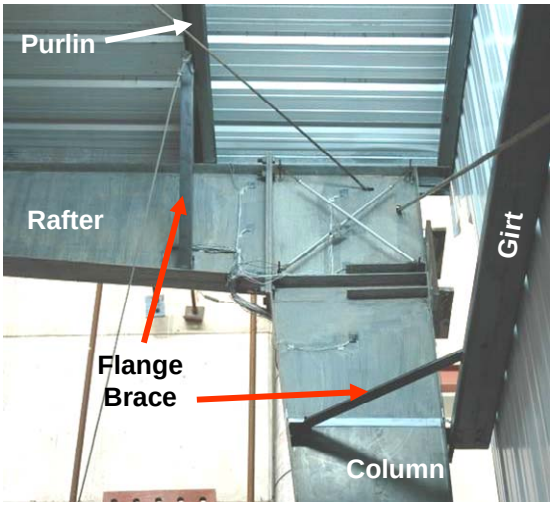

(c) Flange Brace Installation

Figure 3.8 Flange Brace

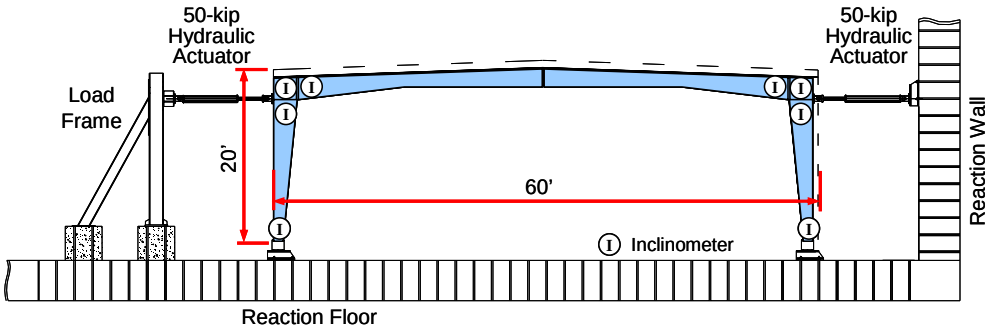

(a) Elevation

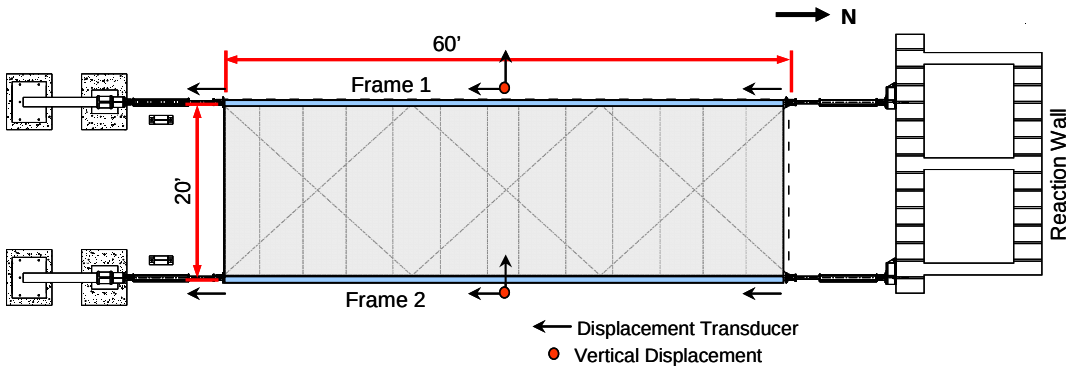

(b) Top View

Figure 3.9 Test Setup

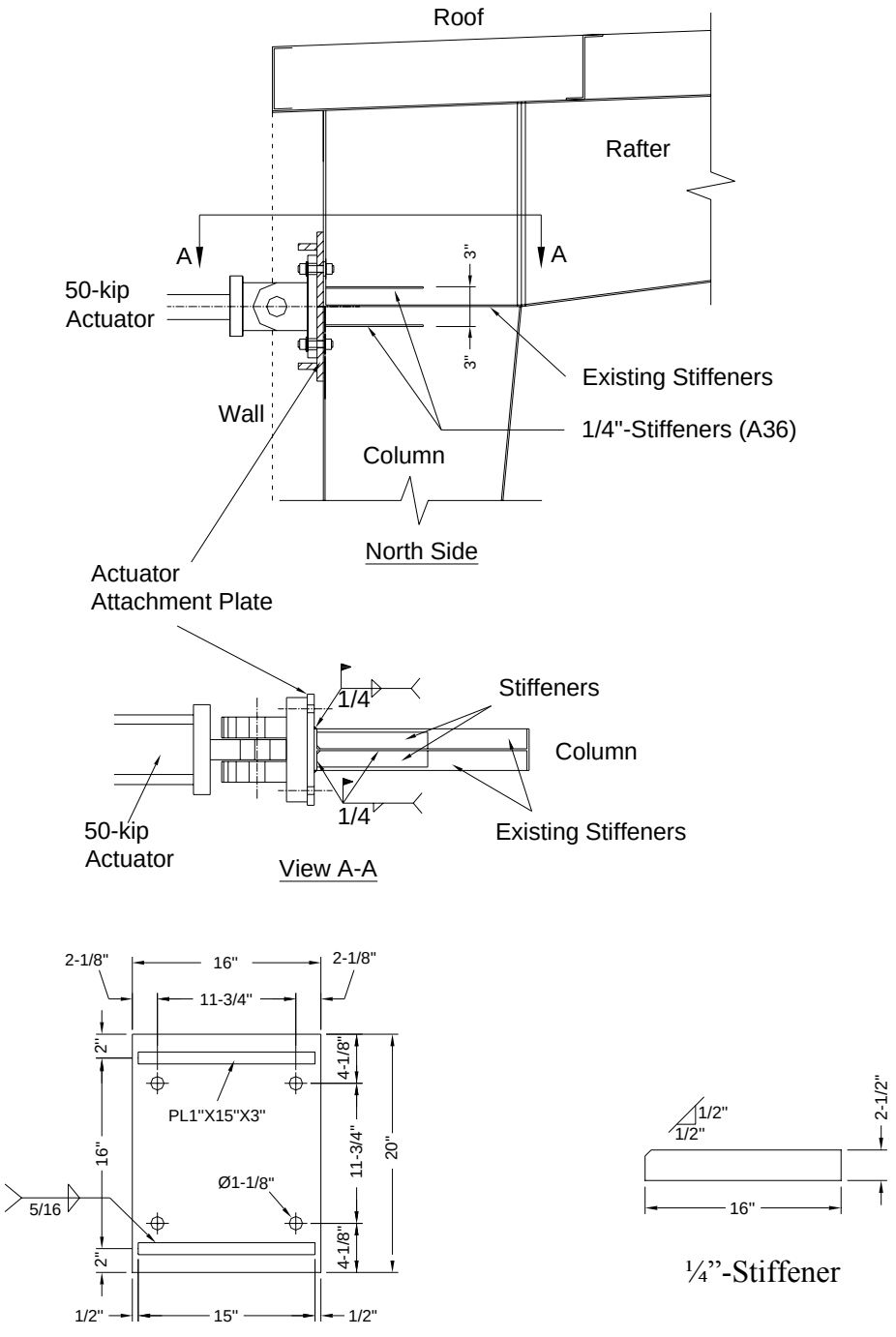

Actuator Attachment Plate

Figure 3.10 Actuator-to-Column Connection Details

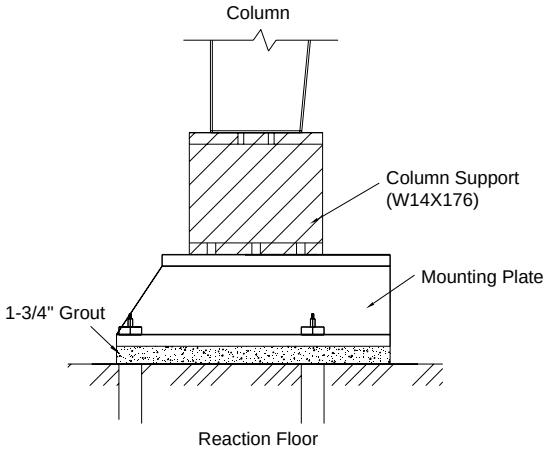

(a) Elevation

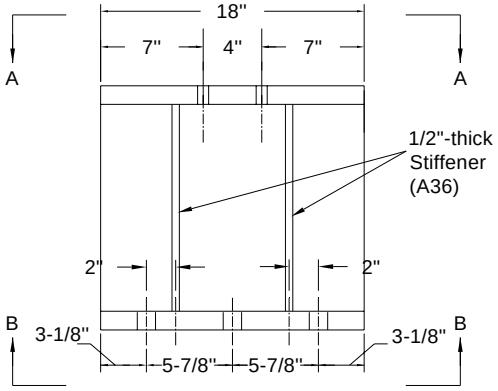

(b) W14×176 Column Support

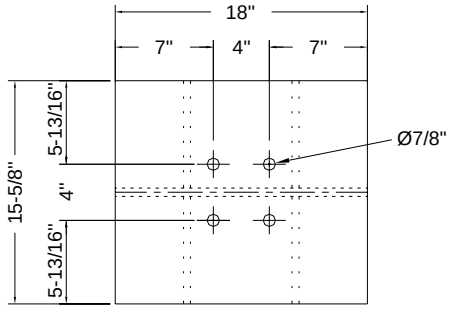

(c) View A-A

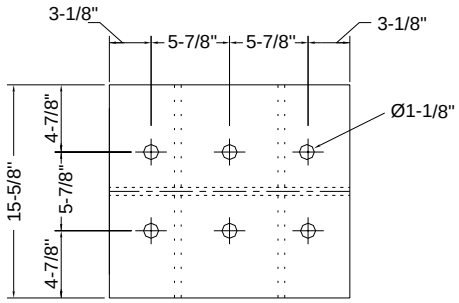

(d) View B-B

(e) Column Base

Figure 3.11 Column Base Connection Details

(a) Panel Zone

(b) End Plate

(c) Column Base

Figure 3.12 Instrumentation for Panel Zone, End Plate, and Column Base

Wood Panel Screwing

Top View after Gravity Load Application

(a) Gravity Load Application

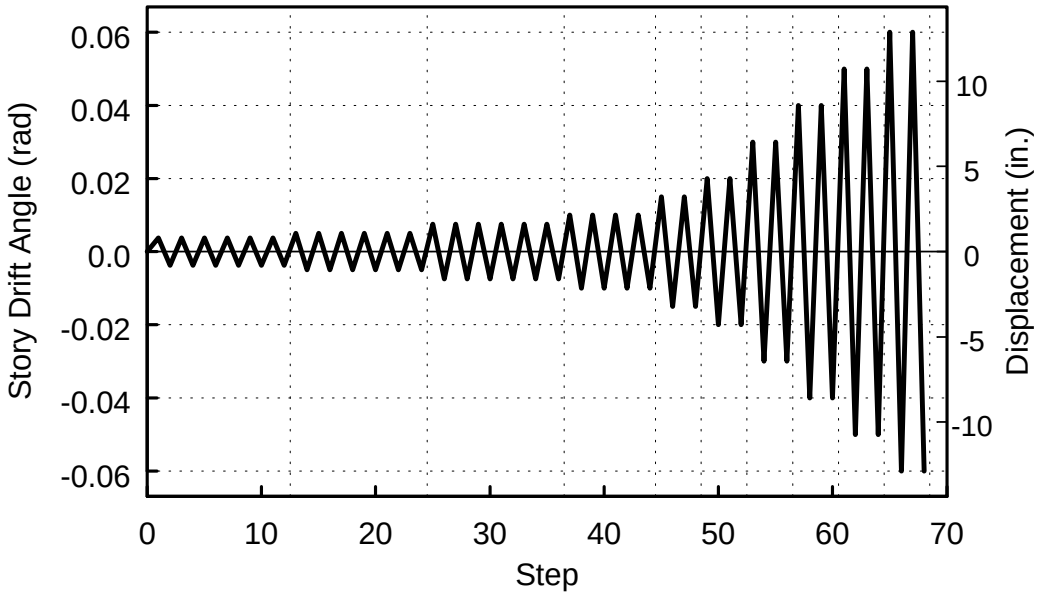

(b) AISC Loading Sequence

Figure 3.13 Gravity Load and Cyclic Load

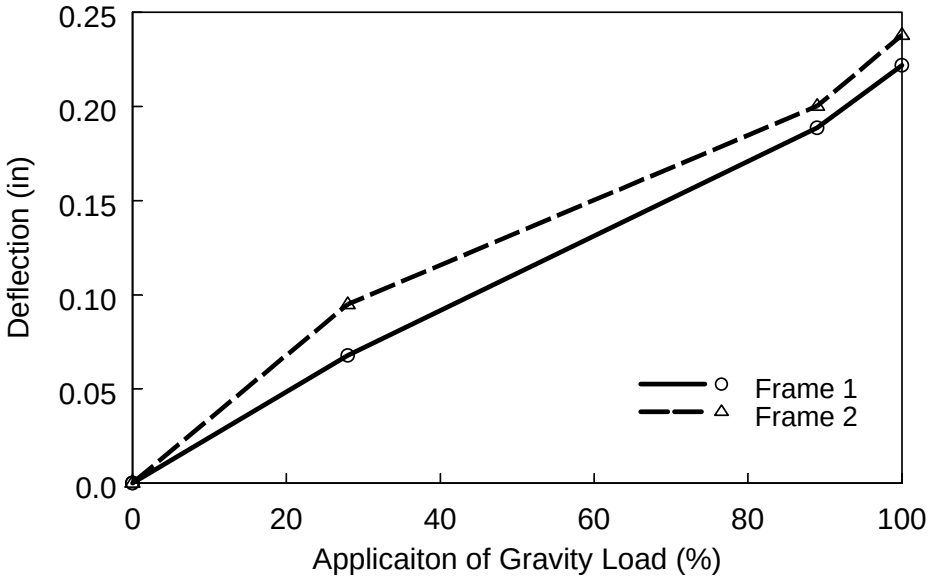

Figure 3.14 Vertical Deflection at Midspan

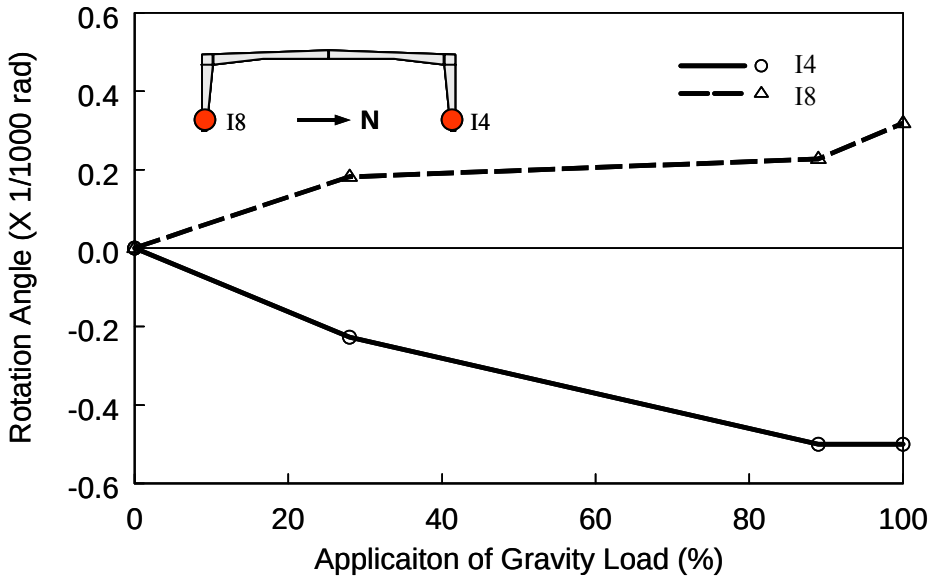

Figure 3.15 Frame 1: Rotation Angle at Column Base

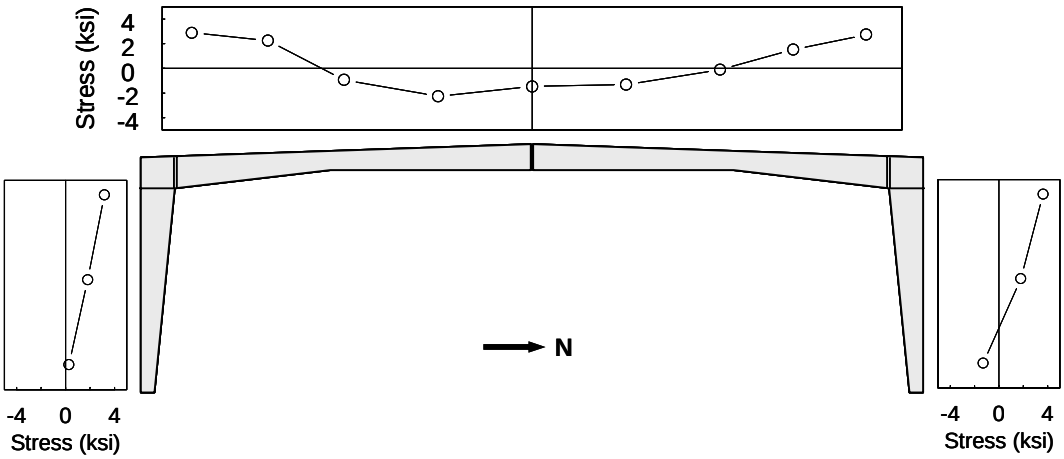

(a) Frame 1

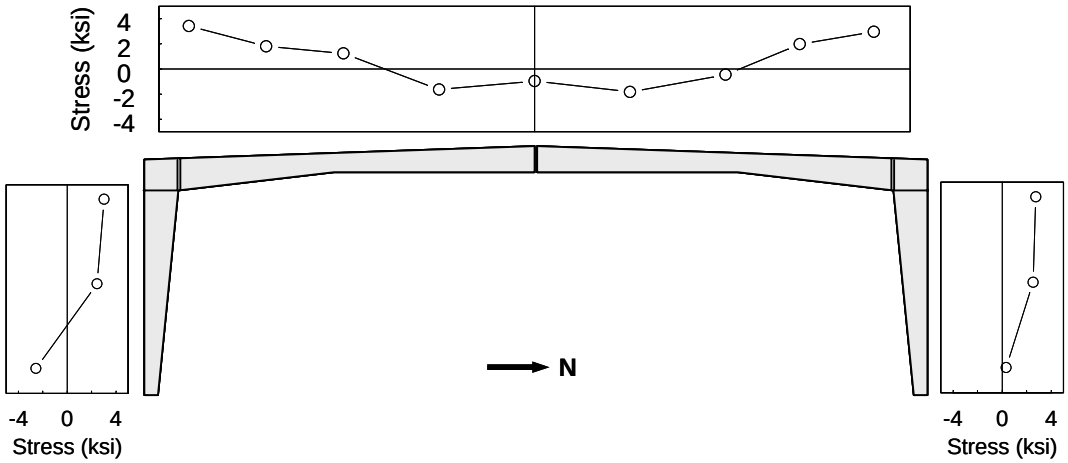

(b) Frame 2

Figure 3.16 Stress Distribution due to Gravity Load

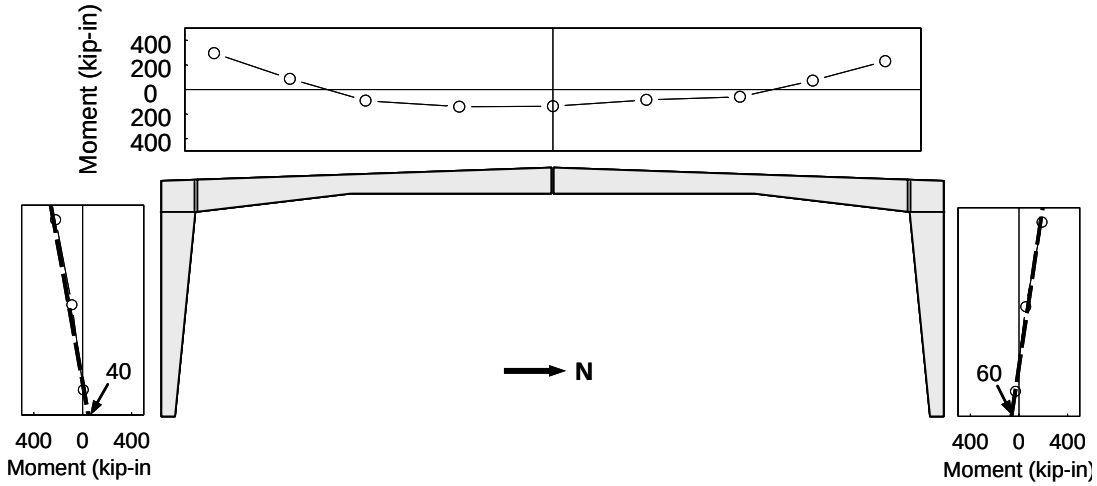

(a) Frame 1

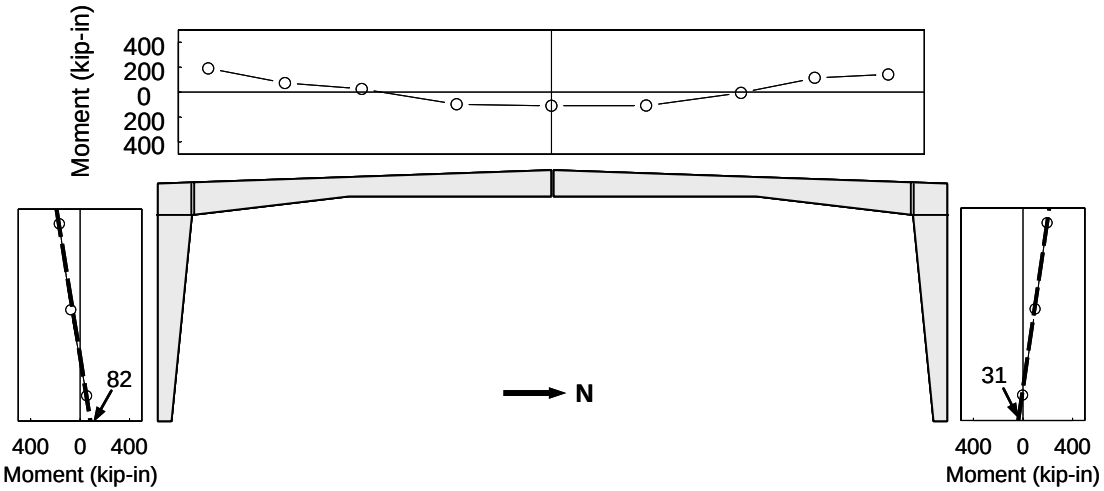

(b) Frame 2

Figure 3.17 Moment Diagram (Gravity Load Only)

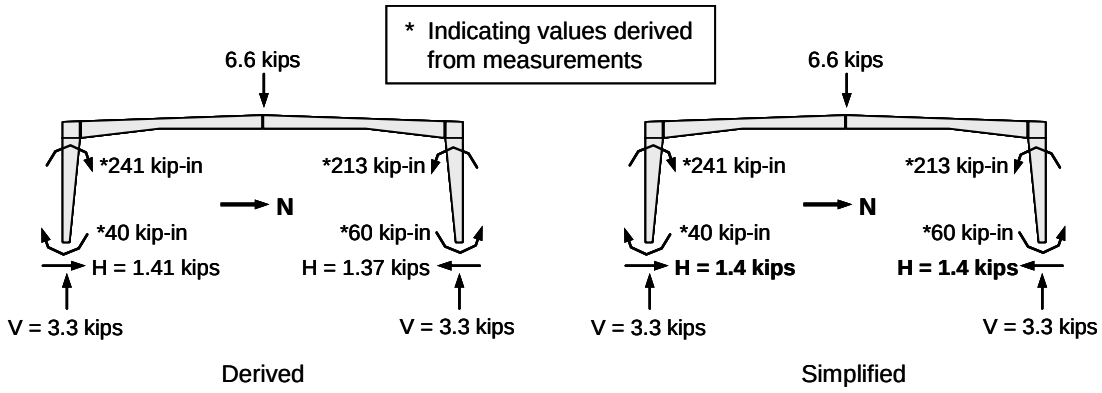

(a) Frame 1

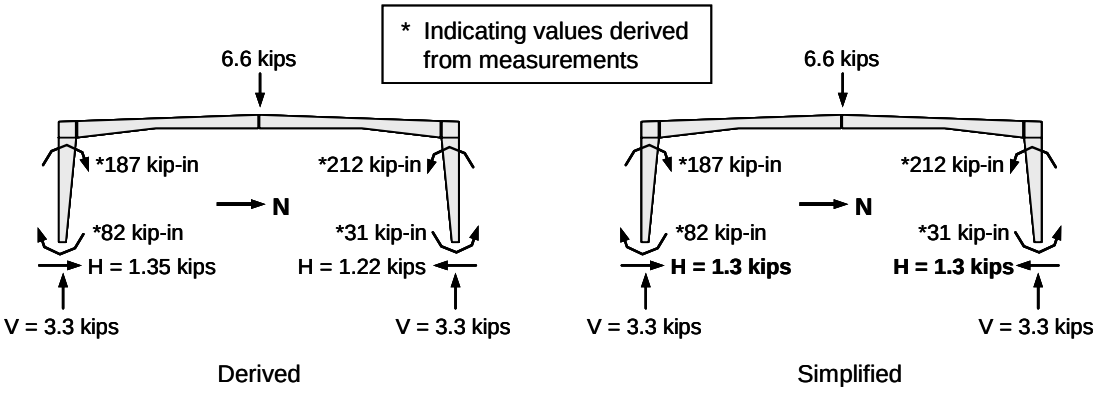

(b) Frame 2

Figure 3.18 Derived and Simplified Support Reactions (Gravity Load Only)

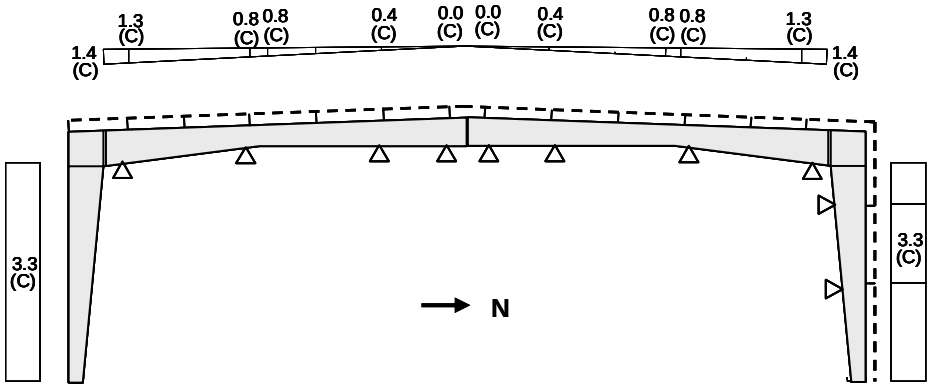

(a) Axial Force Diagram

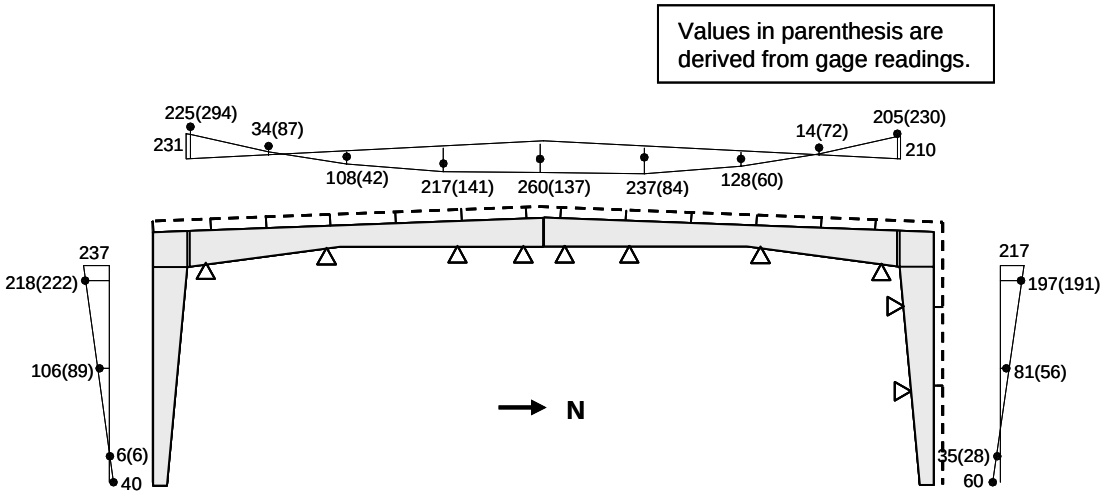

(b) Bending Moment Diagram

Figure 3.19 Frame 1: Axial Force and Bending Moment Diagrams (Gravity Load Only)

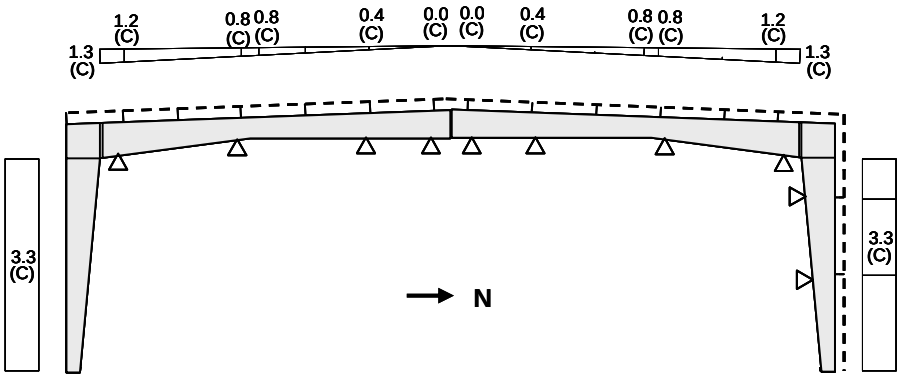

(a) Axial Force Diagram

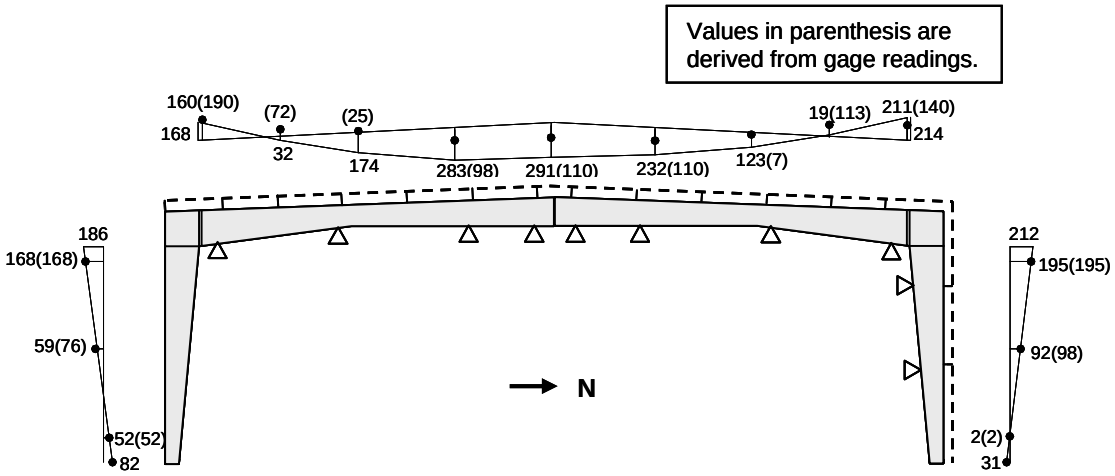

(b) Bending Moment Diagram

Figure 3.20 Frame 2: Axial Force and Bending Moment Diagrams (Gravity Load Only)

(a) North

(b) South

Figure 3.21 Frame 1: Behavior at 1.5% Drift

(a) North

(b) South

Figure 3.22 Frame 2: Behavior at 1.5% Drift

(a) Lateral Buckling

(b) Column

(c) Rafter

Figure 3.23 Lateral Buckling at South Column and Rafter of Frame 2

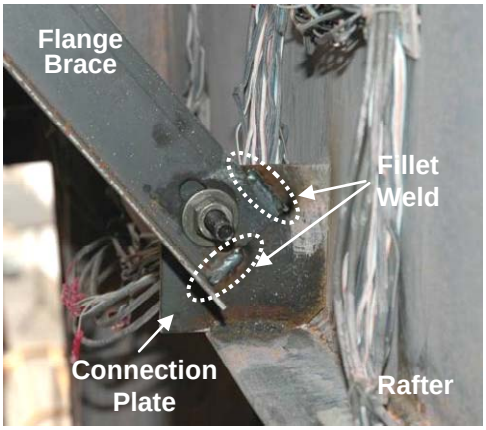

(a) Flange Brace Reinforcement

(b) Additional Flange Brace on South Side of Frame 2

Figure 3.24 Flange Brace Reinforcement and Addition after First 2% Drift

(a) Frame 2

(b) Frame 1

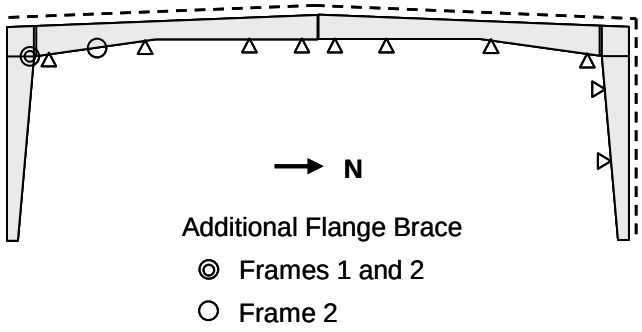

(c) Location of Additional Flange Braces

Figure 3.25 Flange Braces Added during 2% Drift Cycles

(a) South Rafter Lateral Buckling

(b) Close-up View

Figure 3.26 Frame 1: Failure Mode at First Positive Excursion to 3% Drift

(a) South Column Lateral Buckling

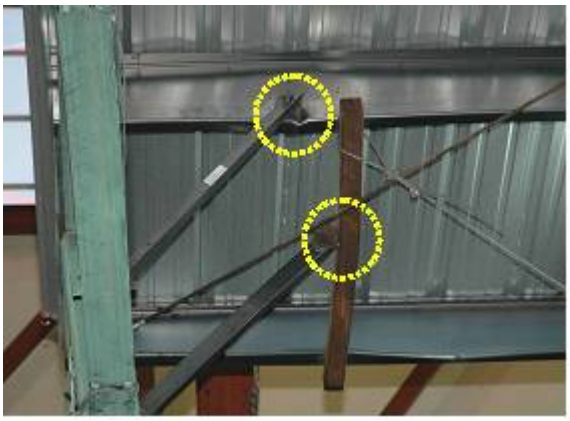

(b) Overload of Brace Support

Figure 3.27 Frame 2: Failure Mode at First Positive Excursion to 3% Drift

(a) North (Closed) Side

(b) South (Open) Side

Figure 3.28 Failure Mode at First Negative Excursion to 3% Drift

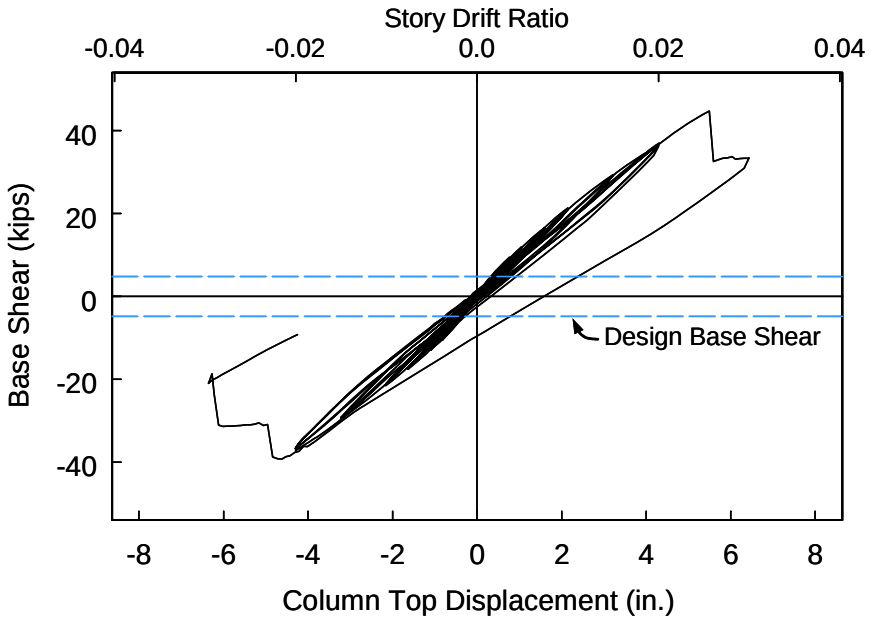

(a) Frame 1

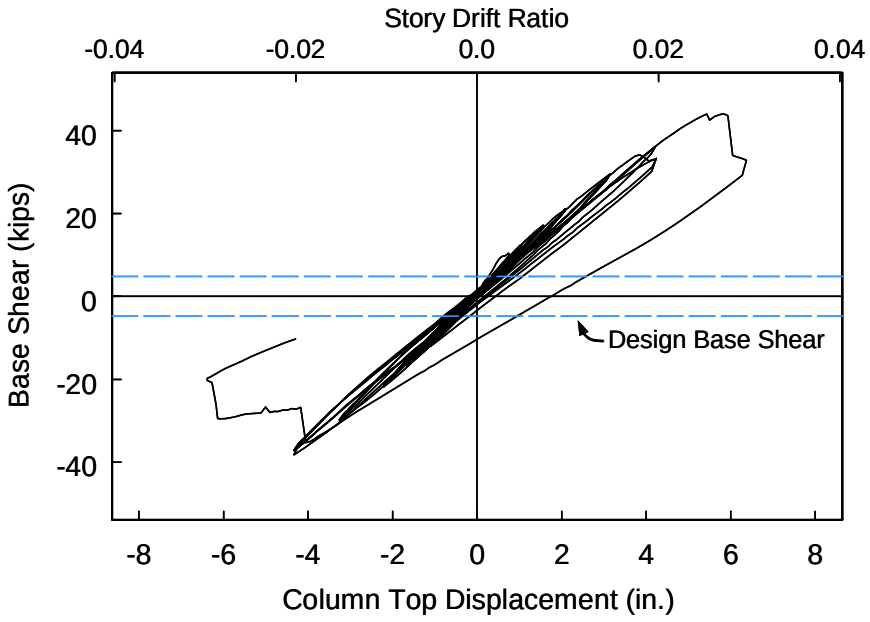

(b) Frame 2

Figure 3.29 Base Shear versus Column Top Displacement

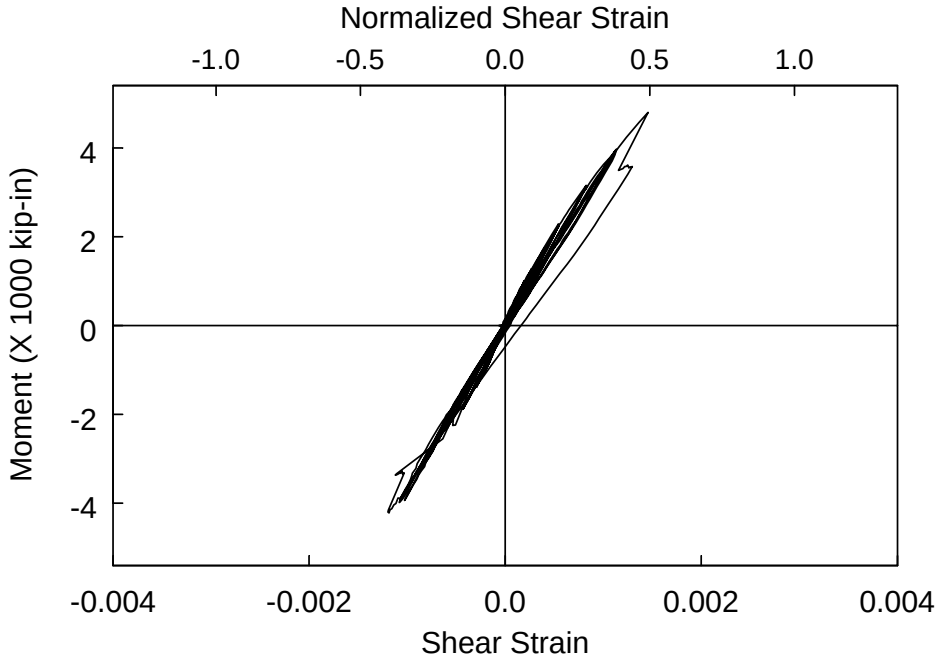

(a) North Panel Zone

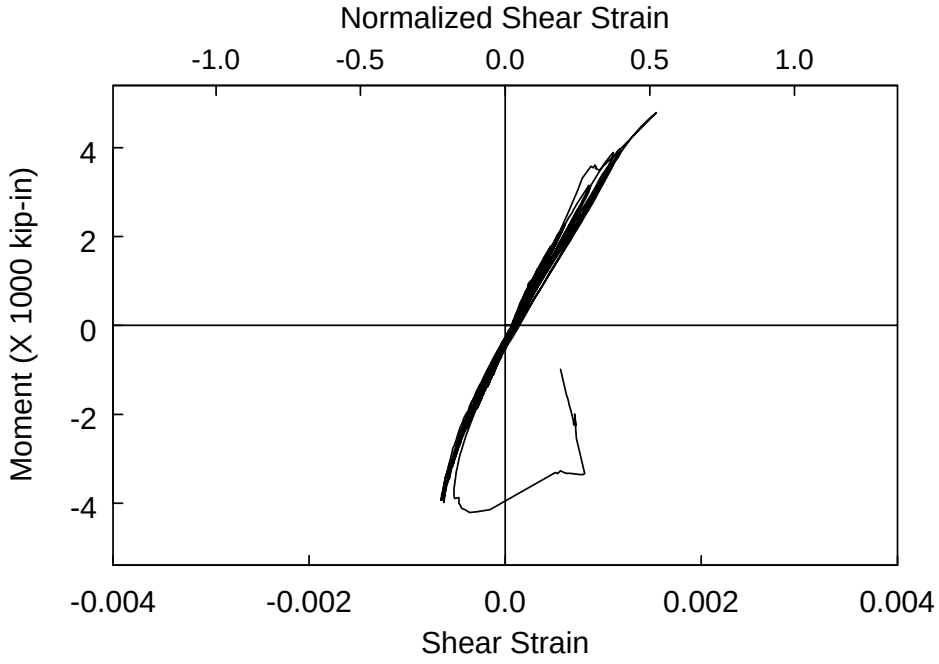

(b) South Panel Zone

Figure 3.30 Frame 1: Moment versus Panel Zone Shear Deformation

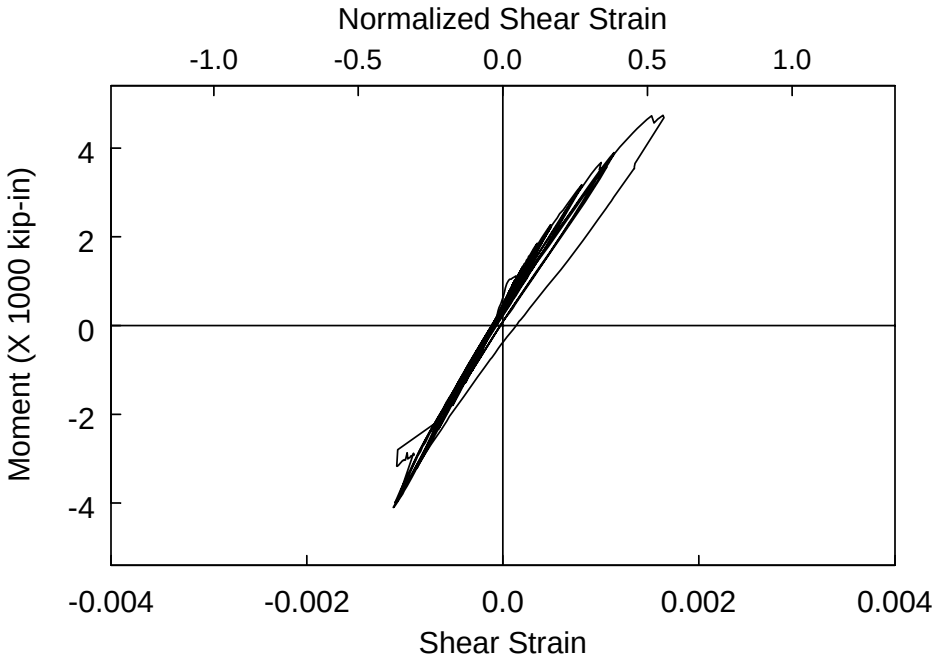

(a) North Panel Zone

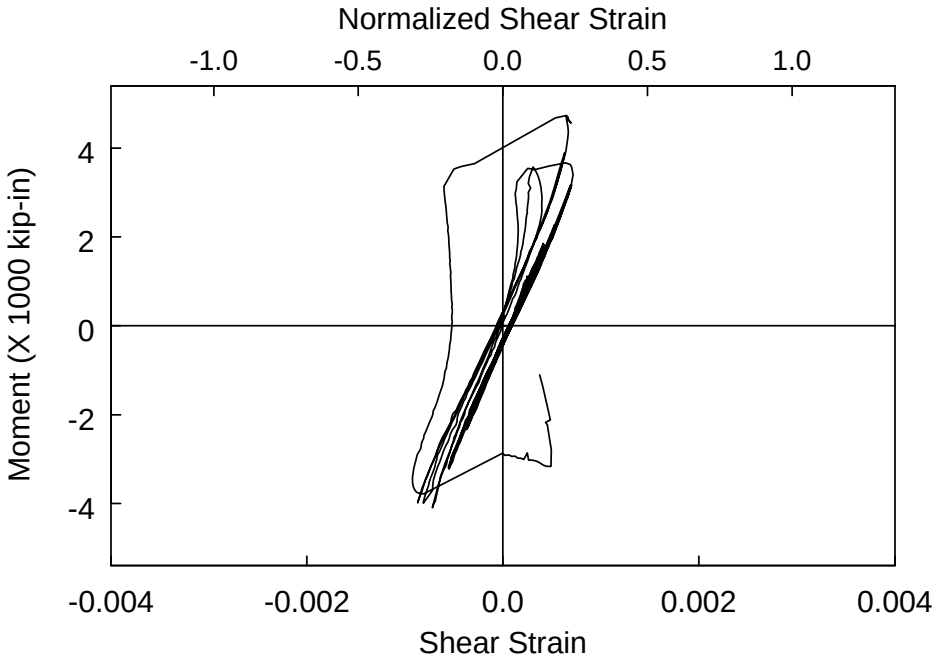

(b) South Panel Zone

Figure 3.31 Frame 2: Moment versus Panel Zone Shear Deformation

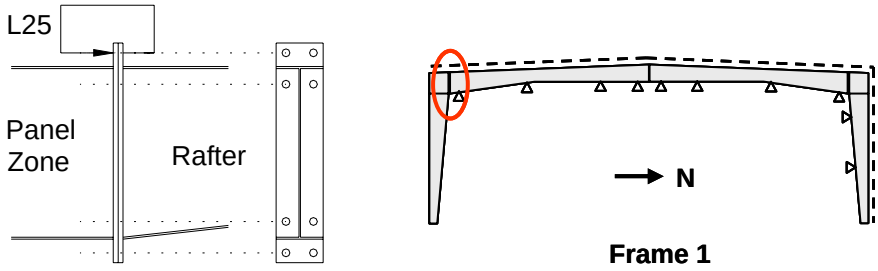

[see Figure 3.12(b)]

(a) Location

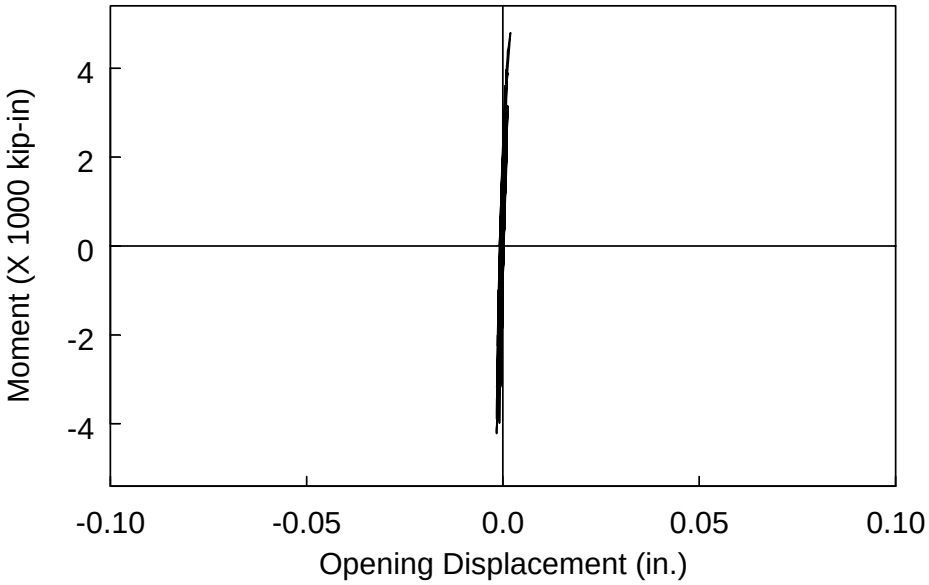

(b) Response

Figure 3.32 Moment versus End-Plate Opening Displacement

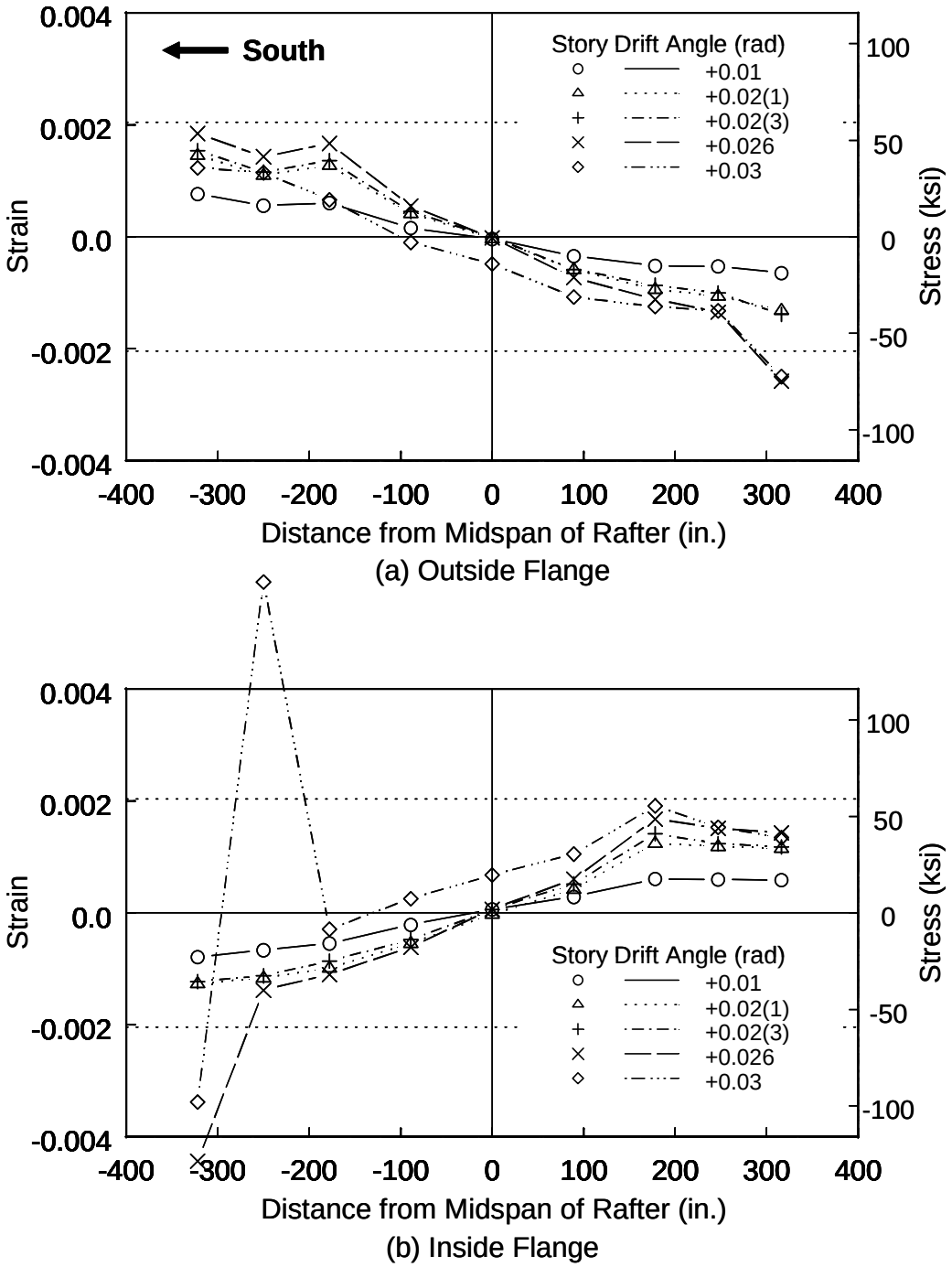

Figure 3.33 Frame 1: Measured Strains at Rafter Flanges (Positive Excursions)

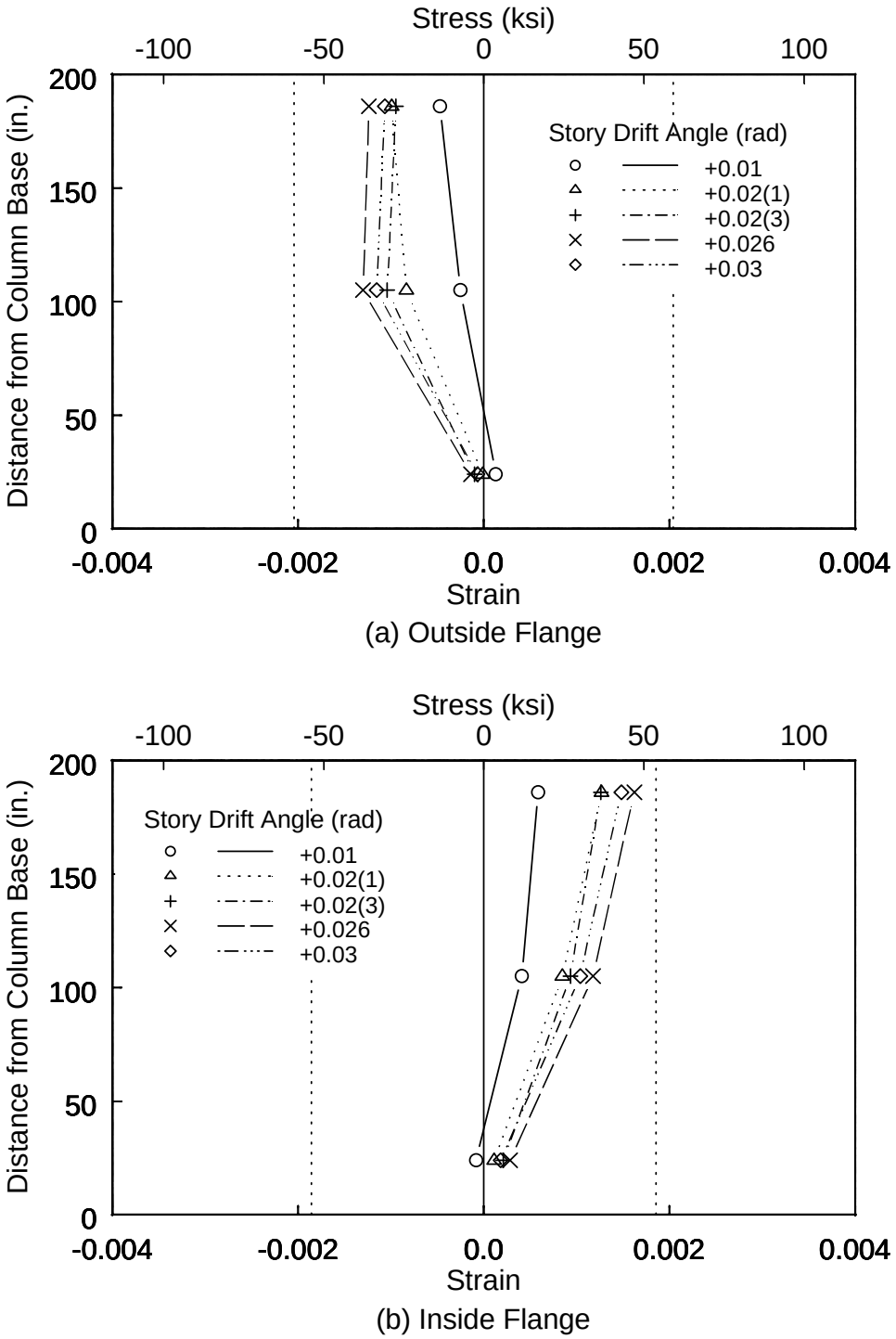

Figure 3.34 Frame 1: Measured Strains at North Column (Positive Excursions)

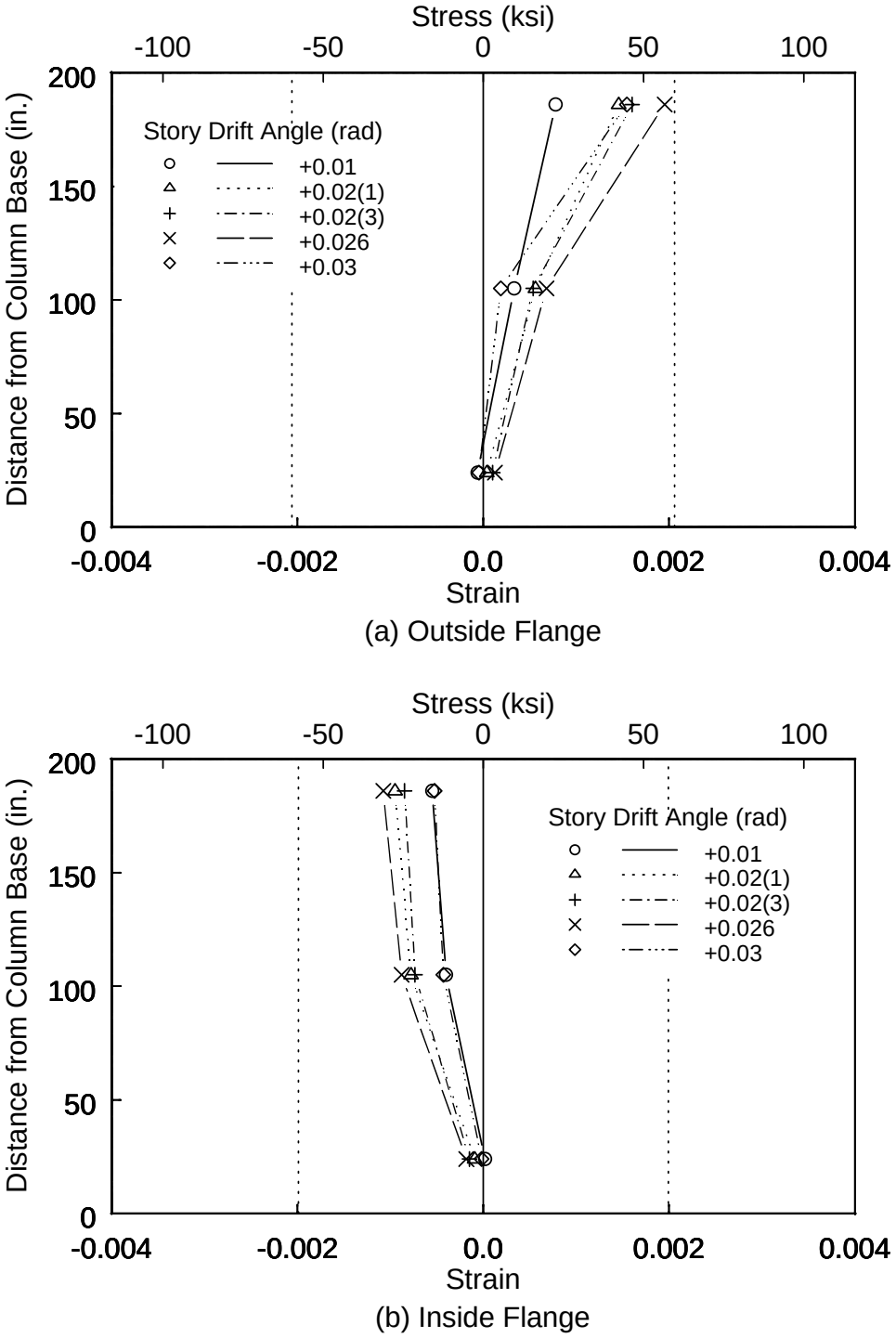

Figure 3.35 Frame 1: Measured Strains at South Column (Positive Excursions)

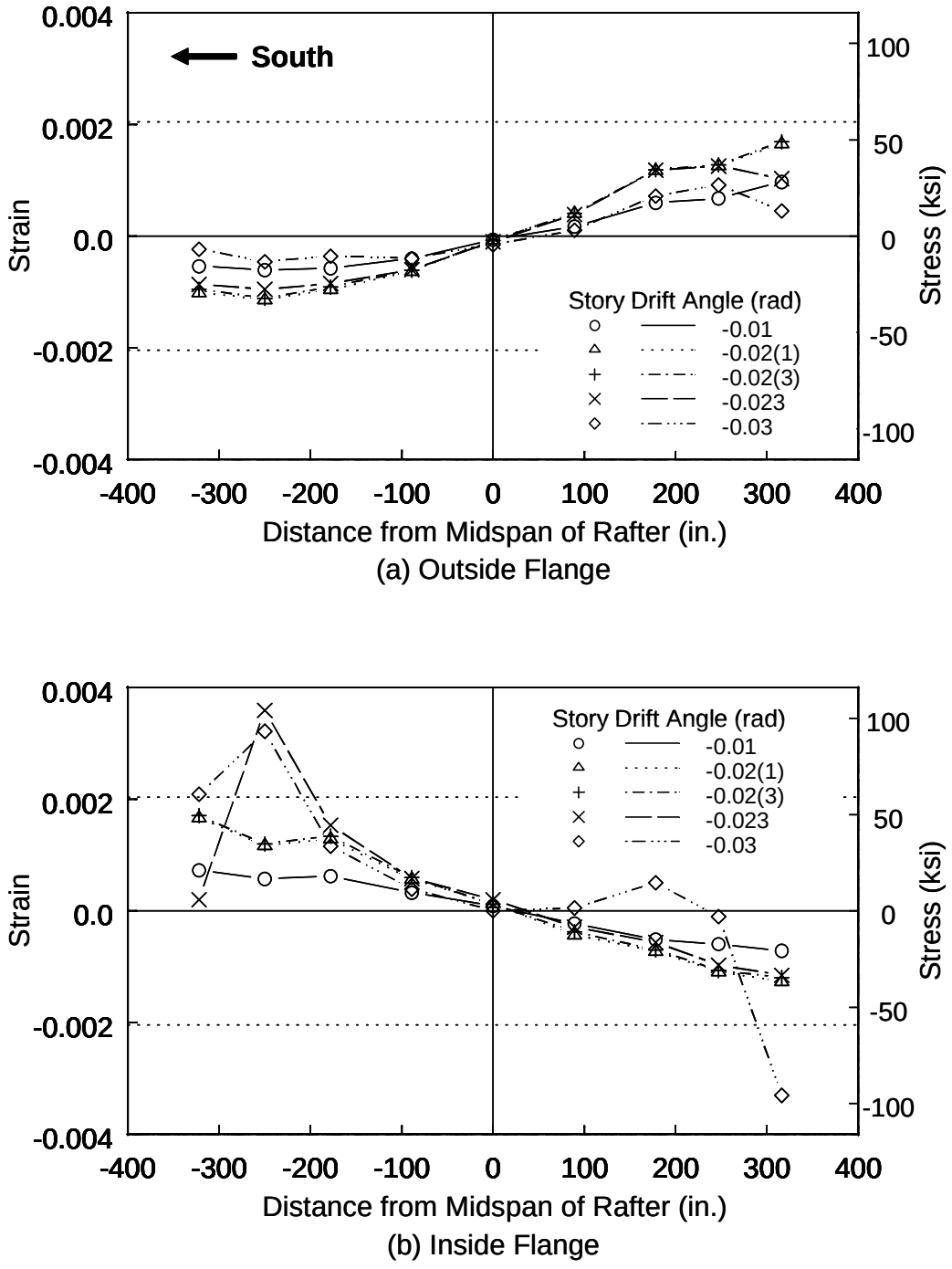

Figure 3.36 Frame 1: Measured Strains at Rafter Flanges (Negative Excursions)

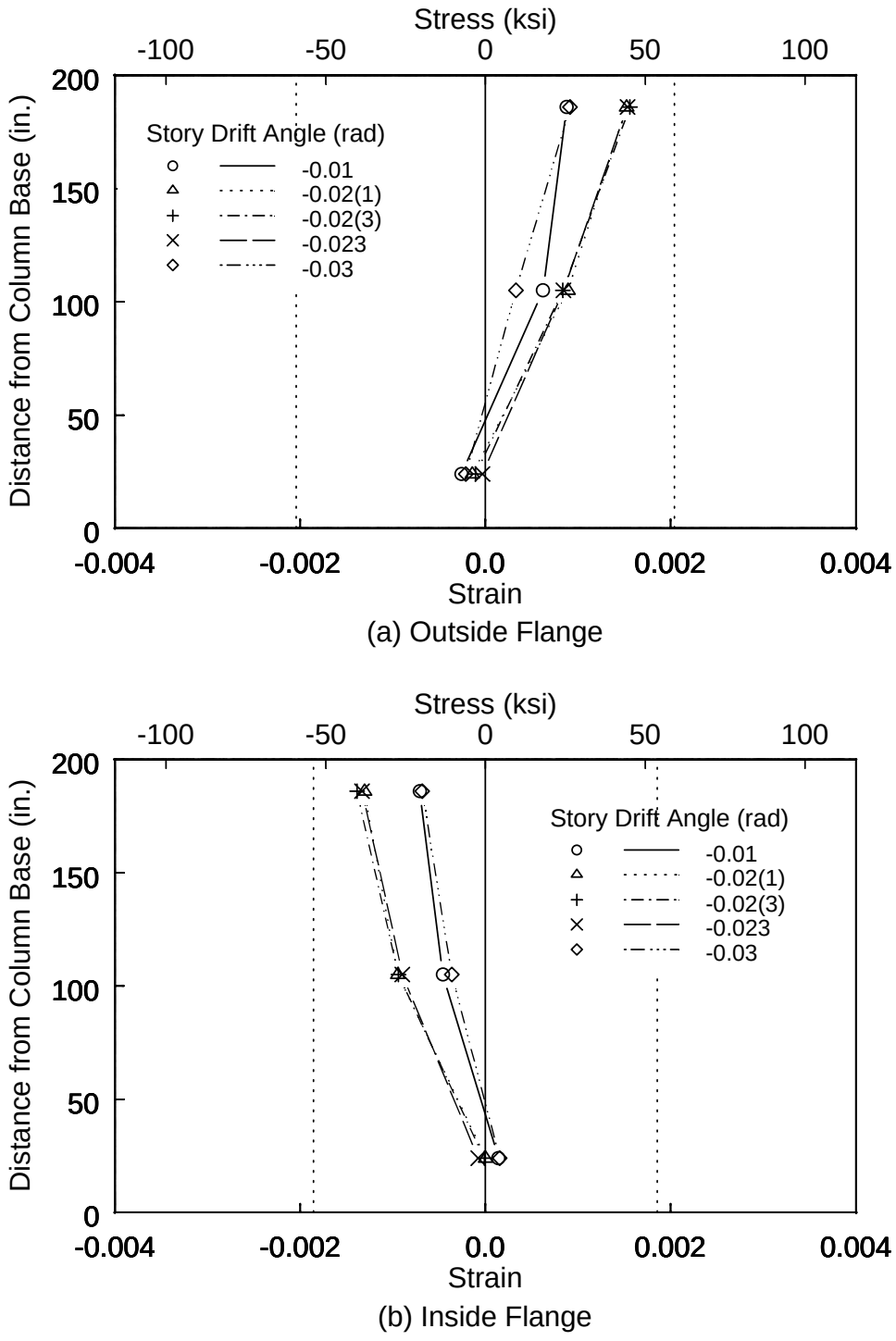

Figure 3.37 Frame 1: Measured Strains at North Column (Negative Excursions)

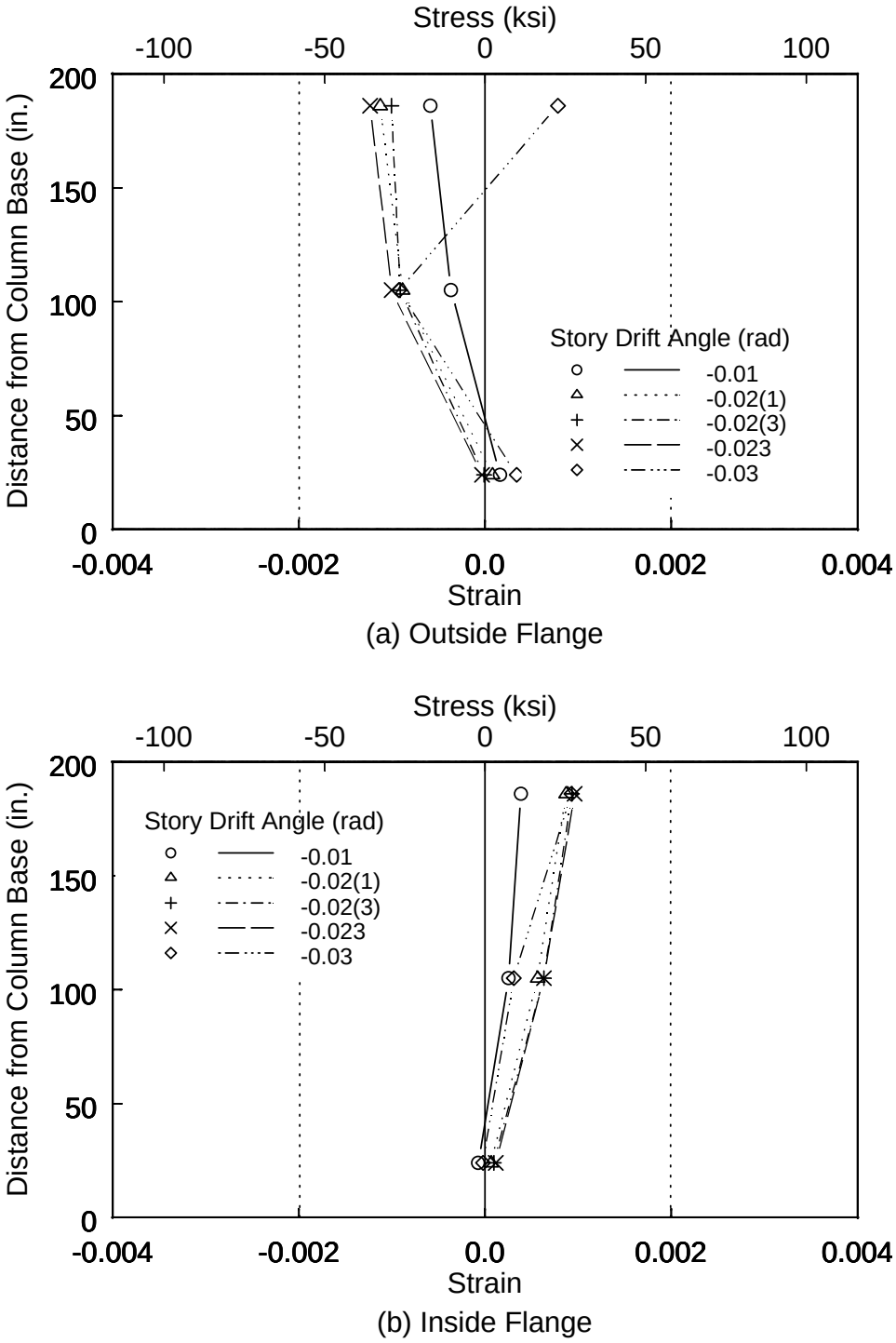

Figure 3.38 Frame 1: Measured Strains at South Column (Negative Excursions)

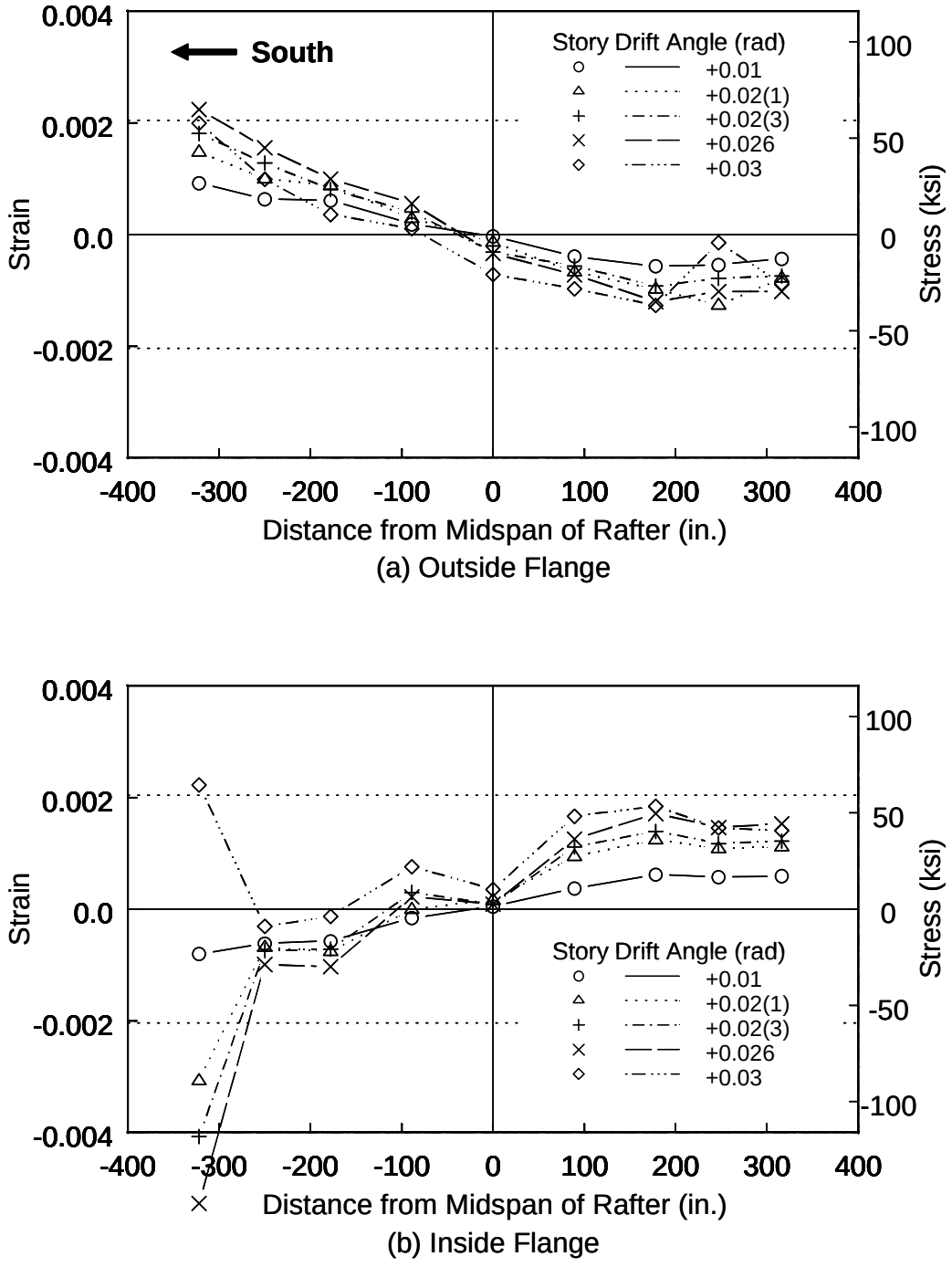

Figure 3.39 Frame 2: Measured Strains at Rafter Flanges (Positive Excursions)

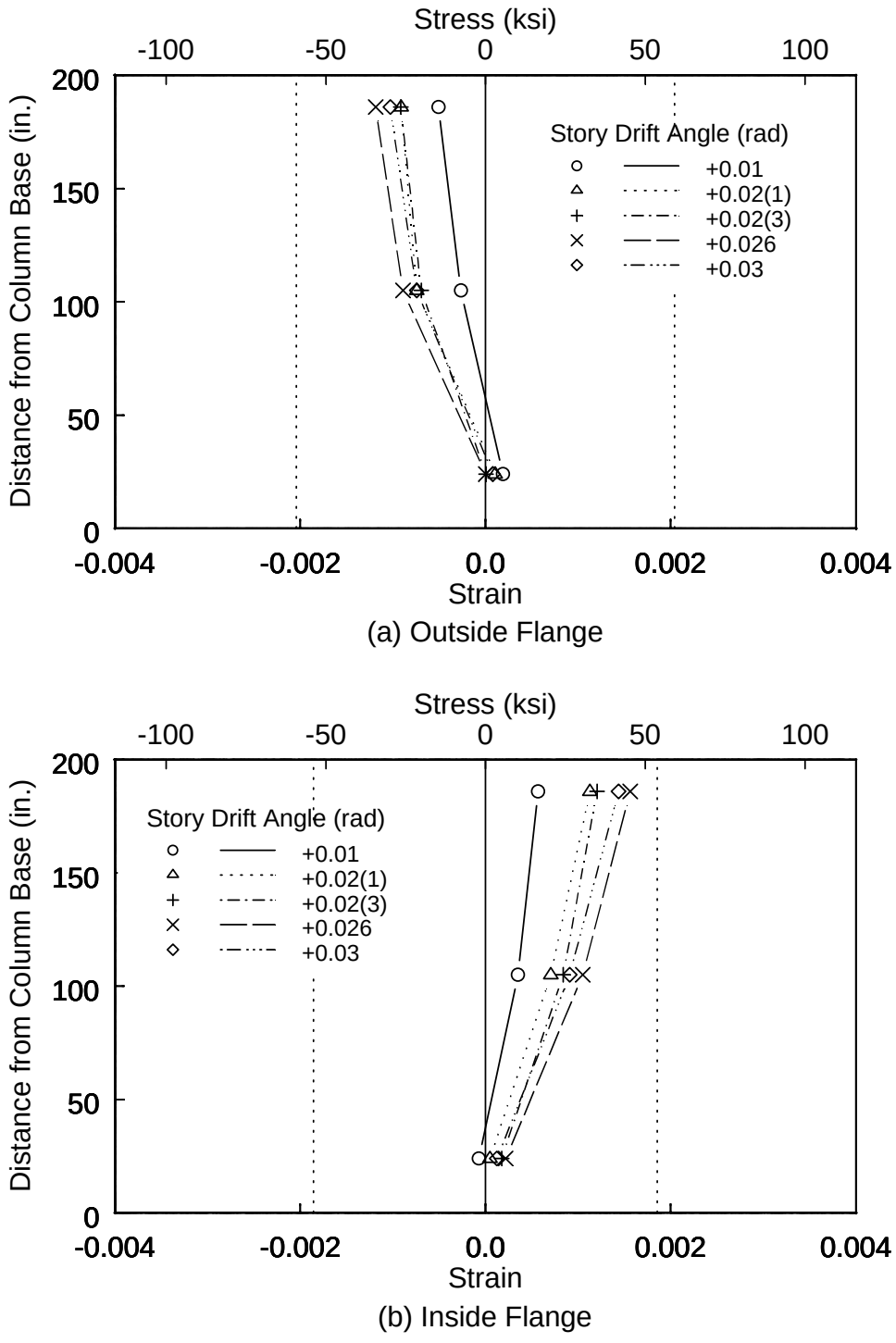

Figure 3.40 Frame 2: Measured Strains at North Column (Positive Excursions)

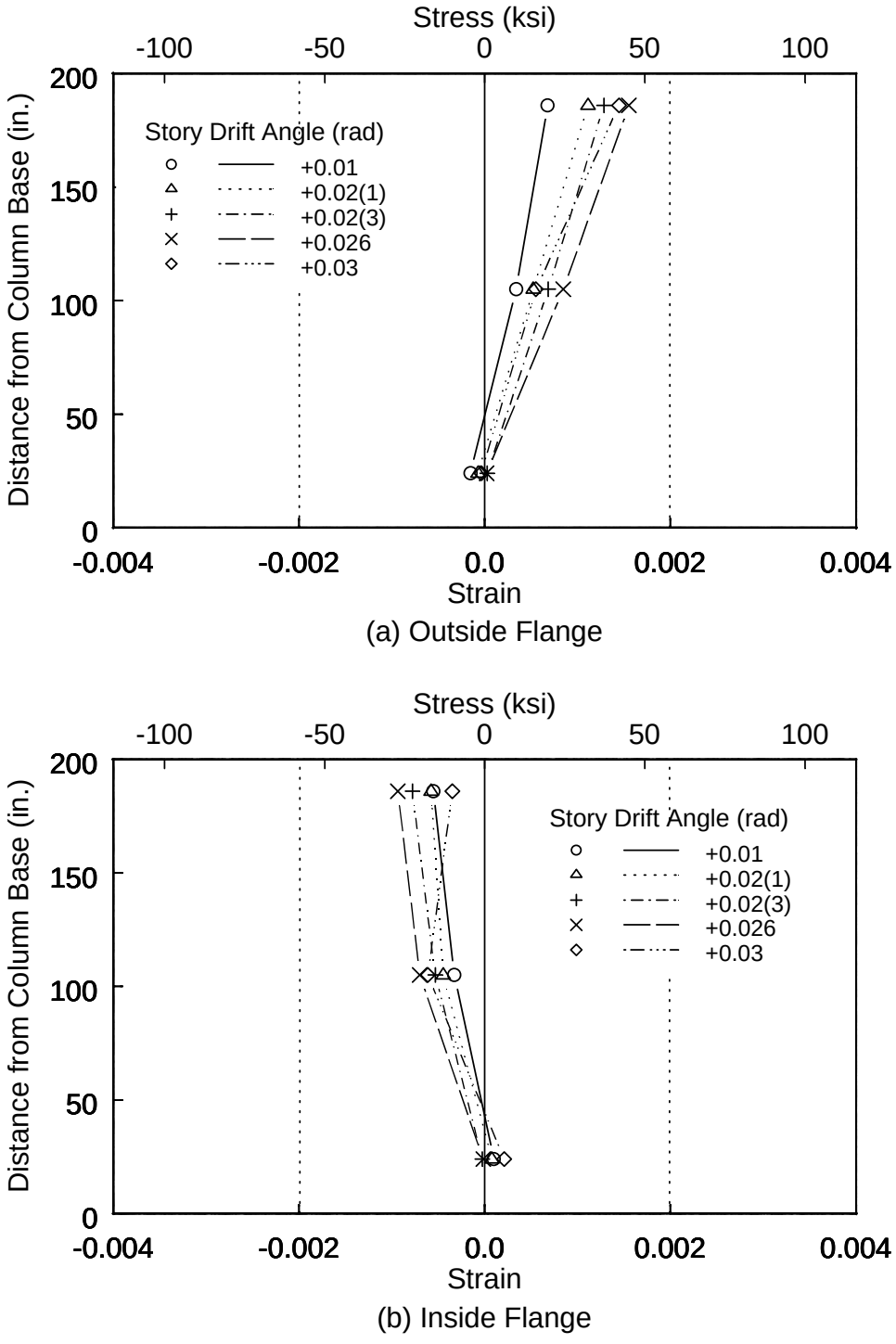

Figure 3.41 Frame 2: Measured Strains at South Column (Positive Excursions)

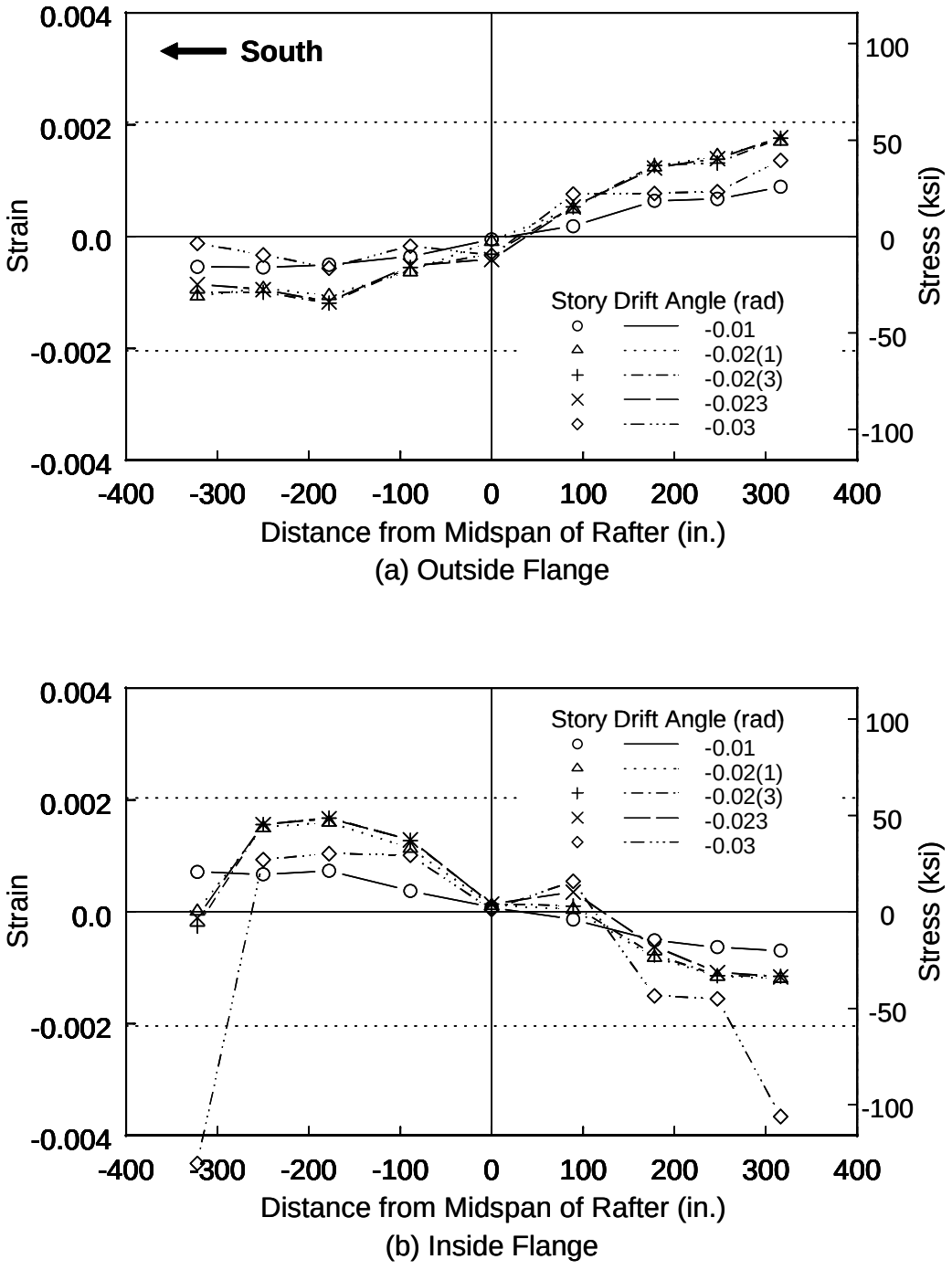

Figure 3.42 Frame 2: Measured Strains at Rafter Flanges (Negative Excursions)

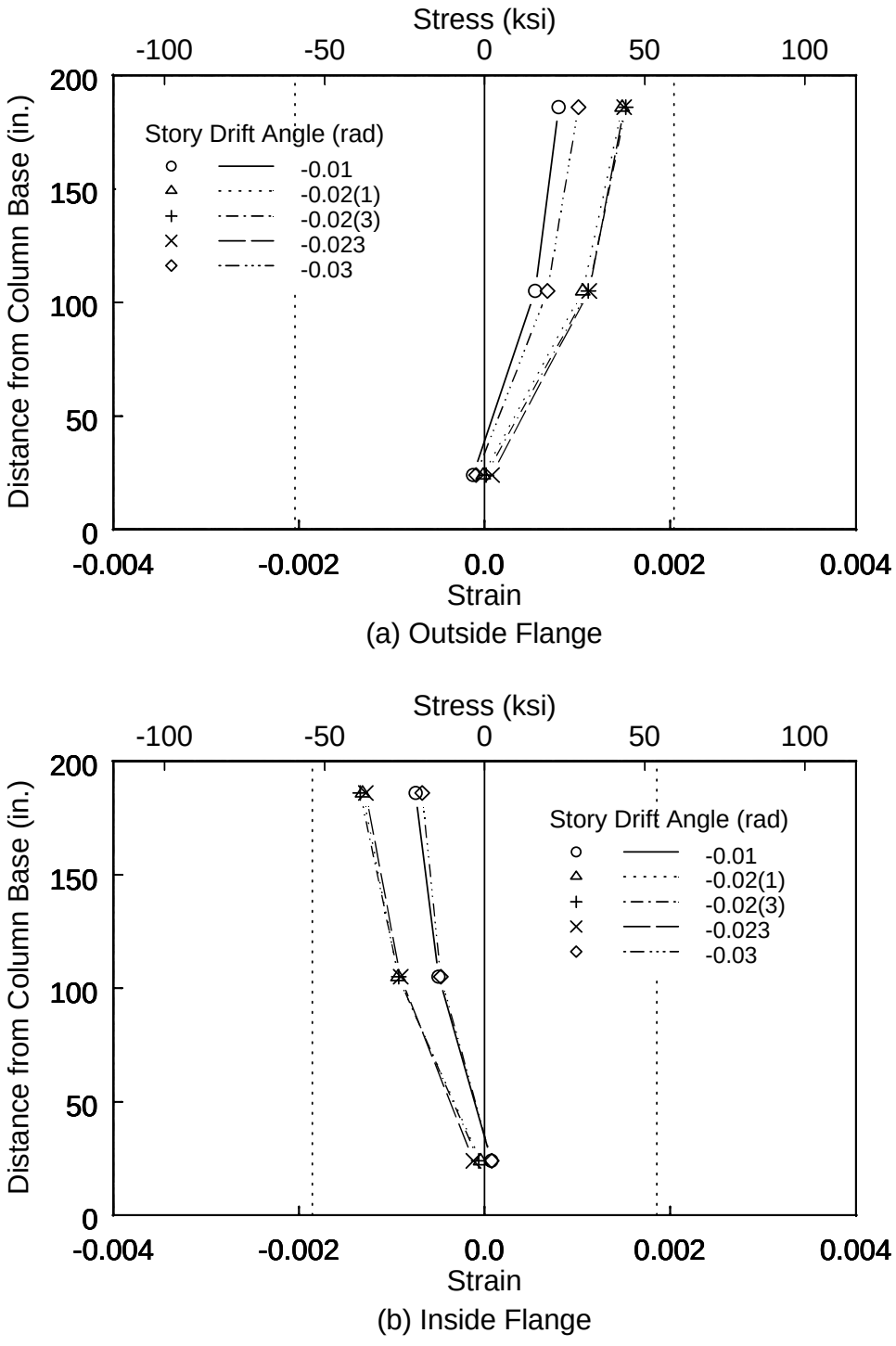

Figure 3.43 Frame 2: Measured Strains at North Column (Negative Excursions)

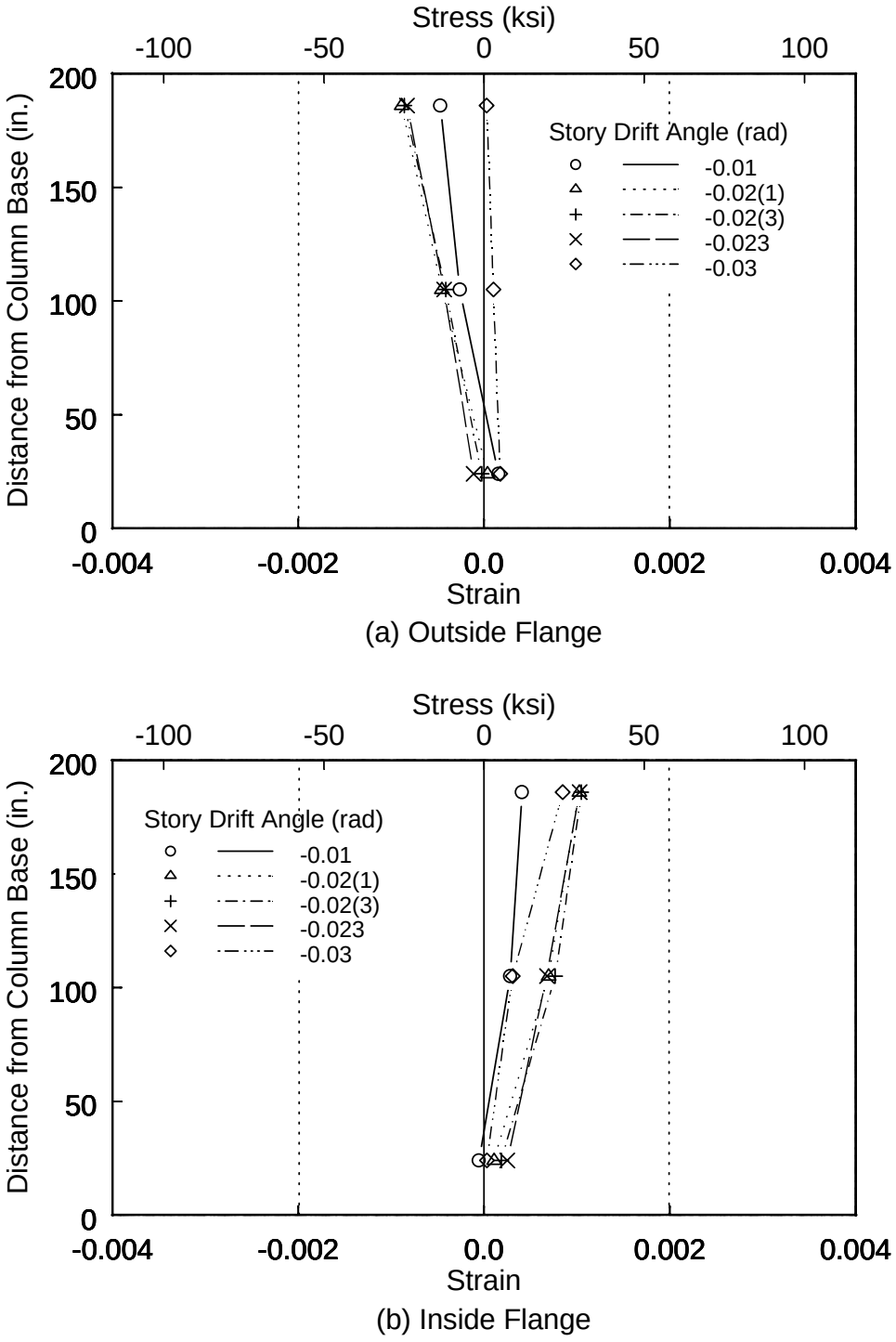

Figure 3.44 Frame 2: Measured Strains at South Column (Negative Excursions)

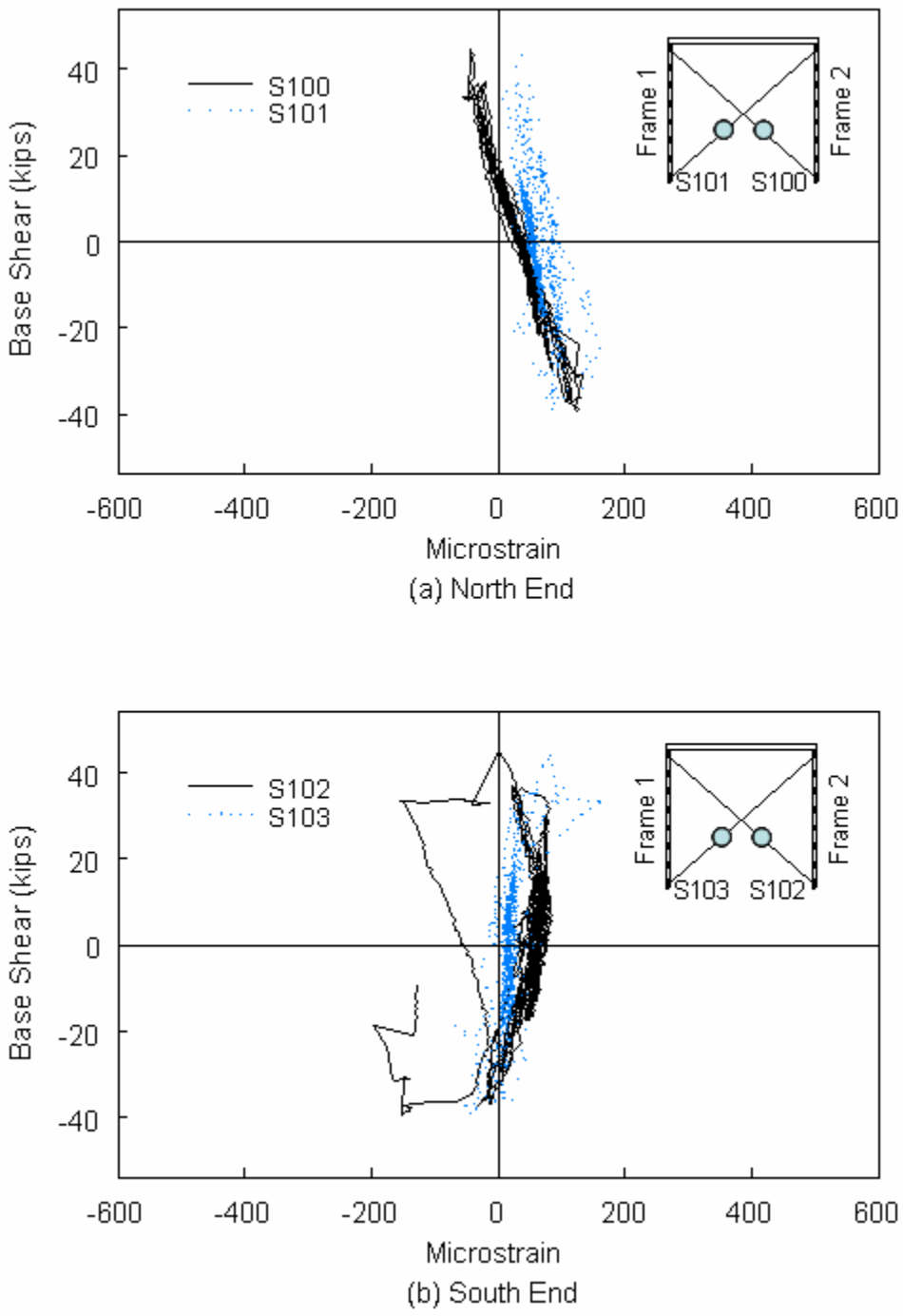

Figure 3.45 Load versus Measured Strain at Rod Braces

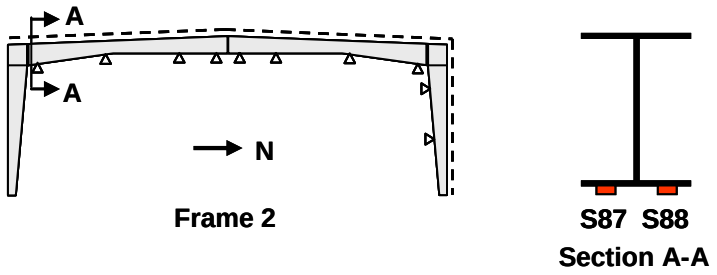

(a) Location

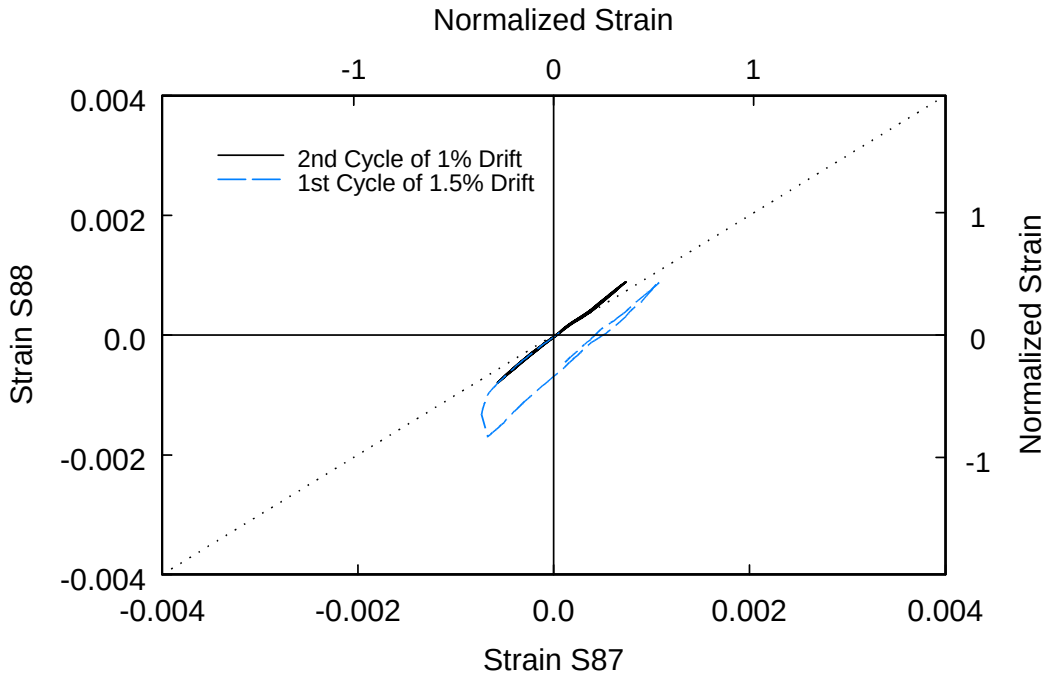

(b) Strain Comparison

Figure 3.46 Strain Deviation at 1.5% Drift

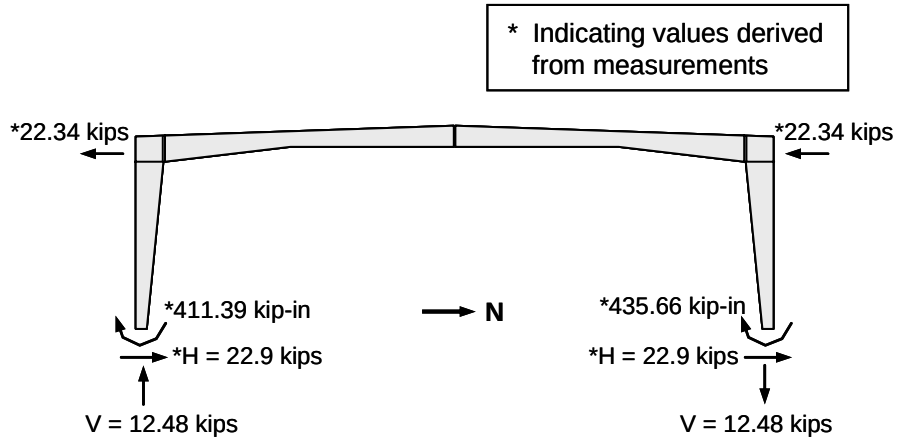

(a) Derived

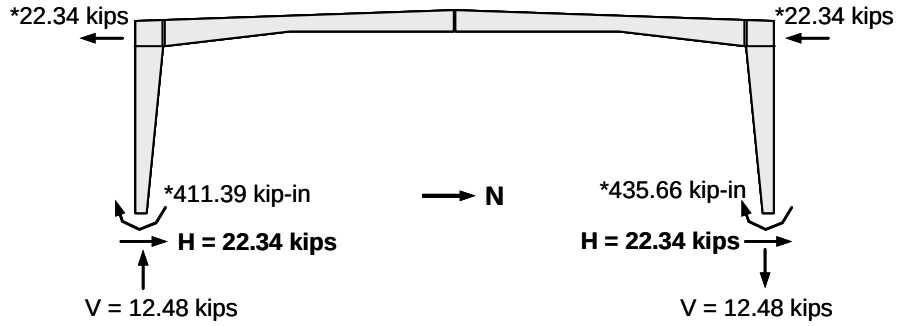

(b) Simplification

Figure 3.47 Support Reactions of Frame 1 at Positive 2.6% Drift (Lateral Load Only)

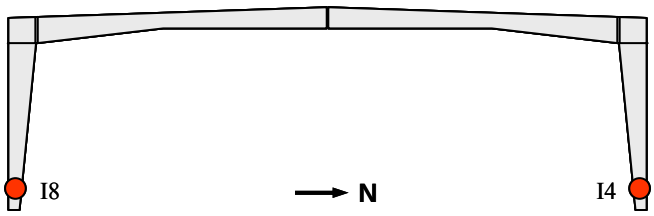

(a) Location of Inclinometers

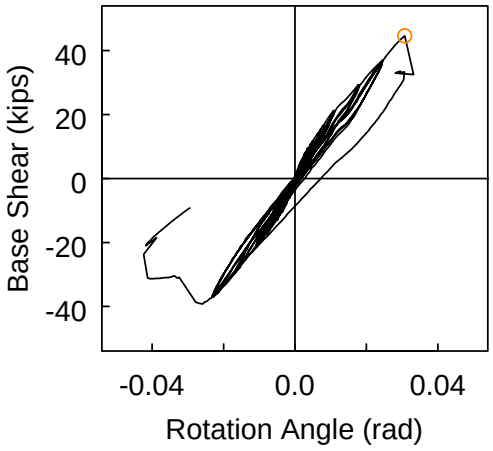

(b) I8

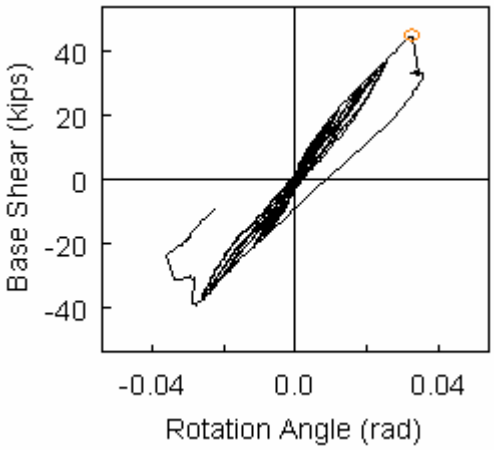

(c) I4

Figure 3.48 Measured Rotation Angle at Column Bases of Frame 1

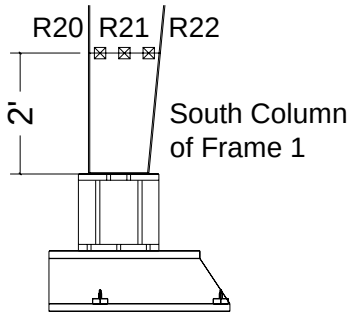

(a) Location

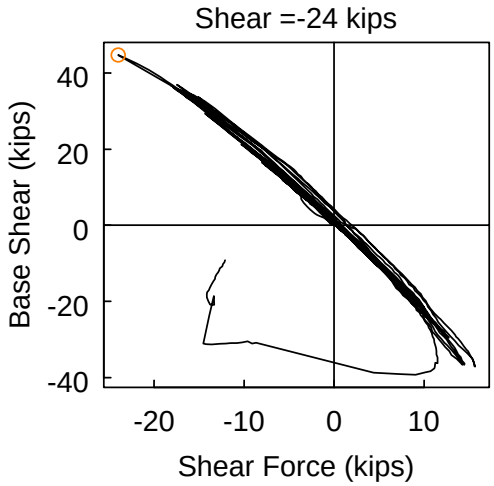

(b) R20

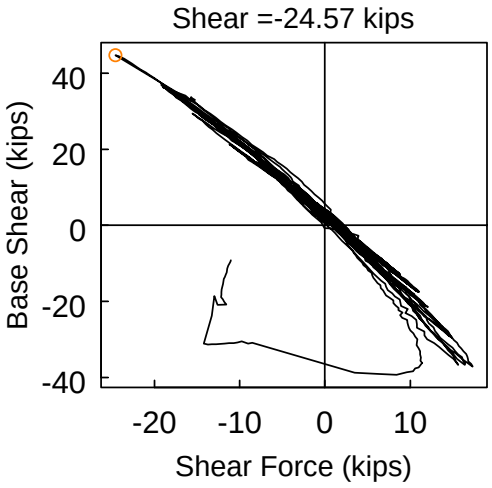

(c) R21

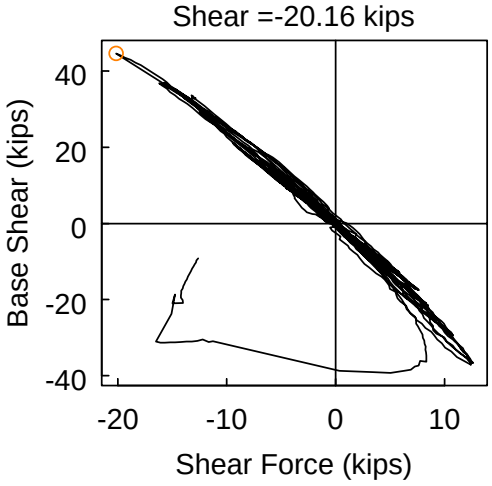

(d) R22

Figure 3.49 Shear Force at South Column of Frame 1

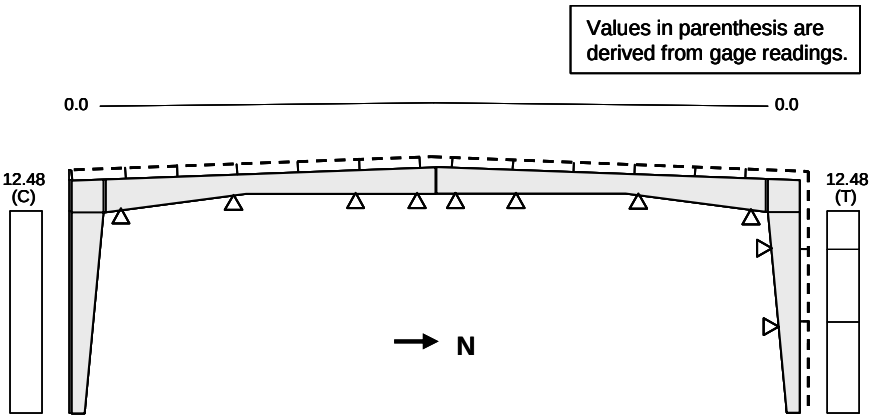

(a) Axial Force Diagram (Frames 1 and 2)

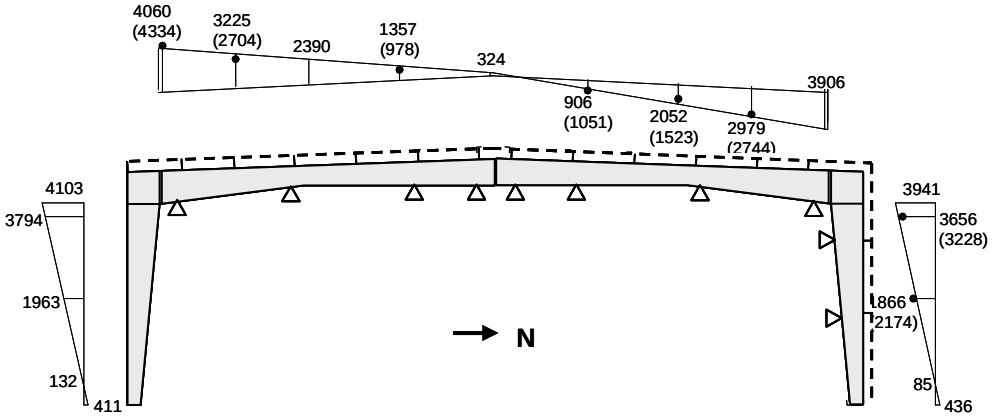

(b) Bending Moment Diagram for Frame 1

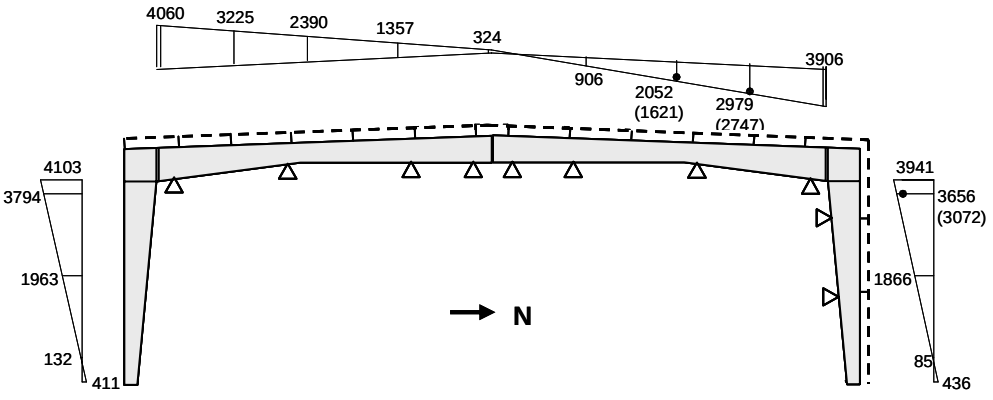

(c) Bending Moment Diagram for Frame 2

Figure 3.50 Internal Forces at Positive 2.6% Drift due to Lateral Load Only

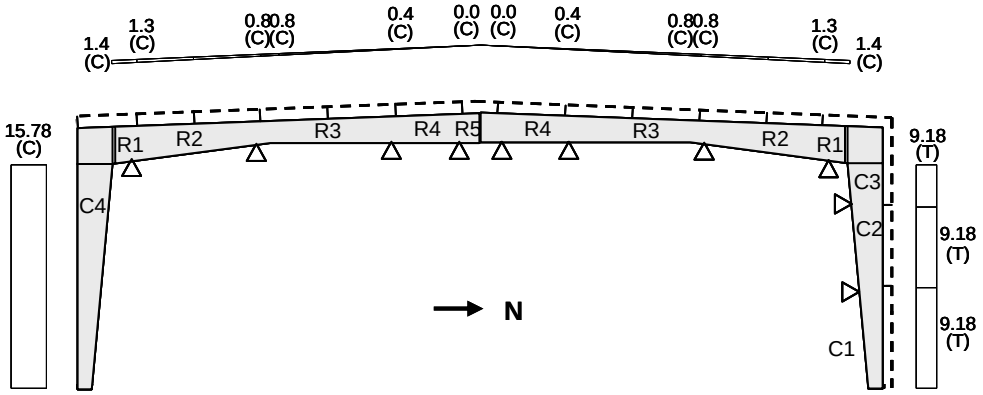

(a) Axial Force Diagram

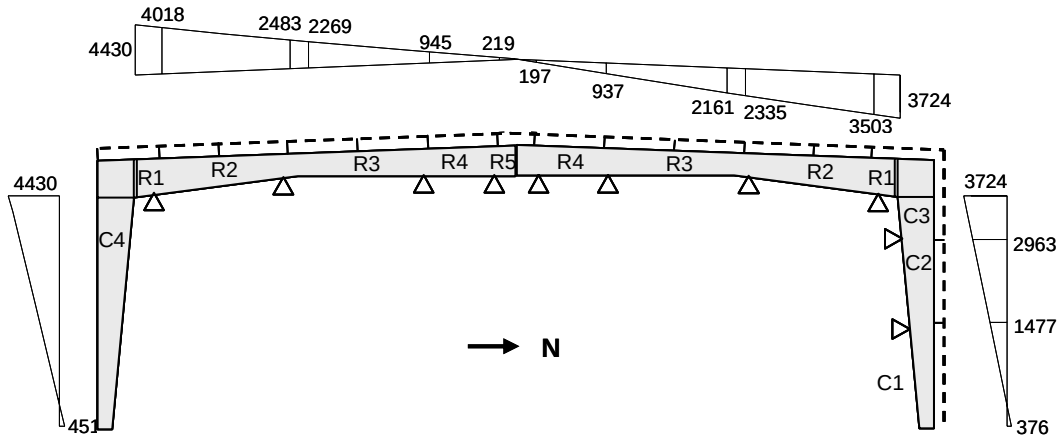

(b) Bending Moment Diagram

Figure 3.51 Frame 1: Internal Forces at Positive 2.6% Drift due to Combined Loads

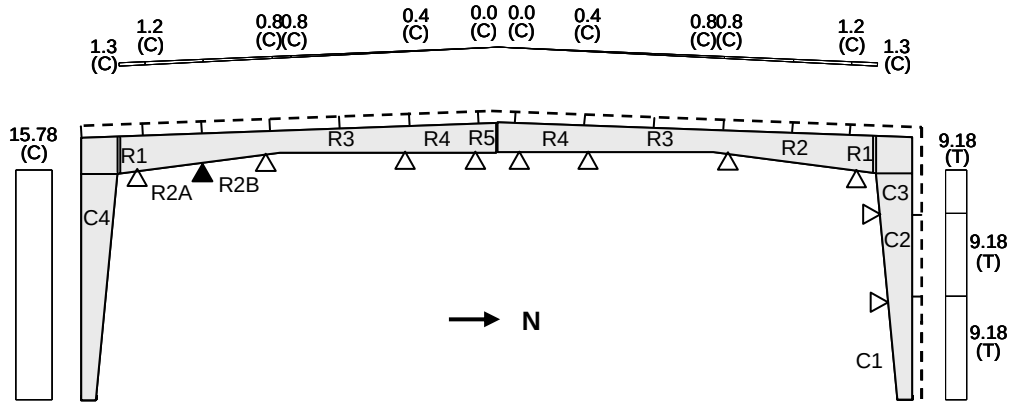

(a) Axial Force Diagram

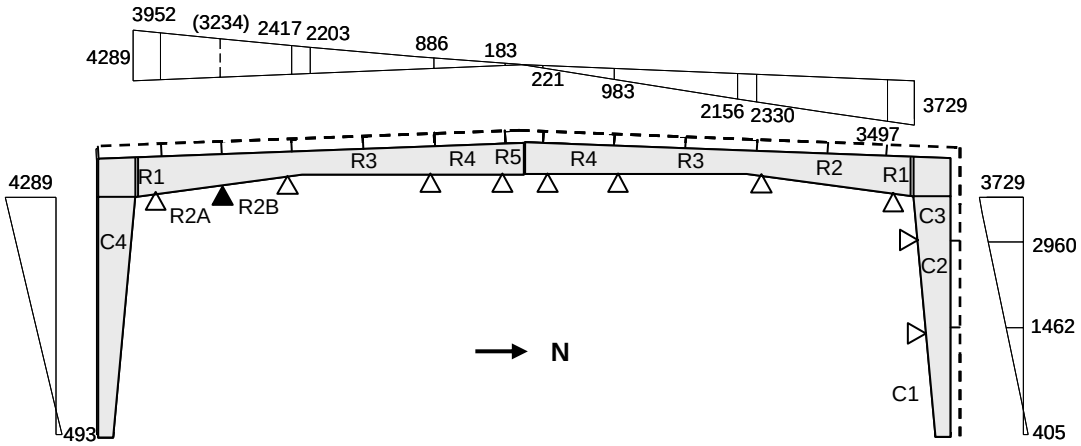

(b) Bending Moment Diagram

Figure 3.52 Frame 2: Internal Forces at Positive 2.6% Drift due to Combined Loads

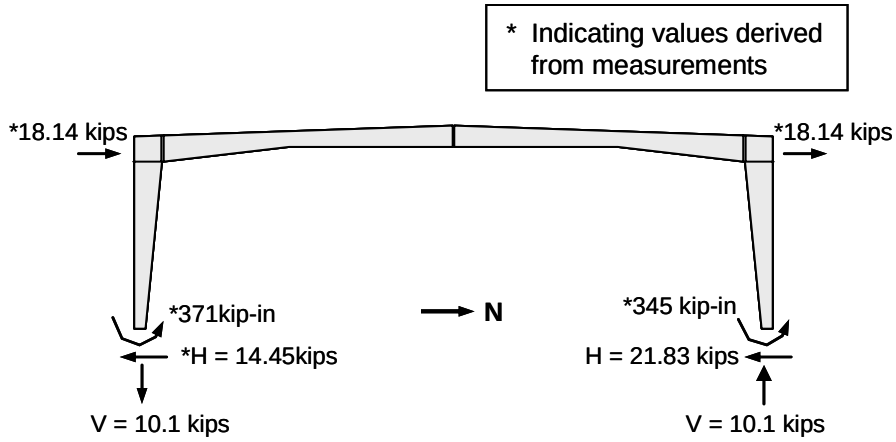

Figure 3.53 Support Reactions of Frame 1 at Negative 2.3% Drift (Lateral Load Only)

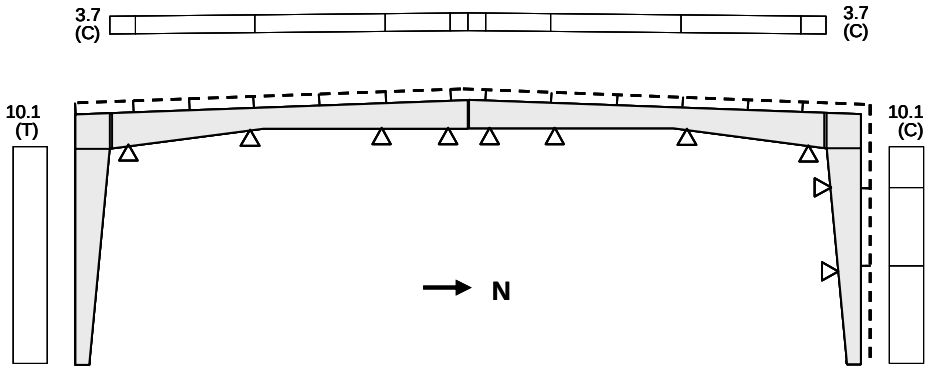

(a) Axial Force Diagram

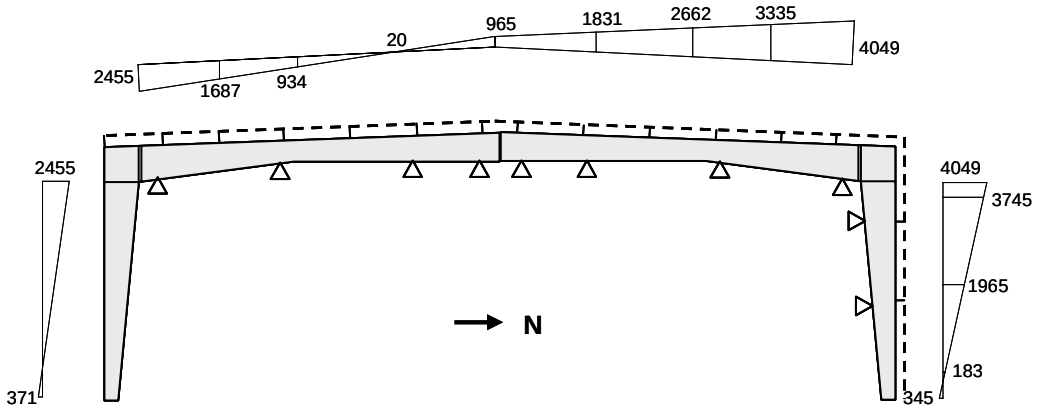

(b) Bending Moment Diagram

Figure 3.54 Internal Forces at Negative 2.3% Drift due to Lateral Load Only

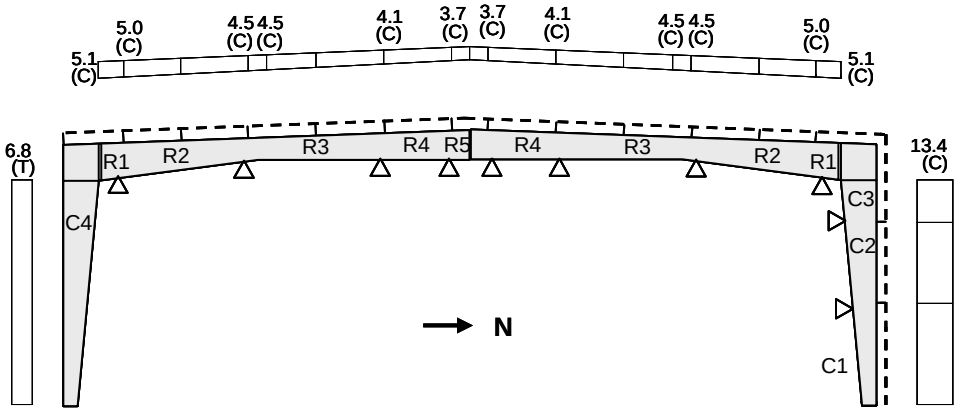

(a) Axial Force Diagram

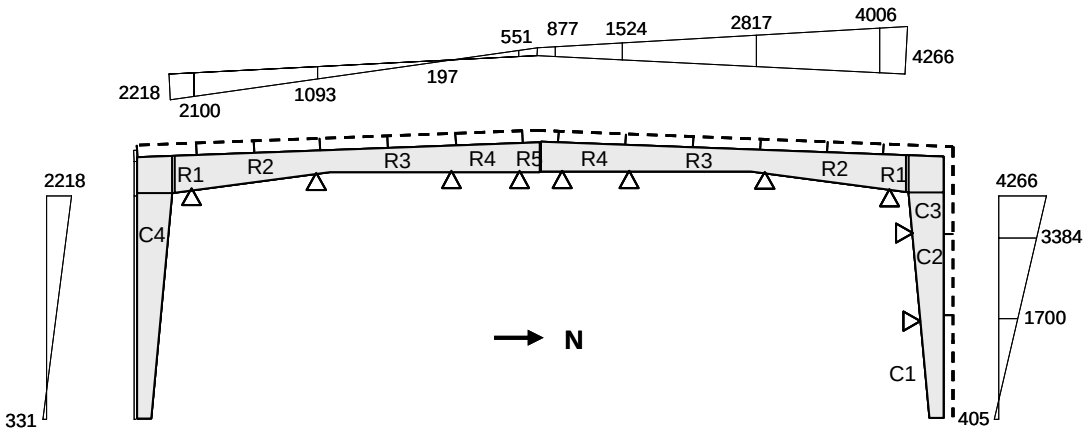

(b) Bending Moment Diagram

Figure 3.55 Frame 1: Internal Forces at Negative 2.3% Drift due to Combined Loads

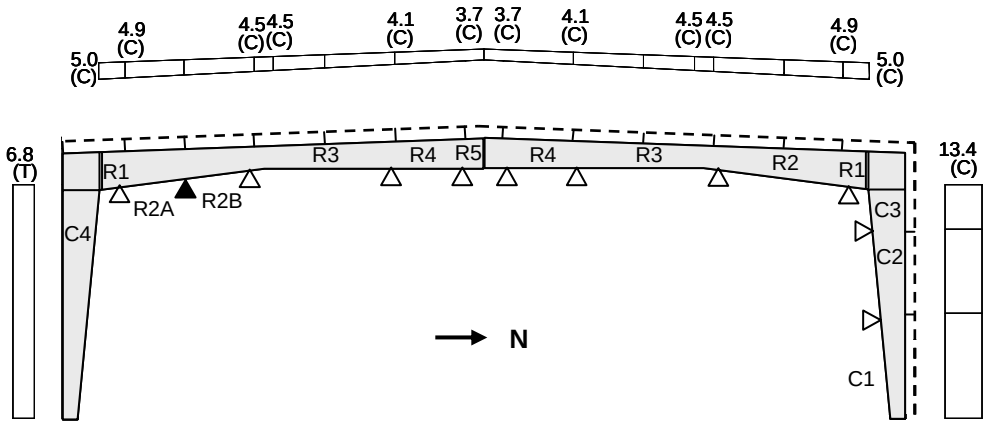

(a) Axial Force Diagram

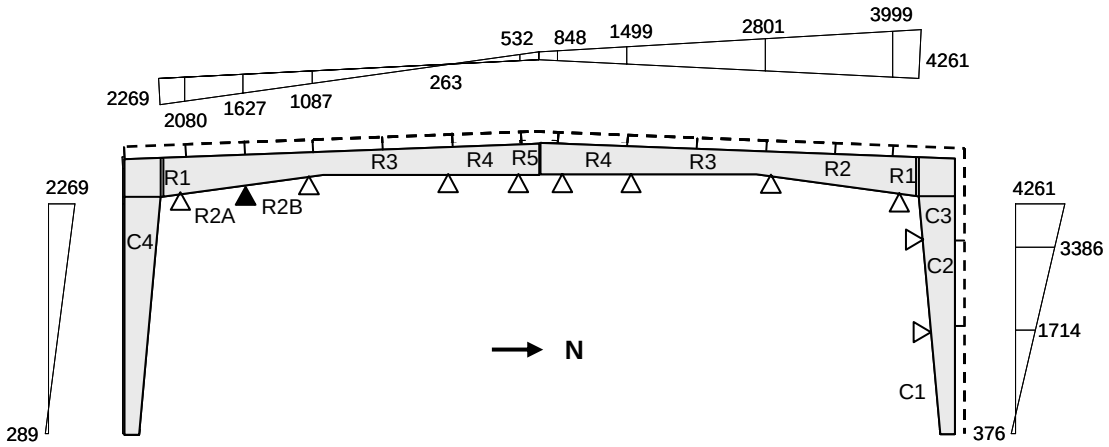

(b) Bending Moment Diagram

Figure 3.56 Frame 2: Internal Forces at Negative 2.3% Drift due to Combined Loads

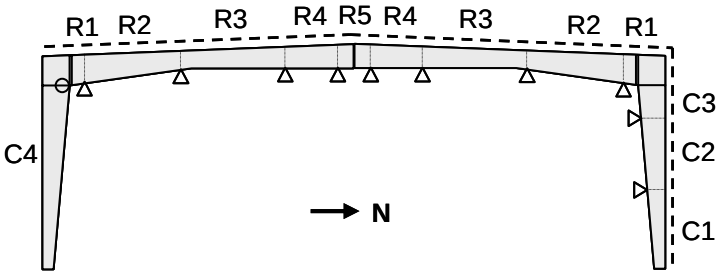

(a) Location

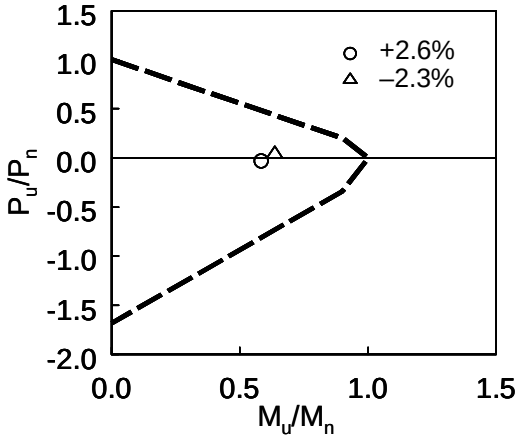

(b) Segment C1

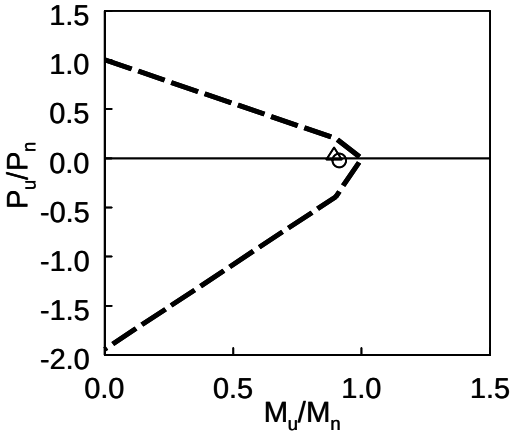

(c) Segment C2

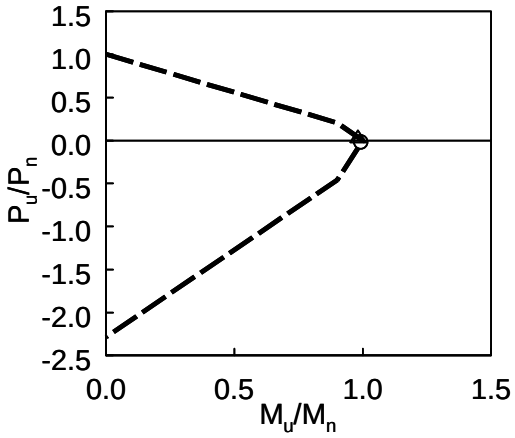

(d) Segment C3

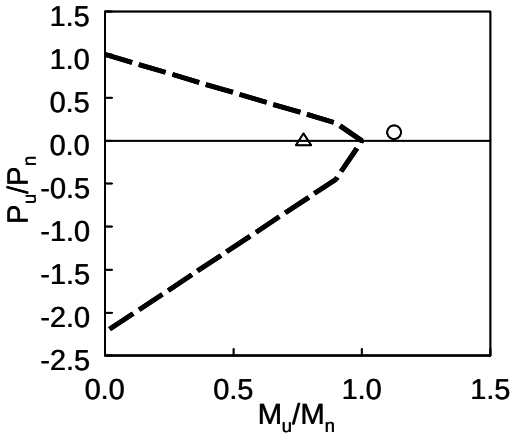

(e) Segment C4

Figure 3.57 Frame 1: Axial Force and Moment Interaction

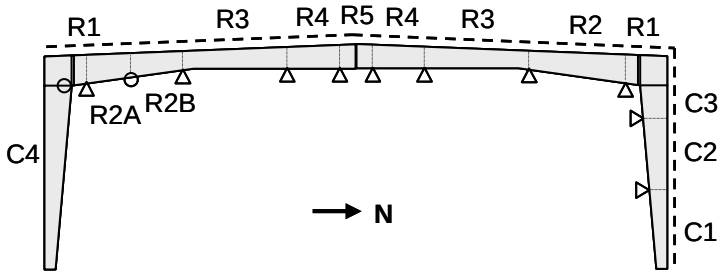

(a) Location

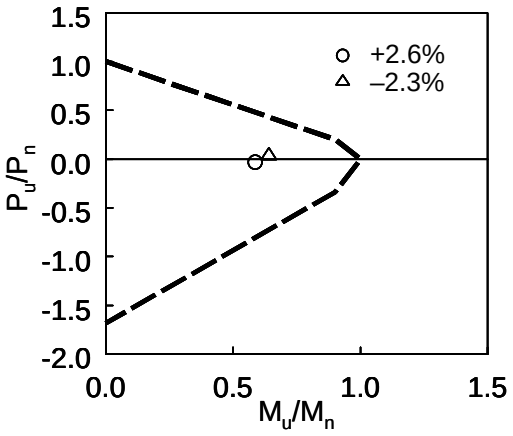

(b) Segment C1

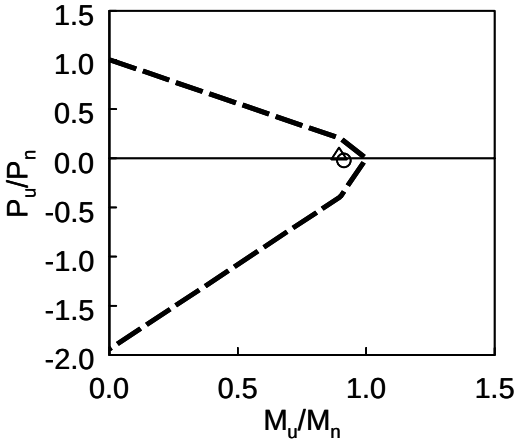

(c) Segment C2

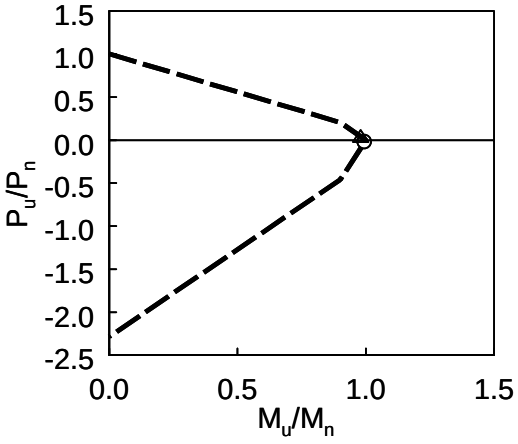

(d) Segment C3

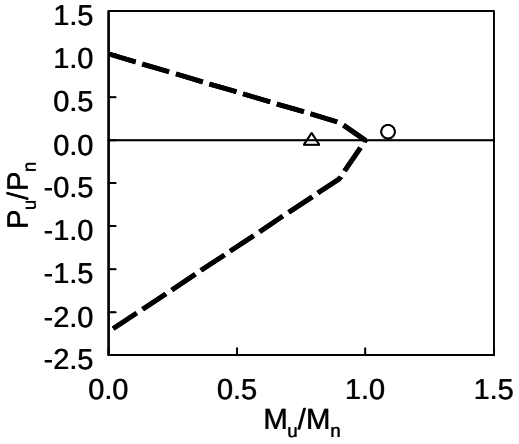

(e) Segment C4

Figure 3.58 Frame 2: Axial Force and Moment Interaction

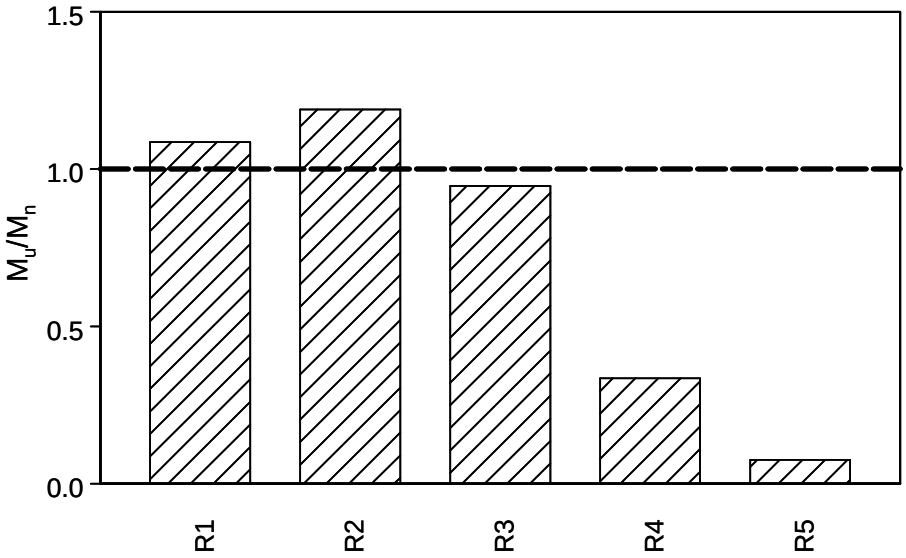

(a) Frame 1

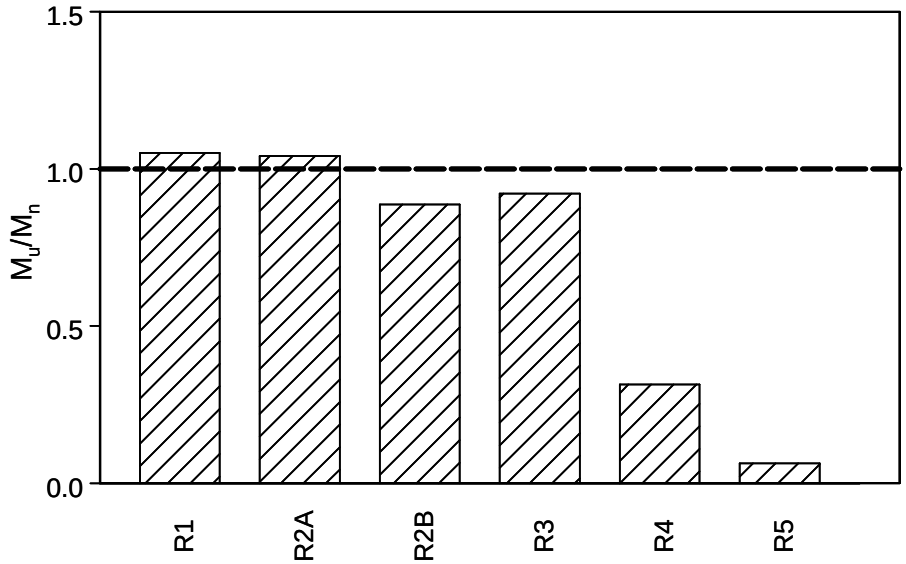

(b) Frame 2

Figure 3.59 South Rafter Strength Check at Positive 2.6% Drift

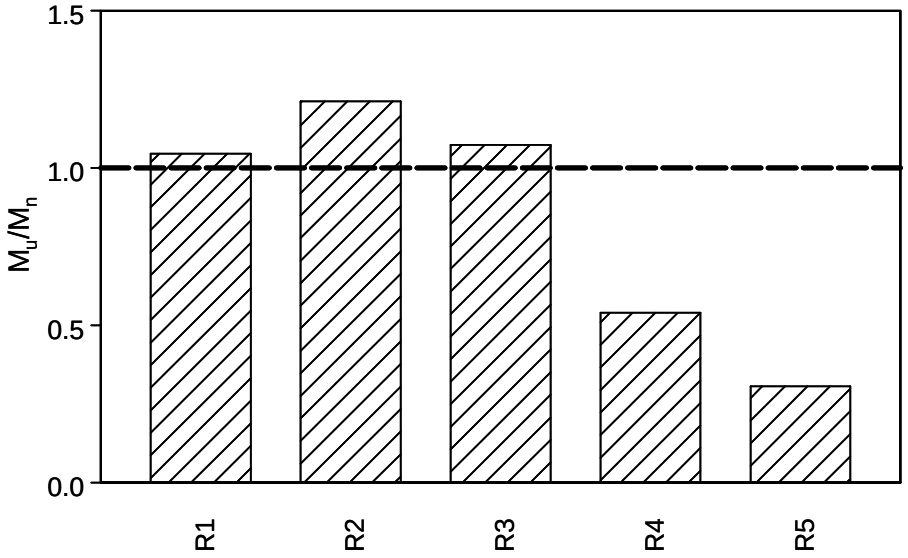

(a) Frame 1

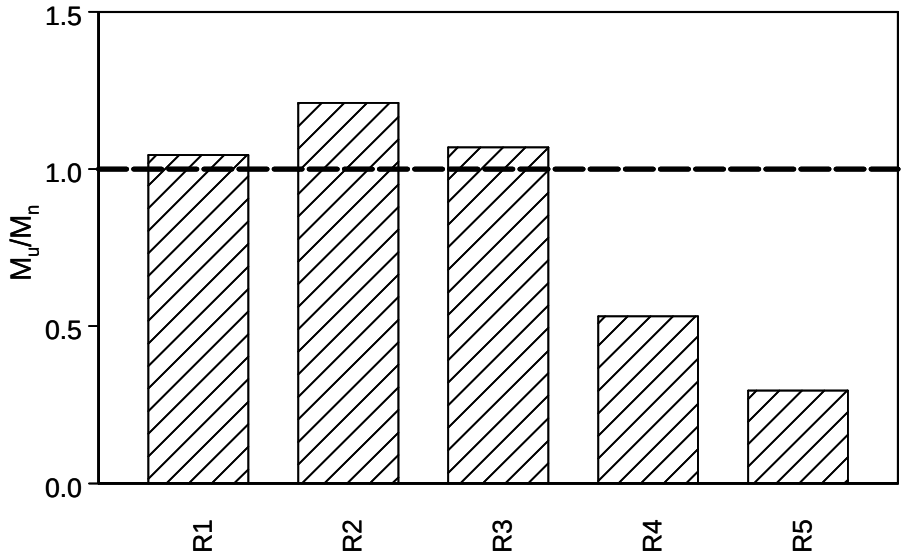

(b) Frame 2

Figure 3.60 North Rafter Strength Check at Negative 2.3% Drift

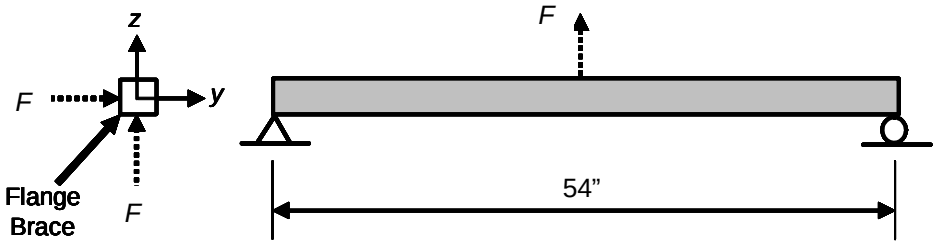

Figure 3.61 Flange Brace Force on HSS Supporting Beam

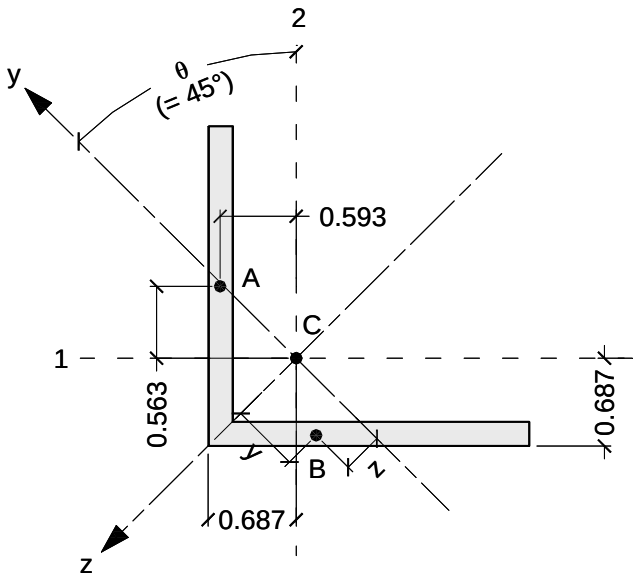

Figure 3.62 Flange Brace Angle Section (L2½×2½×3/16)

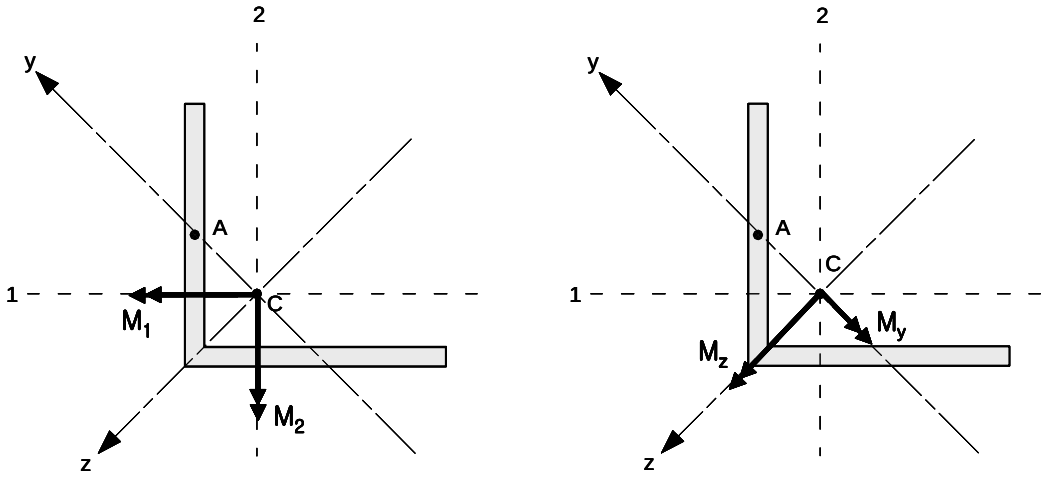

(a) Moment about Axes 1 and 2 (b) Moment about Axes y and z

Figure 3.63 Moment due to Axial Load at Flange Brace

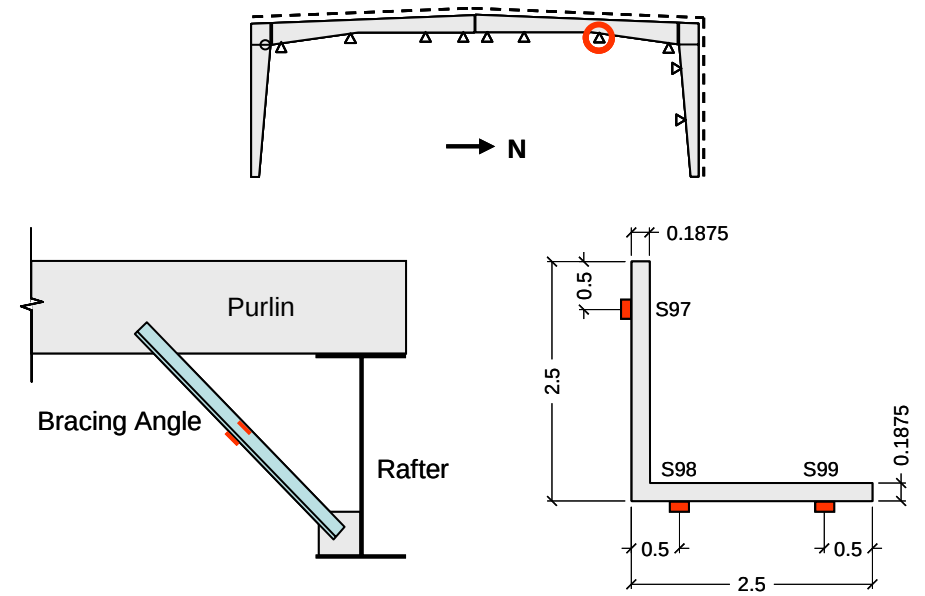

(a) Location

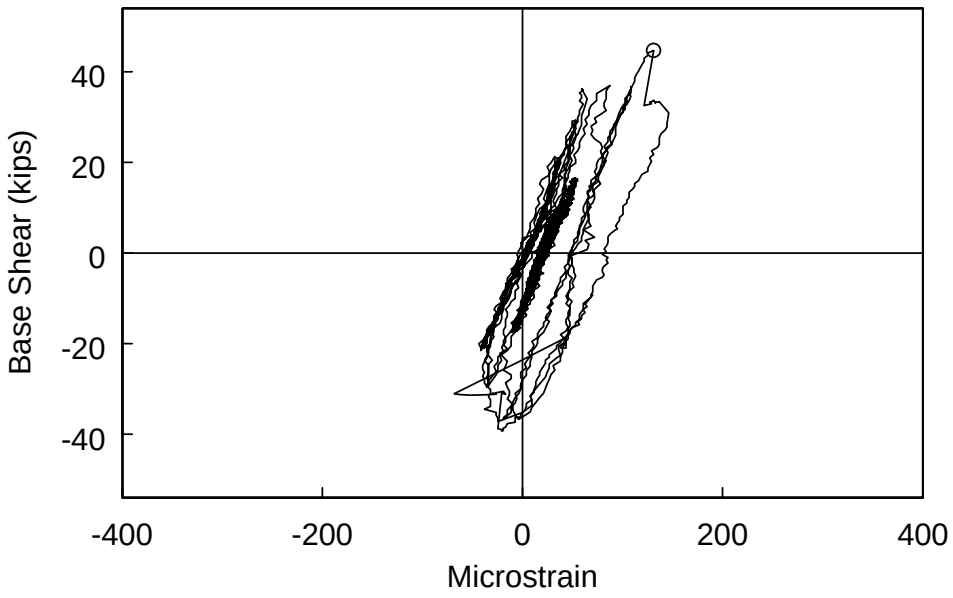

(b) Strain Gage S97

Figure 3.64 Frame 1: Measured Strain at Flange Brace

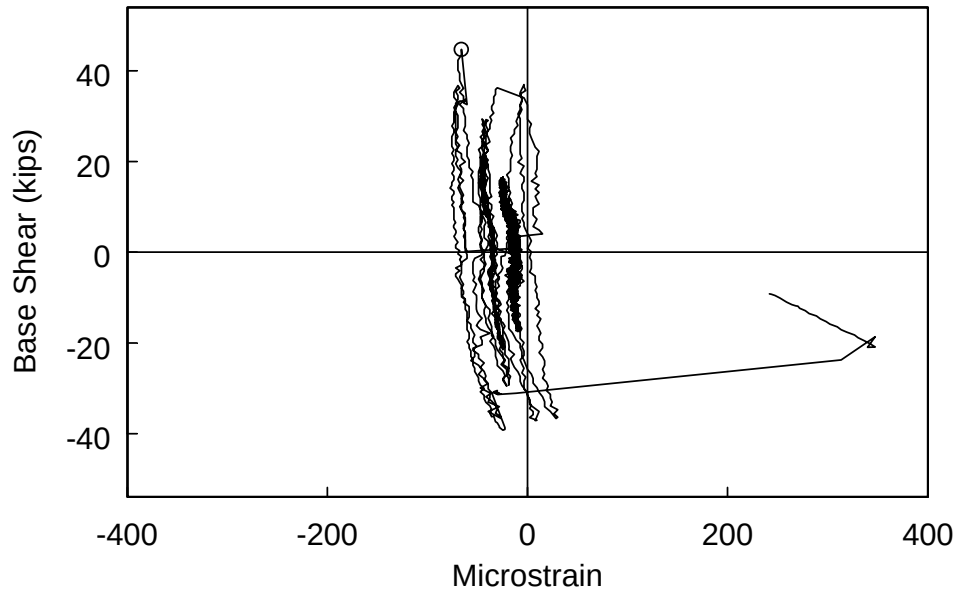

(c) Strain Gage S98

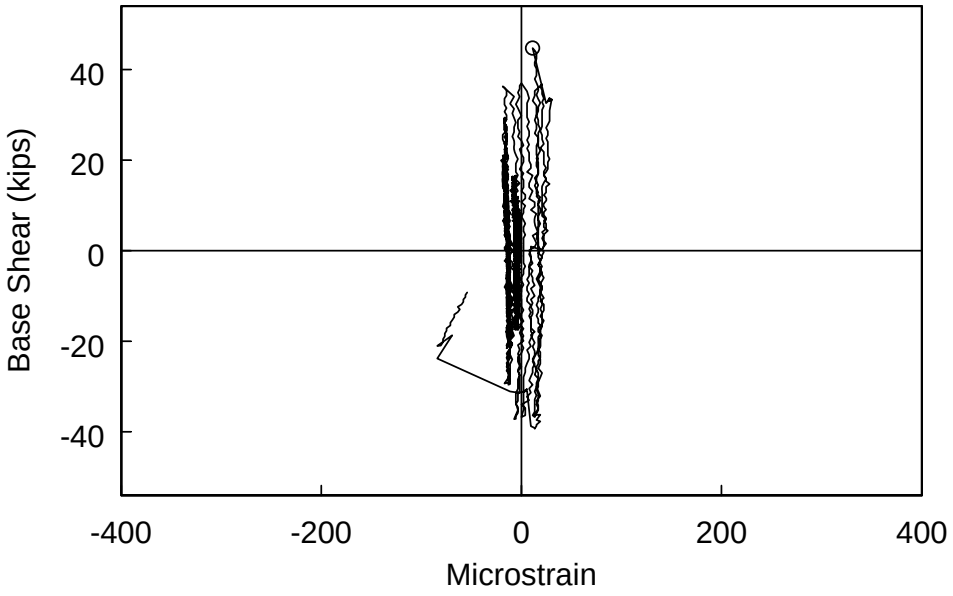

(d) Strain Gage S99

Figure 3.64 Frame 1: Measured Strain at Flange Brace (continued)

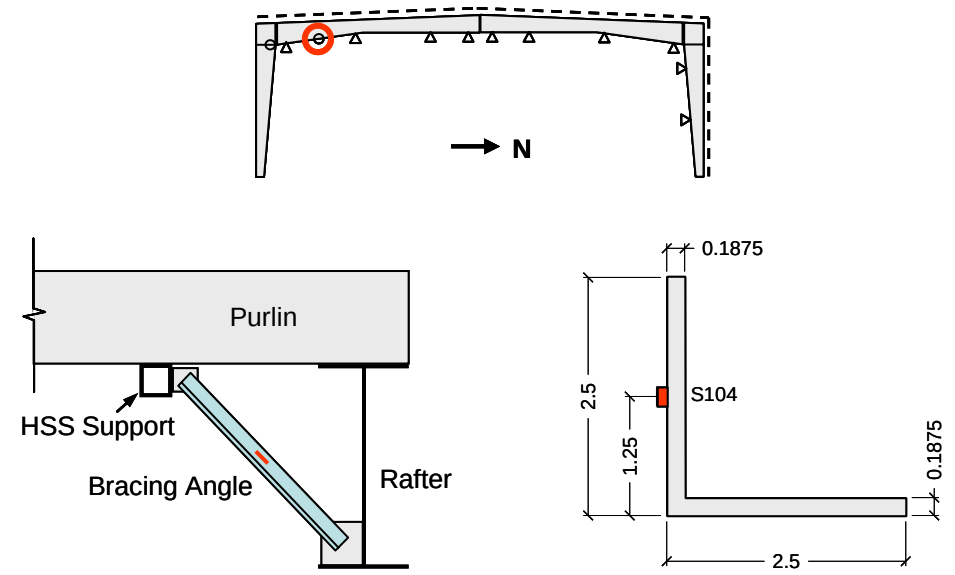

(a) Location

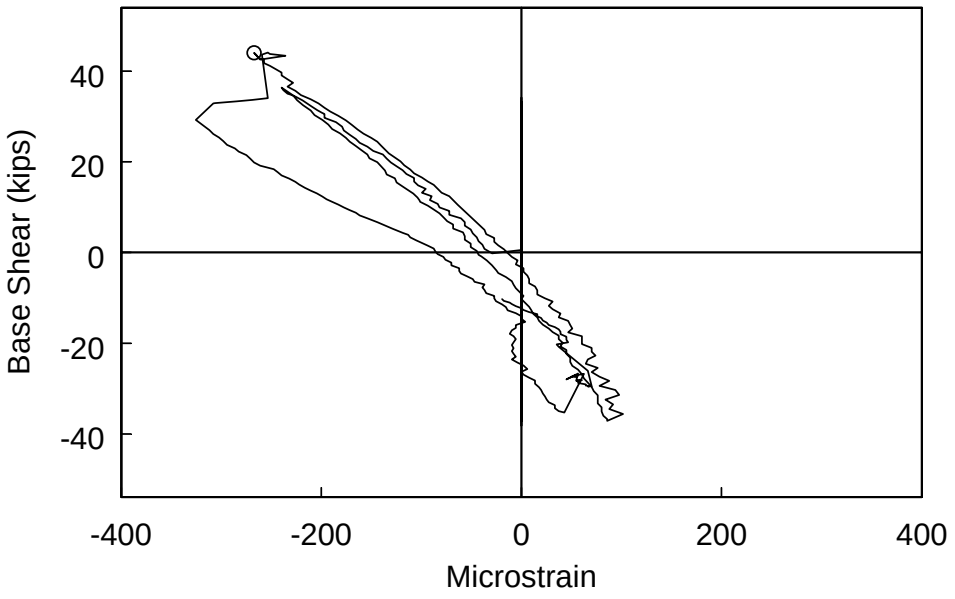

(b) Strain Gage S104

Figure 3.65 Frame 2: Measured Strain at Additional Flange Brace

4 FINITE ELEMENT ANALYSIS OF TEST FRAME

4.1 Introduction

A correlation study with the test results was performed using nonlinear finite element analysis. Section 4.2 addresses the modeling technique used in this study. Models predicted global and local behaviors of the frame and their correlation with test results is presented in Section 4.3. The effect of initial geometric imperfection through a parametric study is discussed in Section 4.4. The findings in this chapter are used to provide proper modeling techniques for this type of building system in Chapter 6.

4.2 Finite Element Modeling Technique

4.2.1 General

Finite element models that simulate geometry and material properties of the test frames were created using the software ABAQUS (ABAQUS Inc. 2005). The results of the finite element analysis complement the laboratory testing and provide additional insight and information on the test frame behavior.

4.2.2 Geometry and Element

The ABAQUS model is shown in Figure 4.1; rather than modeling the entire building explicitly, only one frame was modeled since the two frames were nominally identical. A total of four models were generated considering the column base boundary condition, initial geometric imperfection, and additional flange braces installed during testing (see Table 4.1). The column base was modeled as either a

hinge support or a semi-rigid connection adopting a rotational spring with an average spring constant value of 12,250 kip-in/rad obtained from the test. Initial geometric imperfection with the first buckling mode shape from a linearized eigen buckling analysis was employed for Models 2 through 4 with the amplitude of $L_b/1000$ (= 0.12 in.) based on the findings from Miller and Earls (2003 and 2005). For Models 2 and 3, the imperfection was introduced in the south rafter to simulate failure at positive 2.6% drift (see Figure 4.2). For Model 4, the imperfection was introduced in the south column by applying an 1-in. displacement in the out-of-plane direction at the end plate-to-continuity plate joint as well as in the north rafter using the first eigen buckling mode shape to simulate failure of Frame 2 at negative 2.3% drift. While the first three models represent the original test frame, two additional lateral braces for the rafter in Model 3 were added to represent the strengthened Frame 2 in Model 4 (see Figure 3.25). To incorporate the brace effect in the model, the out-of-plane deformation was fully restrained at the purlin, girt, and flange brace locations. Bolted end-plate connection was assumed rigid based on the test results (see Figure 3.32) and the associated surface interaction between end plates was not considered. Residual stresses were not considered in this study and the slippage of flange braces due to the use of long-slotted holes was also ignored.

Quadrilateral 4-node shell elements, ABAQUS S4R, with 6 degrees of freedom per node (three translational and three in-plane rotations) were used. A reduced integration scheme with one Gauss point in the center of each element was used for computational efficiency. The mesh was refined in the connection region and convergence studies were performed to ensure the mesh refinement was sufficient.

4.2.3 Material Properties

A tri-linear stress-strain relationship was utilized for the models as shown in Figure 4.3 (Mays 2000). Typical steel properties (E = 29,000 ksi, Poisson's ratio = 0.3) were used in the model to describe the elastic material properties, and the yield strength, F_y, of 55 ksi and the tensile strength, F_u, of 70 ksi was assumed. The plasticity in the models was based on a von Mises yield surface and associated flow rule. The plastic hardening was defined by an isotropic hardening law. The isotropic hardening component of the model defines the equivalent stress as a function of the equivalent plastic strain (ABAQUS Inc. 2005).

$$\sigma^0 = \sigma\big|_0 + Q_\infty (1 - e^{-b\bar{\varepsilon}^{pl}}) \tag{4.1}$$

where $\sigma|_0$ is the yield surface size as zero plastic strain, Q_∞ and b are additional material parameters, and $\bar{\varepsilon}^{pl}$ is the plastic strain.

4.2.4 Gravity Load and Monotonic Push

The gravity load (= 16.57 psf) was first applied at the purlin locations as concentrated loads based on their tributary areas. Monotonic lateral load was then applied at column tops, to which the actuators were attached, up to failure; the positive loading (north to south) was applied to Models 1 through 3, while the negative loading (south to north) was imposed to Model 4.

4.2.5 Post-Buckling Response

It is often necessary to obtain nonlinear static equilibrium solutions for unstable problems, where the load-displacement response can exhibit the type of behavior shown in Figure 4.4. This is the case for the test frame since the system is

characterized by a sudden strength degradation due to lateral buckling failure (see Figure 3.29). The modified Riks algorithm (Riks 1970; Crisfleld 1981; and Powell and Simpson 1981) was then used; this solution scheme was selected in order to trace the post-buckling range of the response. The load and/or the displacement may decrease as the solution evolves during periods of the response. It is assumed that the loading is proportional; that is the load magnitude varies with a single scalar parameter. In addition, it is assumed that the response is reasonably smooth so that sudden bifurcations do not occur.

The essence of the method is that the solution is viewed as the discovery of a single equilibrium path in a space defined by the nodal variables and the loading parameter. Development of the solution requires that it traverses the path as far as required. The basic algorithm remains the Newton method; therefore, at any time there will be a finite radius of convergence (ABAQUS Inc. 2005).

4.3 Correlation with Test Results

4.3.1 Gravity Load Analysis

Gravity load analysis was first performed. The predicted vertical deflection at midspan of the frame was 0.31 in. for all models. Note the measured deflections, 0.22 in. and 0.24 in. in Frames 1 and 2, respectively, was less. Normal stress distribution in all models was also similar and the maximum stress at both rafter ends was less than 4 ksi. Figure 4.5 showed the normal stress comparison with the test results. Good correlation was indicated at both rafter ends and column tops but some deviations were observed in the midspan of the rafter. That is probably due to the

stiffening effect from the roof panel and the attached wood panels used for the gravity load [see Figure 3.13(a)] at such low stress level.

4.3.2 Lateral Load Analysis

The analyses were halted at 7.8%, 3.9%, and 4.6% drift in Models 1, 2, and 3, respectively, due to a numerical convergence problem associated with buckling. The analysis of Model 1 which represented a perfectly straight condition showed flange local buckling at the narrowest sections of the rafter (see Figure 4.6), while the observed failure mode in the test was lateral buckling. On the other hand, Models 2 and 3 exhibited lateral buckling failure of the rafter (see Figures 4.7 and 4.8), although flange local buckling followed in Model 3.

Base shear versus lateral displacement of each model was compared with the recorded response in Figure 4.9. Model 1 did not capture the failure point and the predicted ultimate load was much higher than that from test, while Models 2 and 3 predicted the failure location and ultimate load with sufficient accuracy. Lateral stiffness of Model 3 was very close to the measured value due to the inclusion of rotational spring at column base. Models 1 and 2 predicted a lesser lateral stiffness because of the ideal hinge assumption at column base.

The analysis of Model 4 was halted at negative 3.6% drift due to a numerical convergence problem. The analysis results provided a reasonable prediction of the failure mode and the ultimate strength (see Figures 4.10 and 4.11). The predicted ultimate strength in the negative excursion is similar to the measured peak strength in the positive excursion. Since the test frame first experienced lateral buckling in the

positive excursion at 3% drift, a reduced ultimate strength in the subsequent negative excursion is expected.

4.4 Initial Geometric Imperfection

A parametric study on the effect of initial geometric imperfection was carried out with Model 3. First eigen buckling mode shape shown in Figure 4.2 was used as an imperfection with the variation of the maximum amplitude, and the predicted ultimate load was compared with that measured from test.

Regardless of the amplitude, lateral buckling failure mode (see Figure 4.8) was predicted as long as the initial geometric imperfection was introduced. Global responses shown in Figure 4.12 indicated that the ultimate load prediction was not sensitive to the scaling factor of between $L_b/500$ and $L_b/5000$, and corresponded well with the test data. Table 4.2 summarizes the predicted load and the error of each considered case.

4.5 Summary and Conclusions

Finite element analysis of the test frame was conducted using the software ABAQUS (ABAQUS Inc. 2005). First buckling mode shape from the linearized eigen buckling analysis was employed to simulate initial geometric imperfection. To overcome the convergence problems associated with post-buckling in thin structure, modified Riks method was adopted.

(1) All models predicted a vertical deflection at midspan which is about 35% larger than the measured value under gravity load. That is probably due to

the strengthening effect from the roof panel and the attached wood panel (gravity load) which was not considered in the models.

(2) The model without an initial geometric imperfection predicted a different failure mode (flange local buckling) and the ultimate load was much higher than the measured.

(3) Models with an initial imperfection corresponded well with the test results in terms of the buckling failure mode and the ultimate load capacity.

(4) For lateral stiffness and ultimate load, the model with a rotational spring at column base predicted most accurately, but the results from the model with an ideal hinge at column base was also acceptable when an initial geometric imperfection was introduced.

(5) A parametric study showed that the acceptable range of initial imperfection amplitude was between $L_b/500$ and $L_b/5000$; the most accurate prediction was obtained with an amplitude of $L_b/1000$ for the cases considered.

Table 4.1 ABAQUS Modeling Matrix

Model	Column Base	Initial Imperfection[1]	Additional Brace
1	Hinge	N/A – Positive Loading	N/A
2	Hinge	First Eigen Buckling Mode Shape (South Rafter) – Positive Loading	N/A
3	Rotational Spring	First Eigen Buckling Mode Shape (South Rafter) – Positive Loading	N/A
4	Rotational Spring	First Eigen Buckling Mode Shape (north rafter) and 1 in Out-of-Plane Displacement (south column and rafter) – Negative Loading	Two Flange Braces at South Rafter

[1] Amplitude = $L_b/1000$, where L_b is the unbraced length of rafter.

Table 4.2 Initial Imperfection Amplitude Effect on Ultimate Load Prediction

Amplitude[1]	Predicted Ultimate Load (kips)	Error (%)[2]
$L_b/100$ (= 1.2 in.)	38.9	-12.93
$L_b/500$ (= 0.24 in.)	43.7	-2.19
$L_b/1000$ (= 0.12 in.)	45.3	+1.36
$L_b/1500$ (= 0.08 in.)	45.9	+2.75
$L_b/2000$ (= 0.06 in.)	46.3	+3.57
$L_b/5000$ (= 0.024 in.)	47.1	+5.38

[1] Value in parenthesis represents the maximum imperfection amplitude
[2] Positive represents overestimation; Negative represents underestimation

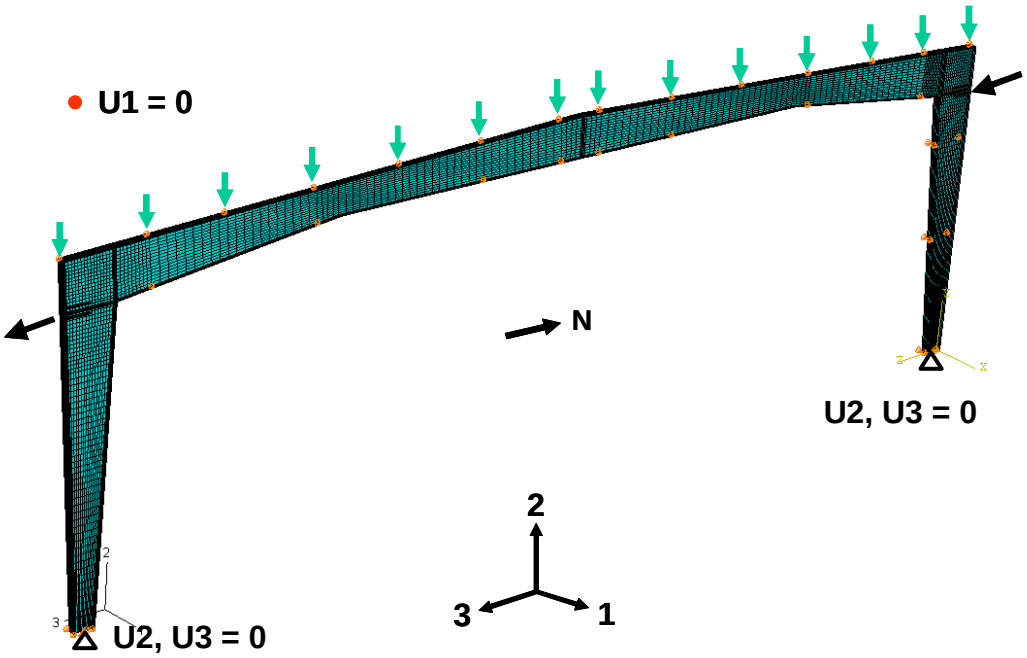

Figure 4.1 ABAQUS Model of Test Frame (Loading in Positive Direction)

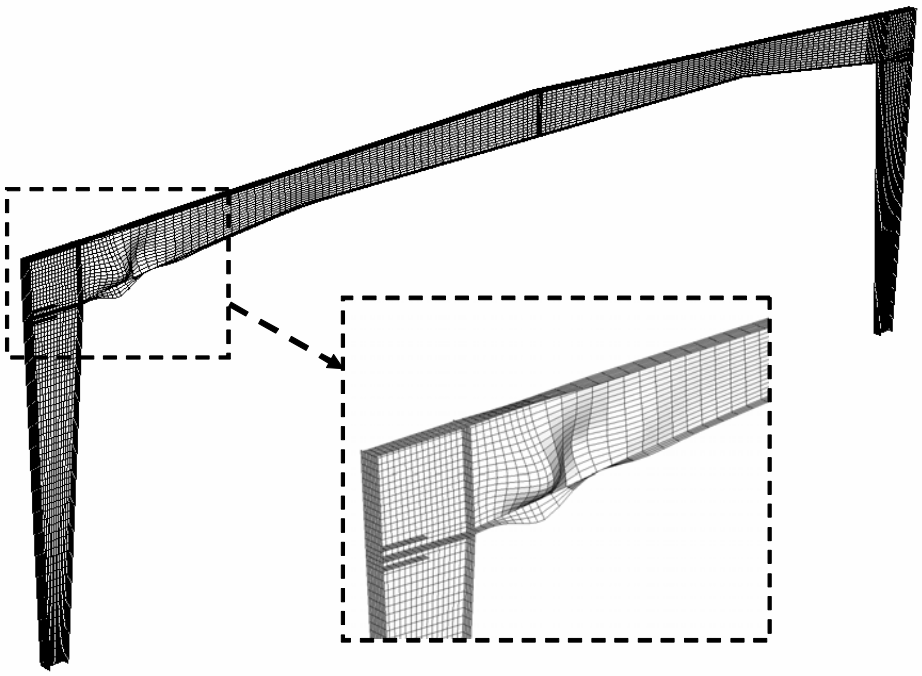

Figure 4.2 First Eigen Buckling Mode Shape for Models 2 and 3

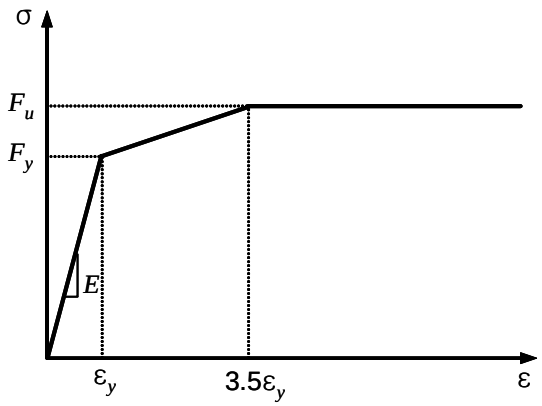

Figure 4.3 Stress-Strain Relationship (Mays 2000)

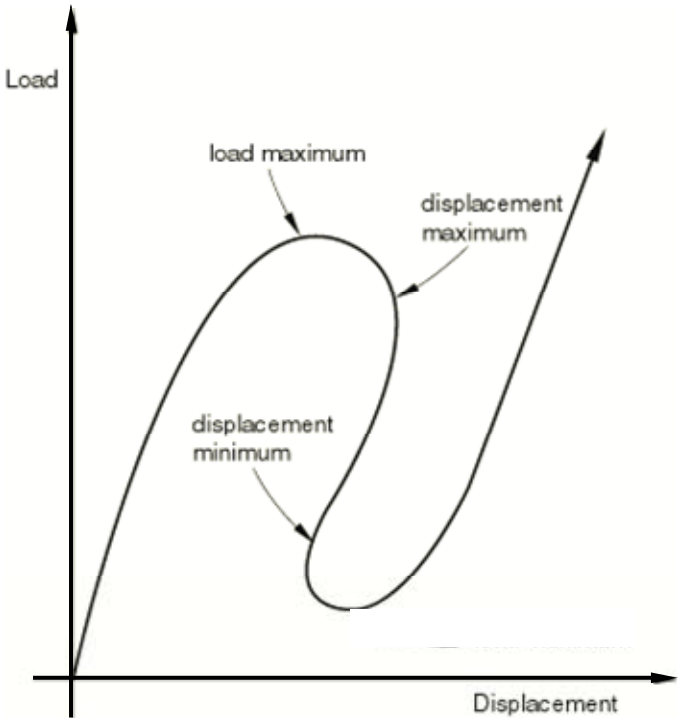

Figure 4.4 Typical Unstable Static Response (ABAQUS Inc. 2005)

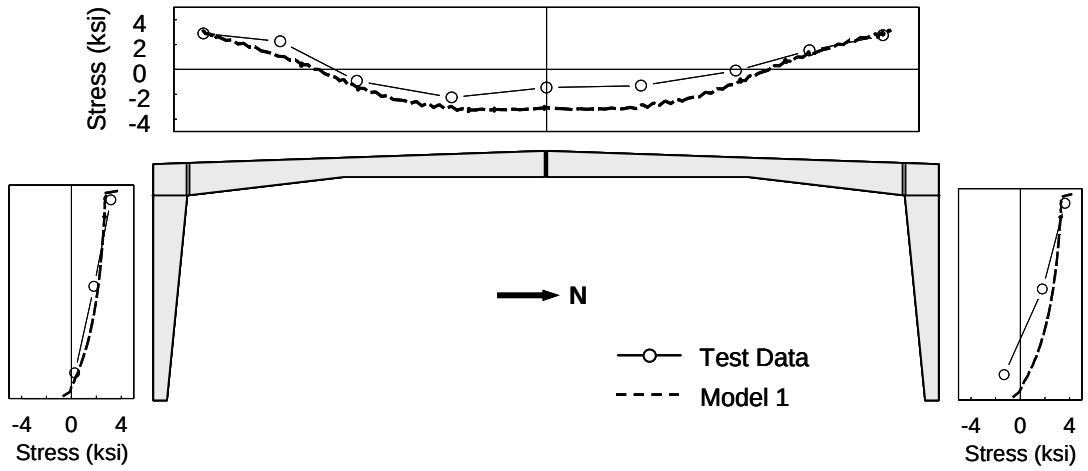

(a) Frame 1

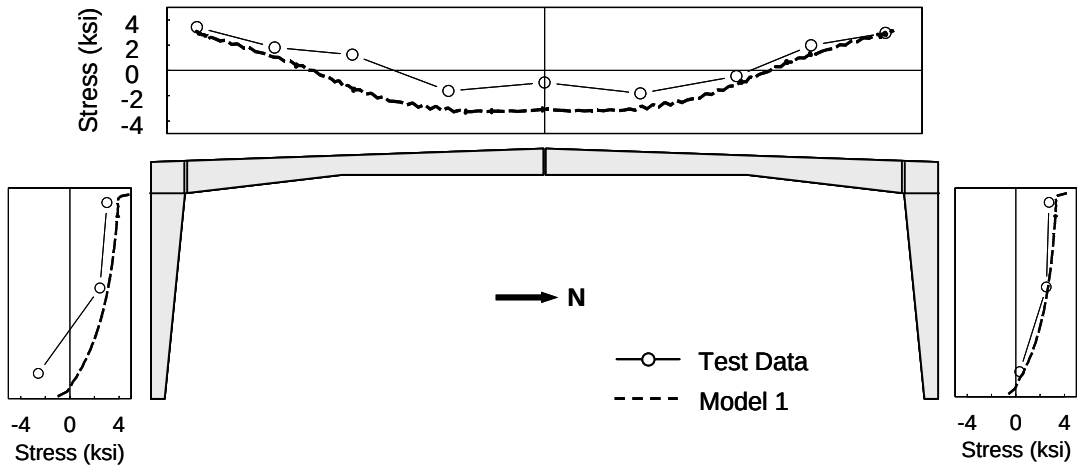

(b) Frame 2

Figure 4.5 Normal Stress Comparison

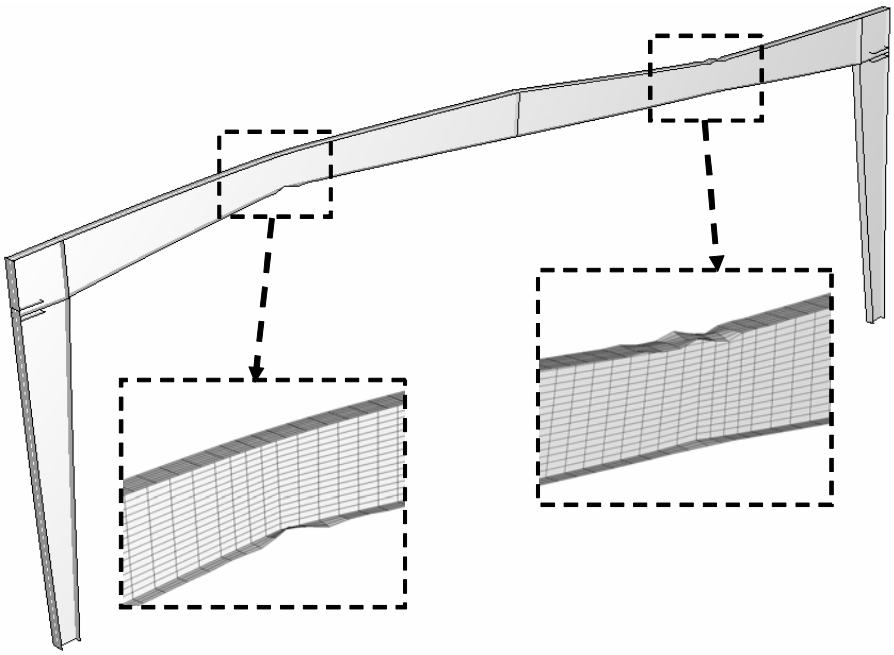

Figure 4.6 Flange Buckling Failure Mode of Model 1

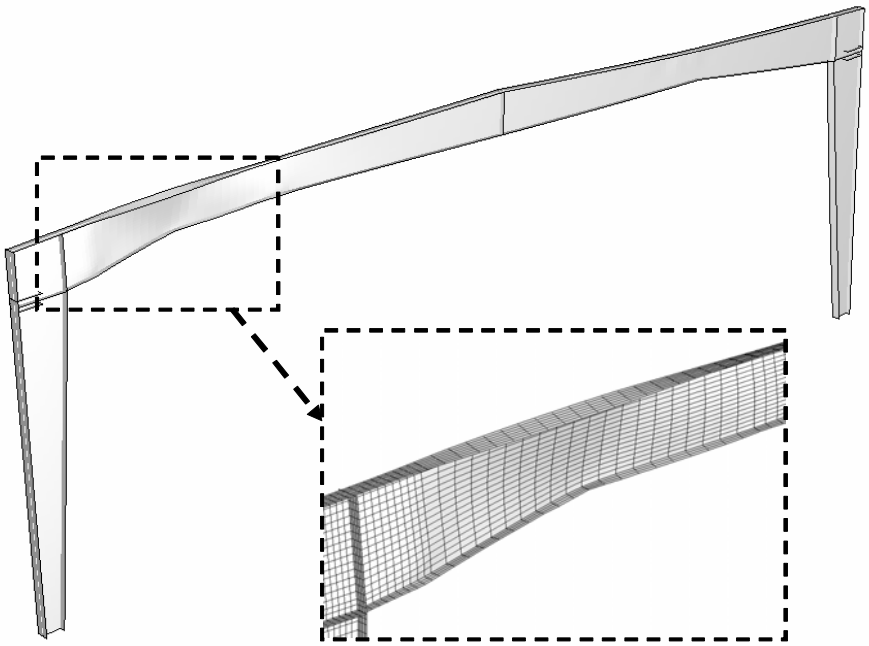

Figure 4.7 Lateral Buckling Failure Mode of Model 2

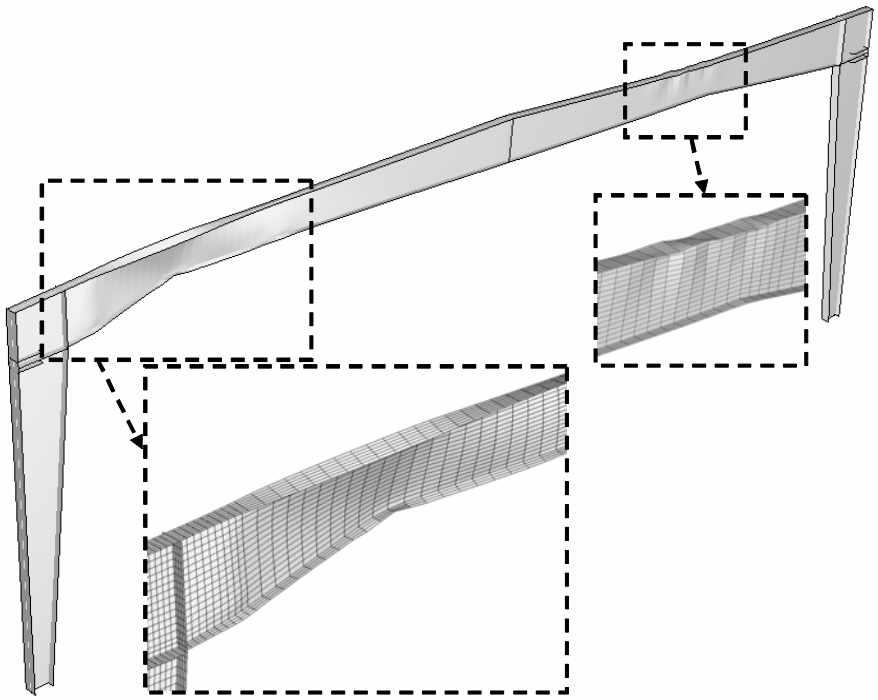

Figure 4.8 Flange Local Buckling and Lateral Buckling Failure Mode of Model 3

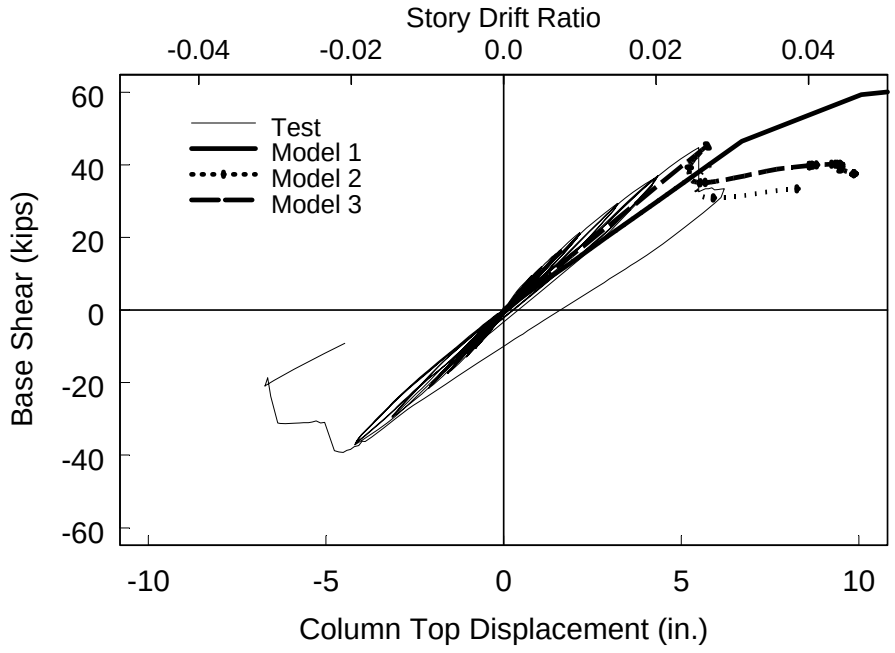

Figure 4.9 Base Shear versus Lateral Displacement Comparison

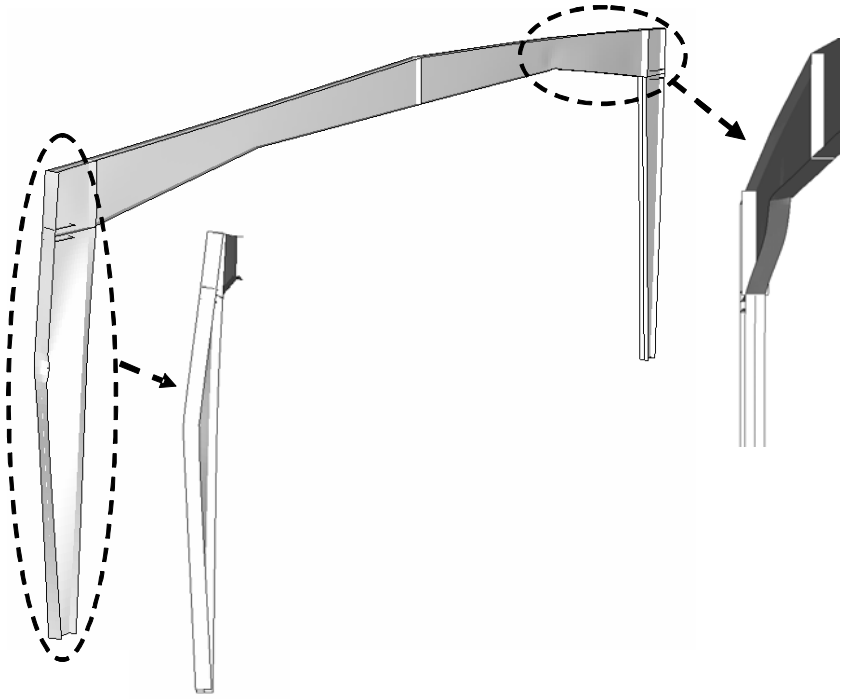

Figure 4.10 Predicted Failure Mode of Model 4

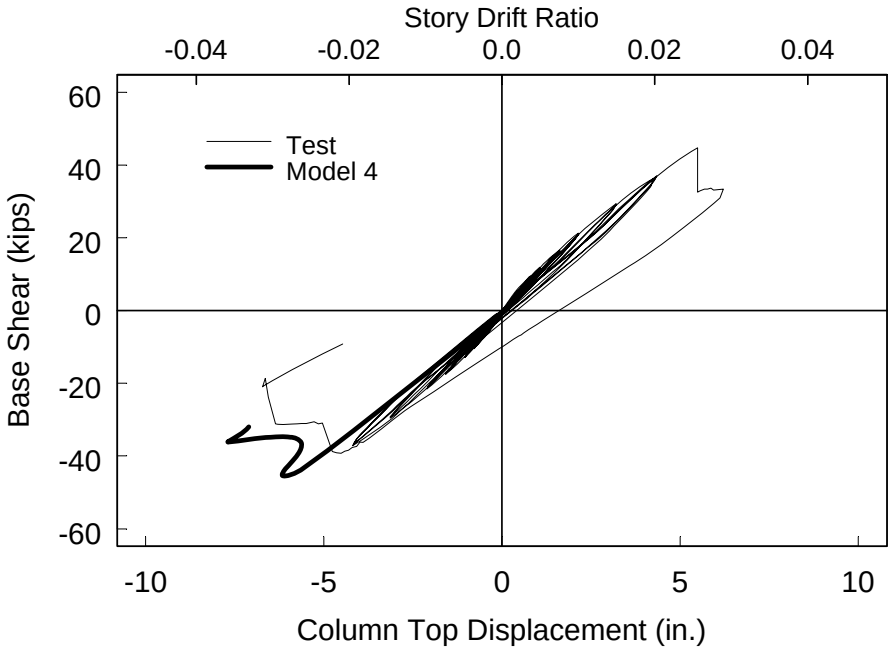

Figure 4.11 Global Response Comparison

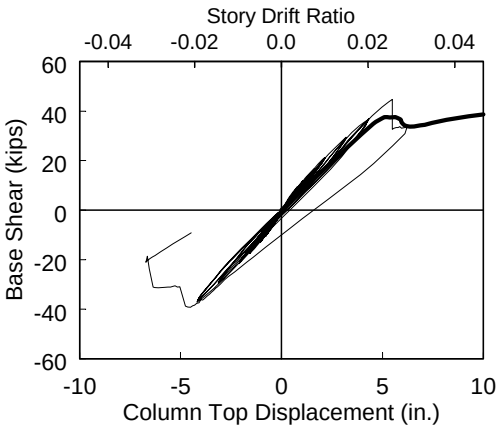

(a) $L_b/100$

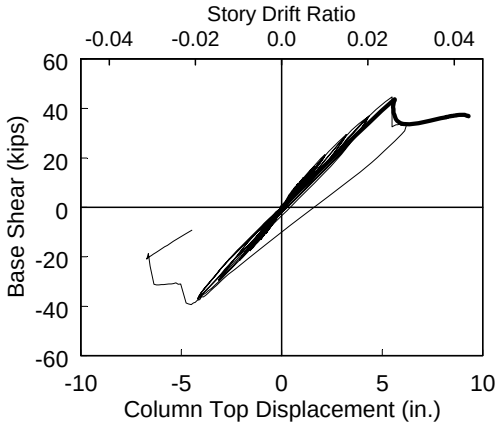

(b) $L_b/500$

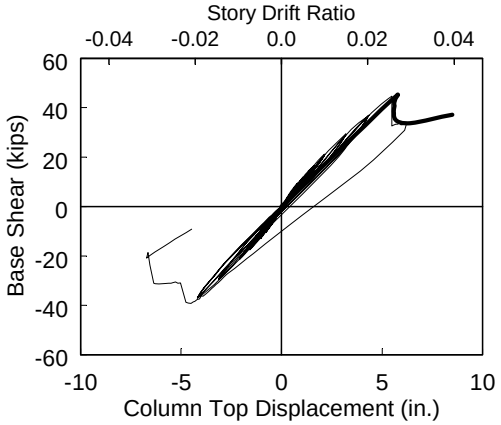

(c) $L_b/1000$

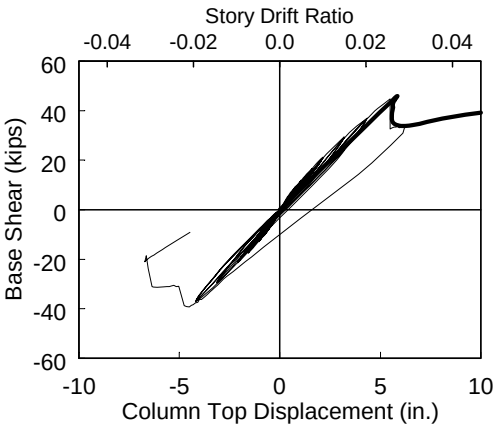

(d) $L_b/1500$

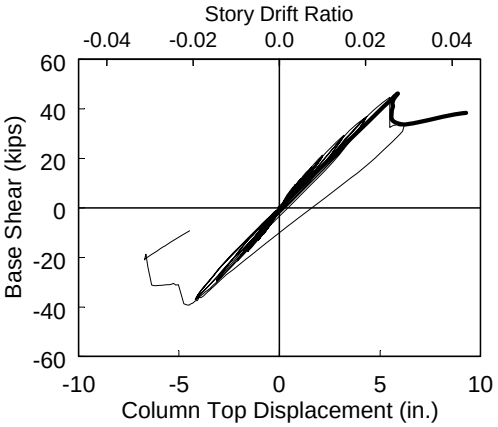

(e) $L_b/2000$

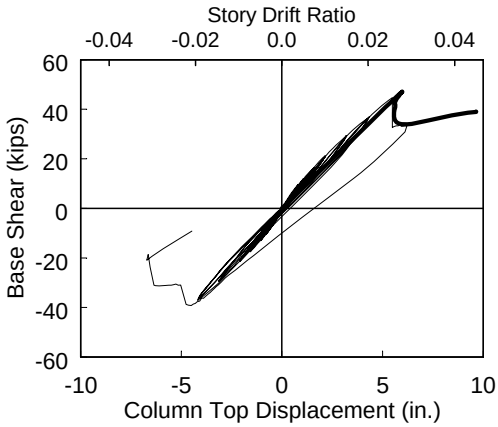

(f) $L_b/5000$

Figure 4.12 Initial Imperfection Effect on Global Response

5 DEVELOPMENT OF A SEISMIC DESIGN PROCEDURE

5.1 Introduction

A new seismic design procedure based on story drift was developed for metal building systems. Section 5.2 addresses the general concept of the new procedure. Sections 5.3 and 5.4 discuss important design parameters that are used in the approach. The effects of the damping ratio (ξ) and the response modification factor (*R*-factor) are investigated in Sections 5.5 and 5.6. Section 5.7 presents the simplified seismic design procedure considering the drift capacity and demand of metal buildings.

5.2 Drift-Based Design Concept

It was shown in the cyclic test of a metal building in Chapter 3 that the system has little ductility; the behavior of the system was characterized by the elastic response and sudden strength degradation as soon as the ultimate load was reached (see Figure 3.29). Test results also demonstrated that the strength evaluation for web-tapered members specified in the code provisions (AISC 2001) is sufficiently accurate. For the development of a new seismic design procedure, it is then assumed that the system behaves elastically, but fails once any one of the members reaches its strength based on the code provisions.

Figure 5.1 shows the general idea of the new seismic design procedure. Consider the governing earthquake load combination, which is usually governed by Eq. (3.7):

$$1.2D + f_1L + f_2S + 1.0E \tag{5.1}$$

where the first three terms represent the gravity load effect, and the last term represents the earthquake load effect. In a routine design the most critical unbraced segment based on the above earthquake load combination can be identified. Consider the axial-flexural interaction domain of this critical member, the yield surface based on the *AISC LRFD Specification* (AISC 2001) is

$$\frac{P_u}{\phi P_n} + \frac{8}{9}\frac{M_u}{\phi M_n} \le 1.0 \quad \text{when} \quad \frac{P_u}{\phi P_n} \ge 0.2 \tag{5.2}$$

$$\frac{P_u}{2\phi P_n} + \frac{M_u}{\phi M_n} \le 1.0 \quad \text{when} \quad \frac{P_u}{\phi P_n} < 0.2 \tag{5.3}$$

The gravity load effect can be represented by vector OA, and the eqrthquake load effect is represented by vector AB. Representing these load effects in the form of demand-capacity ratio (DCR), the DCRs for both the gravity load (i.e., DCR_G) and the earthquake load (i.e., DCR_E) are shown in Figure 5.1(a). If the vector AB is scaled by a multiplier Ω_o such that point B is on the yield surface, the critical member has reached its strength and the frame fails. This multiplier, which can be easily calculated in the design process, is defined as the system overstrength. That is, Ω_o is a multiplier for the code specified design base shear such that the collapse limit state of the frame reached.

Figure 5.1(b) shows the corresponding base shear versus story drift relationship. The required elastic earthquake force, E_D, specified in IBC (point D) is reduced by the response modification factor, R, to the code prescribed design earthquake force level, E_h, (point B). Since the frame lacks ductility, the response is linear elastic until the critical member reaches its strength limit state (point C).

Recall that the system overstrength Ω_o represents the ratio between the strength levels at C and B. Therefore, the story drift capacity, Δ_C, of the frame can also be calculated as follows:

$$\Delta_C = \Omega_o \Delta_S \tag{5.4}$$

The goal of this design procedure is to ensure that the story drift capacity, Δ_C, is larger than the elastic drift demand, Δ_D, due to E_D by a certain safety margin. Further discussions regarding the evaluation of the story drift and the base shear are given in Section 5.4.3.

5.3 System Overstrength Factor, Ω_o

The system overstrength factor, Ω_o, is one of the most important parameters to be calculated in this design procedure. Since the design of this type of building system is typically governed by non-seismic load combinations, the system can have a sufficient reserve of strength for the earthquake load combination. It was shown from the cyclic test that the system overstrength factor was 9.31 and 9.18 for Frames 1 and 2, respectively (see Section 3.5). Test results also indicated that failure in the most critical unbraced member resulted in a significant strength loss at the system level. Hence, the overstrength factor of the critical component is the key parameter to determining the system behavior.

In order to identify the critical segment, a strength check is required based on the axial and flexural interaction, and the overstrength factor is calculated as shown in Figure 5.1(a) for each unbraced segment. Since the DCR for each unbraced segment

is calculated routine design, the calculation of the system overstrength factor is straight forward. That is, the smallest DCRis then the system overstrength factor, Ω_o.

5.4 Fundamental Period

5.4.1 Design Seismic Base Shear

According to ASCE 7-05, the fundamental period of the structure, *T*, in the direction under consideration shall be established in the determination of either the equivalent lateral force or the drift using the structural properties and deformational characteristics of the resisting elements in a properly substantiated analysis. But the fundamental period, *T*, shall not exceed the product of the coefficient (C_u) for upper limit on calculated period from Table 5.1 and the approximate fundamental period, T_a, from Eq. (5.5) for the seismic force determination:

$$T_a = C_t h_n^x \tag{5.5}$$

where h_n is the height in ft above the base to the highest level of the structure and the coefficients C_t and x are determined from Table 5.2. For a building with a sloping roof, the height at the eave of the building should be used (MBMA 2004). As an alternative to performing an analysis to determine the fundamental period, *T*, it is permitted to use the approximate building period, T_a (mostly smaller than *T*), for the evaluation of the design base shear (ASCE 2005). Note that ASCE 7-05 permits that the elastic story drift be computed for seismic design force based on the computed fundamental period of the structure without the upper limit (= $C_u T_a$)

The design seismic base shear, *V*, can be determined as follow:

$$V = C_s W \tag{5.6}$$

where C_s is the seismic response coefficient and W is the effective seismic weight. The seismic response coefficient, C_s, can be determined by dividing the spectral response acceleration, S_a, from the design response spectrum shown in Figure 5.2 by the response modification factor, R.

5.4.2 T versus T_a

Study on dynamic characteristics of metal buildings is very limited. Sockalingam (1988) conducted a vibration test on a single-story metal building (see Figure 5.3); the prototype building was composed of web-tapered rafters and columns, and had a dimension of 130 ft wide by 60 ft long by 22 ft eave high. Three frames (two end frames and one middle frame) were spaced at 30 ft and a gravity column was located at mid-span of each frame. The free vibration test results are summarized in Table 5.3. The measured average frequency for the first mode was about 1.1 Hz, which corresponded to the fundamental period of 0.9 second.

If the fundamental period of the prototype building is estimated based on ASCE 7-05, T_a is 0.33 second [= $(0.028)(22)^{0.8}$]. The approximate method underestimates the fundamental period with an error of almost 300%, and in turn, results in a much higher design base shear. Since the T_a formula in ASCE 7-05 is developed for conventional multi-story buildings and is merely a function of the building height [see Eq. (5.5)], the direct application of T_a to the low-rise metal buildings is not reasonable. Actual period of the frame should always be calculated in the proposed seismic design procedure. The upper limit ($C_u T_a$) on calculated period is also not applicable for the seismic design of metal buildings.

5.4.3 Story Drift Evaluation

In conventional seismic design of multistory frames when inelastic action is expected, the design story drift (i.e., maximum inelastic drift) is calculated by multiplying Δ_S in Figure 5.1(b) by a deflection amplification factor, C_d. Since metal buildings investigated are expected to remain elastic and the frames can be modeled as a single-degree-of-freedom system, the well-known relationship between maximum displacement (i.e., spectral displacement) and spectral acceleration can be used (Chopra 2001):

$$\Delta_D = \left(\frac{T}{2\pi}\right)^2 \times S_a \times g \tag{5.7}$$

where T is the computed (actual) fundamental period, S_a is the spectral response acceleration (see Figure 5.2), and g is the acceleration of gravity.

5.5 Influence of Damping

The design base shear in ASCE 7 is determined utilizing the spectral response acceleration, S_a, based on a damping ratio (ξ) of 5%. When a building has a damping ratio of other than 5%, the use of code-specified spectral acceleration results in an unrealistic design base shear. In such case, S_a needs to be adjusted to reflect the actual damping ratio and the guideline for the adjustment of the spectral response acceleration is defined in FEMA 273 (BSSC 1997).

Figure 5.4 shows the general response spectrum, and the damping coefficients (B_S and B_1) are summarized in Table 5.4. If a damping ratio of 2%, for instance, is considered, the damping coefficients are 0.8 for both B_S and B_1. Then, S_a is increased

by 1/0.8 (= 1.25) and the corresponding design base shear is 25% higher than that from 5% damping.

It is conceived that the damping ratio of metal buildings is relatively low compare to that (5%) generally assumed for conventional steel buildings. Sockalingam (1988) showed that the damping ratio is between 2.3% and 2.8% for the first mode from free vibration tests on a metal building (see Table 5.3). Assuming the damping ratio of a typical metal building is 2.5%, the coefficients of B_S and B_1 are 0.83 from linear interpolation and then, the design base shear is increased by 20% (= 1/0.83).

5.6 Influence of *R*-Factor

Moment frames in metal buildings are typically designed as Ordinary Moment Frames (OMFs) with an *R*-factor of 3.5 (ASCE 2005). Consider the linear relation provided in this design procedure as shown in Figure 5.1(b). If the value of *R* is reduced by half, E_h and Δ_S are doubled. But the system overstrength factor, Ω_o, is also reduced by half, which results in the same Δ_C value. This observation is also true if the value of *R* is doubled. Therefore, this design procedure is independent of the *R* value due to the canceling effect from linear relation.

5.7 Simplified Design Procedure

Based on the background information discussed in Sections 5.2 through 5.6, the proposed seismic design procedure for metal buildings follows (see Figure 5.5):

STEP 1 – Perform preliminary frame design based on IBC and consider all load combinations.

In this step, the response modification factor R = 3.5 and the approximated fundamental period ($T_a = C_t h_n^x$) are assumed for seismic design.

STEP 2 – Compute the actual fundamental period:

$$T = 2\pi\sqrt{\frac{W}{gk}} \tag{5.8}$$

where W = effective weight (kips)

g = acceleration of gravity (= 386.4 in/sec^2)

k = frame lateral stiffness (kip/in), which can be obtained from a static load analysis in Step 1.

STEP 3 – Re-compute the earthquake load and calculate the system overstrength factor.

Revise the earthquake load based on the actual fundamental period, T, without an upper limit (= $C_u T_a$) and determine the system overstrength factor, Ω_o [see Figure 5.1(a)].

STEP 4 – Check if the frame has sufficient margin of safety against collapse:

$$\frac{\Omega_o}{R} \geq 1.4. \tag{5.9}$$

A re-design is needed if the above requirement is not satisfied

Note that Ω_o/R in Eq. (5.9) equals the ratio between the story drift capacity and demand:

$$\frac{\Delta_C}{\Delta_D} = \Delta_S \Omega_o = \frac{\Omega_o}{R} \tag{5.10}$$

A safety factor of 1.4 is recommended. This value also includes the effect of lower damping of the frame which is not considered in routine design.

STEP 5 – Connection design.

The seismic force for the connection design is based on the seismic force from Step 3 multiplied by 1.4*R*.

5.8 Summary and Conclusions

A drift-based seismic design procedure was developed for metal buildings. The design procedure assumes that the frame will respond elastically, and that the failure occurs when any one of the members reaches its ultimate strength. The design goal is to make sure that the drift capacity, Δ_C, of the system is larger than the drift demand, Δ_D, by a sufficient margin, which is assured, by checking if the calculated system overstrength factor, Ω_o, is larger than the response modification factor, *R*, by a factor of safety (= 1.4).

(1) The system overstrength factor, Ω_o, of the critical component is one of the most important parameters in this procedure. The system overstrength factor in a member is the multiplier to the design earthquake load effect such that the strength limit state (buckling) is reached.

(2) The actual fundamental period, *T*, should be used to calculate both the earthquake load and the story drift. The use of *T*, instead of the approximated

fundamental period, T_a, reflects not only the actual earthquake force but also the actual overstrength for the drift determination.

(3) The current design provisions utilize 5% damping although the actual damping ratio of metal buildings is less (≈ 2 to 3%); the proposed factor of safety (= 1.4) partially reflects the non-conservative nature of the current design provisions for metal building design.

(4) The proposed design procedure is independent of the R value due to the canceling effect from linear relationship. Using an R value of 3.5 is appropriate for preliminary design. The adequacy of such design is then verified by the proposed design procedure.

Table 5.1 Coefficient for Upper Limit on Calculated Period (ASCE 7-05)

Design Spectral Response Acceleration Parameter at 1 sec, S_{D1}	Coefficient C_u
≥ 0.4	1.4
0.3	1.4
0.2	1.5
0.15	1.6
≤ 0.1	1.7

Table 5.2 Values of Approximate Period Parameters C_t and x (ASCE 7-05)

Structure Type	C_t	x
Moment-resisting frame systems in which the frames resist 100% of the required seismic force and are not enclosed or adjoined by components that are more rigid and will prevent the frames from deflecting where subjected to seismic forces:		
Steel moment-resisting frames	0.028	0.8
Concrete moment-resisting frames	0.016	0.9
Eccentrically braced steel frames	0.03	0.75
All other structural systems	0.02	0.75

Table 5.3 Dynamic Properties of a Metal Building from Free Vibration Tests (Sockalingam 1988)

Loaded Frame	Mode	Applied Force (lb)	Frequency (Hz)	Damping (%)
Middle	First	15.5	1.162	2.31
		42.0	1.133	2.78
		50.2	1.117	2.84
	Second	41.0	2.670	N/A
	Third	74.4	3.681	9.13
End	First	50.2	1.117	2.80
	Second	41.0	2.670	0.61

Table 5.4 Damping Coefficients B_S and B_1 as a Function of Effective Damping β (FEMA 273)

Effective Damping β (percentage of critical)[1]	B_S	B_1
< 2	0.8	0.8
5	1.0	1.0
10	1.3	1.2
20	1.8	1.5
30	2.3	1.7
40	2.7	1.9
> 50	3.0	2.0

[1.] The damping coefficient should be based on linear interpolation for effective damping values other than those given.

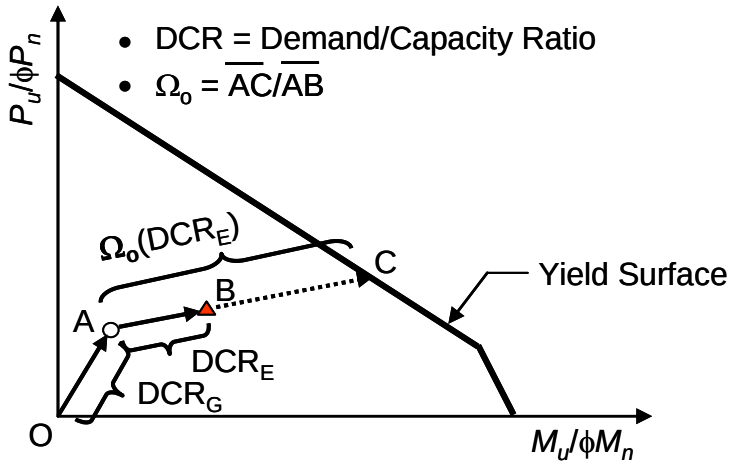

(a) P-M Interaction

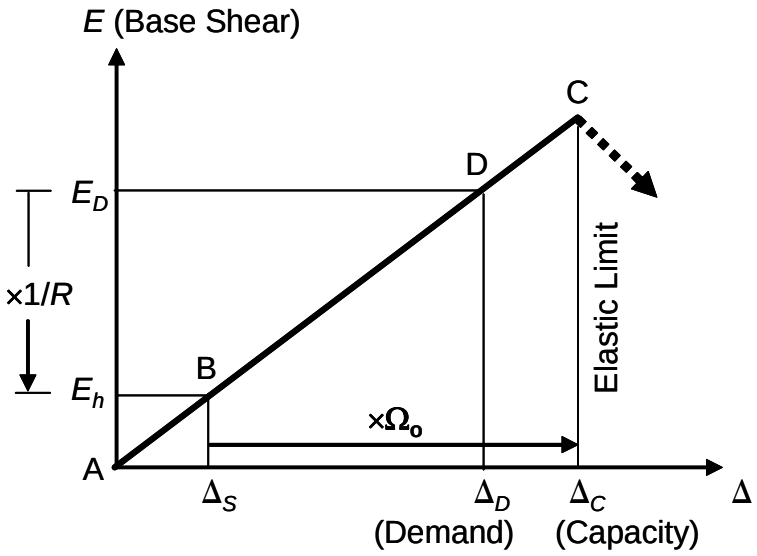

(b) Base Shear versus Story Drift

Figure 5.1 Seismic Design Concept

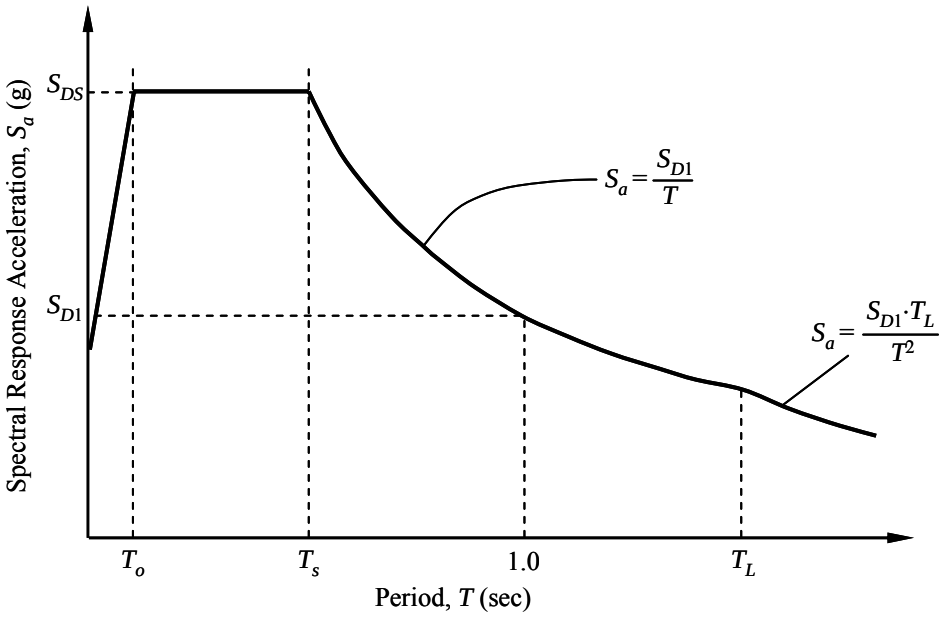

Figure 5.2 Design Response Spectrum (ASCE 7-05)

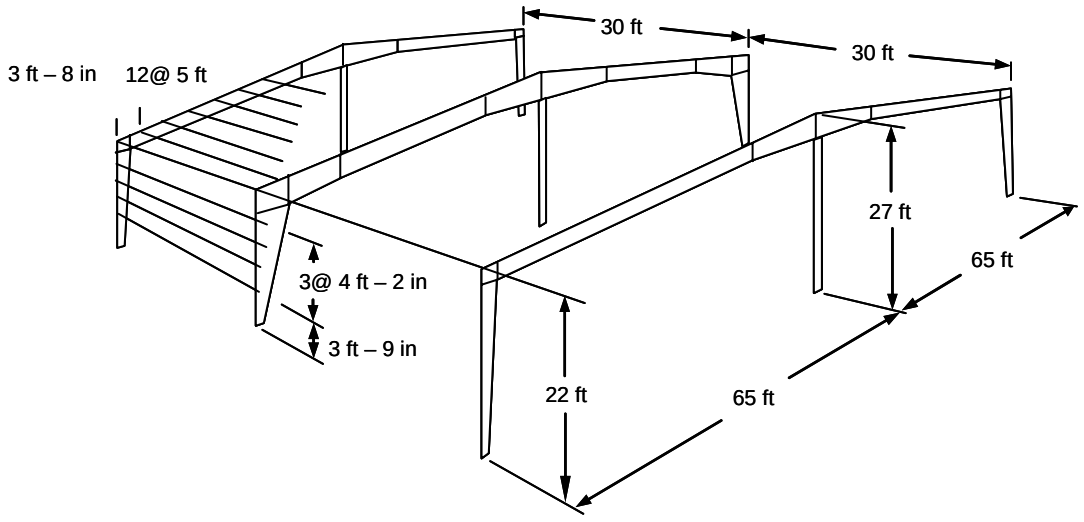

Figure 5.3 Prototype Building for Dynamic Test (Sockalingam 1988)

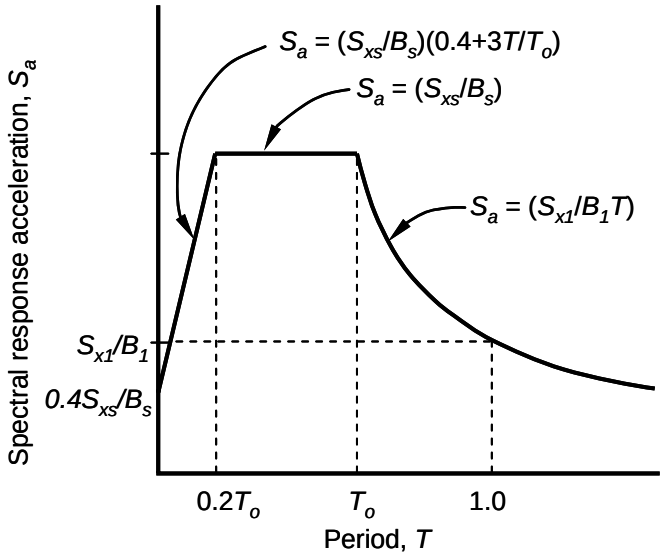

Figure 5.4 General Response Spectrum (FEMA 273)

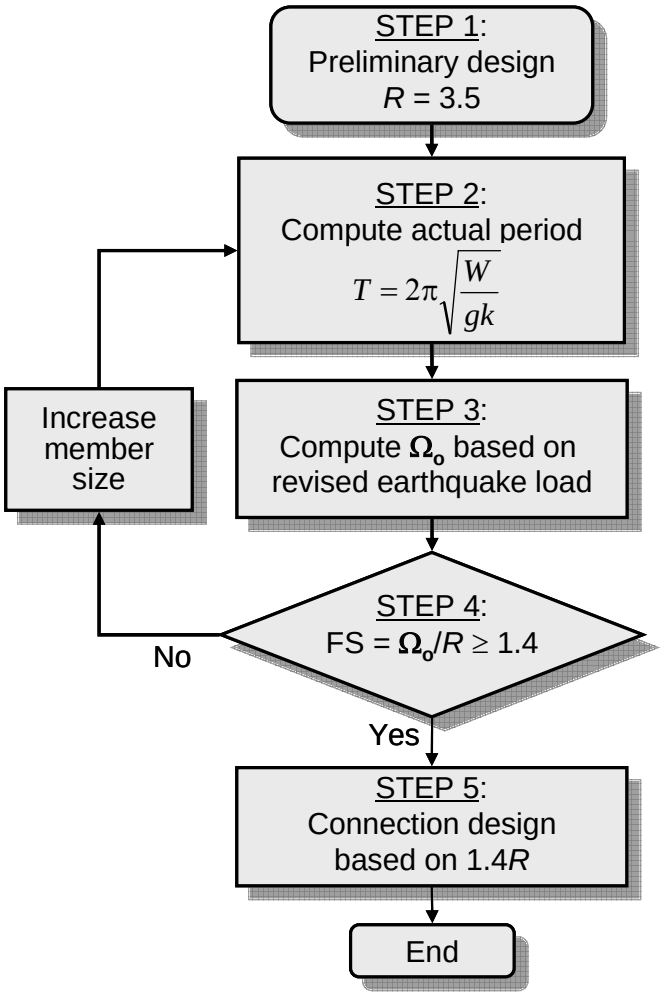

Figure 5.5 General Design Procedure

6 APPLICATIONS OF THE PROPOSED SEISMIC DESIGN PROCEDURE

6.1 Introduction

This chapter demonstrates the application of the drift-based seismic design procedure developed in Chapter 5. Three cases (40 ft wide by 12 ft eave height, 100 ft wide by 20 ft eave height, and 150 ft wide by 20 ft eave height) with frame spacing of 25 ft were considered (Sections 6.2 to 6.4). Each case consists of two example buildings assumed to be located in a high seismic region but with either high wind (Building A) or low wind (Building B) regions. All buildings were first designed in accordance with IBC 2006 (ICC 2006), which corresponded to the preliminary design (Step 1 of the procedure in Section 5.7). The impact of the proposed seismic design procedure on the current design practice is presented (Section 6.5).

6.2 Case 1 (40 ft×12 ft)

6.2.1 Step 1: Preliminary Design

Two example buildings with a dimension of 40 ft width by 12 ft eave height by 25 ft frame spacing and a roof pitch of 2:12 were designed by Nucor Building Systems as shown in Figure 6.1. One side of the building was clad with a metal wall while the other side was opened completely. The design loads are summarized in Table 6.1; the assumed wind loads were 85 mph and 120 mph for Building A and Building B, respectively, and the wind exposure category C was considered for both buildings. The governing load combinations according to IBC 2006 were the non-seismic load combinations:

$$1.2(D+C) + 1.6L_r \text{ (Building A)} \tag{6.1}$$

$$0.9D + 1.6W \text{ (Building B)} \tag{6.2}$$

where D = dead load, C = collateral load, L_r = roof live load, and W = wind load.

The sectional properties from the preliminary design are summarized in Tables 6.2 and 6.3. The critical component of both buildings was the column (C3) without a sidewall, and the demand/capacity ratio was 0.74 and 0.63 for Building A and Building B, respectively, under the governing load combination (see Figure 6.2).

6.2.2 Step 2: Compute Actual Fundamental Period, *T*

The design acceleration spectrum specified in ASCE 7-05 and the corresponding drift are shown in Figure 6.3. The approximated fundamental period, T_a, and the associated drift demand, Δ_{Da}, used in the preliminary design were

$$T_a = C_t h_n^x = (0.028)(12)^{0.8} = 0.20 \text{ sec. (Buildings A \& B)} \tag{6.3}$$

$$\Delta_{Da} = \left(\frac{T_a}{2\pi}\right)^2 \times S_a \times g = \left(\frac{0.20}{2\pi}\right)^2 (1.06)(386.4) = 0.41 \text{ in.} \tag{6.4}$$

In order to calculate the actual fundamental periods of the buildings, modal analysis was conducted using SAP2000 (Computer and Structures 2005). The computed fundamental periods were 0.37 sec. and 0.31 sec., and the corresponding drift demands, Δ_D, were 1.42 in. and 1.01 in. for Building A and Building B, respectively. The use of the actual periods results in the same design lateral force obtained from the approximated period since all of them stay in the plateau area in the spectral acceleration response curve; however, the drift demands are 2.5 to 3.5 times larger. Therefore, the drift demand is underestimated when T_a is used.

The drift at the design seismic force level, Δ_S, are then 0.41 in. (= 1.42/3.5) and 0.29 in. (= 1.01/3.5) for Building A and Building B, respectively.

6.2.3 Step 3: Compute Ω_o Based on the Revised Earthquake Load

Since the actual fundamental periods for both buildings induce the same seismic loads used in their preliminary designs, it is unnecessary to revise the seismic load to compute the overstrength factor, Ω_o. For individual unbraced segment, the overstrength factor should be computed based on the axial and flexural interaction (see Figures 6.4 and 6.5). In the figures, $1.412(D+C)$ is the gravity portion and $1.0E_h$ is the earthquake portion based on the following equation:

$$1.2(D+C) + 1.0E = 1.2(D+C) + 0.2S_{DS}(D+C)+1.0E_h \qquad (6.5)$$

$$= 1.412(D+C) + 1.0E_h$$

where D = dead load, C = collateral load, E_h = horizontal seismic force.

The column (C3) without a sidewall for both buildings is the critical component under the earthquake load combination; the critical component is the same for the governing load combination and the earthquake load combination in this case, but this is not always true. The system overstrength factor at segment C3 is 5.70 and 8.19 for Building A and Building B, respectively.

The corresponding drift capacities, Δ_C, are 2.34 in. (= 0.41×5.70) for Building A and 2.38 in. (= 0.29×8.19) for Building B. These estimated drift capacities are further verified using ABAQUS (ABAQUS Inc. 2005) based on the findings in Chapter 4. The predicted failure mode and the drift capacity corresponded well with the estimations in this procedure (see Figures 6.6 and 6.7). It is notable that plate

buckling developed in the panel zone of Building A provides the ductility in the system (see Figure 6.6), although the inelastic behavior is not considered in this design procedure. The potential for the development of a tension field action as a structural fuse is discussed in Appendix C.

6.2.4 Step 4: Check Ω_o/R Ratio

Based on the overstrength factor computed in Step 3, Ω_o/R is 1.63 (= 5.70/3.5) and 2.34 (= 8.19/3.5) for Building A and Building B, respectively. Both buildings show $\Omega_o/R \geq 1.4$; therefore, the drift capacity is larger than the drift demand with the specified safety margin (= 1.4).

6.2.5 Step 5: Connection Design

Connection design (i.e., end-plate moment connection, panel zone) is based on the seismic force obtained in Step 3 multiplied by $1.4R$ (= 4.9) in accordance with the design code provisions:

$$1.412(D+C) + 1.4R(E_h) = 1.412(D+C) + 4.9E_h \quad (6.6)$$

6.3 Case 2 (100 ft×20 ft)

6.3.1 Step 1: Preliminary Design

Two buildings with a dimension of 100 ft width by 20 ft eave height by 25 ft frame spacing with a roof pitch of 1:12 were designed by Butler Manufacturing Company (see Figure 6.8). Both buildings were symmetric for their mid-spans. The sides were clad with metal walls. The considered design loads are summarized

in Table 6.4. The governing load combinations were the non-seismic load combinations:

$$1.2D + 1.6L_r \text{ (Building A)} \tag{6.7}$$

$$0.9D + 1.6W \text{ (Building B)} \tag{6.8}$$

Tables 6.5 and 6.6 summarize the sectional properties of both buildings. The high demand/capacity ratios under the governing load combinations indicate that the buildings were optimally designed (see Figure 6.9). The unbraced segment C2 was the critical component, and the D/C ratio was 1.00 and 0.95 for Building A and Building B, respectively.

6.3.2 Step 2: Compute Actual Fundamental Period, *T*

The fundamental period from the approximate method presented in ASCE 7-05 is $T_a = C_t h_n^x = (0.028)(20)^{0.8} = 0.31\,\text{sec.}$ and the corresponding drift demand is 0.94 in. for both buildings (see Figure 6.10). The actual fundamental periods, *T*, from the modal analysis using SAP2000 are 0.65 sec. and 0.56 sec., and the drift demands adopting the obtained *T* are then 3.80 in. and 3.07 in. for Building A and Building B, respectively. Therefore, the use of T_a results in the underestimation at 25% to 30% level of the actual drift demand.

The drift, Δ_S, are 1.09 in. (= 3.80/3.5) and 0.88 in. (= 3.07/3.5) for Building A and Building B, respectively.

6.3.3 Step 3: Compute Ω_0 Based on the Revised Earthquake Load

Figure 6.10(a) shows the spectral response acceleration, S_a, at T_a stays in the plateau portion (= 1.00g). The S_a at *T* from Building B is in the descending portion

(= 0.92g) while it is located in the plateau portion (= 1.00g) at T from Building A. Since the design base shear is determined based on the seismic response coefficient, C_s (= S_a/R), shown in Eq. (5.6), the reduction of the seismic force by a factor of 0.92 (= 0.92g/1.00g) is necessary for Building A for the computation of Ω_o.

The critical component under the earthquake load combination [Eq. (6.8)] of both buildings is the segment R4 and the system overstrength factor is 4.90 and 7.29 for Building A and Building B, respectively (see Figure 6.11). The overstength factors of all unbraced segments are summarized in Appendix B. Note the segment C2 was the critical component under the governing load combination for both buildings (Section 6.3.1).

$$1.2D + 1.0E = 1.2D + 0.2S_{DS}D + 1.0E_h = 1.4D + 1.0E_h \quad (6.9)$$

The corresponding drift capacities, Δ_C, are 5.34 in. (= 1.09×4.90) for Building A and 6.42 in. (= 0.88×7.29) for Building B. The predicted failure mode and the drift capacity from ABAQUS analysis are reasonably corresponded with those estimated from this procedure (see Figures 6.12 and 6.13). Flange local buckling without lateral buckling leads to the ductile behavior in Building A while the failure mode of lateral buckling results in a sudden strength degradation in Building B. However, it is very difficult to control the failure only by flange local buckling with no lateral buckling under cyclic loading in this building system.

6.3.4 Step 4: Check Ω_o/R Ratio

Based on the overstrength factor computed in Step 3, Ω_o/R is 1.40 (= 4.90/3.5) and 2.08 (= 7.29/3.5) for Building A and Building B, respectively. Both buildings

show $\Omega_o/R \geq 1.4$; therefore, the drift capacity is larger than the drift demand with the specified safety margin (= 1.4).

6.3.5 Step 5: Connection Design

Connection design is based on the seismic force obtained in Step 3 multiplied by 1.4R (= 4.9):

$$1.4D + 1.4R(E_h) = 1.4D + 4.9E_h \quad (6.10)$$

6.4 Case 3 (150 ft×20 ft)

6.4.1 Step 1: Preliminary Design

Two buildings with a dimension of 150 ft width by 20 ft eave height by 25 ft frame spacing were designed by Nucor Building Systems as shown in Figure 6.14; Building A had a roof pitch of 1:12 while Building B had a roof pitch of 2:12.. Two gravity columns were located in the middle of the span with a distance of 50 ft from the two exterior columns. A full-height 8 in.-thick concrete wall was installed on both sides of the buildings and the connection between the wall and the frame was made at the knee area. The connection details for the wall-to-column and the interior pipe column-to-rafter are shown in Figure 6.15.

The design loads are summarized in Table 6.7. The governing load combination was the seismic load combination:

$$1.412(D+C) + 0.2S + 1.0E_h \text{ (Building A)} \quad (6.11)$$

$$1.412(D+C) + 1.0E_h \text{ (Building B)} \quad (6.12)$$

The sectional properties the buildings are summarized in Tables 6.8 and 6.9. The critical segment was the exterior columns (unbraced segment C1) and the D/C ratio was 0.93 and 1.08 for Building A and Building B, respectively (see Figure 6.16); the D/C ratio larger than the unity (= 1.0) for Building B indicates that the building was under designed.

6.4.2 Step 2: Compute Actual Fundamental Period, *T*

The approximated fundamental period, T_a, is 0.31 sec. for both buildings, which is the same for Case 2 (100 ft×20 ft); Eq. (5.5) totally depends on the height of the building and results in the same fundamental period in the different buildings with the same height. The corresponding drift demand based on T_a is 1.0 in. (see Figure 6.17).

The actual fundamental periods, *T*, from SAP2000 are 0.95 sec. and 0.90 sec. for Building A and Building B, respectively. The spectral response accelerations using *T* is located in the descending portion, and the corresponding drift demands are 6.26 in. and 5.97 in. for Building A and Building B, respectively. The drift demand from T_a is significantly less than that from *T* (1.0 in. vs. 6.26 or 5.97 in.).

The drift, Δ_S, are then1.79 in. (= 6.26/3.5) and 1.71 in. (= 5.79/3.5) for Building A and Building B, respectively.

6.4.3 Step 3: Compute Ω_0 Based on the Revised Earthquake Load

The seismic design loads can be reduced since both spectral response accelerations, S_a, using *T* are located in the descending portion (0.71g for Building A, 0.75g for Building B) while S_a used for the preliminary design is in the plateau (=

1.06g) [see Figure 6.17(a)]. The reduction factor of the seismic force for the computation of Ω_o is 0.67 (= 0.71g/1.06g) and 0.71 (= 0.75g/1.06g) for Building A and Building B, respectively.

The critical component of both buildings is the exterior column (segment C1) and the system overstrength factor is 1.61 for Building A and 1.21 for Building B (see Figure 6.18); the corresponding drift capacity is 2.88 in. (= 1.79×1.61) and 2.07 in. (= 1.71×1.21) for Building A and Building B, respectively. The overstrength factors for all unbraced segments can be found in Appendix B.

The predicted failure mode and the global response from ABAQUS analysis are shown in Figures 6.19 and 6.20. The predicted failure modes at exterior columns correspond well with the critical component estimated in this procedure although the predicted drift capacities are much larger than Δ_C. That is because the interior gravity columns are considered to be hinged at both top and bottom end connections in the design, but the top connections in the ABAQUS models were generated as rigid based on the connection drawing [see Figure 6.15(b)]. Therefore, the connections are able to take some degrees of moment, which results in the moment redistribution of the global system.

6.4.4 Step 4: Check Ω_o/R Ratio

Ω_o/R is less than 1.4 for both buildings [0.46 (= 1.61/3.5) and 0.35 (= 1.21/3.5) for Building A and Building B, respectively]; the returning back to the design Step 2 with the increase of the member sizes is needed.

6.4.5 Step 5: Connection Design

Once Step 4 is satisfied after repeating Steps 2 and 3, the connection design is based on the seismic force obtained in the previous step (Step 3) multiplied by 1.4R (= 4.9).

6.5 Summary and Conclusions

This chapter demonstrats how to apply the drift-based seismic design procedure developed in Chapter 5 with three cases (a total of six preliminary designed buildings) by following the design procedure described in Section 5.7.

(1) The non-seismic load combination was the governing load combination for Case 1 (40 ft×12 ft). The overstrngth factor, Ω_o, of the critical component under the earthquake load combination is 5.70 and 8.19 for Building A and Building B, respectively. $\Omega_o/R \geq 1.4$ is satisfied for both buildings; no re-design is needed.

(2) The governing load combination was the non-seismic load combination for both buildings in Case 2 (100 ft×20 ft). The fact the obtained Ω_o/R is larger than 1.4 for both buildings indicates that the buildings have enough drift capacities to respond elastically under the earthquake event, and no designer-design is needed.

(3) The earthquake load combination was the governing load combination due to the use of the concrete walls for both buildings in Case 3 (150 ft×20 ft). In this case, the increases of member size are required since the elastic drift

capacities are less than the elastic drift demands (Ω_o/R is less than 1.4 for both buildings).

(4) It is shown that metal frames with heavy hard walls based on the current design procedure are vulnerable to collapse. However, the proposed seismic design procedure does not affect the current design of typical metal buildings.

(5) The possibility for the use of the panel zone as a structural fuse is demonstrated through the finite element analysis; the inelastic response utilizing tension field action in the panel zone can be a good source to dissipate the seismic energy in a stable manner.

Table 6.1 Design Loads for Case 1 (40 ft×12 ft)

Load Type	Detail	Data
Dead Load	Dead Load	3.0 psf
	Collateral Load	3.0 psf
	Frame Self Weight	2.0 psf
Live Load	Roof Live Load	12.0 psf
Snow Load	Snow Load	0.0 psf
Wind Load	Wind Speed	85 mph (Building A)
		120 mph (Building B)
	Wind Exposure	C
	Importance Factor	1.0
Earthquake Load	Site Location	California
	Importance Factor	1.0
	Seismic Design Category	D
	R	3.5
	C_s	0.303

Table 6.2 Case 1: Section Properties – Building A

Section	Web Depth (in.)	Web Plate (in.)		Outside Flange (in.)	Inside Flange (in.)
	Start / End	Thick.	Length	W×T×L	W×T×L
RF1	12.0 / 18.0	0.125	124.6	5×1/4×124.6	5×1/4×124.6
RF2	15.0 / 15.0	0.15	217.0	5×1/4×217.0	5×1/4×217.0
RF3	15.0 / 15.0	0.15	217.0	5×1/4×217.0	5×1/4×217.0
RF4	18.0 / 12.0	0.125	124.6	5×1/4×124.6	5×1/4×124.6

* F_y = 55 ksi

Table 6.3 Case 1: Section Properties – Building B

Section	Web Depth (in.)	Web Plate (in.)		Outside Flange (in.)	Inside Flange (in.)
	Start / End	Thick.	Length	W×T×L	W×T×L
RF1	12.0 / 20.0	0.15	119.8	5×1/4×119.8	5×1/4×119.8
RF2	20.0 / 12.0	0.15	214.9	5×1/4×214.9	5×1/4×214.9
RF3	12.0 / 20.0	0.15	214.9	5×1/4×214.9	5×1/4×214.9
RF4	20.0 / 12.0	0.15	119.8	5×1/4×119.8	5×1/4×119.8

* F_y = 55 ksi

Table 6.4 Design Loads for Case 2 (100 ft×20 ft)

Load Type	Detail	Data
Dead Load	Dead Load	2.7 psf
	Collateral Load	0.0 psf
	Frame Self Weight	2.0 psf
Live Load	Roof Live Load	12.0 psf
Snow Load	Snow Load	0.0 psf
Wind Load	Wind Speed	85 mph (Building A)
		120 mph (Building B)
	Wind Exposure	C
	Importance Factor	1.0
Earthquake Load	Site Location	California
	Importance Factor	1.0
	Seismic Design Category	D
	R	3.5
	C_s	0.286

Table 6.5 Case 2: Section Properties – Building A

Section	Web Depth (in.)	Web Plate (in.)		Outside Flange (in.)	Inside Flange (in.)
	Start / End	Thick.	Length	W×T×L	W×T×L
RF1	16.0 / 32.0	0.188	197.2	6×3/8×197.2	6×1/2×197.2
RF2	34.0 / 16.0	0.219 0.16	117.5 120.0	6×3/8×237.5	6×1/2×237.5
	16.0 / 24.0	0.16 0.12	239.3 122.2	6×5/16×362.5	6×1/4×362.5
RF3	24.0 / 16.0	0.12 0.16	122.2 239.2	6×5/16×362.5	6×1/4×362.5
	16.0 / 34.0	0.16 0.219	120.0 117.5	6×3/8×237.5	6×1/2×237.5
RF4	32.0 / 16.0	0.188	197.22	6×3/8×197.2	6×1/2×197.2

* F_y = 55 ksi

Table 6.6 Case 2: Section Properties – Building B

Section	Web Depth (in.)	Web Plate (in.)		Outside Flange (in.)	Inside Flange (in.)
	Start / End	Thick.	Length	W×T×L	W×T×L
RF1	16.0 / 36.0	0.25	191.5	6×3/8×191.5	6×1/2×191.5
RF2	40.0 / 20.0	0.219	237.0	6×1/2×237.0	6×1/2×237.0
	20.0 / 20.0	0.16 0.12	179.8 183.2	6×1/4×179.8 6×3/8×183.2	6×5/16×179.8 6×3/8×183.2
RF3	20.0 / 20.0	0.12 0.16	183.2 179.8	6×3/8×183.2 6×1/4×179.8	6×3/8×183.2 6×5/16×179.8
	20.0 / 40.0	0.219	237.0	6×1/2×237.0	6×1/2×237.0
RF4	36.0 / 16.0	0.25	191.5	6×3/8×191.5	6×1/2×191.5

* F_y = 55 ksi

Table 6.7 Design Loads for Case 3 (150 ft×20 ft)

Load Type	Detail	Data
Dead Load	Dead Load	3.0 psf
	Collateral Load	5.0 psf (Building A)
		3.0 psf (Building B)
	Frame Self Weight	2.0 psf
	Concrete Wall	55.0 psf
Live Load	Roof Live Load	12.0 psf
Snow Load	Snow Load	14.0 psf (Building A)
		0.0 psf (Building B)
Wind Load	Wind Speed	85 mph (Building A)
		120 mph (Building B)
	Wind Exposure	C
	Importance Factor	1.0
Earthquake Load	Site Location	California
	Importance Factor	1.0
	Seismic Design Category	D
	R	3.5
	C_s	0.303

Table 6.8 Case 3: Section Properties – Building A

Section	Web Depth (in.)	Web Plate (in.)		Outside Flange (in.)	Inside Flange (in.)
	Start / End	Thick.	Length	W×T×L	W×T×L
RF1	12.0 / 32.0	0.15	199.2	6×5/16×199.2	6×1/2×199.2
RF2	36.0 / 24.0	0.2	51.0	6×3/8×51.0	6×3/8×51.0
		0.2	165.0	6×3/8×165.0	6×5/16×165.0
		0.15	165.0	6×1/4×165.0	6×1/4×165.0
RF3	24.0 / 32.0	0.2	149.0	6×1/4×149.0	6×3/8×149.0
	32.0 / 18.0	0.2	109.0	6×1/4×109.0	6×3/8×109.0
	18.0 / 18.0	0.15	192.0	6×1/4×192.0	6×1/4×192.0
RF4	18.0 / 18.0	0.15	192.0	6×1/4×192.0	6×1/4×192.0
	18.0 / 32.0	0.2	109.0	6×1/4×109.0	6×3/8×109.0
	32.0 / 24.0	0.2	149.0	6×1/4×149.0	6×3/8×149.0
RF5	24.0 / 32.0	0.15	165.0	6×1/4×165.0	6×1/4×165.0
		0.2	165.0	6×3/8×165.0	6×5/16×165.0
		0.2	51.0	6×3/8×51.0	6×3/8×51.0
RF6	32.0 / 12.0	0.15	199.2	6×5/16×199.2	6×1/2×199.2
C2	Pipe-ϕ×T×L (8.62×0.138×249.2), F_y = 42 ksi				

* F_y = 55 ksi for sections RF1 through RF6

Table 6.9 Case 3: Section Properties – Building B

Section	Web Depth (in.)	Web Plate (in.)		Outside Flange (in.)	Inside Flange (in.)
	Start / End	Thick.	Length	W×T×L	W×T×L
RF1	12.0 / 34.0	0.175	204.4	6×5/16×204.4	6×3/8×204.4
RF2	34.0 / 27.9	0.2	254.8	6×1/4×254.8	6×3/8×254.8
	27.9 / 24.0	0.15	165.0	6×1/4×165.0	6×1/4×165.0
RF3	24.0 / 31.0	0.175	145.9	6×1/4×145.9	6×3/8×145.9
	31.0 / 16.0	0.172	112.1	6×1/4×112.1	6×3/8×112.1
	16.0 / 16.0	0.125	192.0	6×1/4×192.0	6×1/4×192.0
RF4	16.0 / 16.0	0.125	192.0	6×1/4×192.0	6×1/4×192.0
	16.0 / 31.0	0.175	112.1	6×1/4×112.1	6×3/8×112.1
	31.0 / 24.0	0.175	145.9	6×1/4×145.9	6×3/8×145.9
RF5	24.0 / 27.9	0.15	165.0	6×1/4×165.0	6×1/4×165.0
	27.9 / 34.0	0.2	254.8	6×1/4×254.8	6×3/8×254.8
RF6	34.0 / 12.0	0.175	204.4	6×5/16×204.4	6×3/8×204.4
C2	Pipe-ϕ×T×L (8.62×0.138×300.0), F_y = 42 ksi				

* F_y = 55 ksi for sections RF1 through RF6

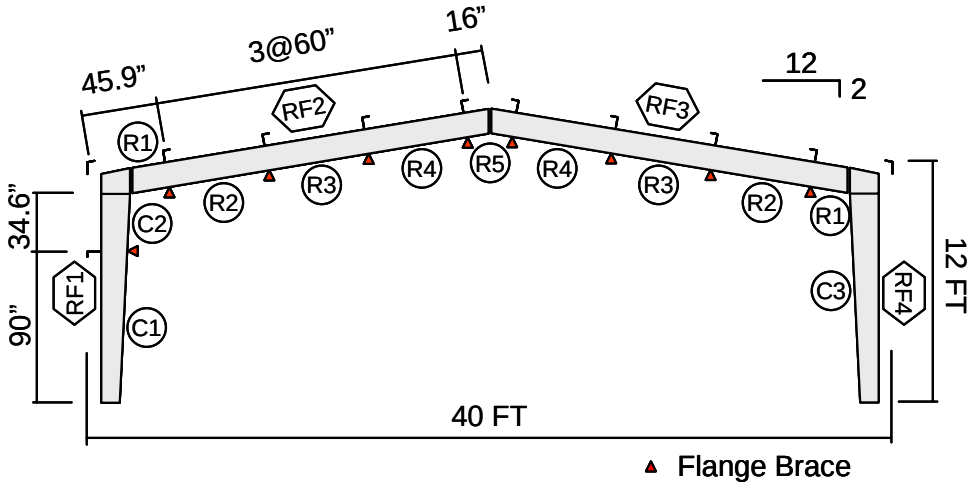

(a) Building 1

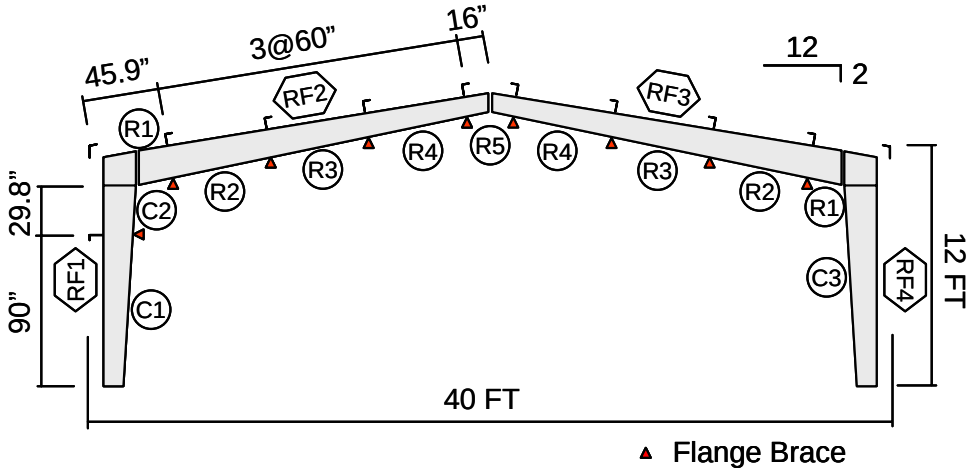

(b) Building 2

Figure 6.1 Case 1 (40 ft×12 ft)

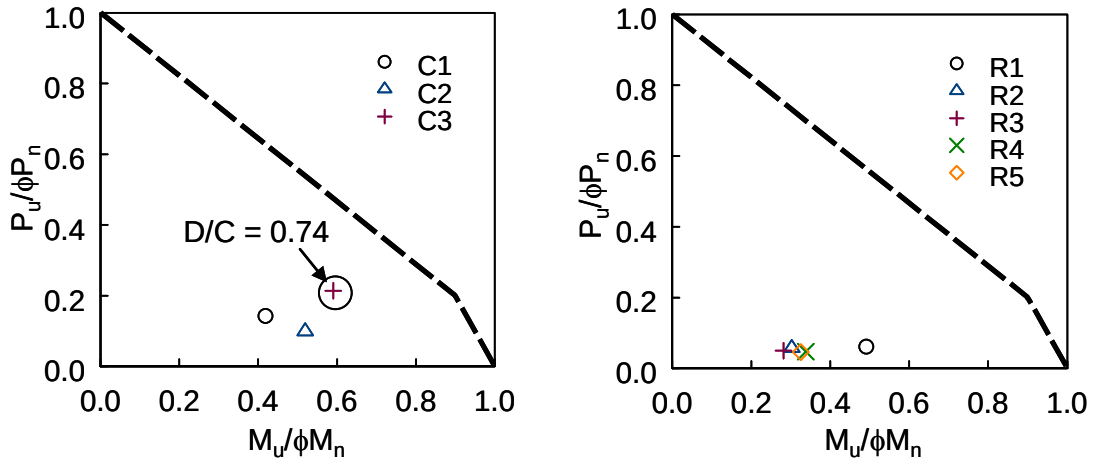

Column Rafter

(a) Building A

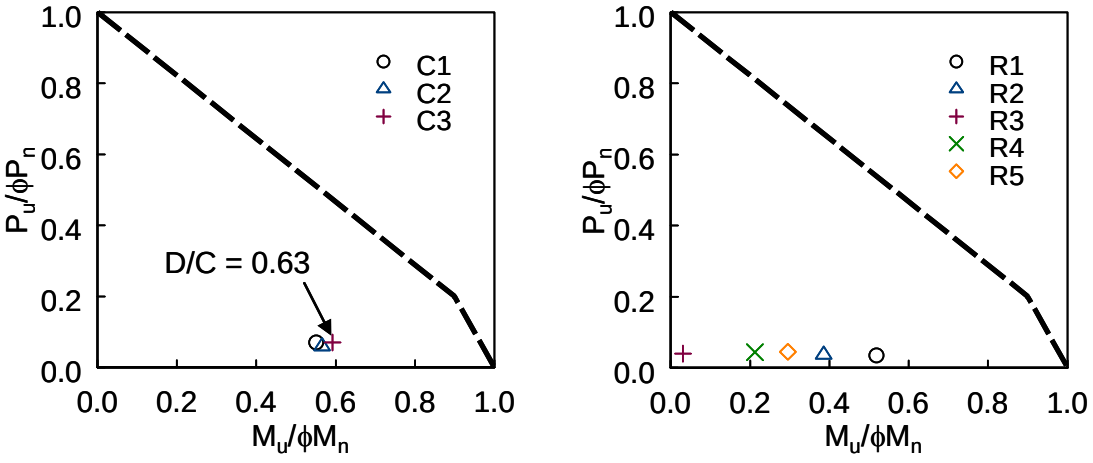

Column Rafter

(b) Building B

Figure 6.2 Case 1: Demand/Capacity Ratio under Governing Load Combination

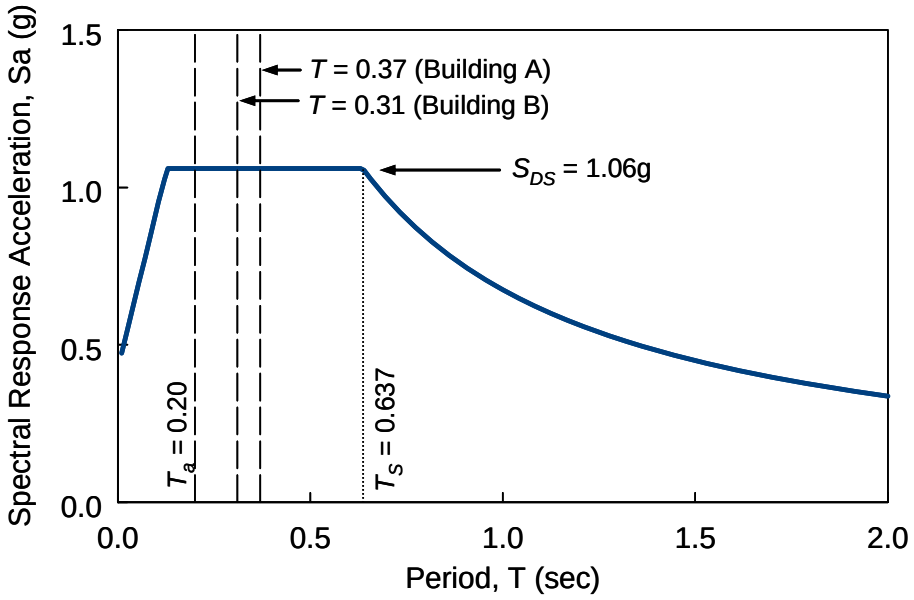

(a) Spectral Response Acceleration

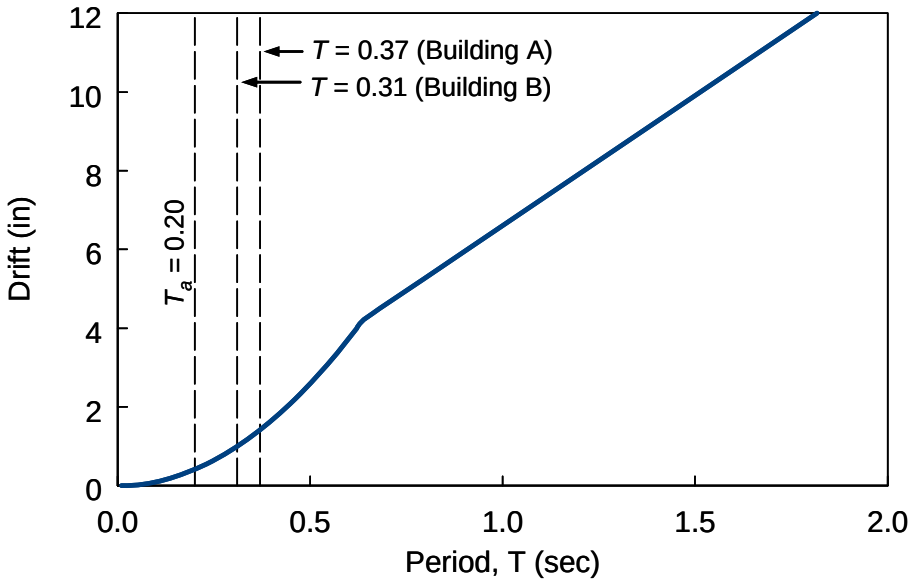

(b) Drift Demand

Figure 6.3 Case 1: Spectral Response Acceleration and Drift Demand

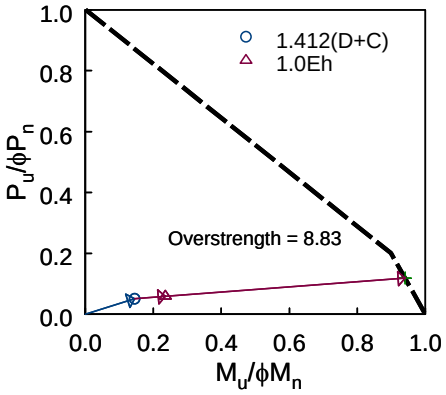

Segment C1

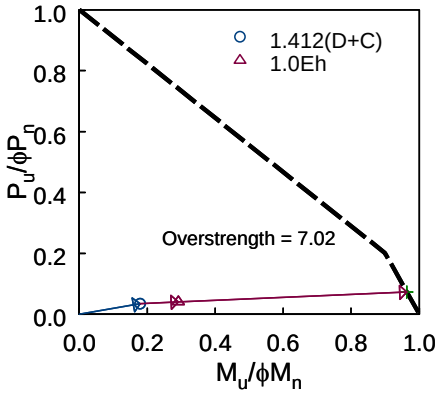

Segment C2

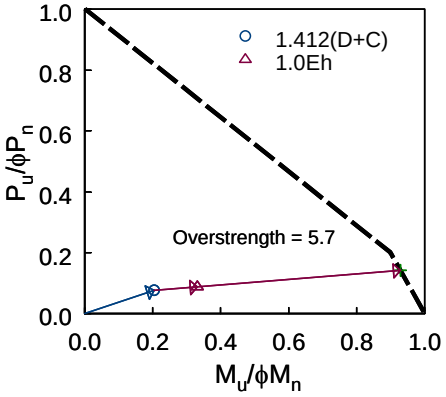

Segment C3

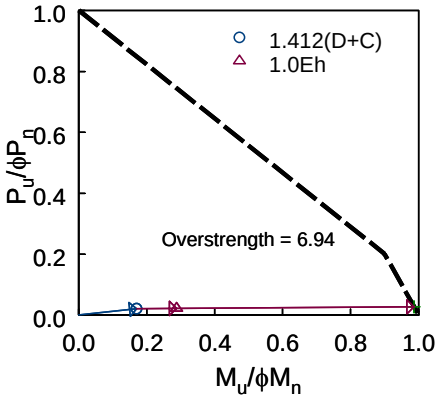

Segment R1

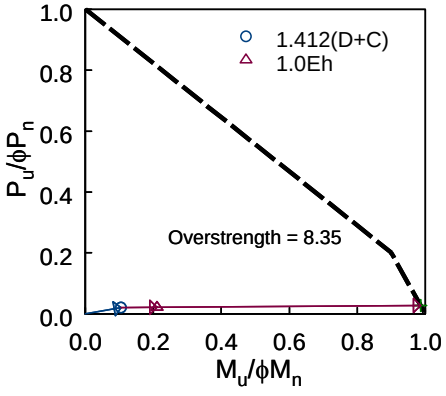

Segment R2

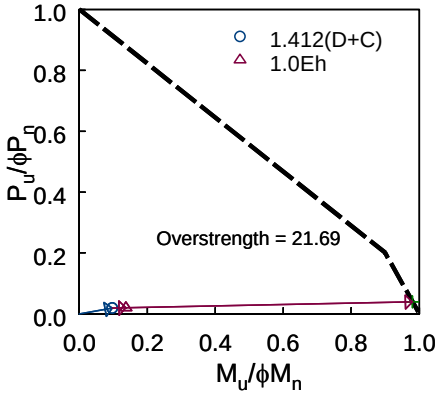

Segment R3

Figure 6.4 Case 1: Overstrength Factor for Building A

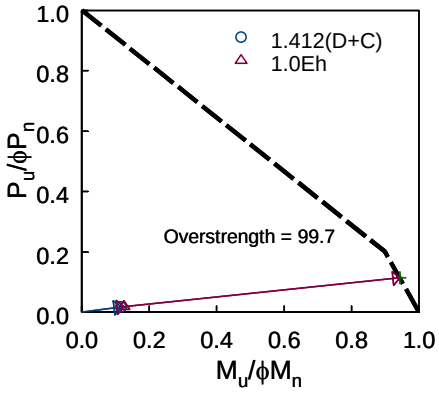

Segment R4

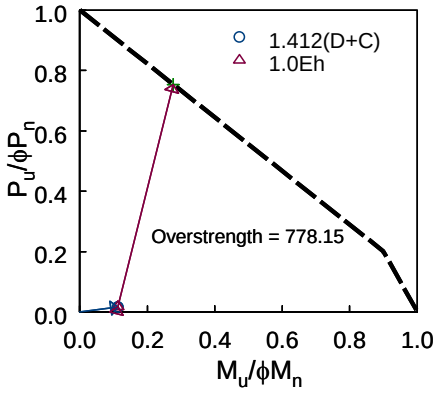

Segment R5

Figure 6.4 Case 1: Overstrength Factor for Building A (continued)

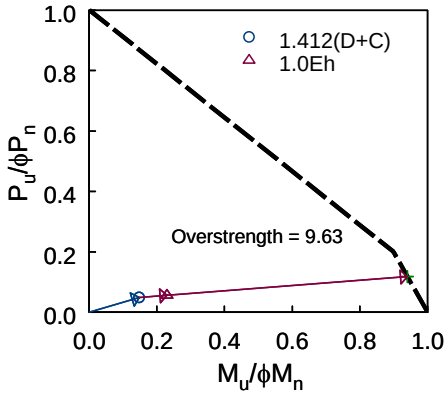

Segment C1

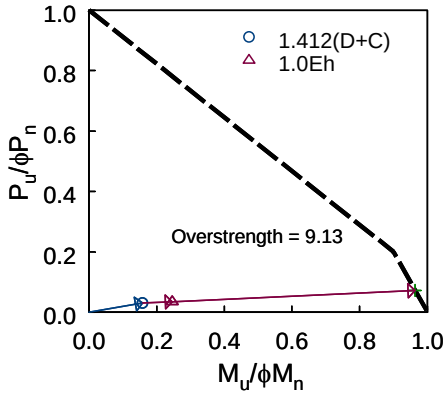

Segment C2

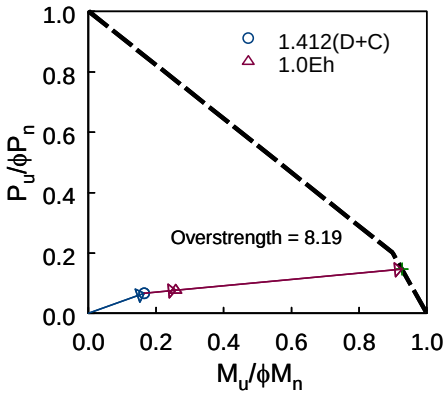

Segment C3

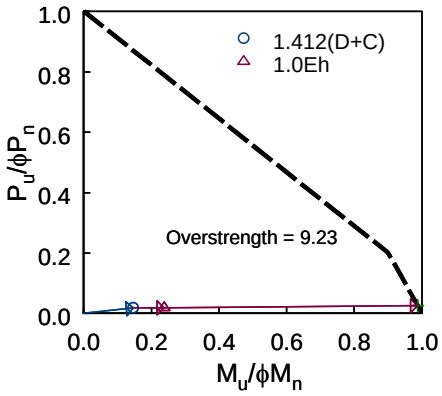

Segment R1

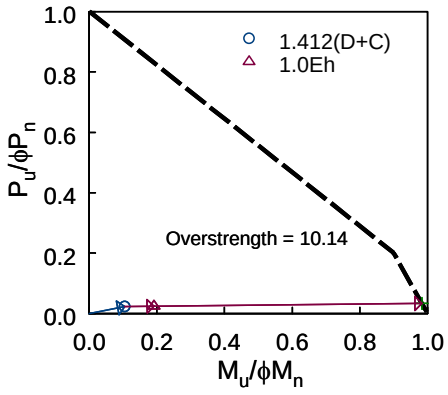

Segment R2

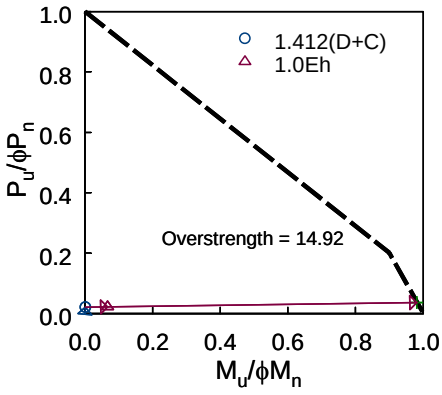

Segment R3

Figure 6.5 Case 1: Overstrength Factor for Building B

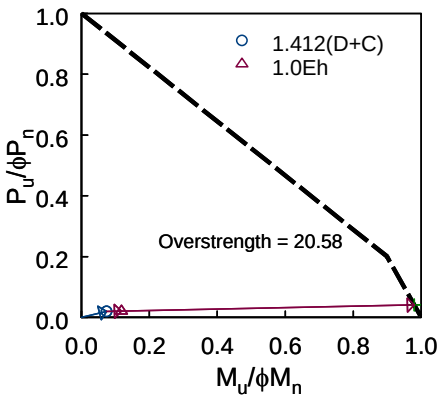

Segment R4

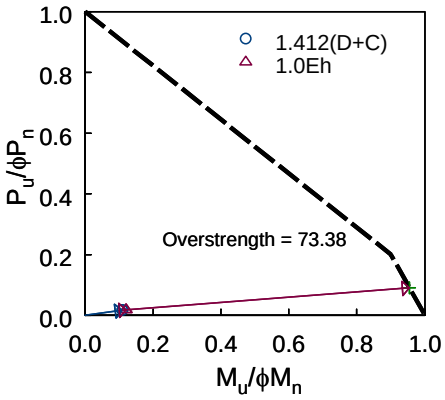

Segment R5

Figure 6.5 Case 1: Overstrength Factor for Building B (continued)

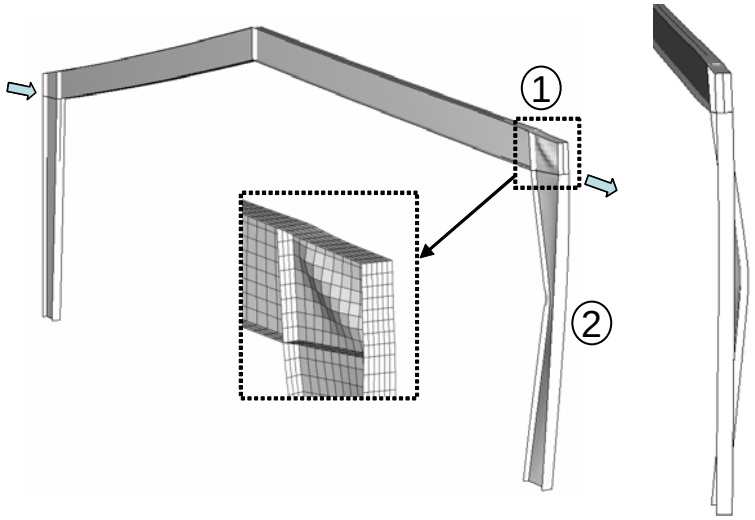

(a) Failure Mode

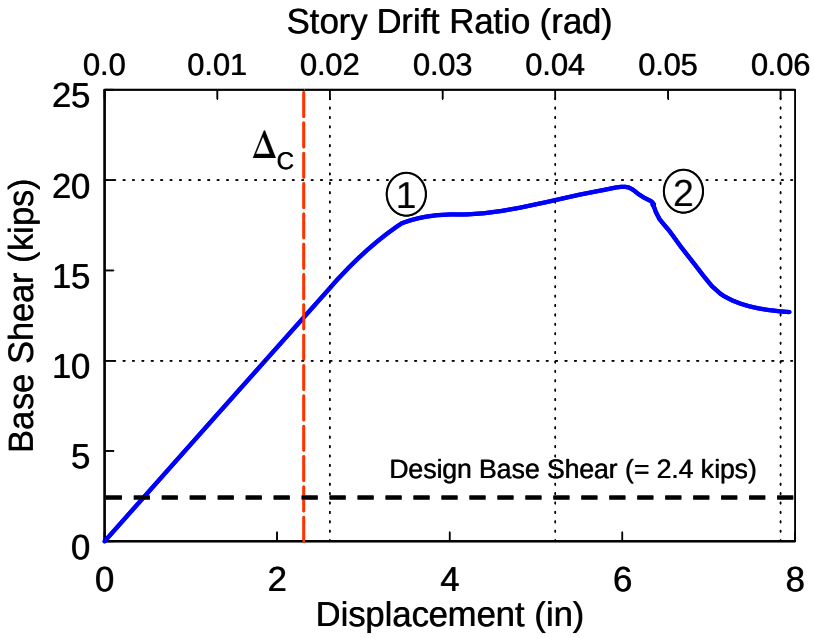

(b) Drift Capacity

Figure 6.6 Case 1: Failure Mode and Drift Capacity Verification of Building A

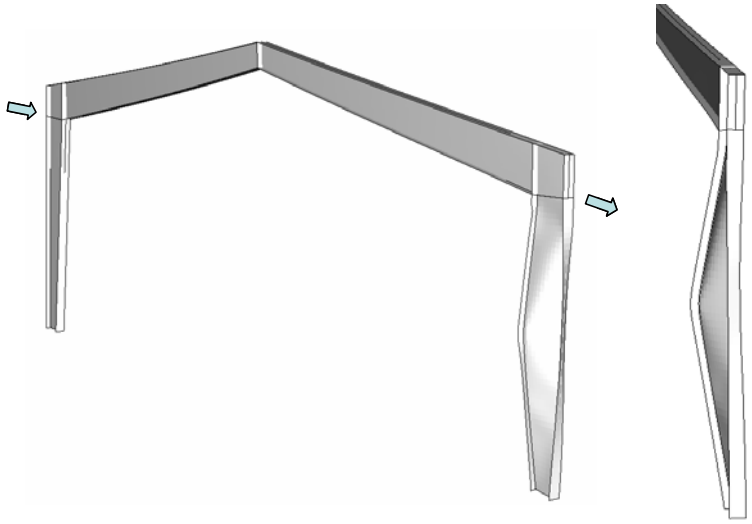

(a) Failure Mode

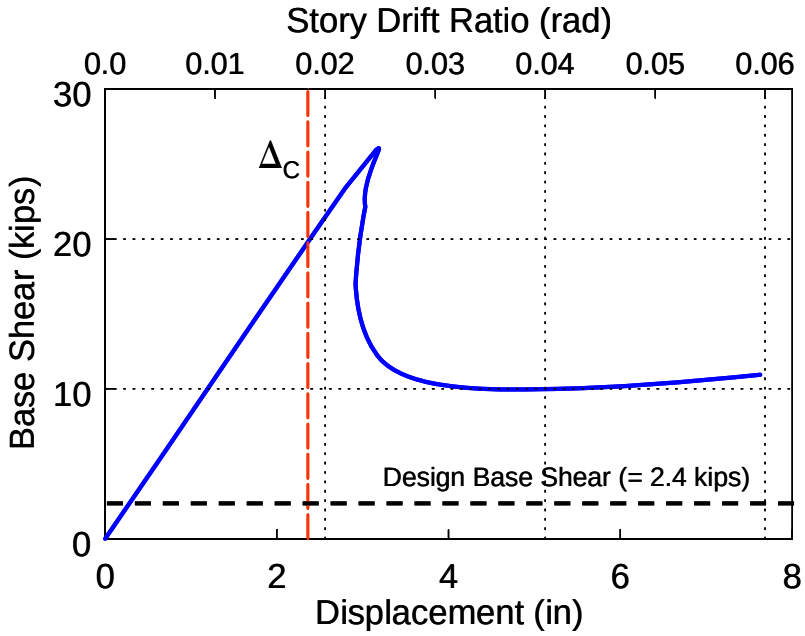

(b) Drift Capacity

Figure 6.7 Case 1: Failure Mode and Drift Capacity Verification of Building B

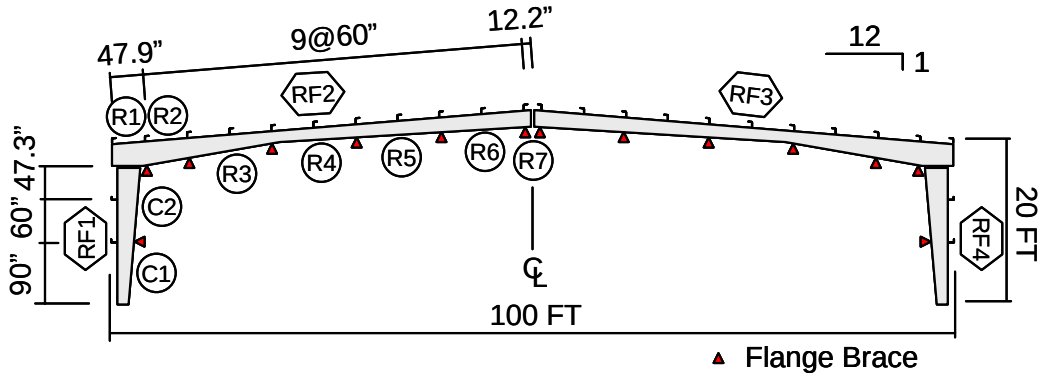

(a) Building A

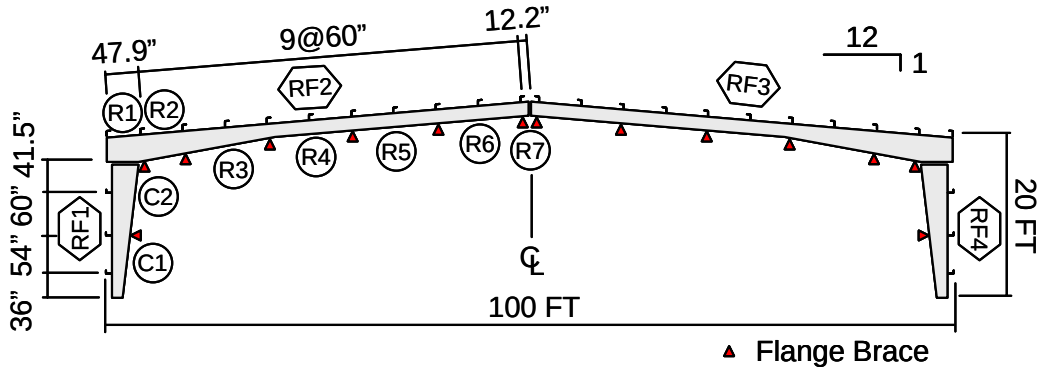

(b) Building B

Figure 6.8 Case 2 (100 ft×20 ft)

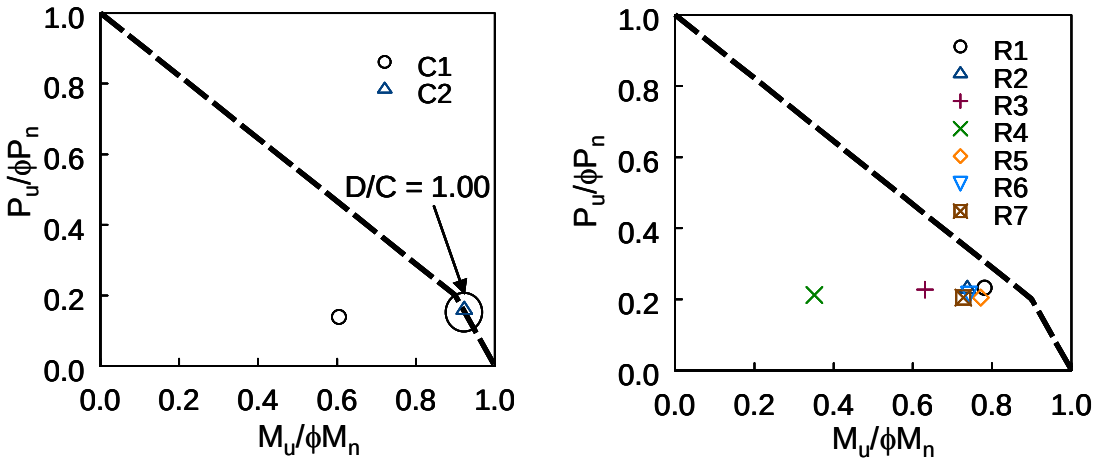

Column Rafter

(a) Building A

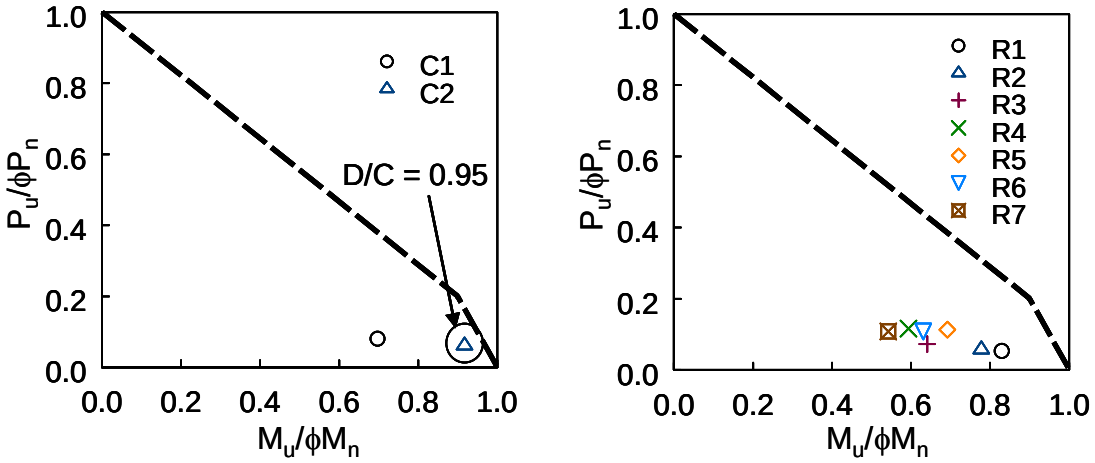

Column Rafter

(b) Building B

Figure 6.9 Case 2: Demand/Capacity Ratio under Governing Load Combination

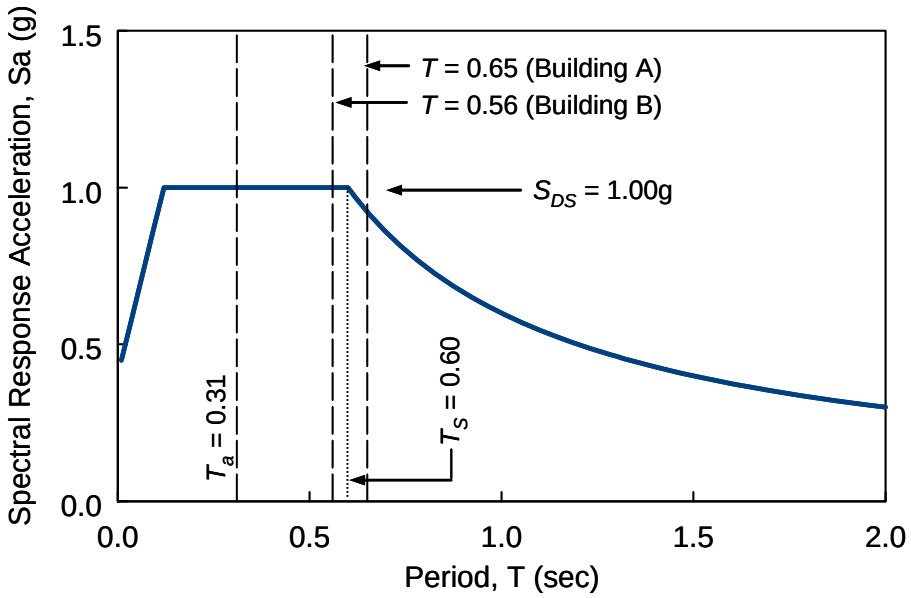

(a) Spectral Response Acceleration

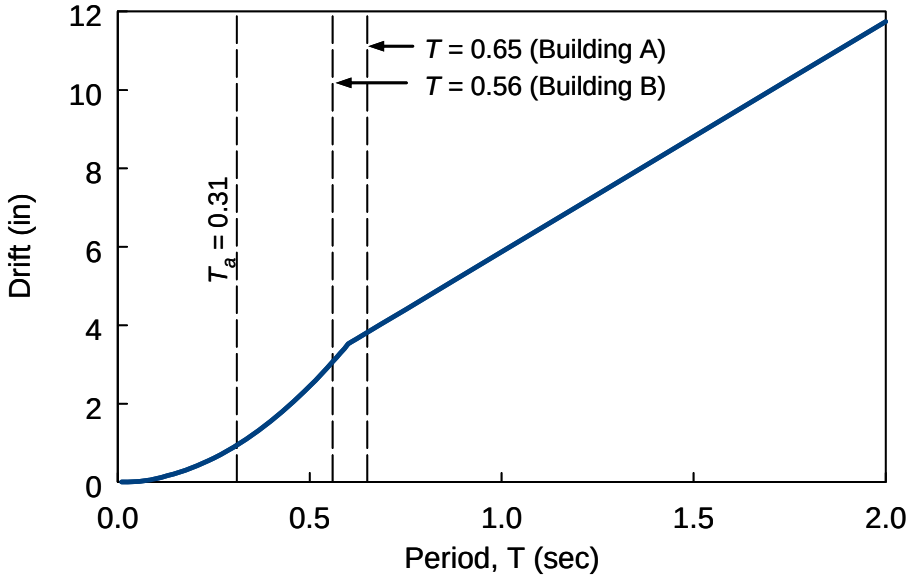

(b) Drift Demand

Figure 6.10 Case 2: Spectral Response Acceleration and Drift Demand

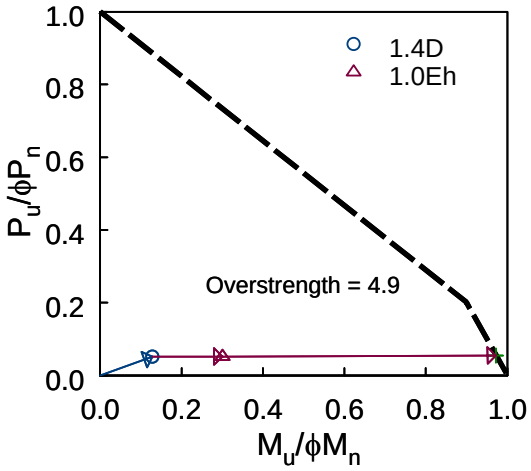

(a) Building A – Segment R4

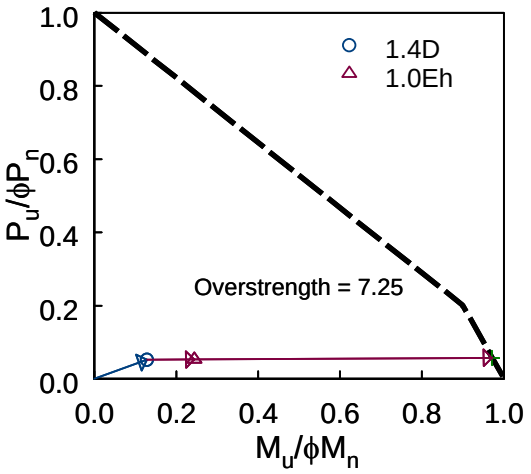

(b) Building B – Segment R4

Figure 6.11 Case 2: Overstrength Factor at Critical Segment

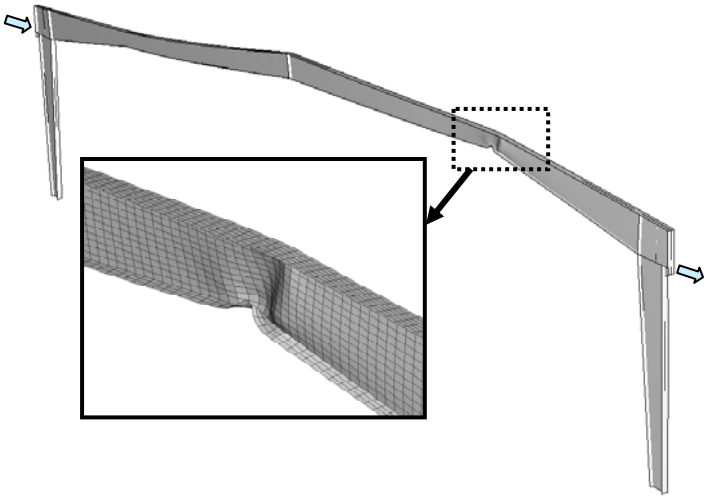

(a) Failure Mode

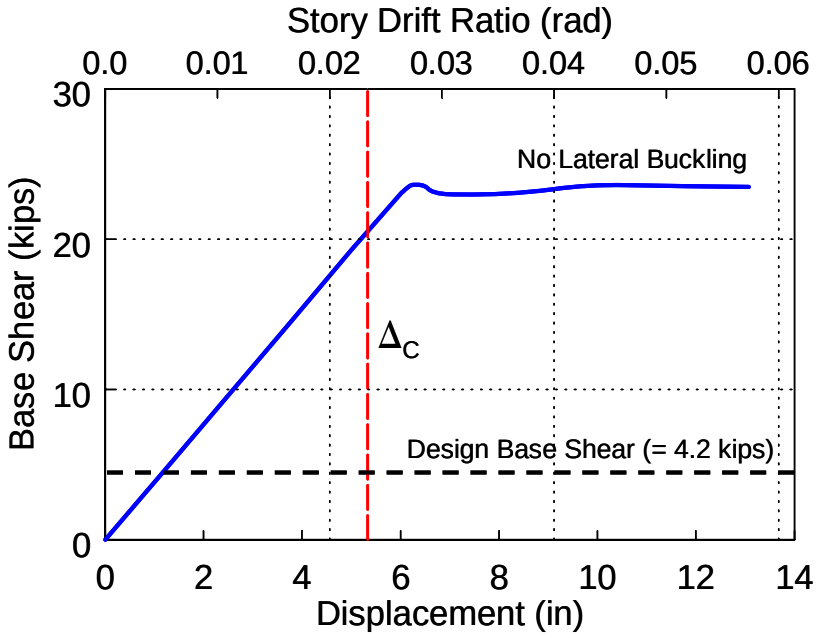

(b) Drift Capacity

Figure 6.12 Case 2: Failure Mode and Drift Capacity Verification of Building A

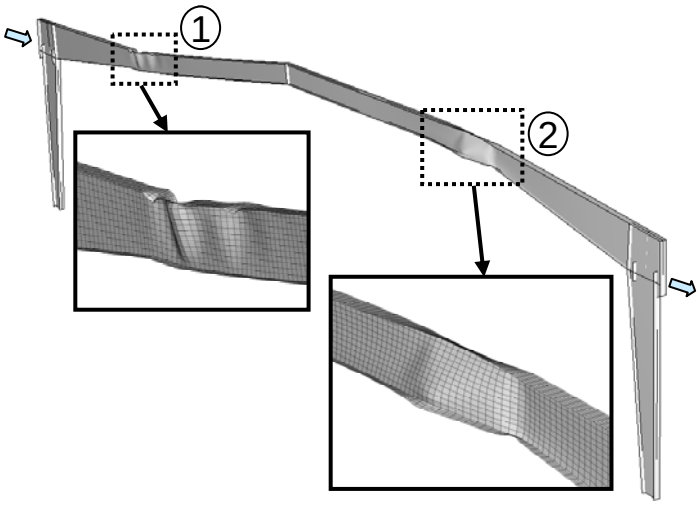

(a) Failure Mode

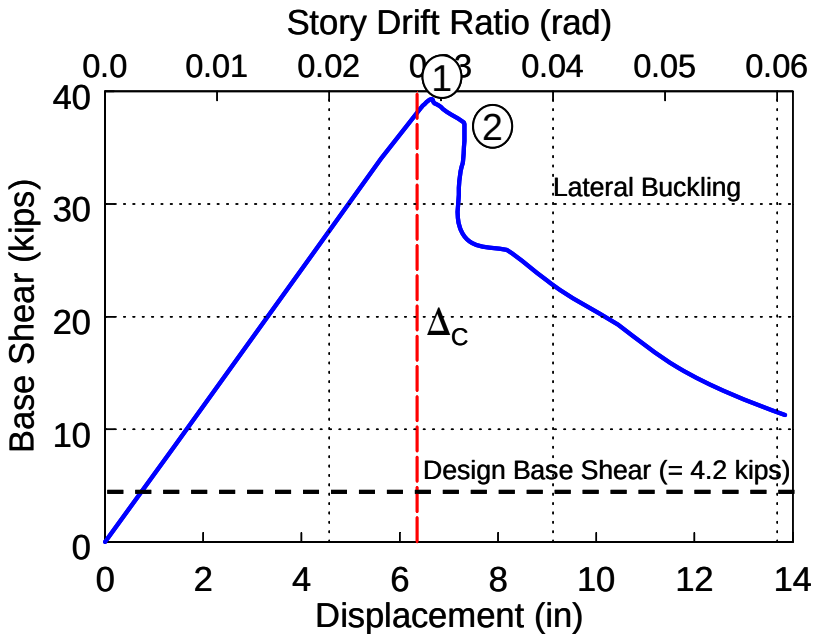

(b) Drift Capacity

Figure 6.13 Case 2: Failure Mode and Drift Capacity Verification of Building B

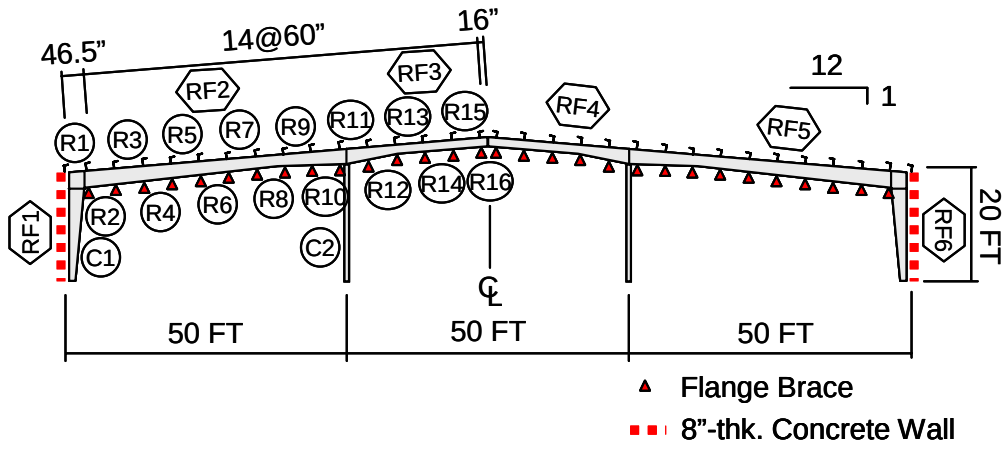

(a) Building 1

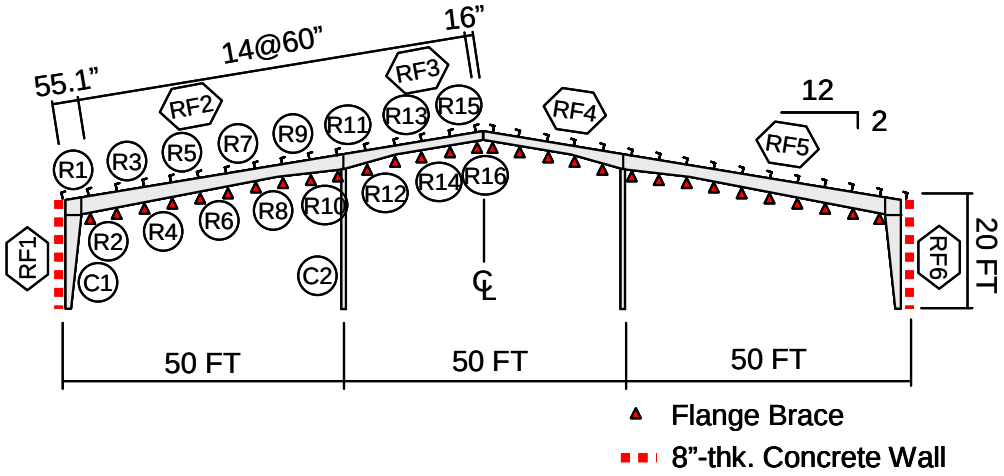

(b) Building 2

Figure 6.14 Case 3 (150 ft×20 ft)

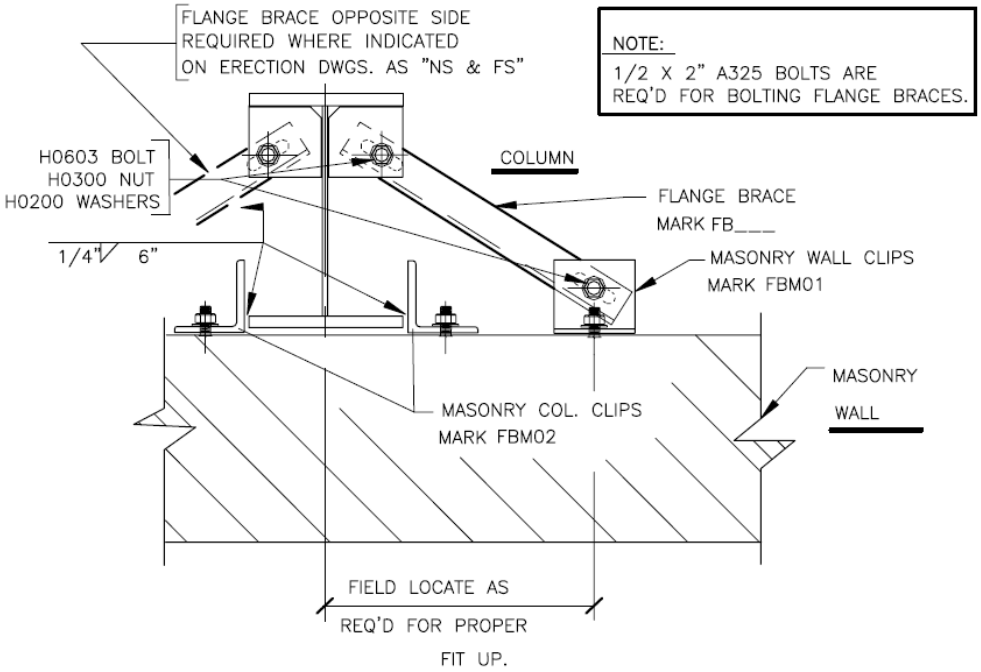

(a) Wall-to-Frame at Knee Area

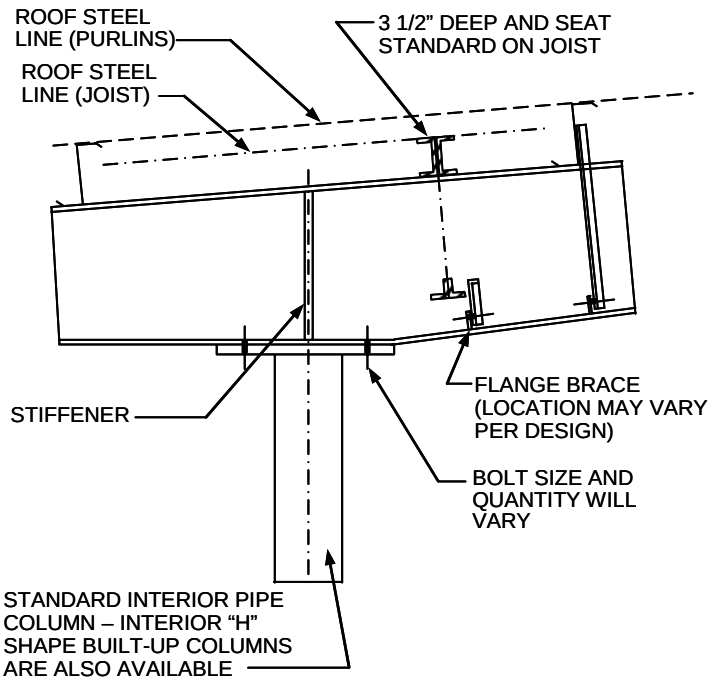

(b) Pipe-to-Rafter

Figure 6.15 Case 3: Connection Details (Nucor Building Systems)

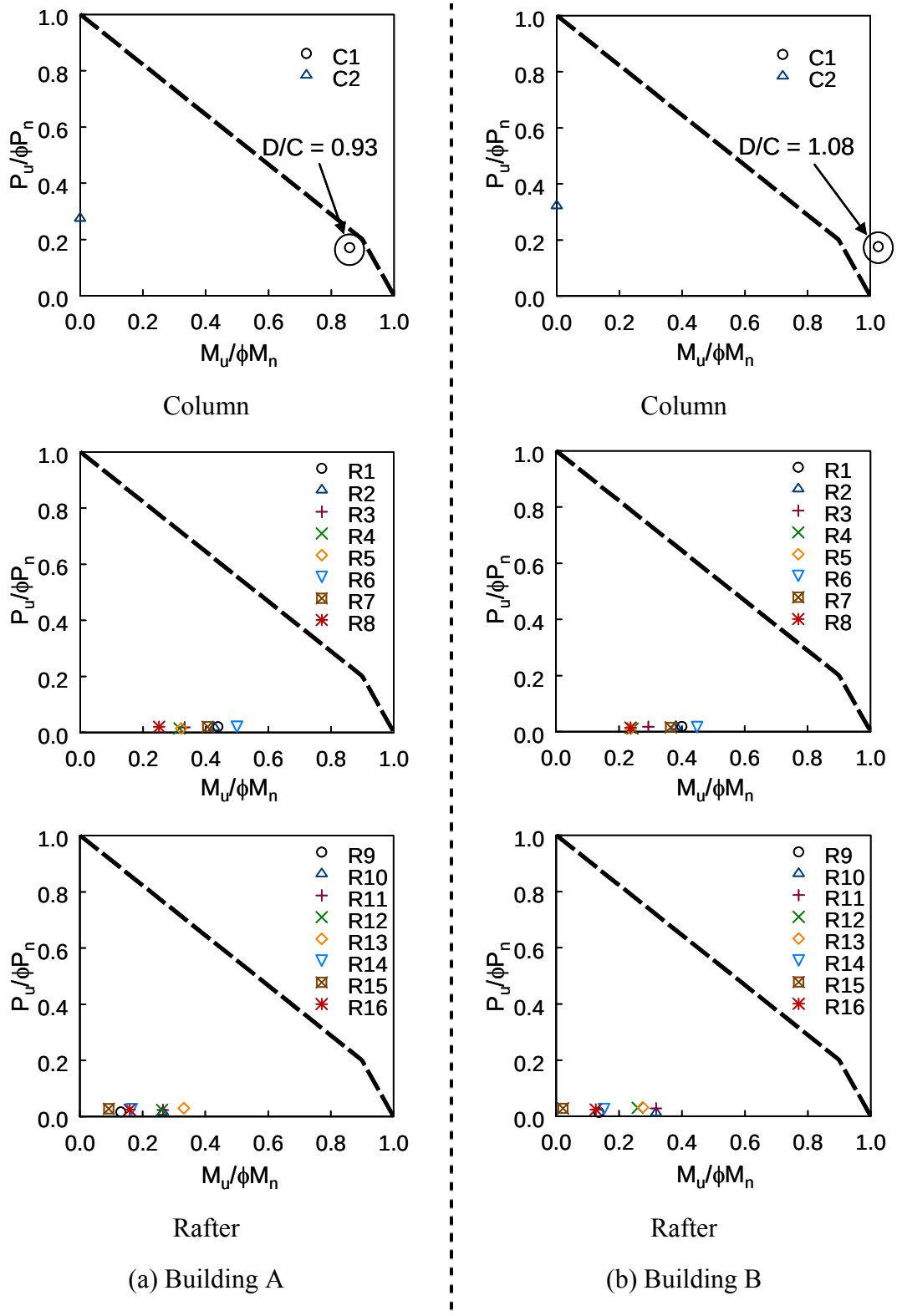

Figure 6.16 Case 3: Demand/Capacity Ratio under Governing Load Combination

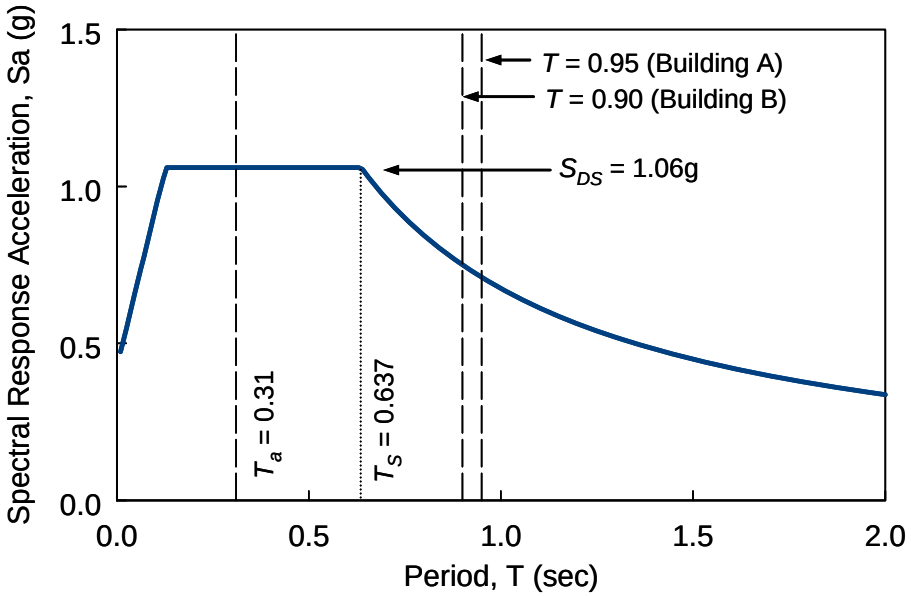

(a) Spectral Response Acceleration

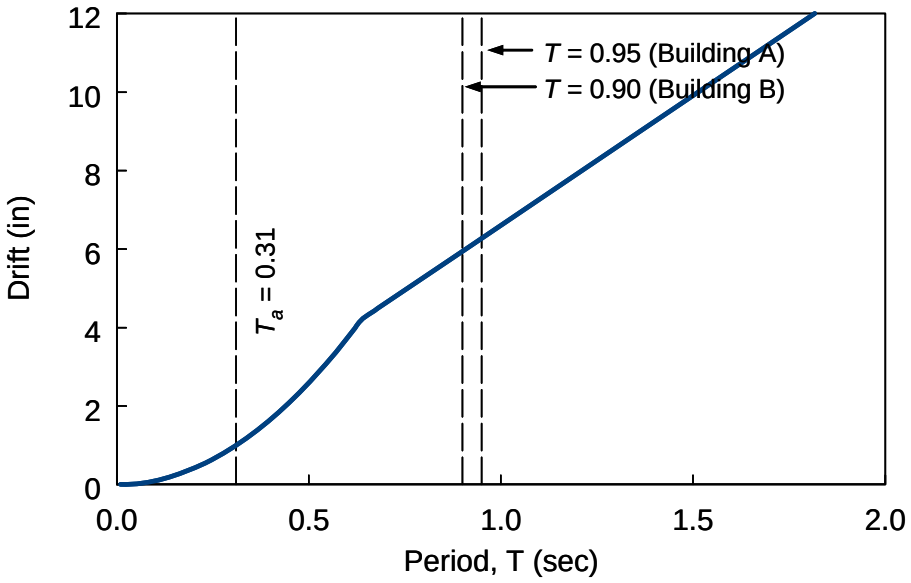

(b) Drift Demand

Figure 6.17 Case 3: Spectral Response Acceleration and Drift Demand

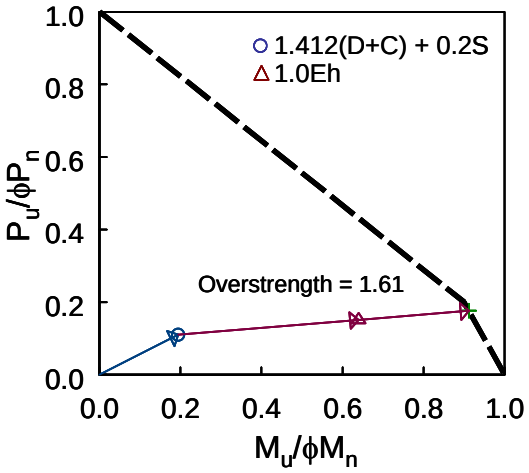

(a) Building A – Segment C1

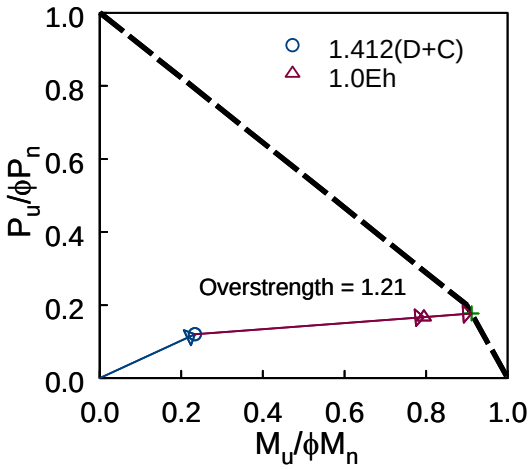

(b) Building B – Segment C1

Figure 6.18 Case 3: Overstrength Factor at Critical Segment

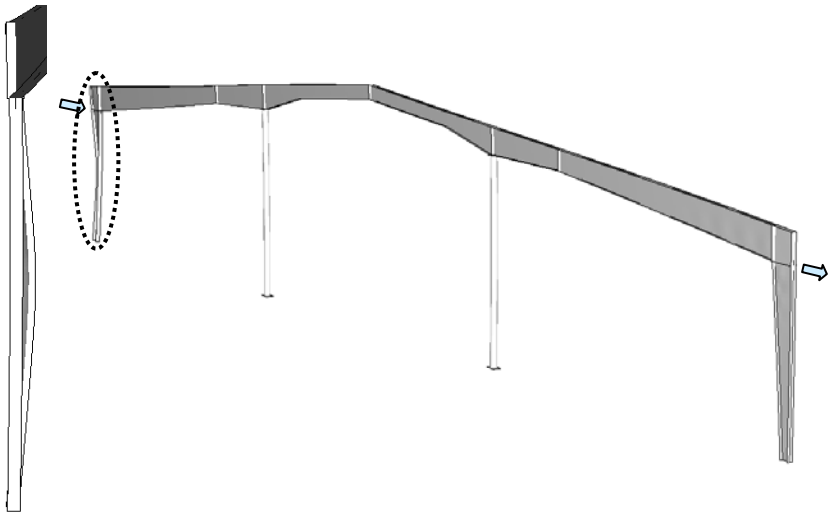

(a) Failure Mode

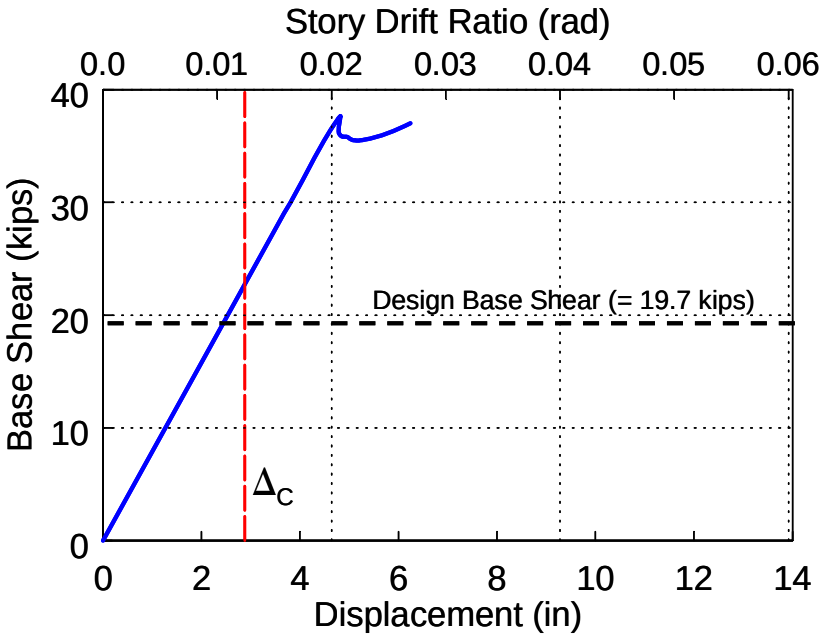

(b) Drift Capacity

Figure 6.19 Case 3: Failure Mode and Drift Capacity Verification of Building A

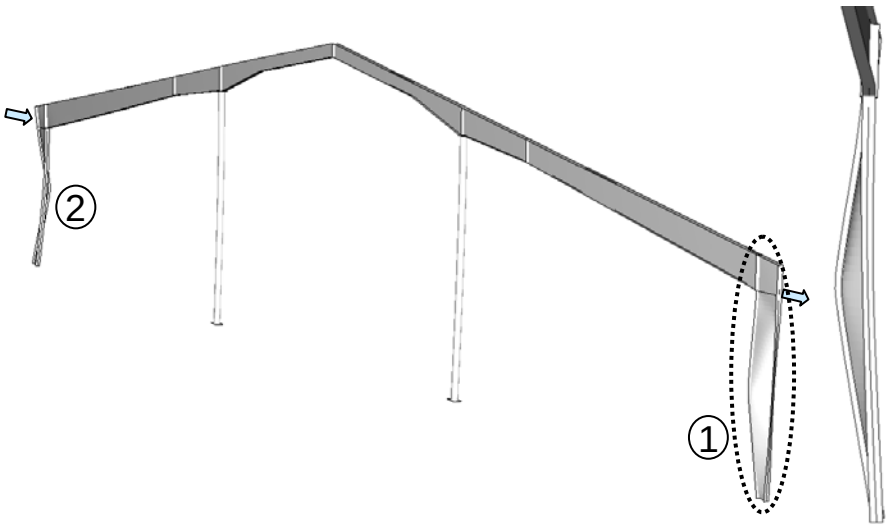

(a) Failure Mode

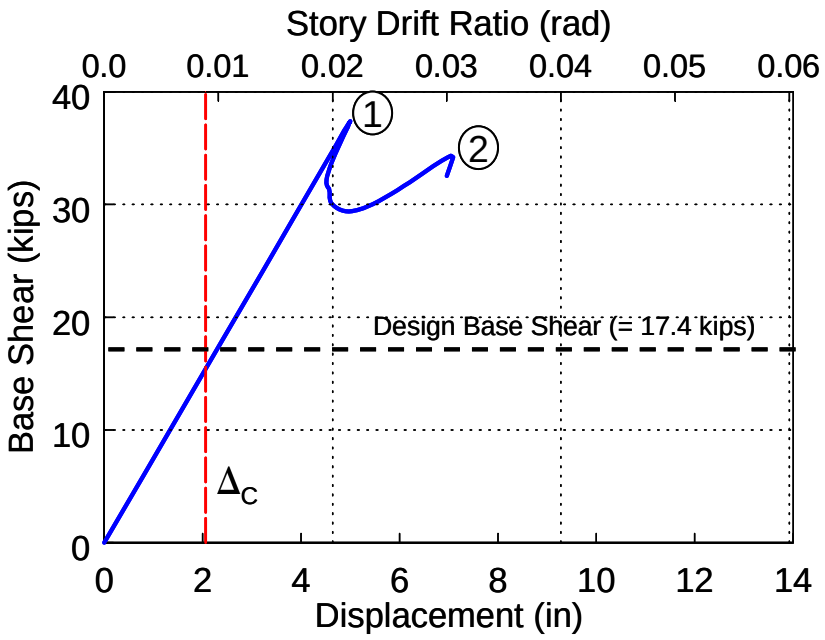

(b) Drift Capacity

Figure 6.20 Case 3: Failure Mode and Drift Capacity Verification of Building B

7 SUMMARY AND CONCLUSIONS

7.1 Summary

Metal building systems are widely used in low-rise (1- or 2-story) building construction in the United States. The primary cornerstone of metal building construction is to minimize the building cost through optimization of the steel weight and the fabrication process; the web-tapered I-shaped built-up sections are usually used and for ease of construction the bolted end-plate moment connections are adopted.

The design of this type of structural system is typically governed by the non-seismic load combinations such as gravity and wind loads. For seismic design in accordance with the *International Building Code* (ICC 2006), the system is designed as an Ordinary Moment Frames (OMFs); the stringent slenderness requirements for both local buckling and lateral buckling are not required, and therefore, non-compact or slender elements are usually used. It is highly questionable whether the plastic moment of the member can be developed. Even if the plastic moment can be developed, it is very difficult to determine the location of the plastic hinge since the section properties are optimized along the member length with respect to moment demand. No specific seismic design guideline is available for this type of system due to lack of research.

Despite the fact that past earthquakes have demonstrated satisfactory performance of light, single-story metal buildings with bolted end-plate moment connections, the stringent seismic design requirements, mainly developed for multi-

story steel moment frames associated with brittle fracture of welded joints after the 1994 Northridge, California earthquake, have also impacted the seismic design of metal building system. In addition, the growing use of heavy exterior walls (i.e., masonry or concrete) challenges the seismic performance of this system under major earthquakes. The development of a seismic design procedure for metal buildings is required.

In this research, a cyclic test of a full-scale metal building with web-tapered members was conducted with the objects of (1) evaluating the cyclic performance, and (2) providing test data for calibration of numerical simulation. Test building with a dimension of 60 ft wide by 20 ft eave height by 20 ft bay spacing and a 0.5:12 roof pitch was designed in accordance with IBC. One side of the building was clad with a metal sidewall, while the other side was completely open. The roof was also covered with the conventional metal roof panels. Non-seismic load combination ($1.2D + 1.6S + 0.8W$) was the governing load combination in the design. For testing purpose, the gravity load component in the earthquake load combination was imposed on top of the roof in the first stage using wood panels. In the second stage, cyclic loading was applied according to the loading sequence for beam-to-column moment connections specified in the *AISC Seismic Provisions* (AISC 2005) since no guideline for cyclic testing of this kind of framing system exists. Correlation study of the test results with the strength evaluations of web-tapered members specified in the *AISC LRFD Specification* (AISC 2001) was conducted. Lateral bracing force in flange braces was also evaluated.

Analytical correlation study with the test data was carried out using the finite element analysis program, ABAQUS (ABAQUS 2005). Rather than modeling the entire building explicitly, only one frame was modeled since the two frames in the test were nominally identical. Gravity load was first applied at the purlin locations as concentrated loads based on their tributary areas. Then monotonic lateral load was applied at column tops, where actuators were attached in the experimental testing, up to failure. The modified Riks algorithm was adopted to trace the post-buckling range of response. Column base boundary conditions were investigated. Sensitivity study on initial geometric imperfection was also conducted.

Together with the cyclic test and the analytical correlation study results, a drift-based seismic design concept was introduced and a seismic design procedure for metal building systems was proposed. Only elastic response of the system is considered up to failure. The design goal is to ensure that the drift capacity of the system is larger than the drift demand by a sufficient margin. Utilizing a linear relationship between base shear and story drift, the proposed design procedure requires checking if the ratio of the system overstrength factor (Ω_o) to the response modification factor (*R*-factor) is larger than a factor of safety (= 1.4). The overstrength factor of an unbraced segment is the multiplier to the earthquake load component in the earthquake load combination such that the strength limit state is reached. The system overstrength factor is then the smallest value among the overstrength factors of all unbraced segments. The factor of safety of 1.4 partially reflects the non-conservative nature of the current design provisions for metal building design; IBC assumes a damping ratio of 5% for determining earthquake load, while the damping ratio from field measurements is

about 2 to 3%. The actual fundamental period of the building, not the empirical period given in IBC, should also be used to calculate both the earthquake load and the story drift.

The impact of the proposed design procedure on the current design of metal buildings was investigated through a series of case studies. Three cases (two without heavy walls and one with heavy walls) were considered. The buildings were designed based on IBC (ICC 2006). The dimensions were 40 ft wide by 12 ft eave height, 100 ft wide by 20 ft eave height, and 150 ft wide by 20 ft eave height for Cases 1, 2 and 3, respectively, and a 25 ft bay spacing was assumed for all cases. Each case consisted of two buildings assumed to be located in a high seismic region with either a low wind (Building A) or high wind (Building B) region.

7.2 Conclusions

Major findings from the experimental testing of a full-scale metal building are:

(1) Gravity load effect ($1.412D + 0.2S$) of the test building was relatively small and the maximum stress due to gravity load was 3 ksi.

(2) System showed high deformability (i.e., flexibility), but little ductility. Elastic behavior was noted up to 2% drift. Non-ductile lateral buckling failure occurred at 2.6% drift, accompanied by sudden strength degradation.

(3) Proper detailing of flange brace connection is required. Premature lateral buckling at rafter and column at 2% drift excursion was observed. Buckling in the subsequent 2% drift cycle was prevented by welding the flange brace to the brace connection plate to avoid slippage.

(4) Internal member forces derived from measurements and associated failure modes corresponded well with strength evaluation of web-tapered members in the *AISC LRFD Specification* (AISC 2001).

(5) The horizontal component of the flange brace force ranged between 1.3% and 2.6% of the nominal yield strength of the rafter compression flange.

Major findings from the analytical correlation study are:

(1) Model assuming either ideal hinges or rotational springs at column bases predicted 35% larger vertical deflection than the measured value from test under gravity load. The strengthening effect from the roof panel and the attached wood panel used for gravity load was not considered in the models.

(2) Proper assumption of initial geometric imperfection was essential to predict the frame behavior. Good correlation with test results was observed in the models with an initial imperfection using the first eigen buckling mode shape. The model without an initial imperfection predicted the different failure mode and the much higher ultimate load.

(3) A parametric study demonstrated that the best correlation was obtained by adopting the first eigen buckling mode shape with an amplitude of $L_b/1000$, where L_b is unbraced length of the member.

(4) A model with rotational springs at column bases, accounting for rotational stiffness of the base plate connection, accurately predicted the response. Results from a model with ideal hinges at the column bases were also

acceptable. Although lateral stiffness was slightly underestimated, ultimate load and associated failure mode corresponded well with test results.

(5) The potential for the development of a tension field action as a structural fuse is addressed. Inelastic plate buckling of panel zone provides system strength and stability in the numerical simulation.

Major findings from the case study of the proposed seismic design procedure are:

(1) Metal buildings with heavy sidewalls following the current design practice are vulnerable to collapse under major earthquake events. Since earthquake load combinations usually govern the design of this class of metal buildings, larger members are needed in accordance with the proposed procedure.

(2) The proposed seismic design procedure does not affect the current design of typical metal buildings without heavy walls. The system has enough reserve strength under earthquake load since non-seismic load combinations govern the design.

APPENDIX A. MEMBER STRENGTH CHECK OF TEST FRMAE

The member strength was checked at three segments, C3, C4, and R2 [see Figure 3.1(a)] in accordance with the Load and Resistance Factor Design Specification (AISC 2001). Nominal yield strength of 55 ksi was used for the calculations.

A1. Unbraced Segment C3

General

The axial force, shear force, and moment were P_u = 34.1 kips, V_u = 16.7 kips, and M_u = 3,370 kip-in, respectively (see Figure 3.6). Section properties were given as follow:

- Inside flange: width (b_{fi}) = 6 in., thickness (t_{fi}) = 5/16 in.
- Outside flange: width (b_{fo}) = 6 in., thickness (t_{fo}) = ¼ in.
- Web: start (h_o) = 27.41 in., end (h) = 31 in., thickness (t_w) = 0.2 in.
- Unbraced length: L_x = 230 in., L_y = 68 in.

Check Axial Compressive Strength

Chapter E and Appendix F3 for web-tapered members of the 2001 LRFD Specification is applicable.

a. Flange Local Buckling

$$k_c = \frac{4}{\sqrt{h_o / t_w}} = \frac{4}{\sqrt{137.1}} = 0.342 \text{; therefore, } k_c = 0.35.$$

$$\lambda_r = 0.64\sqrt{\frac{Ek_c}{F_y}} = 0.64\sqrt{\frac{29000 \times 0.35}{55}} = 8.69$$

Since $\frac{b}{t} = \frac{b_{fo}}{2t_{fo}} = \frac{6}{2 \times 0.25} = 12 > \lambda_r$, the flange is slender.

$$1.17\sqrt{\frac{Ek_c}{F_y}} = 1.17\sqrt{\frac{29000\times 0.35}{55}} = 15.89$$

Since $0.64\sqrt{\frac{Ek_c}{F_y}} < b/t \le 1.17\sqrt{\frac{Ek_c}{F_y}}$, $Q_s = 1.415 - 0.65\left(\frac{b}{t}\right)\sqrt{\frac{F_y}{Ek_c}}$.

The reduction factor for slender unstiffened element is $Q_s = 0.841$.

b. Web Local Buckling

$$\lambda_r = 1.49\sqrt{\frac{E}{F_y}} = 0.64\sqrt{\frac{29000}{55}} = 34.2$$

Since $h_o/t_w = 137.1$, the web is slender.

$1.49\sqrt{E/f} = 1.49\sqrt{29000/31.24} = 45.39 < h_o/t_w = 137.1$

where f is taken as ϕF_{cr} with F_{cr} calculated based on Q_a = 1.0. $S_x = (K_\gamma L/r)_x$ = $1.28\times 230/10.56 = 27.87$ and $S_y = (KL/r)_y = 1.0\times 68/1.07 = 63.55$. $\phi = 0.85$.

$$(\lambda_{eff})_x = \frac{S_x}{\pi}\sqrt{\frac{F_y}{E}} = 0.39 < (\lambda_{eff})_y = \frac{S_y}{\pi}\sqrt{\frac{F_y}{E}} = 0.88.$$

Since $(\lambda_{eff})_y\sqrt{Q} = 0.88\times\sqrt{0.841} = 0.74 < 1.5$, $F_{cr} = Q\left[0.658^{Q\lambda_{eff}^2}\right]F_y = 36.76$ ksi.

The effective width is determined as follow:

$$b_e = 1.92t\sqrt{\frac{E}{f}}\left[1 - \frac{0.34}{(b/t)}\sqrt{\frac{E}{f}}\right]$$

$$= 1.92(0.2)\sqrt{\frac{29000}{31.24}}\left[1 - \frac{0.34}{(137.1)}\sqrt{\frac{29000}{31.24}}\right] = 6.70 \text{ in.} < 27.41 \text{ in.}$$

The reduction factor for the first iteration is $Q_a = 0.53$.

ϕF_{cr} based on $Q = Q_s \times Q_a$ =0.45 from the first iteration is 18.52 ksi, which is very different from the assumed value of f (= 31.24 ksi). Using $f = \phi F_{cr}$, after few iterations, b_e = 8.12 in., Q_a = 0.55, Q = 0.47, and ϕF_{cr} = 20.63 ksi.

c. Nominal Compressive Strength

$\phi P_n = \phi F_{cr} A_g = 20.63 \times 8.86 = 182.7$ kips.

Check Flexural Strength

a. Classification

$$\frac{h}{t_w} = 155.0$$

$$\lambda_r = 5.70\sqrt{\frac{E}{F_y}}\left(1 - 0.74\frac{P_u}{\phi_b P_y}\right) = 5.7\sqrt{\frac{29000}{55}}\left(1 - 0.74\frac{34.1}{0.9 \times 487.3}\right) = 124.8 < \frac{h}{t_w}$$

where ϕ_b = 0.9, $P_y = A_g F_y$ = 487.3 kips. Since $\lambda_r < \frac{h}{t_w}$, the web is slender and Chapter G for Plate Girders specified in the 2001 LRFD Specification is applicable.

b. Flange Local Buckling

$$\frac{b}{t} = \frac{b_{fi}}{2t_{fi}} = \frac{6}{2 \times 0.3125} = 9.6$$

$$\lambda_p = 0.38\sqrt{\frac{E}{F_{yf}}} = 0.38\sqrt{\frac{29000}{55}} = 8.73$$

$$\lambda_r = 1.35\sqrt{\frac{E}{F_{yf} / k_c}} = 1.35\sqrt{\frac{29000}{55/0.35}} = 18.34$$

Since $\lambda_p < \lambda < \lambda_r$, $F_{cr} = F_{yf}\left[1 - \frac{1}{2}\left(\frac{\lambda - \lambda_p}{\lambda_r - \lambda_p}\right)\right] = 52.5$ ksi.

The bending strength reduction factor, R_{pg}, is determined as follow:

$$R_{PG} = 1 - \frac{a_w}{1200 + 300a_w}\left(\frac{h}{t_w} - 5.7\sqrt{\frac{E}{F_y}}\right) = 0.968 \le 1.0$$

where $a_w = \frac{ht_w}{b_{fc}t_{fc}} = 3.31 \le 10$ (inside flange is in compression).

The nominal moment for flange local buckling is

$\phi_b M_n = \phi_b S_{xc} R_{PG} F_{cr} = 0.9(86.79)(0.968)\ (52.5) = 3{,}971$ kip-in.

b. Lateral-Torsional Buckling

The flexural strength of tapered flexural members for the limit state of lateral-torsional buckling is specified in Appendix F3-4 of the 2001 LRFD Specification.

$\gamma = \frac{d_L - d_o}{d_o} = \frac{31.56 - 27.97}{27.97} = 0.13$ and the radius of gyration, r_{To},= 1.43 (based on compression flange plus one-third of the compression web area).

$$F_{s\gamma} = \frac{0.41E}{h_s L d_o / A_f} = \frac{0.41(29000)}{(1.09)(68)(27.97)/(1.875)} = 10.7\,\text{ksi}.$$

$$F_{w\gamma} = \frac{5.9E}{(h_w L / r_{To})^2} = \frac{5.9(29000)}{[(1.003)(68)/(1.43)]^2} = 75.24\,\text{ksi}.$$

where $h_s = 1.0 + 0.023\gamma\sqrt{Ld_o / A_f} = 1.09$, $h_w = 1.0 + 0.00385\gamma\sqrt{L / r_{To}} = 1.003$.

The factor, *B*, considering the effect of moment gradient is determined as follow [Case (b)]:

$$B = 1.0 + 0.58\left(1.0 + \frac{f_{b1}}{f_{b2}}\right) - 0.7\gamma\left(1.0 + \frac{f_{b1}}{f_{b2}}\right)$$

$$= 1.0 + 0.58\left(1.0 - \frac{28.8}{38.8}\right) - 0.7(0.13)\left(1.0 - \frac{28.8}{38.8}\right) = 1.13$$

$$F_{b\gamma} = \frac{2}{3}\left[1 - \frac{F_y}{6B\sqrt{F_{s\gamma}{}^2 + F_{w\gamma}{}^2}}\right] = \frac{2}{3}\left[1 - \frac{55}{6(1.13)\sqrt{(10.7)^2 + (72.24)^2}}\right]$$

$= 32.74$ ksi $< 0.6F_y$ (= 33 ksi).

The nominal moment for lateral-torsional buckling is

$$\phi_b M_n = \phi_b (5/3) S_x^{'} F_{b\gamma r} = 0.9(5/3)(86.79)(32.74) = 4{,}262 \text{ kip-in},$$

where $S_x^{'}$ is the elastic section modulus of the larger end.

c. Nominal Flexural Strength

$\phi_b M_n = 3{,}971$ kip-in. (flange local buckling governs.)

Check P-M Interaction

$$\frac{P_u}{\phi P_n} = \frac{34.1}{182.7} = 0.187 < 0.2$$

$$\frac{P_u}{2\phi P_n} + \frac{M_u}{\phi_b M_n} = \frac{0.187}{2} + \frac{3370}{3971} = 0.942 \ < 1.0 \text{ (O.K.)}$$

Check Shear Strength

$V_u = 16.7$ kips

Since $\left[3.07\sqrt{E/F_{yw}} = 70.49\right] < \left[\frac{h_o}{t_w} = 137.1\right] < 260$,

$$\phi_v V_n = \phi_v A_w \left[\frac{4.52E}{(h/t_w)^2}\right]$$

$$= 0.9(27.97)(0.2)\left[\frac{4.52(29000)}{(137.1)^2}\right] = 35.1 \ \text{ kips} > V_u \text{ (O.K.)}$$

A2. Unbraced Segment C4

General

The axial force, shear force, and moment were P_u = 32.3 kips, V_u = 14.8 kips, and M_u = 3,110 kip-in, respectively. Section properties were given as follow:

- Inside flange: width (b_{fi}) = 8 in., thickness (t_{fi}) = 3/8 in.
- Outside flange: width (b_{fo}) = 8 in., thickness (t_{fo}) = ¼ in.
- Web: start (h_o) = 12 in., end (h) = 31 in., thickness (t_w) = 0.2 in.
- Unbraced length: L_x = 230 in., L_y = 230 in.

Check Axial Compressive Strength

a. Flange Local Buckling

$$k_c = \frac{4}{\sqrt{h_o / t_w}} = \frac{4}{\sqrt{60}} = 0.516$$

$$\lambda_r = 0.64\sqrt{\frac{Ek_c}{F_y}} = 0.64\sqrt{\frac{29000 \times 0.516}{55}} = 10.56$$

Since $\frac{b}{t} = \frac{b_{fo}}{2t_{fo}} = \frac{8}{2 \times 0.25} = 16 > \lambda_r$, the flange is slender.

$$1.17\sqrt{\frac{Ek_c}{F_y}} = 1.17\sqrt{\frac{29000 \times 0.516}{55}} = 19.31$$

Since $0.64\sqrt{\frac{Ek_c}{F_y}} < b/t \le 1.17\sqrt{\frac{Ek_c}{F_y}}$, $Q_s = 1.415 - 0.65\left(\frac{b}{t}\right)\sqrt{\frac{F_y}{Ek_c}} = 0.785$.

b. Web Local Buckling

$\left[\lambda_r = 1.49\sqrt{\frac{E}{F_y}} = 0.64\sqrt{\frac{29000}{55}} = 34.2\right] <$ [h_o/t_w = 60]; the web is slender.

After few iterations, $1.49\sqrt{E/f} = 1.49\sqrt{29000/18.44} = 59.09 < h_o/t_w = 60$

where $S_x = (K_\gamma L/r)_x = 1.40 \times 230/5.37 = 60.0$,

$S_y = (KL/r)_y = 1.0 \times 230/1.90 = 121$,

$$(\lambda_{eff})_x = \frac{S_x}{\pi}\sqrt{\frac{F_y}{E}} = 0.83 < (\lambda_{eff})_y = \frac{S_y}{\pi}\sqrt{\frac{F_y}{E}} = 1.37 .$$

Then, $b_e = 7.32$ in., $Q_a = 0.873$, $Q = 0.685$.

$$(\lambda_{eff})_y \sqrt{Q} = 1.37 \times \sqrt{0.685} = 1.13 \ < 1.5, \ \phi F_{cr} = \phi Q \left[0.658^{Q\lambda_{eff}^2}\right] F_y = 18.68 \text{ ksi}.$$

c. Nominal Compressive Strength

$\phi P_n = \phi F_{cr} A_g = 18.68 \times 7.4 = 138.2$ kips.

Check Flexural Strength

a. Classification

$$\frac{h}{t_w} = 155.0$$

$$\lambda_r = 5.70\sqrt{\frac{E}{F_y}}\left(1 - 0.74\frac{P_u}{\phi_b P_y}\right) = 5.7\sqrt{\frac{29000}{55}}\left(1 - 0.74\frac{32.3}{0.9 \times 407}\right) = 122.3 < \frac{h}{t_w}$$

where $\phi_b = 0.9$, $P_y = A_g F_y = 407.03$ kips. Since $\lambda_r < \frac{h}{t_w}$, the web is slender.

b. Flange Local Buckling

$$\frac{b}{t} = \frac{b_{fi}}{2t_{fi}} = \frac{8}{2 \times 0.375} = 10.67$$

$$\lambda_p = 0.38\sqrt{\frac{E}{F_{yf}}} = 0.38\sqrt{\frac{29000}{55}} = 8.73$$

$$\lambda_r = 1.35\sqrt{\frac{E}{F_{yf}/k_c}} = 1.35\sqrt{\frac{29000}{55/0.35}} = 18.34$$

Since $\lambda_p<\lambda<\lambda_r$, $F_{cr} = F_{yf}\left[1-\frac{1}{2}\left(\frac{\lambda-\lambda_p}{\lambda_r-\lambda_p}\right)\right] = 49.5$ ksi.

$$R_{PG} = 1-\frac{a_w}{1200+300a_w}\left(\frac{h}{t_w}-5.7\sqrt{\frac{E}{F_y}}\right) = 0.981 \le 1.0$$

where $a_w = \frac{ht_w}{b_{fc}t_{fc}} = 2.07 \le 10$ (inside flange is in compression).

The nominal moment for flange local buckling is

$\phi_b M_n = \phi_b S_{xc} R_{PG} F_{cr} = 0.9(117.6)(0.981)(49.5) = 5{,}133$ kip-in.

b. Lateral-Torsional Buckling

$$\gamma = \frac{d_L - d_o}{d_o} = \frac{31.63-12.63}{12.63} = 1.50\,,\ r_{To} = 2.19.$$

$$F_{s\gamma} = \frac{0.41E}{h_s L d_o / A_f} = 5.91 \text{ ksi.},\quad F_{w\gamma} = \frac{5.9E}{(h_w L / r_{To})^2} = 13.79 \text{ ksi.}$$

where $h_s = 1.0+0.023\gamma\sqrt{Ld_o/A_f} = 2.08$, $h_w = 1.0+0.00385\gamma\sqrt{L/r_{To}} = 1.059$.

$$B = \frac{1.75}{1.0+0.25\sqrt{\gamma}} = \frac{1.75}{1.0+0.25\sqrt{1.50}} = 1.34 \text{ [Case (d)]}$$

$$F_{b\gamma} = \frac{2}{3}\left[1-\frac{F_y}{6B\sqrt{F_{s\gamma}{}^2+F_{w\gamma}{}^2}}\right] = 19.94 \text{ ksi} \le 0.6F_y\ (= 33 \text{ ksi}).$$

The nominal moment for lateral-torsional buckling is

$\phi_b M_n = \phi_b (5/3) S_x^{'} F_{b\gamma r} = 0.9(5/3)(117.6)(19.94) = 3{,}517$ kip-in.

c. Nominal Flexural Strength

$\phi_b M_n = 3{,}517$ kip-in. (lateral-torsional buckling governs.)

Check P-M Interaction

$$\frac{P_u}{\phi P_n} = \frac{32.3}{138.2} = 0.234 > 0.2$$

$$\frac{P_u}{\phi P_n} + \frac{8}{9}\frac{M_u}{\phi_b M_n} = 0.234 + \frac{8}{9}\left(\frac{3110}{3517}\right) = 1.019 \quad \approx \quad 1.0 \text{ (say O.K.)}$$

Check Shear Strength

V_u = 14.8 kips

Since $\left[3.07\sqrt{E/F_{yw}} = 70.69\right] < \left[\frac{h_o}{t_w} = 102.3\right] < 260$,

$$\phi_v V_n = \phi_v 0.6 F_{yw} A_w \left(\frac{2.45\sqrt{E/F_{yw}}}{h/t_w}\right)$$

$$= (0.9)(0.6)(55)(12.63)(0.2)\left(\frac{2.45\sqrt{(29000/55)}}{60}\right) = 70.3 \text{ kips} > V_u. \text{ (O. K.)}$$

A3. Unbraced Segment R2

General

The axial force, shear force, and moment were P_u = 17.6 kips, V_u = 30.9 kips, and M_u = 2,111 kip-in, respectively. Section properties were given as follow:

- Inside flange: width (b_{fi}) = 6 in., thickness (t_{fi}) = ¼ in.
- Outside flange: width (b_{fo}) = 6 in., thickness (t_{fo}) = ¼ in.
- Web: start (h_o) = 23.01 in., end (h) = 30.38 in., thickness (t_w) = 0.225 in.
- Unbraced length: L_x = 356 in., L_y = 110 in.

Check Axial Compressive Strength

a. Flange Local Buckling

$$k_c = \frac{4}{\sqrt{h_o / t_w}} = \frac{4}{\sqrt{102.3}} = 0.396$$

$$\lambda_r = 0.64\sqrt{\frac{Ek_c}{F_y}} = 0.64\sqrt{\frac{29000 \times 0.396}{55}} = 9.25$$

Since $\frac{b}{t} = \frac{b_{fo}}{2t_{fo}} = \frac{6}{2 \times 0.25} = 12 > \lambda_r$, the flange is slender.

$$1.17\sqrt{\frac{Ek_c}{F_y}} = 1.17\sqrt{\frac{29000 \times 0.396}{55}} = 16.90$$

Since $0.64\sqrt{\frac{Ek_c}{F_y}} < b/t \le 1.17\sqrt{\frac{Ek_c}{F_y}}$, $Q_s = 1.415 - 0.65\left(\frac{b}{t}\right)\sqrt{\frac{F_y}{Ek_c}} = 0.875$.

b. Web Local Buckling

$$\lambda_r = 1.49\sqrt{\frac{E}{F_y}} = 0.64\sqrt{\frac{29000}{55}} = 34.2$$

Since $h_o/t_w = 102.3$, the web is slender.

After few iterations, $1.49\sqrt{E / f} = 1.49\sqrt{29000/19.53} = 57.41 < h_o/t_w = 102.3$

where $S_x = (K_\gamma L/r)_x = 0.79 \times 356/8.81 = 31.9$,

$S_y = (KL/r)_y = 1.0 \times 110/1.05 = 104.8$,

$$(\lambda_{eff})_x = \frac{S_x}{\pi}\sqrt{\frac{F_y}{E}} = 0.44 < (\lambda_{eff})_y = \frac{S_y}{\pi}\sqrt{\frac{F_y}{E}} = 1.07.$$

Then, $b_e = 9.0$ in., $Q_a = 0.614$, $Q = 0.538$.

$(\lambda_{eff})_y\sqrt{Q} = 1.07 \times \sqrt{0.583} = 0.817 < 1.5$, $\phi F_{cr} = \phi Q\left[0.658^{Q\lambda_{eff}^2}\right]F_y = 19.40$ ksi.

c. Nominal Compressive Strength

$\phi P_n = \phi F_{cr} A_g = 19.40 \times 8.2 = 159.1$ kips.

Check Flexural Strength

a. Classification

$$\frac{h}{t_w} = 135.0$$

$$\lambda_r = 5.70\sqrt{\frac{E}{F_y}}\left(1 - 0.74\frac{P_u}{\phi_b P_y}\right) = 5.7\sqrt{\frac{29000}{55}}\left(1 - 0.74\frac{17.6}{0.9 \times 449.7}\right) = 126.7 < \frac{h}{t_w}$$

where $\phi_b = 0.9$, $P_y = A_g F_y = 487.3$ kips. Since $\lambda_r < \frac{h}{t_w}$, the web is slender.

b. Flange Local Buckling

$$\frac{b}{t} = \frac{b_{fi}}{2t_{fi}} = \frac{6}{2 \times 0.25} = 12$$

$$\lambda_p = 0.38\sqrt{\frac{E}{F_{yf}}} = 0.38\sqrt{\frac{29000}{55}} = 8.73$$

$$\lambda_r = 1.35\sqrt{\frac{E}{F_{yf} / k_c}} = 1.35\sqrt{\frac{29000}{55 / 0.35}} = 18.34$$

Since $\lambda_p < \lambda < \lambda_r$, $F_{cr} = F_{yf}\left[1 - \frac{1}{2}\left(\frac{\lambda - \lambda_p}{\lambda_r - \lambda_p}\right)\right] = 45.6$ ksi.

$$R_{PG} = 1 - \frac{a_w}{1200 + 300a_w}\left(\frac{h}{t_w} - 5.7\sqrt{\frac{E}{F_y}}\right) = 1.02 > 1.0\text{; therefore, } R_{PG} = 1.0$$

where $a_w = \frac{ht_w}{b_{fc}t_{fc}} = 4.56 \le 10$ (inside flange is in compression).

The nominal moment for flange local buckling is

$\phi_b M_n = \phi_b S_{xc} R_{PG} F_{cr} = 0.9(79.62)(1.0)(45.6) = 3{,}268$ kip-in.

b. Lateral-Torsional Buckling

$$\gamma = \frac{d_L - d_o}{d_o} = \frac{30.88 - 23.51}{23.51} = 0.31\,,\ r_{To} = 1.38.$$

$$F_{s\gamma} = \frac{0.41E}{h_s L d_o / A_f} = \frac{0.41(29000)}{(1.30)(110)(23.51)/(1.5)} = 5.29 \ \text{ ksi.}$$

$$F_{w\gamma} = \frac{5.9E}{(h_w L / r_{To})^2} = \frac{5.9(29000)}{[(1.011)(110)/(1.38)]^2} = 26.23 \ \text{ ksi.}$$

where $h_s = 1.0 + 0.023\gamma\sqrt{Ld_o / A_f} = 1.30$, $h_w = 1.0 + 0.00385\gamma\sqrt{L / r_{To}} = 1.011$.

$$B = 1.0 + 0.58\left(1.0 + \frac{f_{b1}}{f_{b2}}\right) - 0.7\gamma\left(1.0 + \frac{f_{b1}}{f_{b2}}\right)$$

$$= 1.0 + 0.58\left(1.0 - \frac{14.8}{35.9}\right) - 0.7(0.31)\left(1.0 - \frac{14.8}{35.9}\right) = 1.21 \ \text{ [Case (b)].}$$

$$F_{b\gamma} = \frac{2}{3}\left[1 - \frac{F_y}{6B\sqrt{F_{s\gamma}{}^2 + F_{w\gamma}{}^2}}\right] = 26.30 \ \text{ ksi} < 0.6F_y \ (= 33 \text{ ksi}).$$

The nominal moment for lateral-torsional buckling is

$$\phi_b M_n = \ \phi_b (5/3) S_x^{'} F_{b\gamma r} = 0.9(5/3)(79.62)(26.30) = 3{,}141 \text{ kip-in.}$$

c. Nominal Flexural Strength

$\phi_b M_n$ = 3,141 kip-in. (lateral-torsional buckling governs.)

Check Unity

$$\frac{P_u}{\phi P_n} = \frac{17.6}{159.1} = 0.107 < 0.2$$

$$\frac{P_u}{2\phi P_n} + \frac{M_u}{\phi_b M_n} = \frac{0.107}{2} + \frac{2111}{3141} = 0.73 \ \text{ (O.K.)}$$

Check Shear Strength

V_u = 30.9 kips

Since $\left[3.07\sqrt{E/F_{yw}} = 70.49\right] < \left[\frac{h_o}{t_w} = 102.3\right] < 260$

$$\phi_v V_n = \phi_v A_w \left[\frac{4.52E}{(h/t_w)^2}\right]$$

$$= 0.9(23.51)(0.225)\left[\frac{4.52(29000)}{(102.3)^2}\right] = 59.63 \quad \text{kips} > V_u \text{ (O.K.)}.$$

APPENDIX B. OVERSTRENGTH FACTOR OF EXAMPLE BUILDINGS

B1. Example Building – Case 2 (100 ft×20 ft)

B1.1 Building A

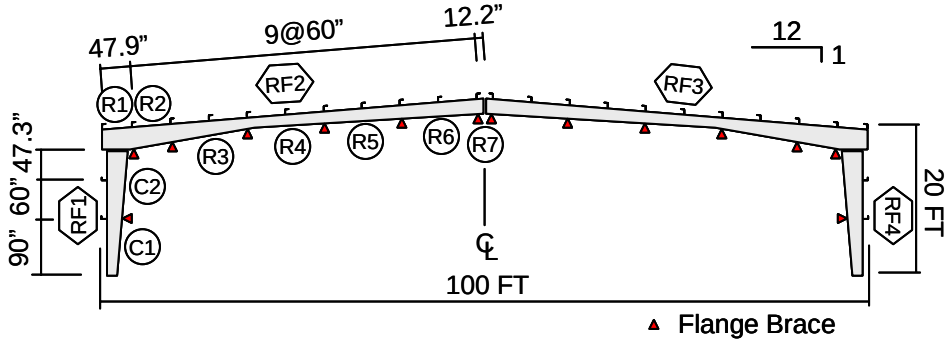

Figure B1 Case 2: Unbraced Segment Designation for Building A

- **Overstrength Factor under Earthquake Load Combination**

Earthquake Load Combination = $1.4D + 1.0E_h$

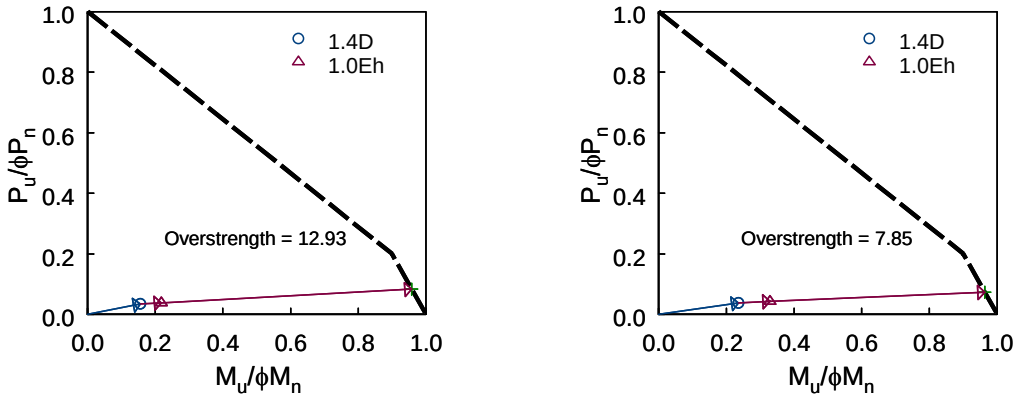

Segment C1 Segment C2

Figure B2 Case 2: Overstrength Factor of Building A

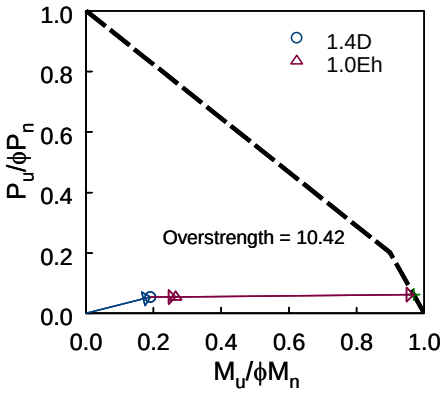

Segment R1

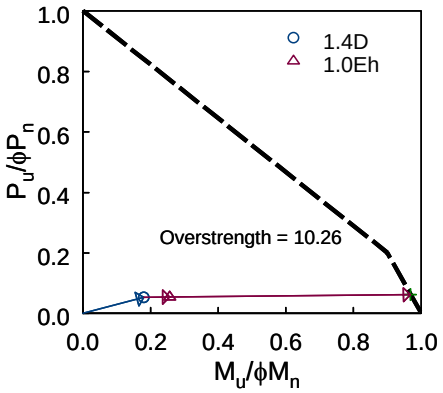

Segment R2

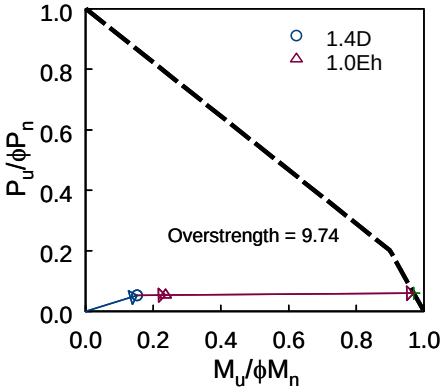

Segment R3

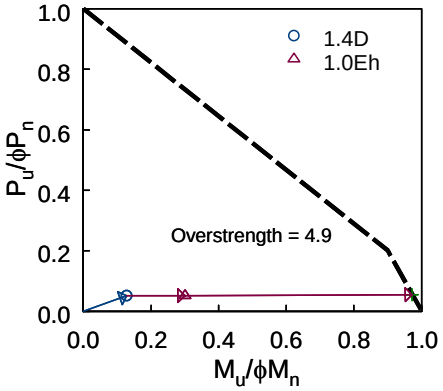

Segment R4

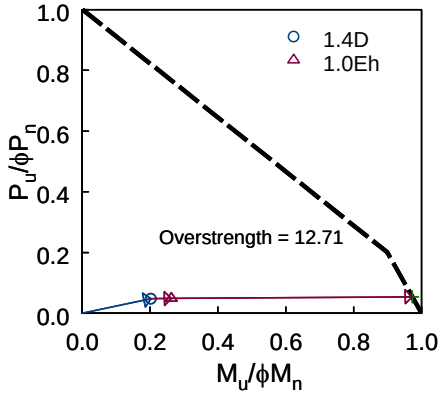

Segment R5

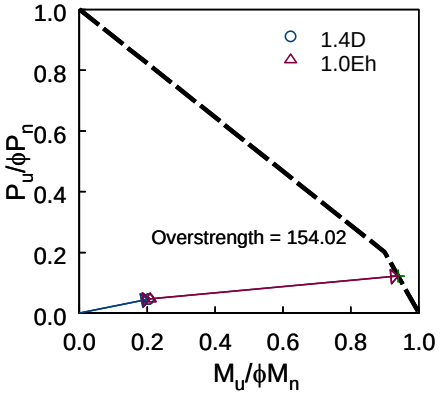

Segment R6

Figure B2 Case 2: Overstrength Factor of Building A (continued)

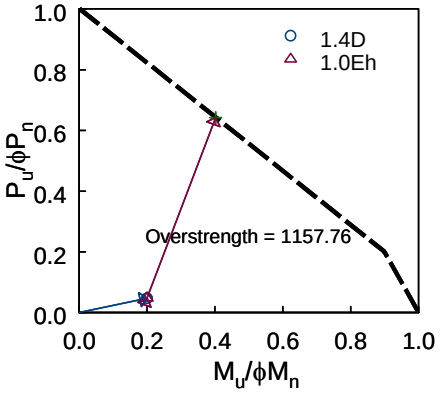

Segment R7

Figure B2 Case 2: Overstrength Factor of Building A (contimued)

B1.2 Building B

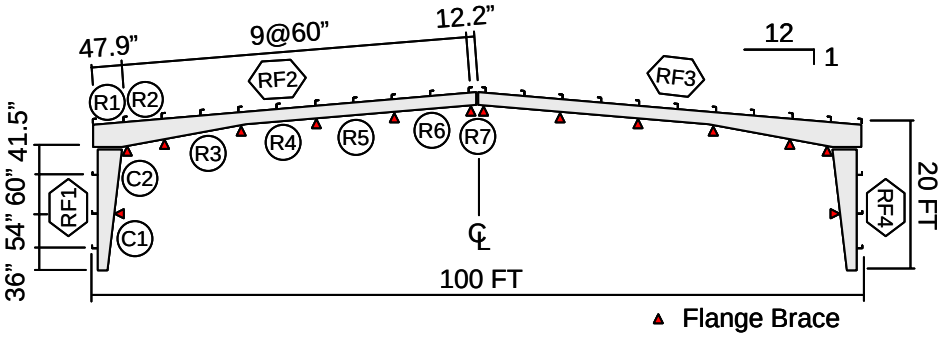

Figure B3 Case 2: Unbraced Segment Designation for Building B

- **Overstrength Factor under Earthquake Load Combination**

Earthquake Load Combination = $1.4D + 1.0E_h$

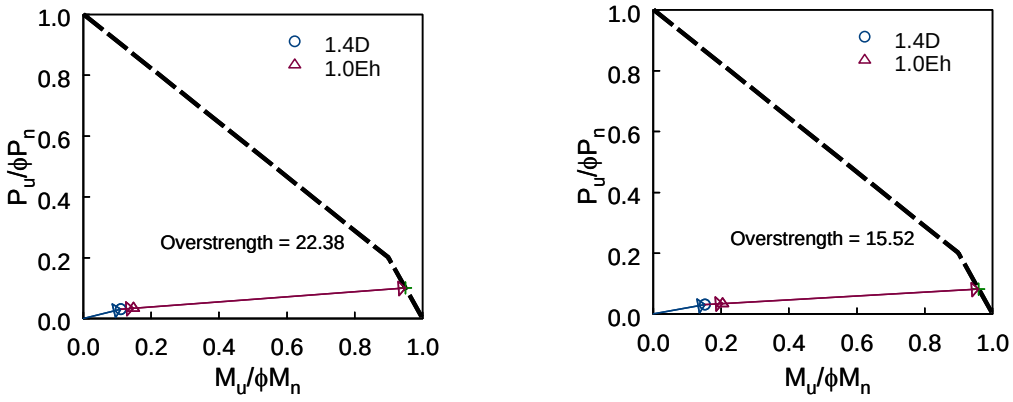

Segment C1 Segment C2

Figure B4 Case 2: Overstrength Factor of Building B

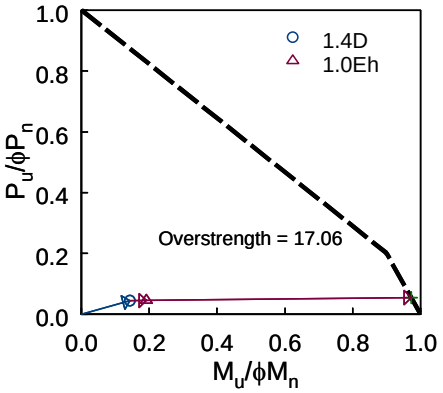

Segment R1

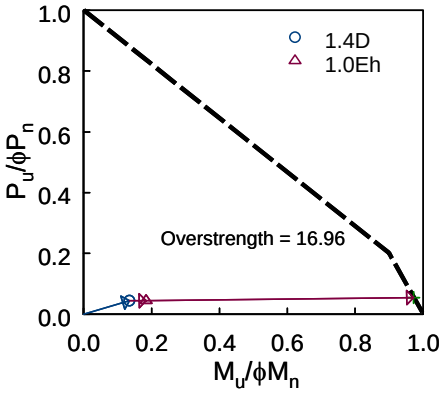

Segment R2

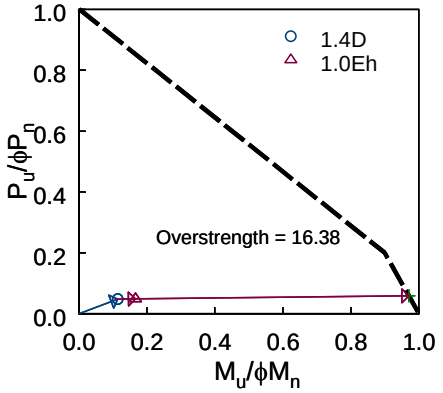

Segment R3

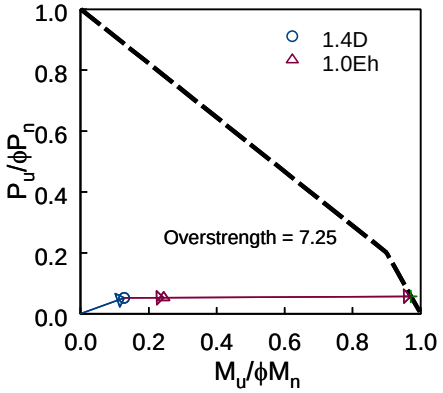

Segment R4

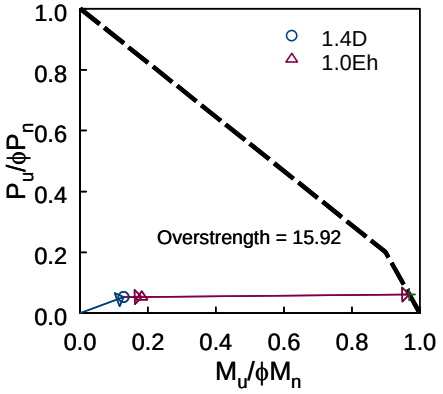

Segment R5

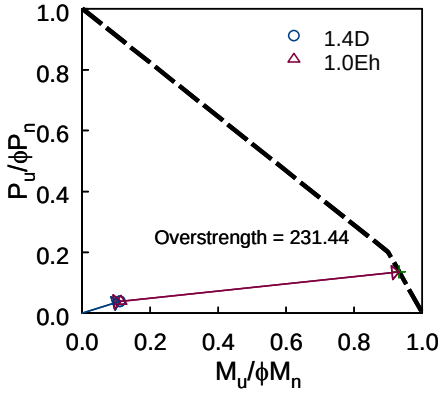

Segment R6

Figure B4 Case 2: Overstrength Factor of Building B (continued)

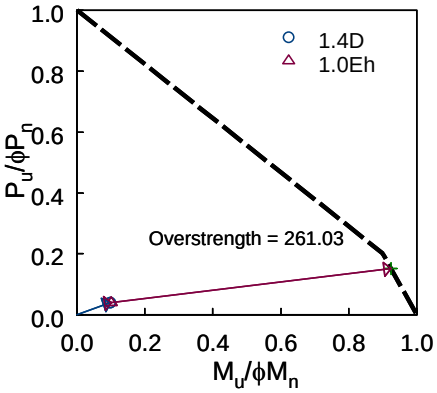

Segment R7

Figure B4 Case 2: Overstrength Factor of Building B (continued)

B2. Example Building – Case 3 (150 ft×20 ft)

B2.1 Building A

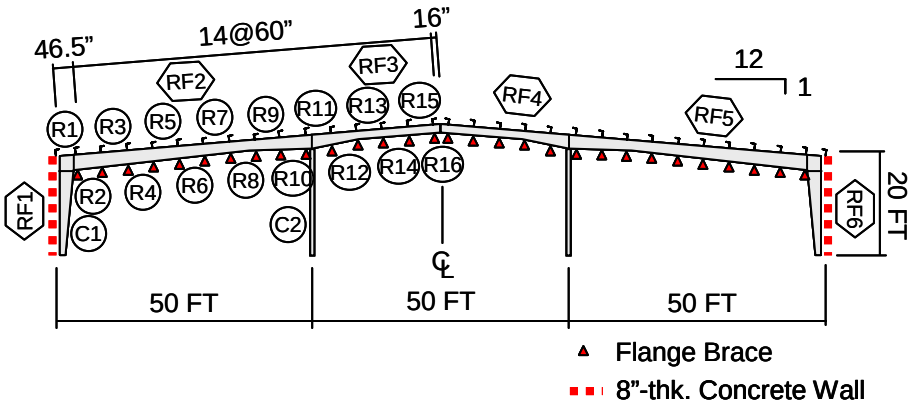

Figure B5 Case 3: Unbraced Segment Designation for Building A

- **Overstrength Factor under Earthquake Load Combination**

Earthquake Load Combination = $1.412(D+C) + 0.2S + 1.0E_h$

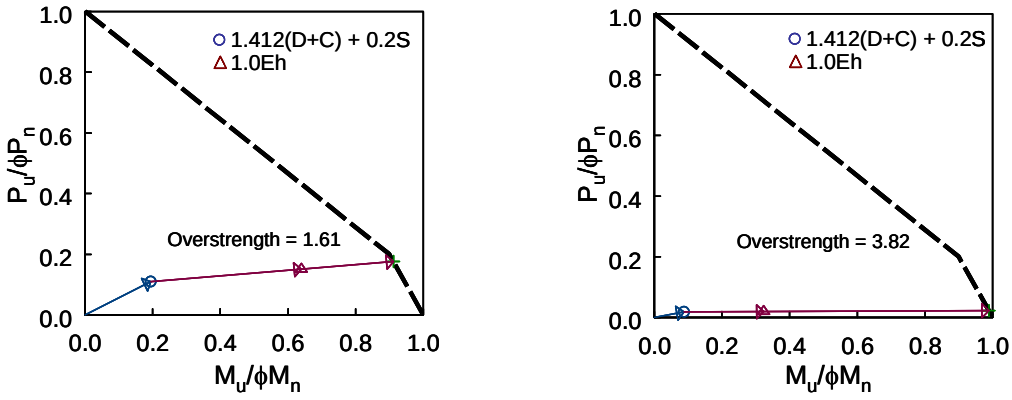

Segment C1 Segment R1

Figure B6 Case 3: Overstrength Factor of Building A

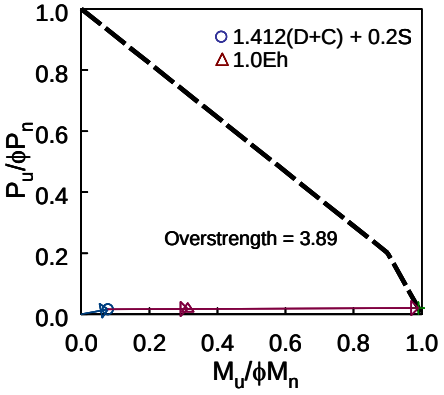

Segment R2

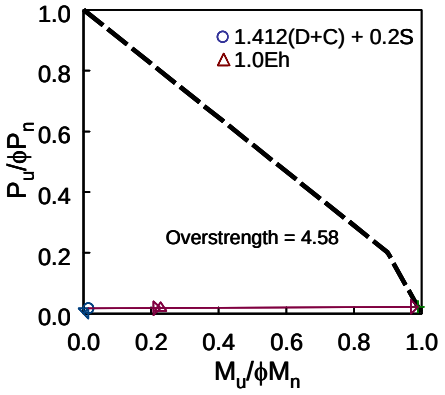

Segment R3

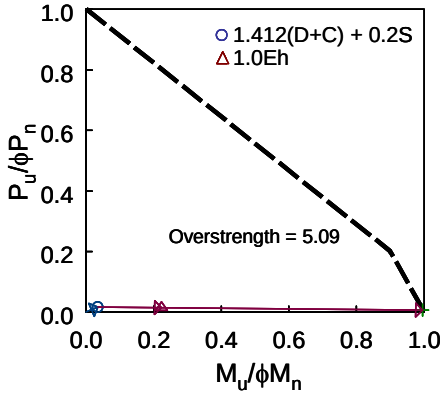

Segment R4

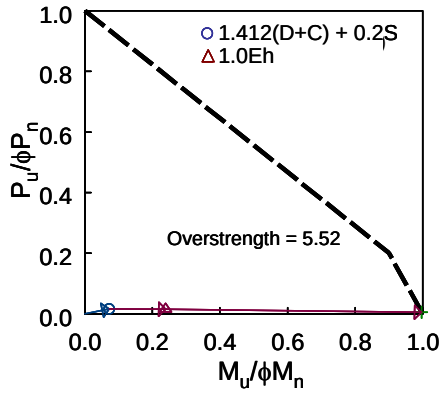

Segment R5

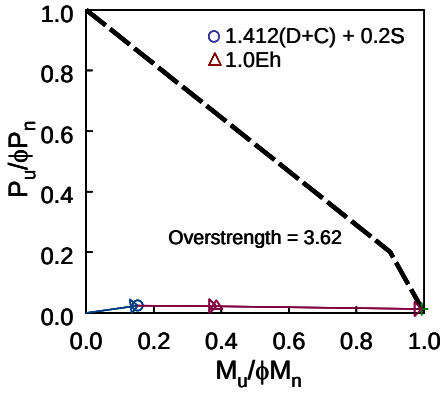

Segment R6

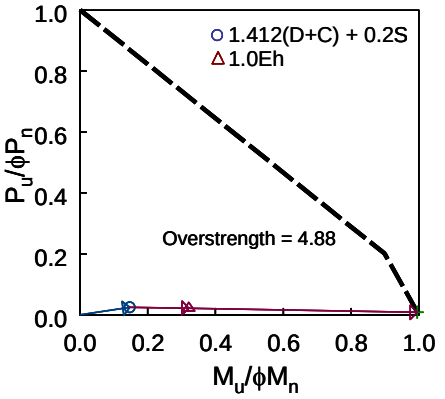

Segment R7

Figure B6 Case 3: Overstrength Factor of Building A (continued)

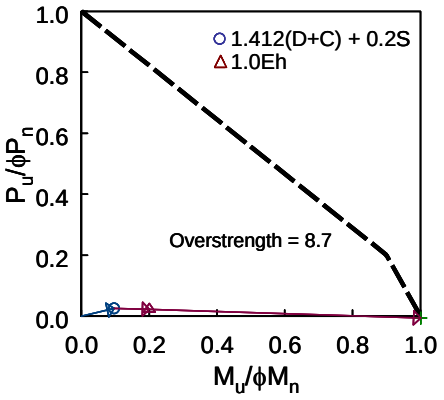

Segment R8

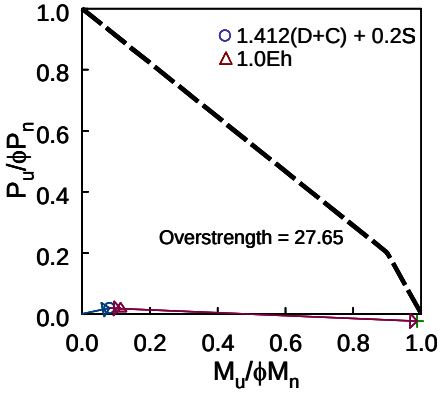

Segment R9

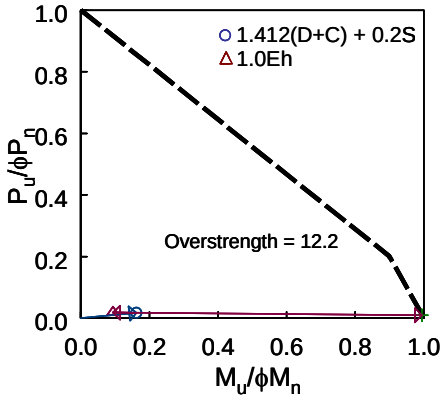

Segment R10

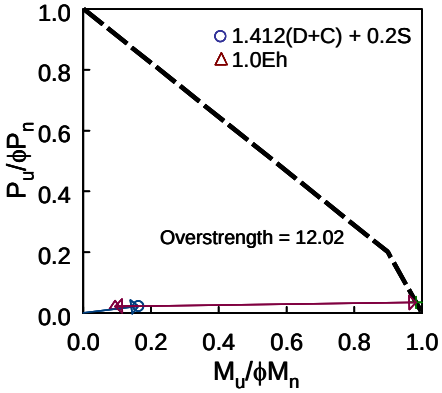

Segment R11

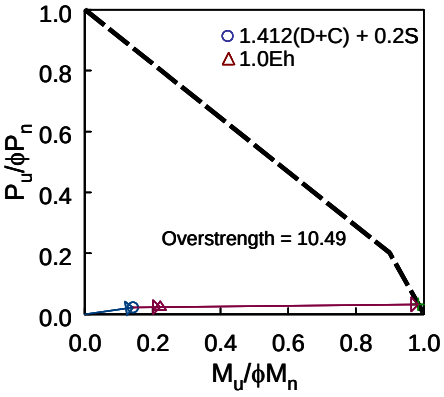

Segment R12

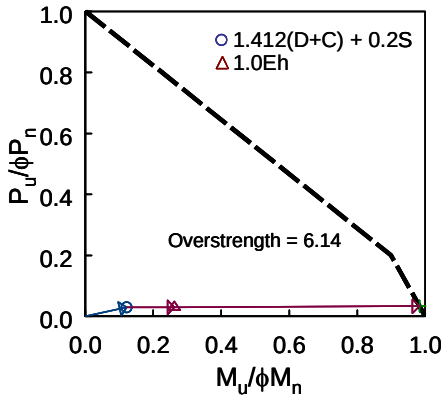

Segment R13

Figure B6 Case 3: Overstrength Factor of Building A (continued)

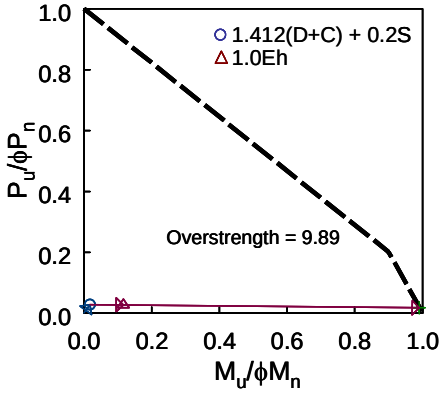

Segment R14

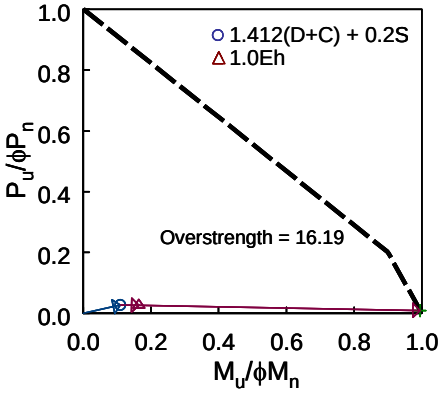

Segment R15

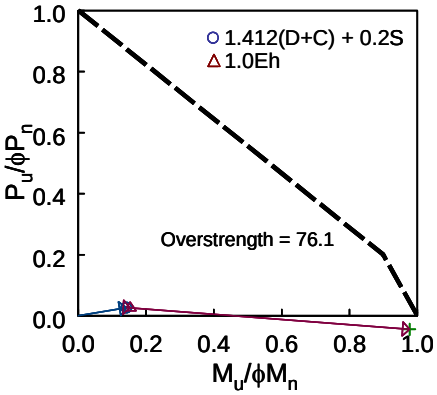

Segment R16

Figure B6 Case 3: Overstrength Factor of Building A (continued)

B2.2 Building B

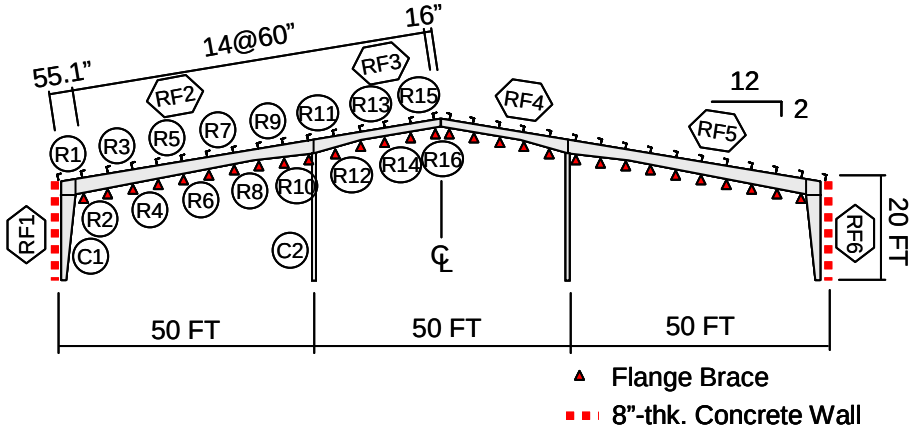

Figure B7 Case 3: Unbraced Segment Designation for Building B

- **Overstrength Factor under Earthquake Load Combination**

Earthquake Load Combination = $1.412(D+C) + 1.0E_h$

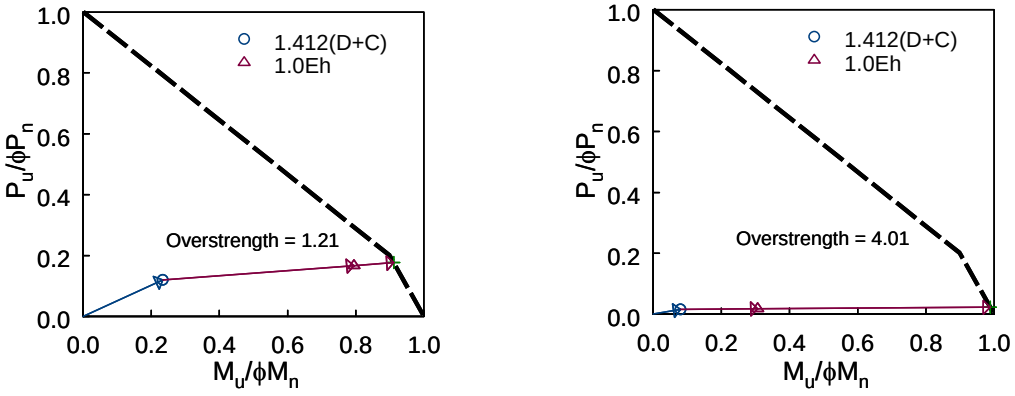

Segment C1 Segment R1

Figure B8 Case 3: Overstrength Factor of Building B

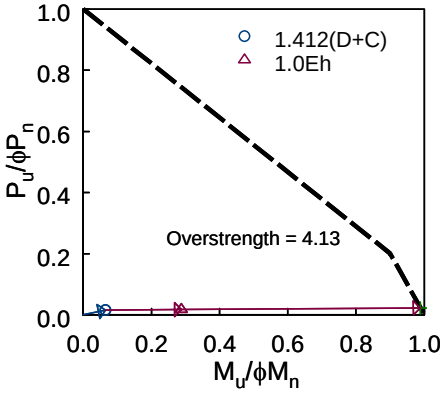

Segment R2

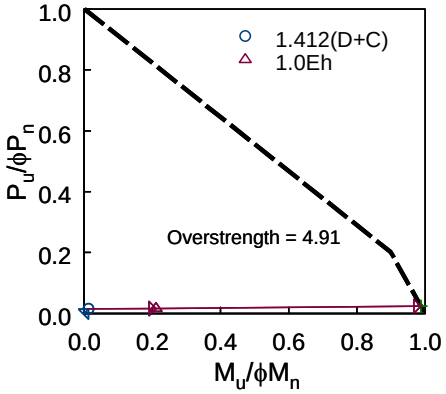

Segment R3

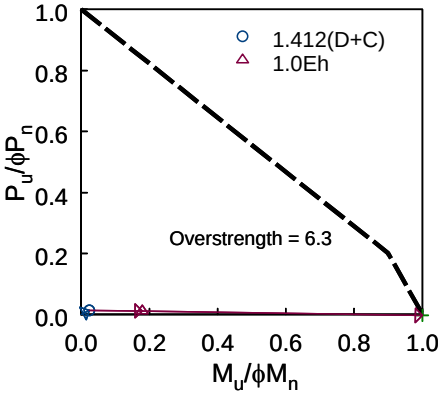

Segment R4

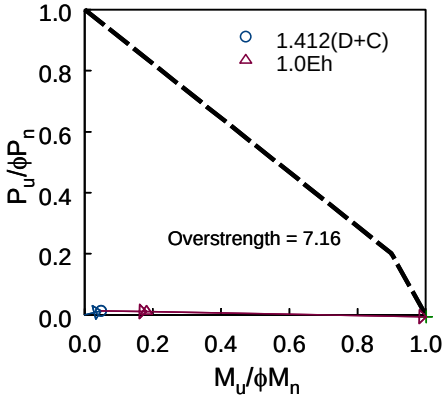

Segment R5

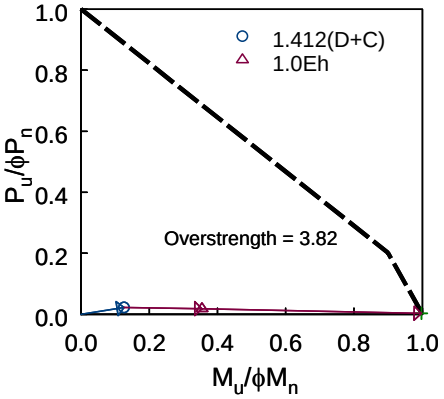

Segment R6

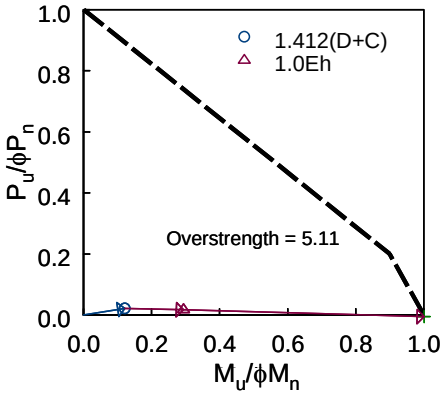

Segment R7

Figure B8 Case 3: Overstrength Factor of Building B (continued)

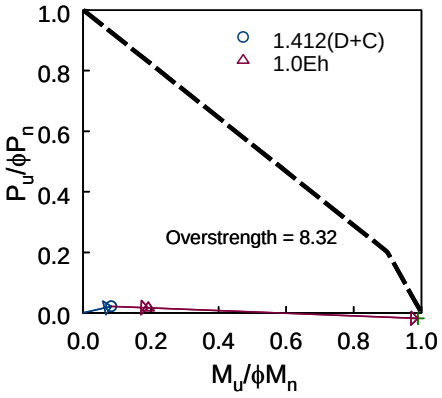

Segment R8

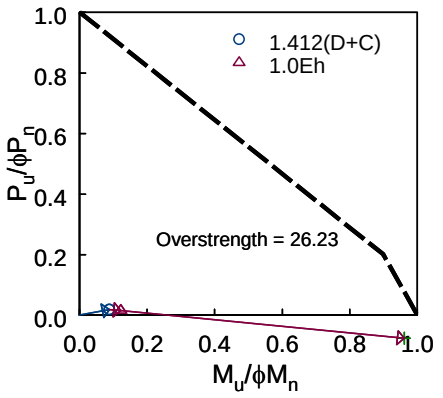

Segment R9

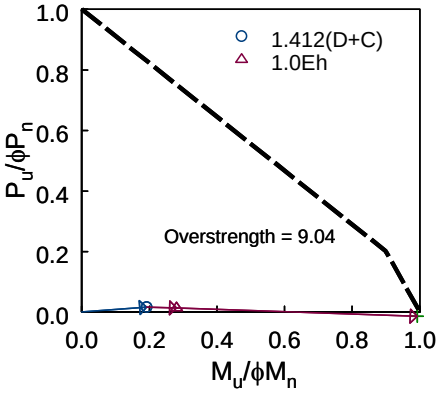

Segment R10

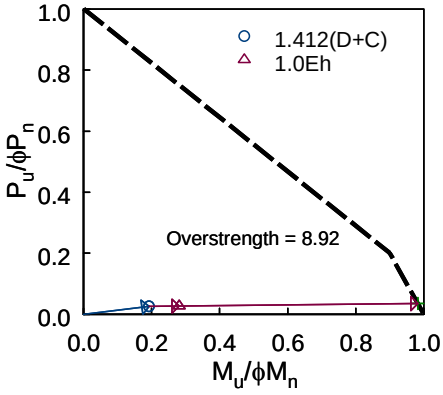

Segment R11

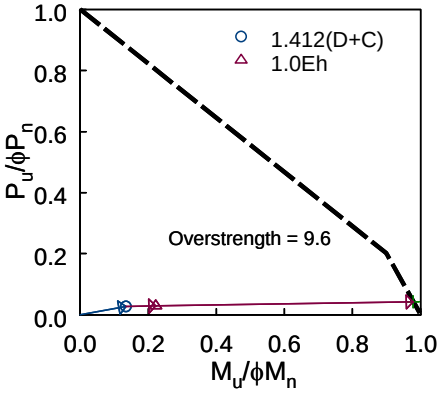

Segment R12

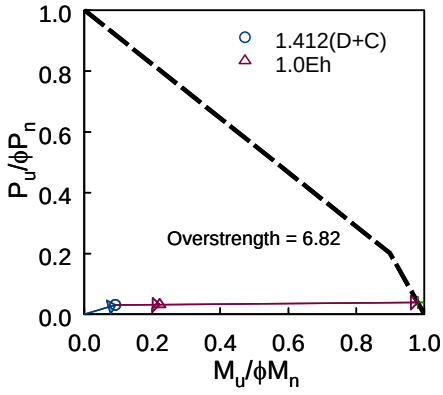

Segment R13

Figure B8 Case 3: Overstrength Factor of Building B (continued)

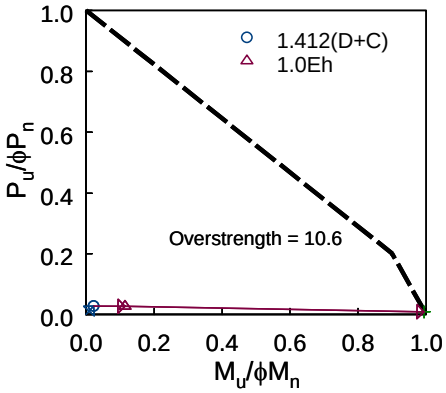

Segment R14

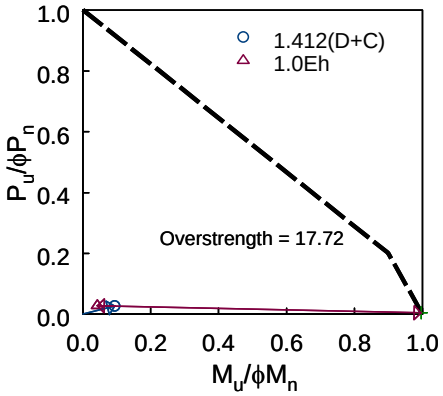

Segment R15

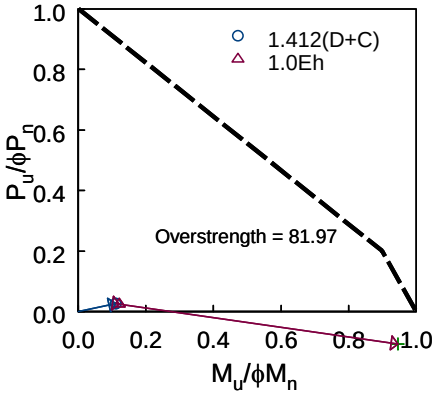

Segment R16

Figure B8 Case 3: Overstrength Factor of Building B (continued)

APPENDIX C. PARAMETRIC STUDIES ON PANEL ZONE THICKNESS

Finite element analysis results of Building A of Case 1 indicated that the system ductility could be provided by inelastic deformation of the panel zone (see Figure 6.6); tension field action after panel zone plate buckling attributed to the stable and ductile behavior of the system until failure. Parametric studies on the panel zone thickness were performed to investigate the potential of utilizing panel zone deformation as a structural fuse.

Case 1 and Case 3 (total four buildings) in Chapter 6 were considered. ABAQUS models used for drift capacity verification were employed with the variation of the panel zone thickness.

C1. Case 1

C1.1 Building A

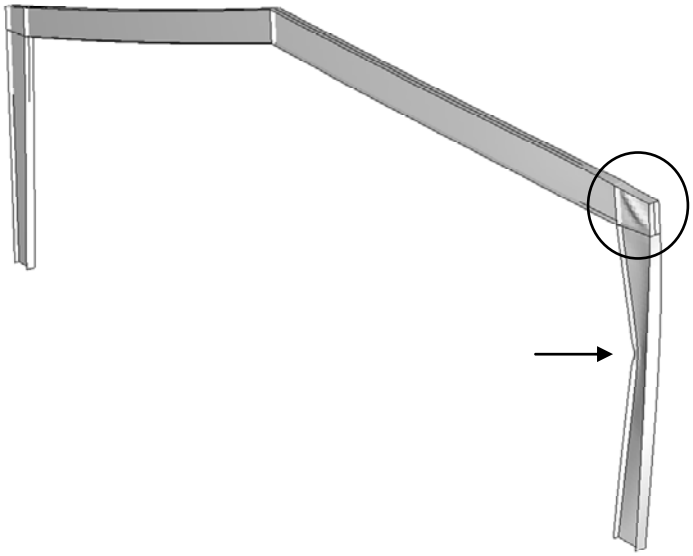

(a) t_{pz} = 0.15 in. (Building A)

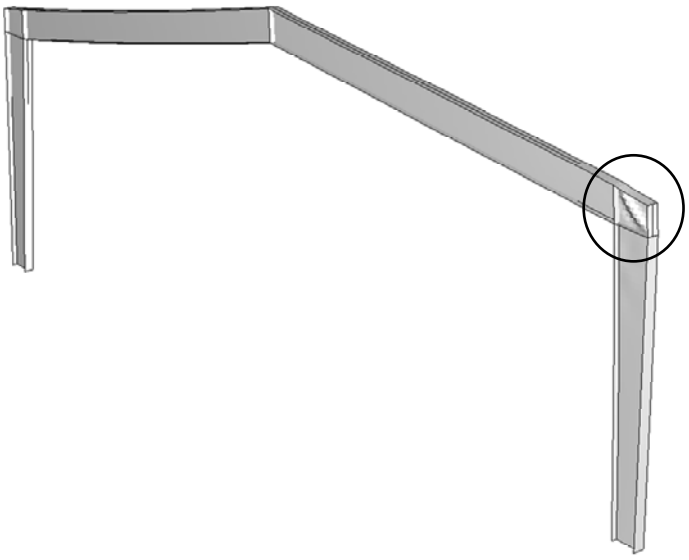

(b) t_{pz} = 0.14 in.

Figure C1 Case 1: Building A – Failure Mode

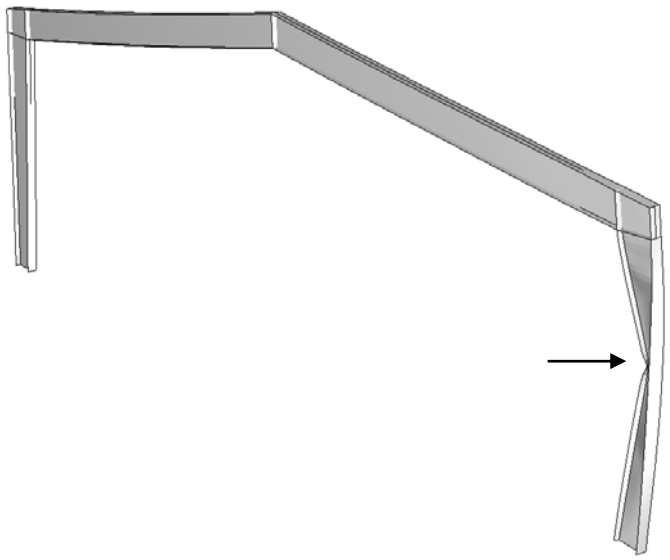

(c) t_{pz} = 0.175 in.

Figure C1 Case 1: Building A – Failure Mode (continued)

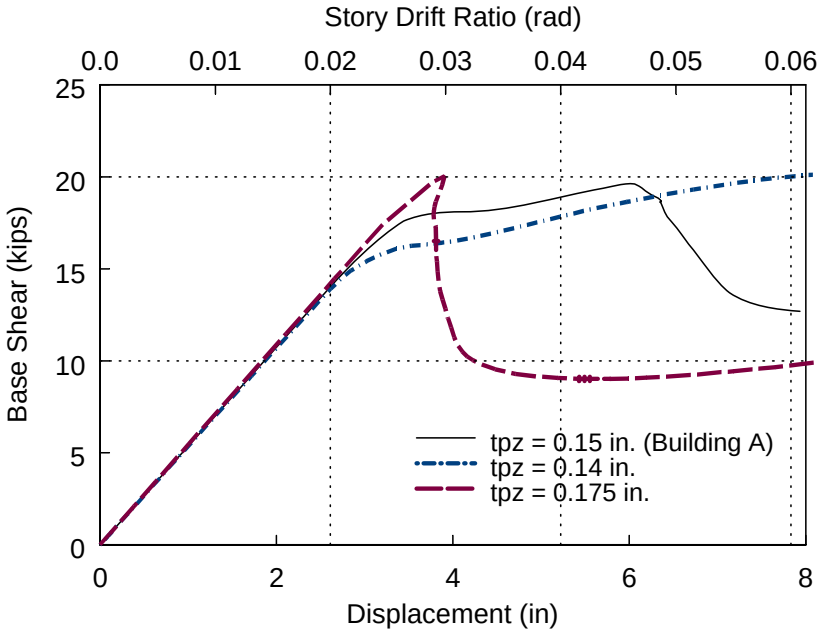

Figure C2 Case 1: Building A – Global Response Comparison

C1.2Building B

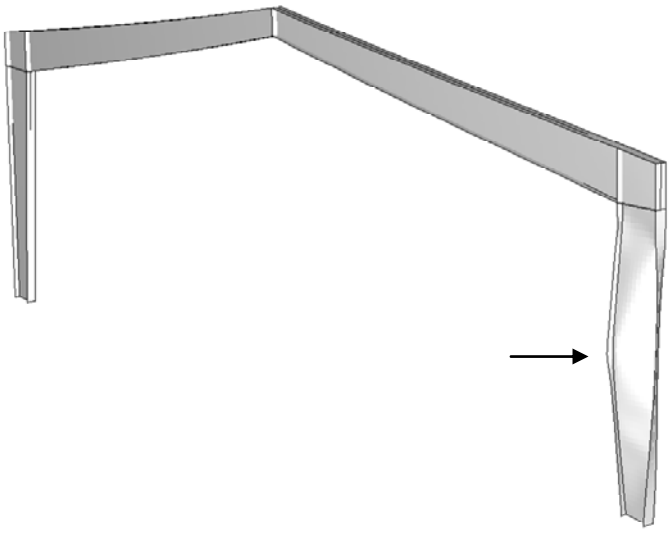

(a) t_{pz} = 0.175 in. (Building B)

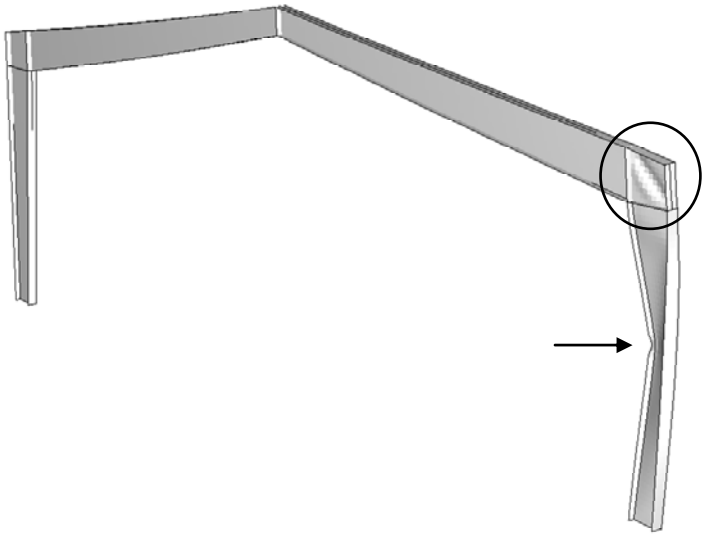

(b) t_{pz} = 0.14 in.

Figure C3 Case 1: Building B – Failure Mode

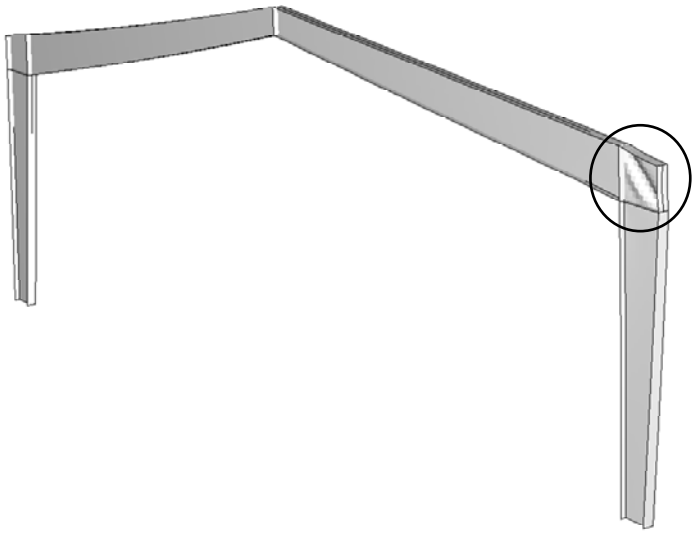

(c) t_{pz} = 0.125 in.

Figure C3 Case 1: Building B – Failure Mode (continued)

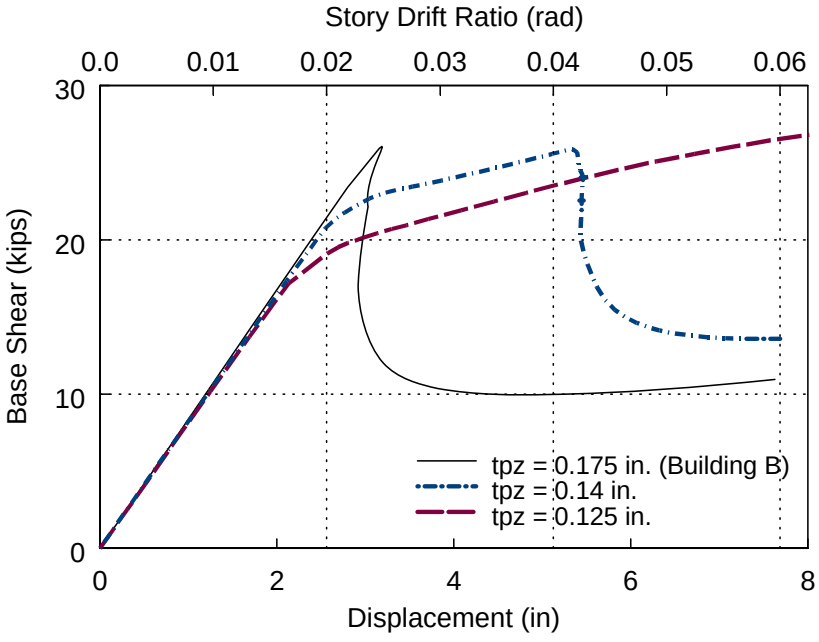

Figure C4 Case 1: Building B – Global Response Comparison

C2. Case 3

C2.1 Building A

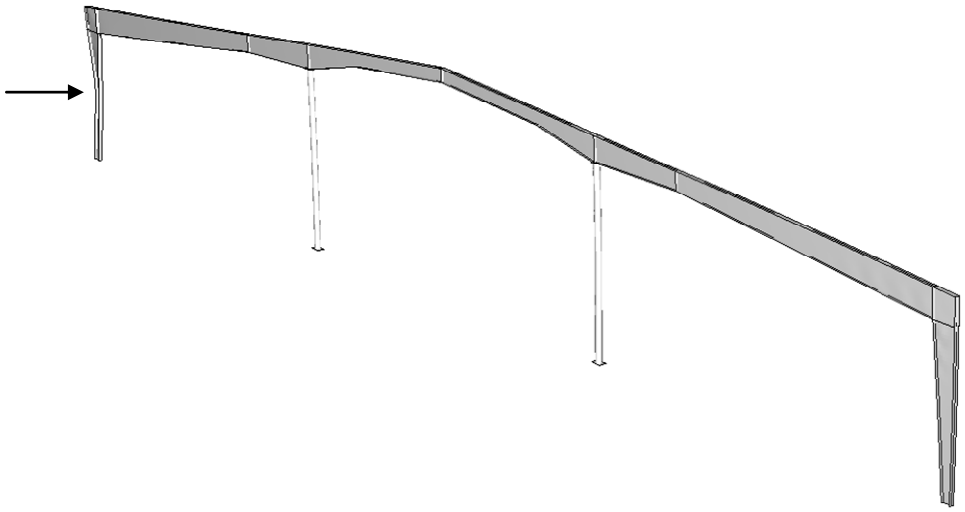

(a) t_{pz} = 0.225 in. (Building A)

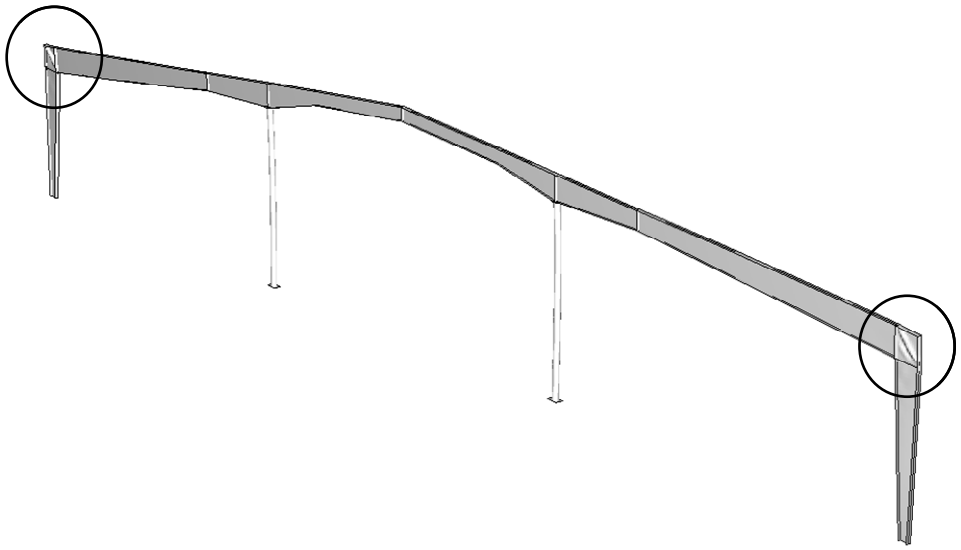

(b) t_{pz} = 0.125 in.

Figure C5 Case 3: Building A – Failure Mode

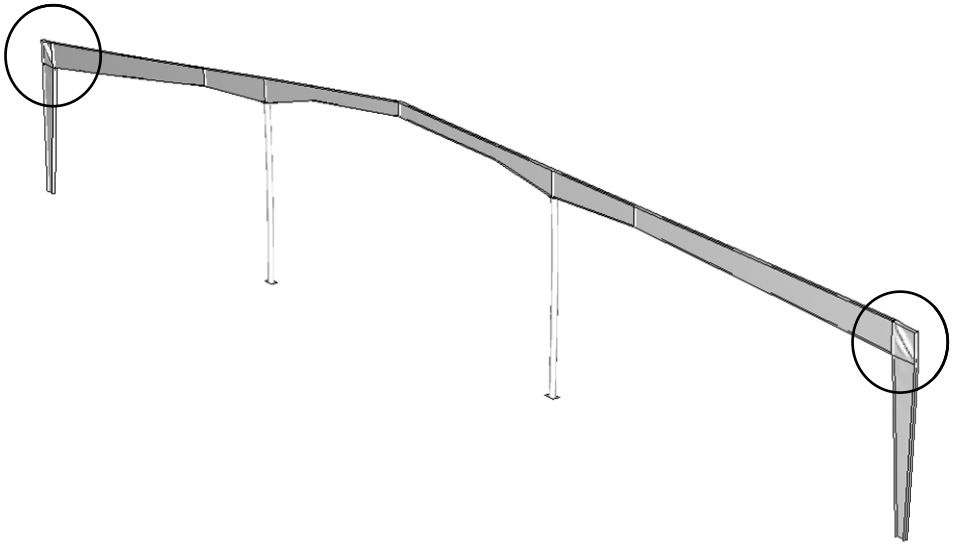

(c) t_{pz} = 0.10 in.

Figure C5 Case 3: Building A – Failure Mode (continued)

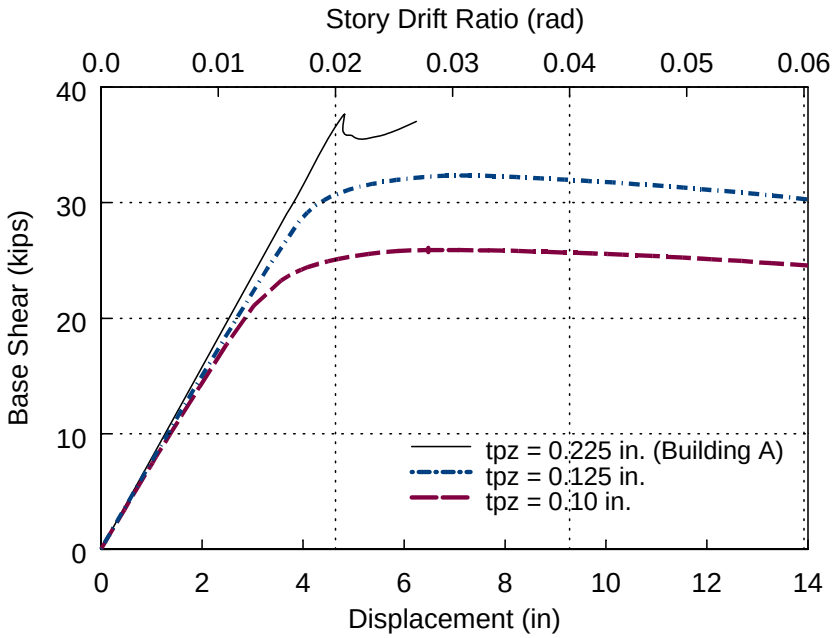

Figure C6 Case 3: Building A – Global Response Comparison

C2.2Building B

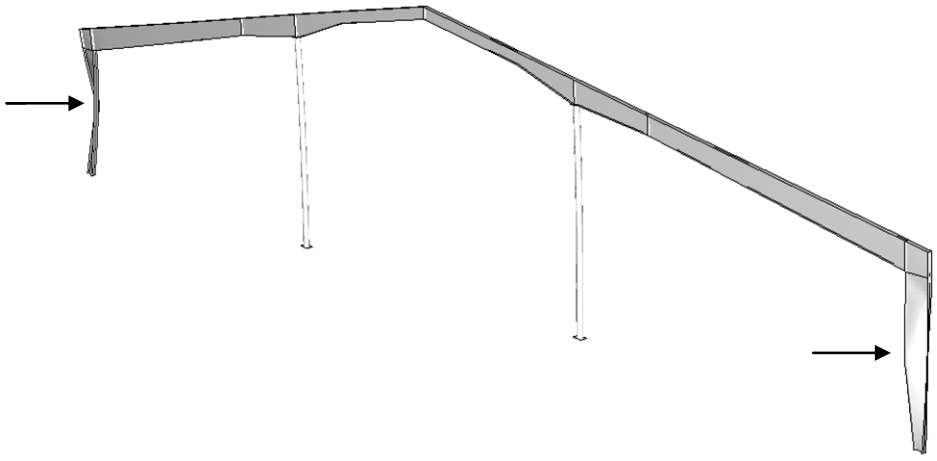

(a) t_{pz} = 0.225 in. (Building B)

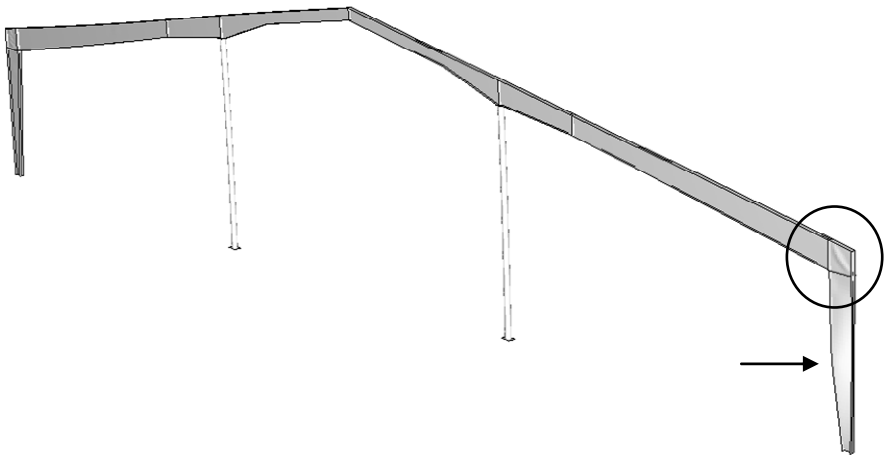

(b) t_{pz} = 0.125 in.

Figure C7 Case 3: Building B – Failure Mode

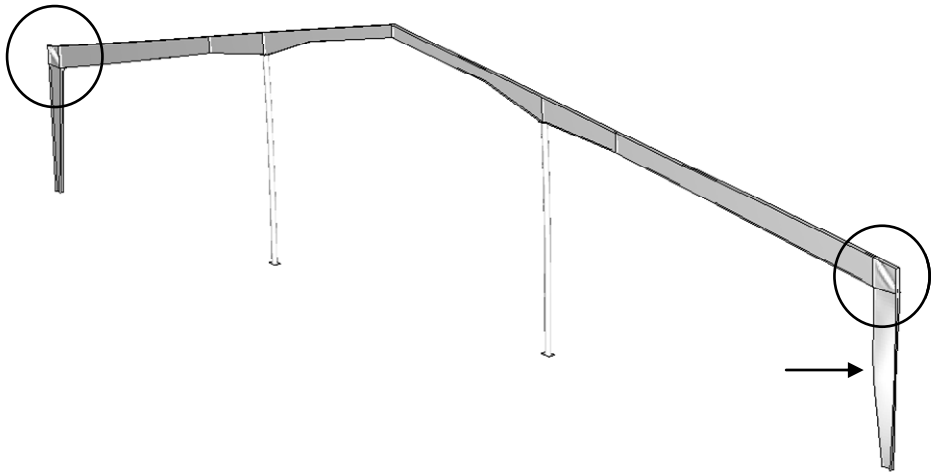

(c) t_{pz} = 0.125 in.

Figure C7 Case 3: Building B – Failure Mode (continued)

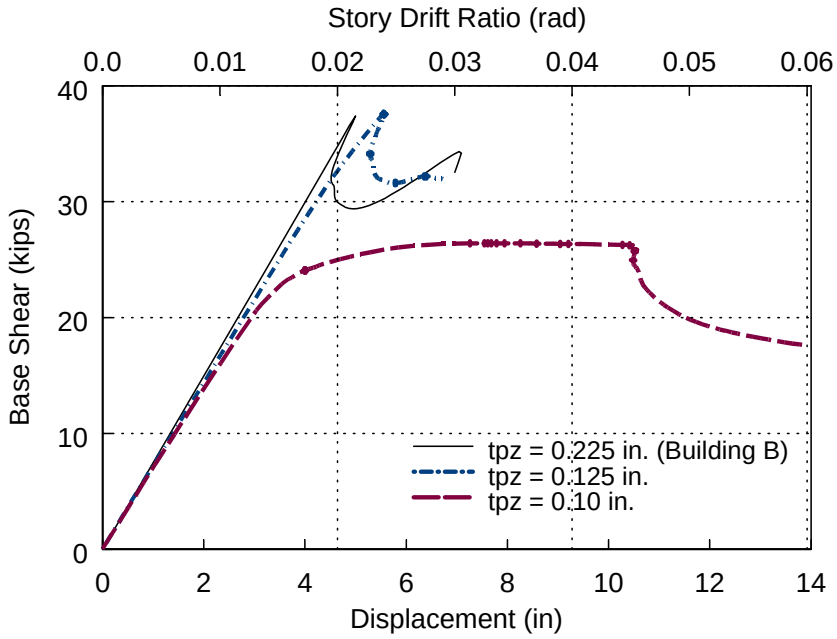

Figure C8 Case 3: Building B – Global Response Comparison

REFERENCES

[1] ABAQUS. (2005). *ABAQUS Standard Users Manual*, *Version 6.5*, ABAQUS Inc. Providence, RI.

[2] AISC. (2002). *AISC/MBMA Steel Design Guide 16: Flush and Extended Multiple-Row Moment End-Plate Connections*, American Institute of Steel Construction, Chicago, IL.

[3] AISC. (1989). *Manual of Steel Construction: Allowable Stress Design*, Ninth Edition, American Institute of Steel Construction, Chicago, IL.

[4] AISC. (2001). *Manual of Steel Construction: Load and Resistance Factor Design*, Third Edition, American Institute of Steel Construction, Chicago, IL.

[5] AISC. (2005). *Seismic Provisions for Structural Steel Buildings*, American Institute of Steel Construction, Chicago, IL.

[6] ASCE. (2002). *Minimum Design Loads for Buildings and Other Structures*, ASCE 7-02, American Society of Civil Engineers, Reston, VA.

[7] ASCE. (2005). *Minimum Design Loads for Buildings and Other Structures*, ASCE 7-05, American Society of Civil Engineers, Reston, VA.

[8] Ashakul, A. and Murray, T. M. (2006). "LRFD versus ASD Frame Design Study," *Report No. CE/VPI-ST 02/02*, Virginia Polytechnic Institute and State University, Blacksburg, VA.

[9] Bachman, R. E. and Shoemaker, W. L. (2004). "MBMA Seismic Design Guide for Metal Building Systems 2000 IBC," *CD Proceedings*, *2004 ASCE Structures Congress*, 1-8.

[10] Building Seismic Safety Committee. (1997). *NEHRP Guidelines for the Seismic Rehabilitation of Buildings*, FEMA 273, Federal Emergency Management Agency, Washington, D.C.

[11] Building Seismic Safety Committee. (2000). *Recommended Seismic Design Criteria for New Steel Moment-Frame Buildings*, EEMA 350, Federal Emergency Management Agency, Washington, D.C.

[12] Building Seismic Safety Committee. (2003). *NEHRP Recommended Provisions for Seismic Regulations for New Buildings and Other Structures*, FEMA 450, Federal Emergency Management Agency, Washington, D.C.

[13] Chen, Y., Wu, X., Tian, H., Zhao, J., and Ma, Y. (2006). "Experiment on Non-compact H-shaped Members and Frames Subjected to Cyclic Loads and the

Prediction of Capacities," *International Journal of Steel Structures*, Korean Society of Steel Construction, 6(3), 215-226.

[14] Chopra, A. K. (2001). *Dynamics of Structures: Theory and Applications to Earthquake Engineering*, Second Edition, Prentice Hall, Upper Saddle River, NJ.

[15] Crisfleld, M. A. (1981). "A Fast Incremental/Iterative Solution Procedure That Handles Snap-through," *Computers and Structures*, Vol.13, 55–62.

[16] Davids, D. B. (1996). *LRFD Evaluation of Full-Scale Metal Building Rigid Frame Tests*, Master Thesis, Virginia Polytechnic Institute and State University, Blacksburg, VA.

[17] Forest, R. and Murray, T. M. (1982). "Rigid Frame Studies," *Research Report No. FSEL/STAR 82-01*, University of Oklahoma, Oklahoma City, OK.

[18] Galambos, T. V. (1998). *Guide to Stability Design Criteria For Metal Structures*, Fifth Edition, John Willey & Sons, Inc., New York, NY.

[19] Gil, H. and Yura, J. A. (1999). "Bracing Requirements of Inelastic Columns," *Journal of Constructional Steel Research*, Elsevier, Vol.51. 1-19.

[20] Heldt, T. J. and Mahendran, M. (1998). "Full Scale Experiments of a Steel Portal Frame Building," *Journal of the Australian Institute of Steel Construction*, Australian Institute of Steel Constructions, 32(4), 2-15.

[21] HKS. (1996). *ABAQUS Standard Users Manual*, Version 5.6, Hibbitt, Karlsson, and Sorensen Inc., Providence, RI.

[22] ICC. (2003). *International Building Code*. International Code Council, Inc., Whittier, CA.

[23] ICC. (2006). *International Building Code*. International Code Council, Inc., Whittier, CA.

[24] Lee, G. C., Chen, Y. C., and Hsu, T. L. (1979). "Allowable Axial Stress of Restrained Multi-Segment, Tapered Roof Girders," *Welding Research Council*, Bulletin No. 248.

[25] Lee, G. C., Ketter R. L., and Hsu, T. L. (1981). *The Design of Single Story Rigid Frames*, Metal Building Manufacturers Association, Cleveland, OH.

[26] Lee, G. C. and Morrell, M. L. (1975). "Application of AISC Design Provisions for Tapered Members," *Engineering Journal*, AISC, First Quarter, 1-13.

[27] Lee, G. C., Morrell, M. L., and Ketter, R. L. (1972). "Design of Tapered Members," *Welding Research Council*, Bulletin No. 173.

[28] Mays, T. (2000). *Application of the Finite Element Method to the Seismic Design and Analysis of Large Moment End-Plate Connections*, Ph.D. Thesis, Virginia Polytechnic Institute and State University, Blacksburg, VA.

[29] MBMA. (2002). *Metal Building Systems Manual*, Metal Building Manufacturers Association, Cleveland, OH.

[30] MBMA. (2004). *Seismic Design Guide for Metal Building Systems Based on the 2000 IBC*, Metal Building Manufacturers Association, Cleveland, OH.

[31] Miller, B. S. and Earls, C. J. (2003). "Behavior of Web-Tapered Built-up I-Shaped Beams", *Report CE/ST 28*, University of Pittsburgh, Pittsburgh, PA.

[32] Miller, B. S. and Earls, C. J. (2005). "On Moment Capacity and Flexural Ductility in Doubly Symmetric Web-Tapered I-Girders," *Engineering Journal,* Third Quarter (2005), 123-141.

[33] Morrell, M. L. and Lee, G. C. (1974). "Allowable Stresses for Web-Tapered Beams with Lateral Restraints," *Welding Research Council*, Bulletin No. 192.

[34] Murray, T. M. (1986). "Stability of Gable Frame Panel Zone Plates," *Proceedings of the Structural Stability Research Council Annual Technical Session*, Structural Stability Research Council, 317-325.

[35] Newman, A (2003). *Metal Building Systems: Design and Specifications*, Second Editioin, McGraw-Hill, New York, NY.

[36] Nucor Building Systems website (http://www.nucorbuildingsystems.com).

[37] Powell, G. and Simons, J. (1981). "Improved Iterative Strategy for Nonlinear Structures," *International Journal for Numerical Methods in Engineering*, Wiley InterScience, Vol. 17, 1455–1467.

[38] Prawel, S. P., Morrell, M. L. and Lee, G. C. (1974). "Bending and Buckling Strength of Tapered Structural Members," *Welding Research Journal Supplement*, Vol.53, 75-84.

[39] Riks, E. (1970). "On the Numerical Solution of Snapping Problems in the Theory of Elastic Stability," *SUDAAR No. 401*, Stanford University, Stanford, CA.

[40] SAP2000. (2005). *SAP 2000 User's Manual*, *Version 10.02*, Computers and Structures Inc. Berkeley, CA.

[41] SEAOC. (1999). *Recommended Lateral Force Requirements and Commentary*, Seventh Edition, Structural Engineers Association of California, Sacramento, CA.

[42] Sockalingam, B. (1988). *A Dynamic Test Procedure for Analyzing Low-Rise Metal Buildings,* Master Thesis, Clemson University, Clemson, SC.

[43] Sumner, E., A. (1995). *Experimental and Analytical Investigation of the LRFD Strength of Tapered Members*, Master Thesis, Virginia Polytechnic Institute and State University, Blacksburg, VA.

[44] Uang, C. M. (1991). "Establishing R (or R_w) and C_d Factors for Building Seismic Provisions," *Journal of Structural Engineering*, ASCE, Vol.117, No.1, 1991, 19-28.

[45] Winter, G. (1960). "Lateral Bracing of Columns and Beams," *Transactions*, ASCE, Vol.125, 807-845.

[46] Young, J. and Murray, T. M. (1996). "Experimental Investigation of Positive Bending Moment Strength of Rigid Knee Connections," *Research Report No. CE/VPI-ST 9617*, Department of Civil Engineering, Virginia Polytechnic Institute and State University, Blacksburg, VA.

[47] Yura, J. A. and Li, G. (2002). "Bracing Requirements for Inelastic Beams," *2002 SSRC Annual Stability Conference*, Structural Stability Research Council.